# Studies on coacervation phase behavior of sequence-controlled polyelectrolytes

Inaugural Dissertation

to obtain the academic degree

Doctor rerum naturalium (Dr.rer.nat)

of the Faculty of Mathematics and Natural Science

of Heinrich-Heine-University Düsseldorf

presented by

**Michele Denise Illmann**

from Hilden

Düsseldorf, August 2024

From the Institute of Organic Chemistry and Macromolecular Chemistry at the Heinrich Heine-University Düsseldorf

Published by permission of the

Faculty of Mathematics and Natural Science at

Heinrich-Heine-University Düsseldorf

1st Reviewer: Prof. Dr. Laura Hartmann

2nd Reviewer: PD Dr. Klaus Schaper

Date of the oral examination: 05.12.2024

This thesis was accomplished in the period between April 2019 and December 2022 in the Institute of Organic Chemistry and Macromolecular Chemistry at the Heinrich Heine University in Düsseldorf, in the group of Prof. Dr. Laura Hartmann.

I hereby declare that the thesis submitted is my own work without making use of impermissible aids, considering the “Rules of the Principles of Safeguarding Good Scientific Practice at Heinrich-Heine-University Düsseldorf”. All direct or indirect sources used are acknowledged in the bibliography as references. I further declare that I have not submitted this or a similar thesis at any other examination board in order to obtain a degree.

Düsseldorf, August 2024

Michele Denise Illmann

*Don’t be afraid of hard work. Nothing worthwhile comes easily. Don’t let others discourage you or tell you that you can’t do it. In my day I was told women didn’t go into chemistry. I saw no reason why we couldn’t.*

*Gertrude Belle Elion (Biochemist and Pharmacologist)*

# Table of contents

# Abstract

Many biologically relevant molecules are polyelectrolytes e.g., DNA or proteins, but also synthetic polyelectrolytes are of great importance in our everyday life e.g., as superabsorbers or adhesives. When two polyelectrolytes are mixed together, a polyelectrolyte complex is formed, which can occur in the form of coacervates. Coacervation describes a liquid-liquid phase separation, in which most of both polymers are deposited in one of the two phases – the polymer-rich phase or coacervate. This process is based on the electrostatic interaction between the charged groups of the polymers and is induced at a certain polymer and salt concentration. Coacervate formation is again relevant both for natural and synthetic polyelectrolytes. An example from nature is the velvet worm: coacervate formation of its hunting slime enables its unique hunting skill by forming stiff fibers through mechanical shear forces out of this slime. Another example is a cell, where phase separation of intrinsically disordered proteins (IDPs) leads to the formation of membraneless organelles and can thus protect internal cell processes from the cytoplasm without an additional solid cell membrane. Despite the wide relevance, the formation of coacervates is not yet fully understood, as not only polymer-related parameters such as chain length, charge sequence and -density are key indicators. Many external influences such as salt concentration, temperature or the pH value can have an impact on the phase separation process by affecting the net charge of the polymer complex. To gain deeper insights, the tailor-made synthesis of polyelectrolytes with controllably variable structures supports the research of coacervation formation. In the present work, the aim was to synthesize sequence-controlled polyelectrolytes in order to investigate the impact of placing the same charged groups at different positions within the overall polyelectrolyte structure on the coacervate formation and to explore new possible applications in the field of biomimetic systems.

The first part of the thesis focuses on the synthesis of such sequence-controlled polyelectrolytes. Previous studies of coacervation behavior focused on the synthesis of sequence-controlled polyelectrolytes using solid-phase synthesis, a well-known approach for the sequential assembly of building blocks towards peptide structures. However, this type of synthesis is limited in its number of repeating units. Solid-phase synthesis was used in this work in combination with polymer analogous reactions to access brush-shaped polyelectrolytes and polyampholytes. For this purpose, oligo-electrolytes and oligo-ampholytes were sequentially synthesized using Fmoc-based solid-phase synthesis, which were subsequently coupled onto active ester polymers using the “grafting to” method. The method benefits from using the same polymer backbone for the conversion to the polyelectrolyte and polyampholyte structures, which contributed to greater comparability in the further process. The challenge during oligomer synthesis was to find a suitable protection group to keep the

amino acids side chains inactive during the overall synthesis to prevent crosslinking during polymer analogous reaction. Alloc and Allyl protection groups were used to protect lysine and glutamic acid side chains, because of their good stability in both acidic and alkaline conditions as well as their general applicability on oligo-electrolyte and oligo-ampholyte synthesis. Active ester polymers were produced by polymerizing pentafluoro phenyl monomers via RAFT polymerization. The obtained polyactive ester derivatives were used as a polymer backbone for the subsequent substitution of the pentafluoro phenyl side chains with terminal primary amine groups of the oligomers. Comparable linear structures were obtained by conjugating active ester polymers with glycine and ethanolamine. The targeted functionalization degree of the oligomers into the polymer was chosen to compare with the linear charged polyelectrolytes. Final cleavage of the amino acid side chain Alloc and Allyl protection groups after polymer conversion was challenging, as currently existing cleavage protocols were optimized on solid-phase synthesis systems which required an adaption to a reaction in solution. A result of this work is the successful synthesis of sequence-controlled polyelectrolytes and polyampholytes as well as their characterization by $^{1}$H-, $^{19}$F-NMR and GPC.

In the second part of this work, the synthesized polyelectrolytes and polyampholytes were investigated for their coacervation behavior. For the linear charged polyelectrolytes, a phase diagram was obtained in dependance of the salt- and polymer-concentration in order to define the liquid-liquid phase separation range. The influence of polymer chain length confirmed coacervation behavior of longer polyelectrolytes, which lead to a higher salt resistance and thus to an enhanced phase separation area. However, this increase could only be observed up to a certain polymer concentration, beyond this concentration salt resistance of longer polymer backbone dropped drastically and the polyelectrolytes were present in a precipitated form and no longer in a liquid phase. When comparing linear polyelectrolytes with the brush-shaped polyelectrolytes, the salt resistance of the coacervate phase decreases significantly. Also, solubilities of the polymers were strongly impaired by this polymer structure and were therefore only analyzed at lower polymer concentrations.

The investigation of linear, ampholytic polymers, on the other hand, did not lead to any phase separation, which could be due to an insufficient accumulation of charges. Coacervation was found to be favored by high charge densities of equally charged groups, which could not be guaranteed with this purely randomly constructed polyampholytes. When synthesizing polyampholytes from sequence-defined oligo-ampholytes, a system with an increased charge density was obtained to exhibit liquid-liquid phase separation at low salt concentrations. The first coacervate droplets were already observed from polymer with oligo-ampholytes with two consecutive, identical charges, even though these systems exhibited significantly lower salt resistance compared to the linear polyelectrolytes. Nevertheless, a successful initial

investigation of the coacervation behavior was carried out and the first comparisons of brush-shaped polyelectrolytes and polyampholytes were made regarding their polymer length, charge distribution and charge density.

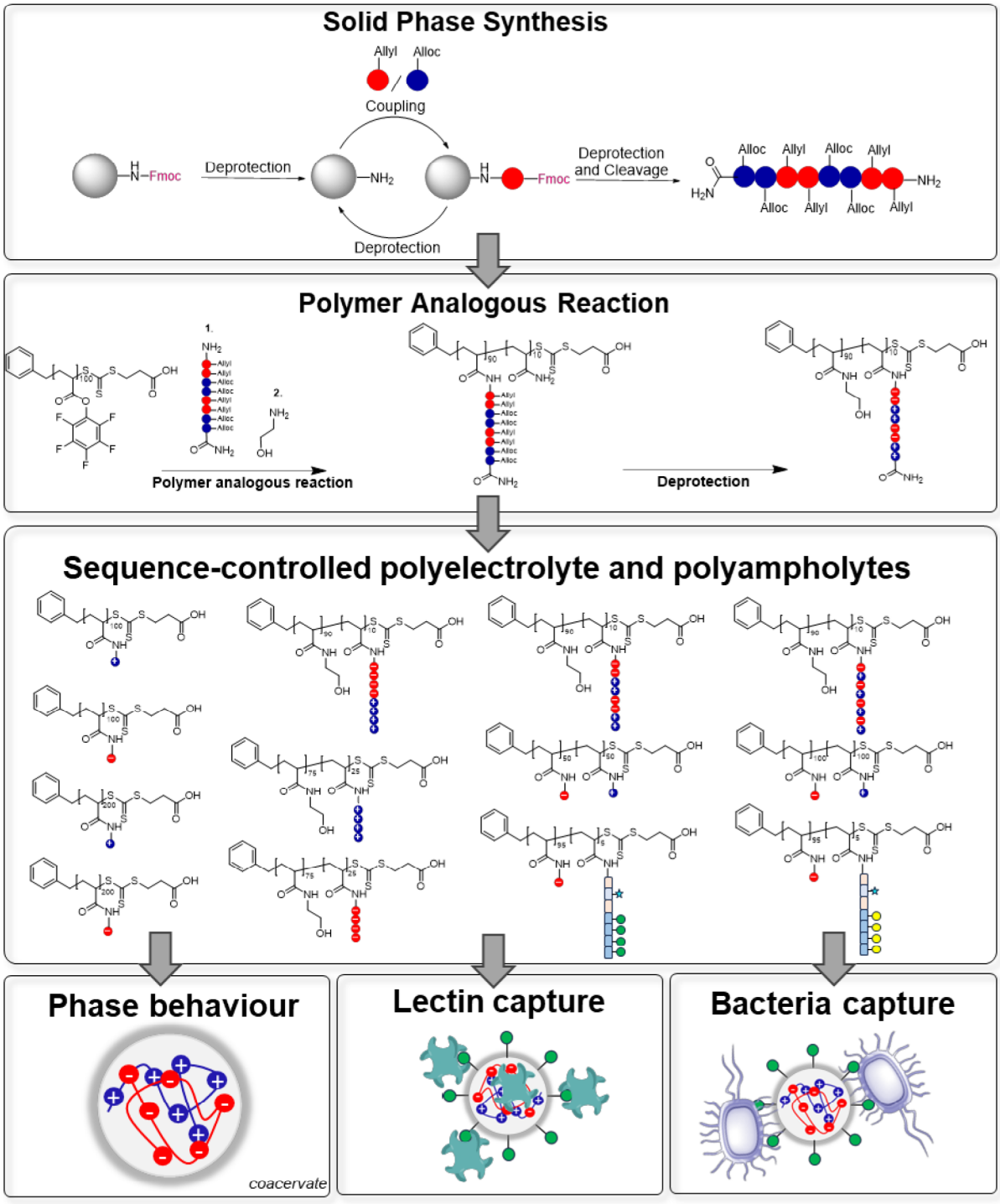


*Figure 1: Schematic overview of different parts in this thesis*

In the final part of this work, glycan presenting polyelectrolytes were synthesized and investigated for their phase behavior as well as their biomolecular interactions with lectins and bacteria. For this purpose, mannose and galactose functionalized oligomers were prepared by

solid-phase synthesis and converted to polyelectrolytes via polymer analogous reaction, using the same method as described before. First coacervation tests in solution showed that coacervate droplets can also be formed with these glycan presenting polyelectrolytes, which, however, show significantly slower phase separation. This may be due to a lower charge density caused by the carbohydrate units present. Furthermore, these coacervate droplets were analyzed in biological assays for their specific interactions with lectins and bacteria. It was found that the coacervates bearing mannose units were able to capture significantly more of the lectin Concanavalin A, a mannose-specific binding protein, than galactose-containing or non-glycan presenting coacervate droplets. Furthermore, in first studies with *E. coli* bacteria it was observed that both, the mannose-bearing and the unfunctionalized coacervates showed interaction with the bacteria. This suggests that also non-glycan interactions, most likely from the charges of the polyelectrolytes, have an influence on the capture of the bacteria within the coacervate phase. Indeed, *E. coli* presents a surface charge as well which was investigated by Zeta potential measurements. If, however, the mannose functionality is blocked by an access of methyl α-D-mannopyranosid or coacervates containing galactose are used, an almost shielding effect can be observed, which not only leads to "non-capture" of the *E. coli* bacteria but actually repelled them. To summarize this, the introduction of specific binding units into liquid condensates opens up new possibilities for the investigation of lectin-carbohydrate interactions and the design of new functional materials.

Overall, this work provides an extended synthesis route that allows access to sequence-controlled polyelectrolytes and polyampholytes. In addition, initial investigations not only allowed further conclusions to be drawn about the phase behavior of coacervates, but also revealed potential for application in the field of biomimetics.

# List of Publications

## Publications included in this thesis

Illmann, M. D.; Schafl, L.; Drees, F.; Hartmann, L.; Schmidt, S. Glycan-Presenting Coacervates Derived from Charged Poly(active esters): Preparation, Phase Behavior, and Lectin Capture. *Biomacromolecules* **2023**

Own contributions:

Collaborative synthesis of sequence-defined oligomers containing mannose and galactose moieties, as well as an AIE Dye. Collaborative synthesis of polyelectrolytes containing glyco-oligomers via polymer analogous reaction. Investigation of their phase behavior by variation of polymer and salt concentration. Investigation of incorporation of Concanavalin A within glycan coacervates. Determination of capture effectivity. Collaborative manuscript writing.

# 1. Introduction

## 1.1. Polyelectrolytes

Polyelectrolytes (PEs) are polymeric structures featuring dissociating groups in the side chain that are either positively or negatively charged under suitable pH and solvent conditions. Polymers that contain both negative and positive charges are called polyampholytes. If the groups are not dissociated, PEs behave like ordinary macromolecules.[1, 2] However, if the state of a single group changes from an uncharged to a charged state, the behavior of the polymer and its properties such as dissolution behavior, ionic strength etc. will change. These changes are closely linked to the number of charged groups in the macromolecules, so that PEs represent two essential categories that can be investigated in combination: 1) polymeric structures with a 2) high number of charges. Polyelectrolytes can be categorized into different types based on their origin, charge, shape, composition, charge density or the position of it as described in Figure 2.

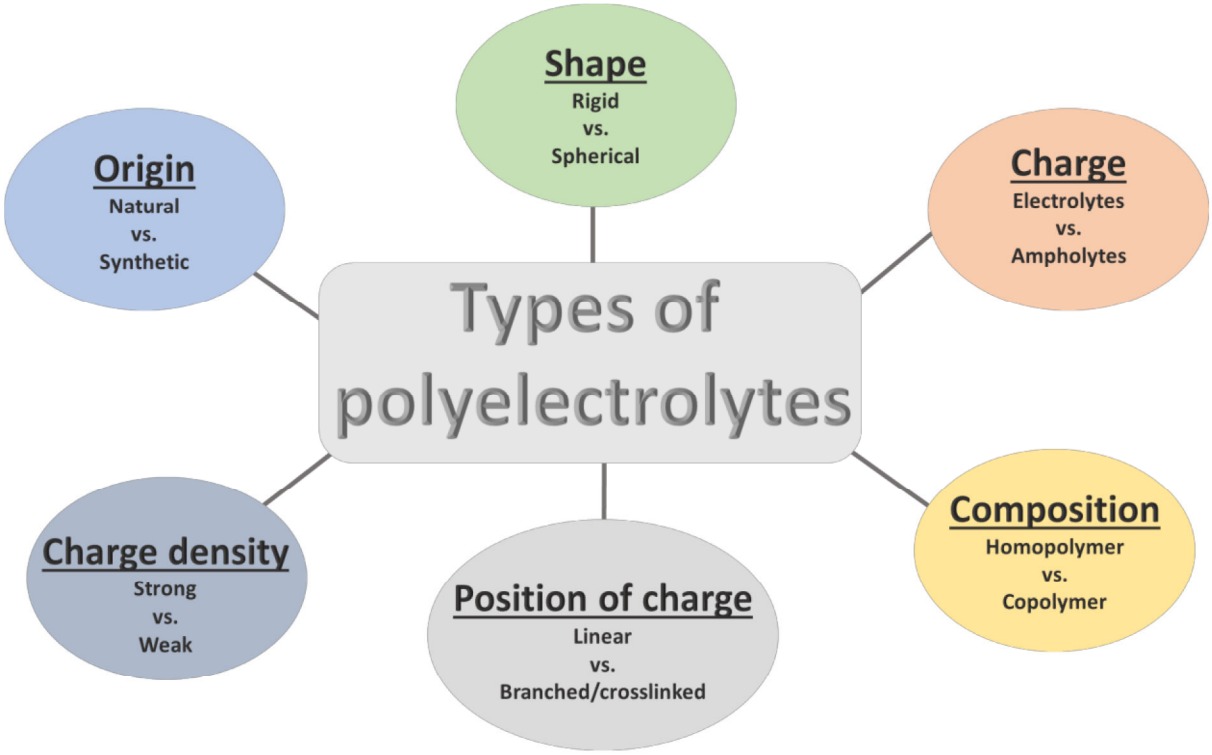


*Figure 2: Types of polyelectrolytes based on their origin, shape, charge, composition, charge density and position of the charge (graphic based on[1]).*

The diversity among polyelectrolyte types leads to complex interactions that are often challenging to understand. In general, interactions of polyelectrolytes are driven by the two major points, solubility and electrostatic interactions. They can be influenced, for instance, by the salt concentration or the pH value. Hence, the solubility of PEs can be categorized in different stages:[3, 4]

Stage 1 Dissolved polyelectrolytes in water can built up more complex structures.

Stage 2 Dissociated groups are surrounded by counterions. Di- or higher valent counterions can lead to “bridging” effect between two charged polymer chains, while the polyelectrolytes stay in solution.

Stage 3 With increasing charge density due to high volumes of polymer, PEs can go from a diluted, liquid stage into a precipitate form, which is also driven by the concentration of salt within the solution.

Stage 4 At a certain salt concentration, the PEs revert from a solid state to a solution, as the polymer ions are shielded by the salt ions.

With this, applications for PEs can derive from fields like pharmaceutical industry and medicine, over to the cosmetic and food industry. In pharmaceutical field PEs can be used as swellable controlled polymers, coating materials or surfactant, but also as injectable drug delivery systems. The range of applications expands even further when considering not only individual polyelectrolytes, but a mixture of differently charged PEs.[5-9]

### 1.1.1. Polyelectrolyte complexes and coacervate formation

Polyelectrolytes tend to interact with oppositely charged polyelectrolytes, and therefore form Polyelectrolyte complexes (PECs) in aqueous solutions. Interaction between these two charged polymers is mainly driven by the electrostatic interaction of the opposite charges and an entropy gain, which arises from the release of counterions.[10] As early as 1896, *Kossel* was the first to provide an explanation for the phase separation of natural proteins and carbohydrates, which he attributed to the opposite charges and the resulting electrostatic interactions.[11] Further observations were made in 1911 by *Tiebackx*, who noted the phase behavior of different acids in solution with gelatin and gum arabic and in 1961 when *Michaels* investigated PECs with the synthesis and analysis of poly(4-vinylbenzyltrimethylammonium) in combination with poly(styrene sulfonate).[12 13]

The formation of PECs is divided into three major steps. In the first step, a so-called primary complex is formed and results in a spontaneous arrangement and interaction of the oppositely charged polyelectrolytes, without the formation of an ordered structure. In the second step, an intramolecular rearrangement occurs, in which an ordered secondary complex is formed. During this process, new connections and conformations of the polymer chains are formed. In the last step, the secondary complex aggregates, which is highly influenced by hydrophobic interactions and leads to insolubility in standard solvents.[14, 15] Therefore, as an supramolecular order between the polymer chains, two models for PECs are considered here: the chain-ordered ladder-like model and the disordered scrambled-egg model.[1, 13, 16]

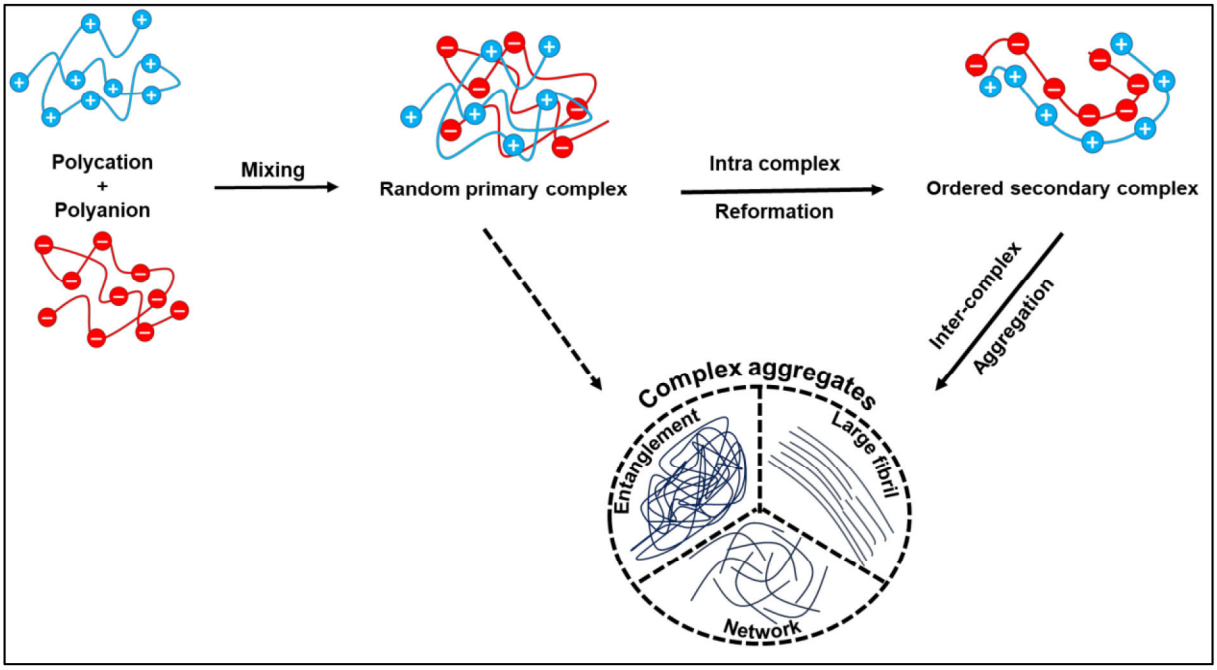


*Figure 3: Schematic representation of complex aggregate formation of polyelectrolyte complexes. Representation shows three major steps in PECs aggregation process: First random primary complex, ordered secondary complex after intramolecular construction and inter-complex aggregation leading to complex aggregates.*

Once created, a variety of conditions can readily affect the state of the polyelectrolytes for instance the concentration of polymers, the pH level, or the ionic strength of the PEs. Therefore, polyelectrolyte complexes can be classified broadly into three types based on their phase behavior in aqueous solution:[1, 16]

1. *Water soluble PECs*, the macroscopically homogenous systems based on smaller PEC aggregates.
2. *Turbid colloidal stable PECs*, which represent a transition stage preceding phase separation.
3. *Complex Coacervates*, a liquid-liquid phase separation PEC system.[17]

**Complex Coacervation**

Complex coacervation was first described in 1930 by *Bungenberg de Jong* and *Kruyt,* when they observed a liquid-liquid phase separation of a gelatin and gum arabic mixture. They began to use the term of “coacervation” to describe the intermediate state of segregation, the origin being based on the latin word "acervus", which can be translated as "heap", while the prefix "co-" refers to the prior assembly.[18] The liquid-liquid phase system is formed by a separation into a polymer-rich (coacervate phase) and a dilute phase (supernatant).[19] However, coacervate formation is not limited to the presence of two oppositely charged polyelectrolytes. Polyampholytes can also lead to the formation of coacervates, whereby the term self-coacervation is used here.[20, 21] This phenomenon is mainly driven by electrostatic interaction

between differently charged species and the interaction results in a release of the associated counter ions, which in turn is associated with an entropy gain.[22]

Usually, the initial indications of coacervate formation are visible to the unaided eye. Turbidity begins to appear in the solutions due to the formation of small coacervate droplets.[23, 24] However, these droplets are usually not stable and can coalesce very easily over time to form larger droplets. At a certain point, enough droplets have accumulated to form a separate phase that settles to the bottom, like a water-oil separation, which can be accelerated by external forces such as centrifugation. Nevertheless, stable coacervate droplets that either do not coalesce or require a significantly longer period to do so can also be formed, based on the molecular structure of the polyelectrolytes. For example, polyelectrolytes containing large uncharged blocks in the chain can form micelle-like coacervates that are less prone to coalescence. They work especially well as a stable encapsulation technique for encapsulating and delivering proteins or antigens.[25]

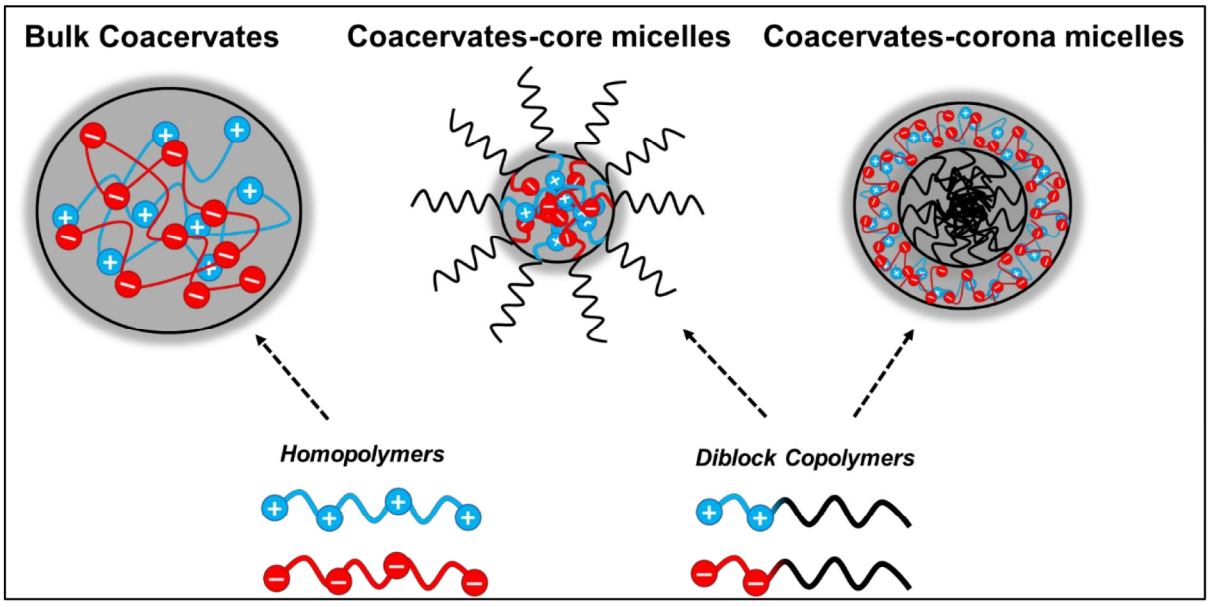


*Figure 4: Schemes of different architectural coacervates based on their polyelectrolyte structure* [26]

The coacervation phase is sensitive to a variety of external parameters, similar to other forms of PECs. These conditions include temperature, ionic strength, pH value, polymer concentration, and many more.[27, 28] Regarding the salt concentration, there is less interaction between the charged polymer chains as the amount of salt in the solution increases, because the charged groups of the polymer are more thoroughly covered with the counterions of the salt. The interaction between the polymer chains becomes so insignificant above a specific concentration of salt that they shift from a liquid-liquid phase separation to a dissolved system. This effect appears when exceeding the critical salt concentration (CSC).[23, 29]

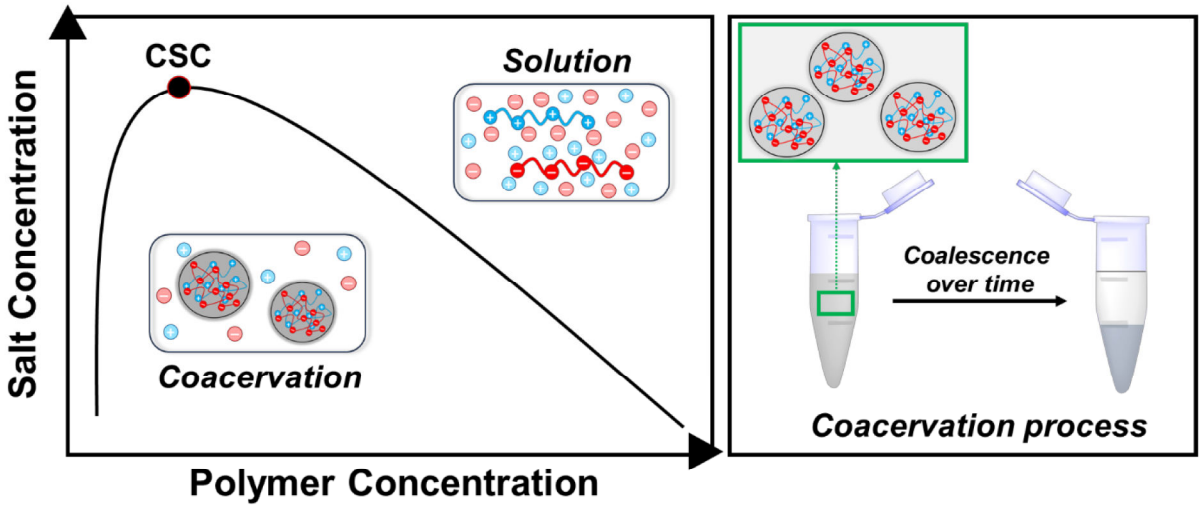


*Figure 5: Coacervation phase behavior. a) Schematic phase diagram of coacervation process as a function of salt and polymer concentration. At a certain salt concentration two phase system transfers to a one phase solution (critical salt concentration, CSC). b) Coacervation droplets coalescence over time and settle down two a visible two-phase separation.*

The length of the polymer chains, the polymer concentration in the solution, and the valence of the ions can all affect when the point of CSC is reached.[30] The range of the stable two-phase system also shifts when the polymer concentration is increased concurrently. However, if the polymer concentration is too high, the system will precipitate because of the excessive interaction between the polymer chains.

Prior research performed by the group of *Perry* has demonstrated the influence of charge density and distribution for the coacervation phase. Here, it was shown that the charge sequence of polyampholytes is crucial for coacervate formation and that a high charge density significantly favors stronger coacervate formation. Intrinsically disordered proteins (IDPs) serve as the basis for these investigations and refer to proteins lacking a defined 3D-structure. Because they typically possess both positive and negative charges, the majority of them are also categorized as polyampholytes and are essential to the formation of membraneless organelles It has been demonstrated that the effects of the polyampholyte studies and the chain extension of homopolymeric polyelectrolytes on coacervation formation are comparable. The coacervation phase can be increased by lengthening the charge sequence (or, in the case of homopolymers, the chain length). [31-33]

Apart from investigating the behavior of coacervates in response to external factors, they are currently being investigated for their use in industries like food, cosmetics, and pharmaceuticals.[34, 35] A study on the use of coacervates to enhance the thermostability of attenuated live virus vaccines was published in 2020.[36] Vaccines must be kept well cooled for a longer period of time in order to maintain their effectiveness. Should this cold chain be broken, the vaccine's efficacy might be affected. Porcine parvovirus (PPV) was encapsulated within the coacervate phase through the use of poly(D,L-glutamic acid) and poly(L-lysine) as

polyelectrolytes. This enabled the viruses to maintain their stability for several weeks at relatively high temperatures, whereas viruses not embedded in coacervate can only maintain their stability for a few days at comparable temperatures.[36]

The aforementioned examples demonstrate how the coacervate process is a highly beneficial mechanism that is specifically influenced by several kinds of conditions. However, in nature there are multiple examples of coacervates and their significant roles and functions. Current studies and investigations are still in the early stages of examining these processes and exploiting them to establish specific applications.[37-40]

### 1.1.2. Coacervates in biology

An essential class of naturally occurring polyampholytes are proteins. Organized structures such as beta sheets and alpha helices can be formed through the precise arrangement of different amino acids, hydrogen bonds or the interaction of charged or hydrophobic units. These formations are particularly important for assuming biological functions in the body, such as receptor domains for cell-cell communication. With protein structures that are intrinsically disordered, this is not the case. In this instance, the protein maintains a partially linear or partially random coil arrangement and either no or only a partial superordinate structure form. Their organization is not entirely disorganized, though. Because they typically contain a higher percentage of charged groups and fewer hydrophobic side chains, IDPs are particularly soluble in water. Hence, the abundance of charged groups ensures the protein's strong electrostatic interactions and may lead to the formation of coacervate structures. They can be found as membraneless organelles in the cytoplasm of cells. Since they don't have a cell membrane that protects them from the cytoplasm, these membraneless organelles rely on the compartmentalization of IDPs to maintain their functionality. [41-45]

The velvet worm's secretion of "super glue" is another outstanding example from nature utilizing coacervation.[46] The worm is an example of the group of soft-skinned invertebrates that produces a mucus that it uses as for prey hunting or for defence. The worm sprays this fluid through the mucus papillae next to the jaw region, which turns from a mucus into a solid fiber, due to the shear forces that have been exerted. As a result, the fiber renders the competitor or victim immobile. Upon closer inspection, the mucus is found to be composed of tiny droplets rich in proteins identified as coacervate droplets. Unlike IDP, these originate from the oppositely charged regions of the proteins and can assemble into nanoparticles because they typically form an ordered beta sheet structure. The mechanism of spraying out ensures that these particles aggregate with each other and transition from a liquid-liquid phase separation to the formation of solid fibers. This process is reversible. As soon as the fiber is exposed to water, it dissolves and, at the appropriate concentration, reverts to a coacervate phase.[46-48]

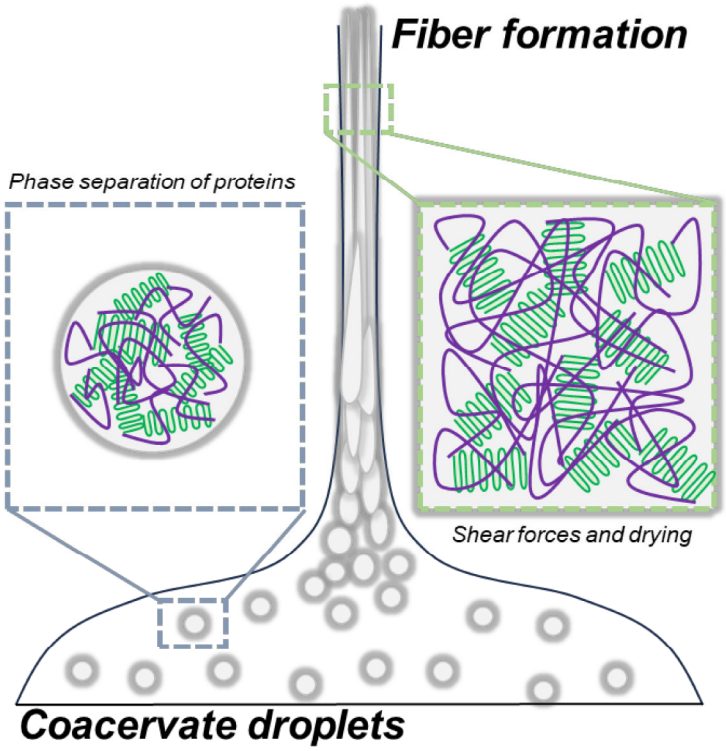


*Figure 6: Mechanism of fiber formation of the stumpy-footed worm through shear forces and drying. The fibers are formed from tiny coacervate droplets that coalesce through the shearing and thus trigger fiber formation. The coacervate droplets are formed by the electrostatic interaction of proteins (purple: disordered protein structure, green: beta sheet structure), (Adapted from [49]).*

While nature uses the formation of coacervates in a targeted manner,[38, 50, 51] research has also been able to show the benefits of coacervates, such as their use in the encapsulation of proteins or vaccines.[26, 36, 52-54] The disadvantage here is that no selectivity toward the capsules molecules can be achieved. Since the principle is based purely on the interaction of charged structures, no selection can be made, for example, regarding which proteins are encapsulated, as long as they all contain sufficiently charged subunits. Nature does, however, also provide alternative methods for targeting specific proteins.

## 1.2. Carbohydrates in nature

Carbohydrates are one of the key players in many biological processes in our body. They represent the third major group of biomacromolecules besides proteins and nucleic acids. The smallest subunits of carbohydrates are called monosaccharides, such as glucose, fructose, or galactose. Based on monosaccharide units, disaccharide structures like lactose or sucrose as well as larger, more complex polysaccharide structures can be formed including cellulose, starch and chitin. By forming glycosidic bonding between monosaccharides units larger di- and poly saccharides structures can be formed to build up a wide range of different carbohydrates. In general, carbohydrates, along with proteins and lipids, are rather known from the field of nutrition and some carbohydrates provide energy supply to biological systems. However, in recent decades, the carbohydrates have become central to the research of biological

processes.[55, 56] Starting from the interaction and communication between different cells, to the fact that they function as a receptor for bacteria causing infections.[57, 58] These processes are caused by the interaction of the so-called glycocalyx, a complex layer of carbohydrate structures covering every eukaryotic cell, and some carbohydrate binding proteins, the lectins.[59, 60] These lectins are also present on the outside of a cell and lead to the ability for the cells to specifically interact with each other. The glycocalyx can have a thickness of around 100 nm, whereby the carbohydrates are anchored in the cell membrane as glycoconjugates such as glycoproteins and glycolipids.[61]

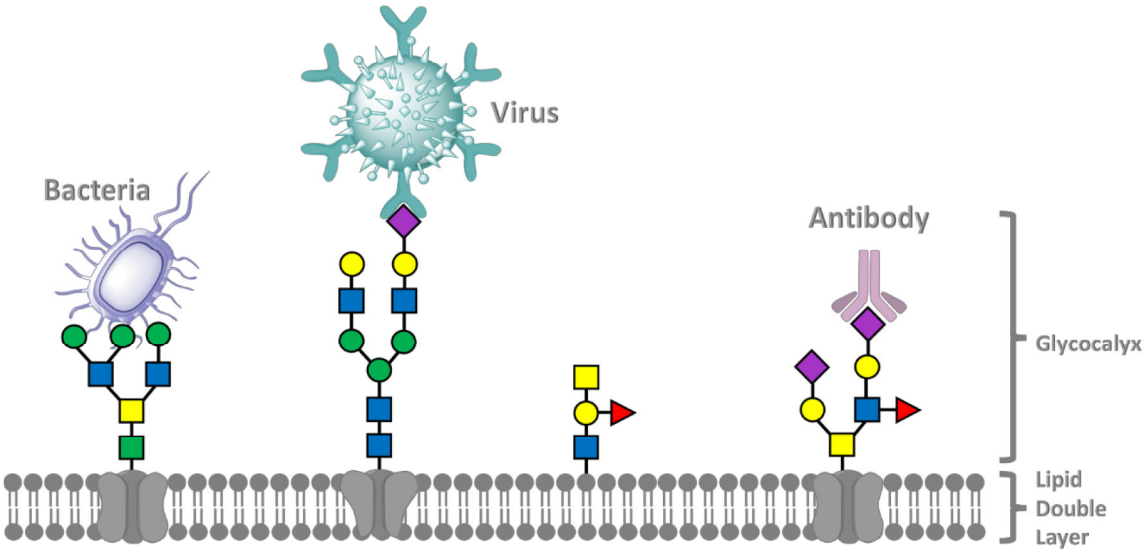


*Figure 7: Schematic representation of the complex carbohydrate layer (glycocalyx) which is partly bound by lipid proteins in the lipid double layer. The glycocalyx forms the connection site for receptors of bacteria, viruses, or antibodies, for example.[61]*

### 1.2.1 Carbohydrates as recognition motifs in biology

Lectins are a class of biomacromolecules that can specifically recognize and bind carbohydrate structures. They can be derived from plant, animal or bacterial sources.[62] The term “lectin” was first introduced by *Boyd et al.* in 1954 and comes from the Latin word “lego”, which translates as “to choose” or “to pick out”.[63] The carbohydrates are then recognized via the so-called carbohydrate recognition domain (CRD), which binds the corresponding mono- or disaccharide structure. They are classified in different lectin types as C-Type, I-Type, or L-Type lectins, which, among other things, describes the localization or their function.[64-67] One of the most investigated lectins is the C-type Concanavalin A (ConA). In 1919, ConA was the first lectin to be isolated from jack beans by *Sumner* and was also the first lectin example with a fully revealed amino acid sequence and quaternary structure.[68, 69] This good understanding of ConA structure is a reason for being the most investigated lectin by far and was often used to study carbohydrate lectin interactions.[70-73] It belongs to the class of C-Type lectins and therefore requires $Ca^{2+}$-ions to bind carbohydrate structures. ConA is able to recognize specific α-D-mannopyranoside (Man) and α-D-glucopyranoside (Glc) carbohydrate motifs and is

usually composed of a total of four subunits, each of which has a CRD. This tetrameric structure is present at neutral pH value, whereas at lower, acidic pH values the substructure changes to a dimeric form which has an impact on carbohydrate binding behavior.[74-77] The orientation and position of the carbohydrate hydroxy groups lead to the formation of the hydrogen bonds within the CRD, providing the foundation for identifying the carbohydrate structures. This results in the fact that in the CRD of ConA, mannose can form hydrogen bonds via the position of the proteins amino acids, while galactose is unable to show binding to ConA via the axial position of the hydroxyl group at C4. This fact makes galactose a sufficient negative control for non-binding units in ConA protein assays.

Also, bacteria utilize lectin-carbohydrate binding interactions to infect cells. *E. coli* is a bacteria strain that can cause urinary tract infections which is usually treated medically by taking antibiotics. The so-called fimbriae or pili have lectins on their surface that allow them to attach and penetrate a cell. The fimbriae interacts with the glycocalyx of a host cell and *E. coli* contains the adhesin FimH on the tip of the fimbriae. Mannose units are recognized and bound by the adhesin FimH. By specifically blocking these receptors, the bacteria can be prevented from attaching to the cells, which thus prevents the subsequent infection process.[78-85]

A more comprehensive investigation of the binding process between carbohydrates and lectins is necessary to gain a deeper understanding of both cell communication and the bacterial process of infection. Because there is no covalent bond between proteins and carbohydrates—rather, a variety of secondary reversible interactions, including hydrogen bonds and van der Waals forces — the interactions between single ligand-receptor motifs are very weak. These interactions are reinforced by the multivalency principle.[76, 86-90] This indicates that numerous occurrences of the same event taking place on the surface of the cell or bacteria give these single, weak interactions strength in higher numbers. *Y. C. Lee* noted this multivalency of carbohydrate-lectin interactions in his research during the 1970s.[91, 92] This effect can strengthen weak, non-covalent bonding events due to entropic reasons. Higher numbers of ligands on the same backbone result in a significant increase in overall avidity, since a single pair of receptor and ligand only has low affinity constants.[93] Note that various binding scenarios that can occur to represent multivalency are explained in Figure 8, covering four different mechanisms: statistical rebinding, steric shielding, clustering, and the chelate effect.[94]

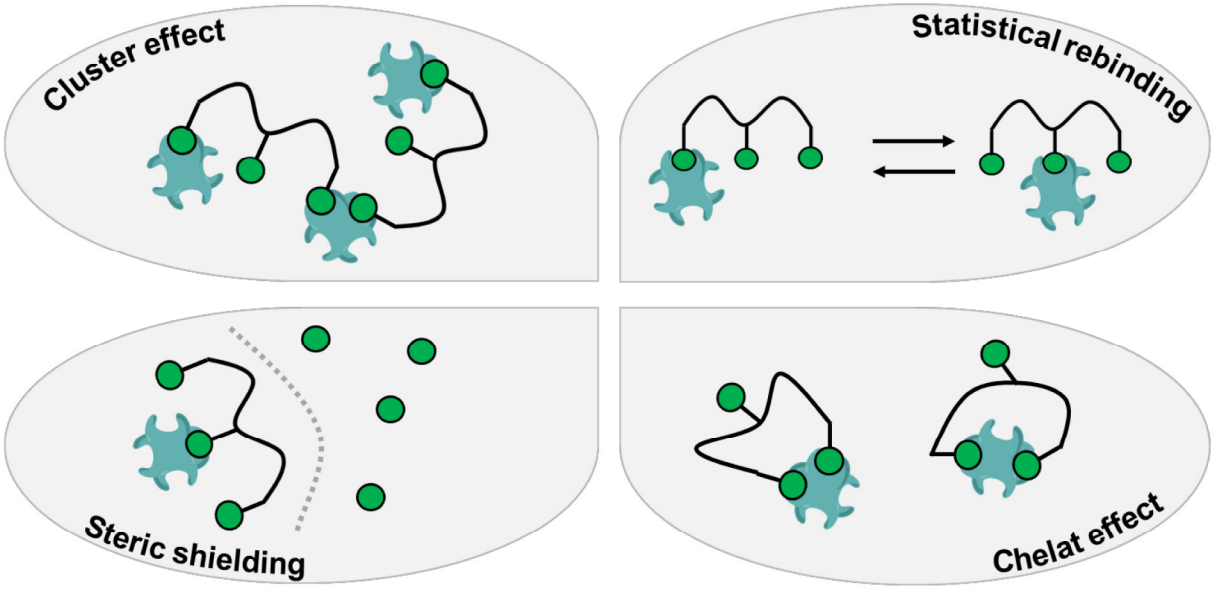


*Figure 8: Schematic representation of multivalency binding effects: cluster effect, statistical rebinding, steric shielding and chelate effect.*[95]

The lectin-carbohydrate bond is a very weak bond and can therefore be easily dissociated, but also easily rebound. This process, where one ligand is replaced by another, non-bound ligand, is called **statistical rebinding**.[94, 96, 97]

Clustering, or **cluster effect** describes the ability of a multivalent ligand to bind to multiple receptors, resulting in increased binding affinity. Depending on the concentration of the ligands, this effect functions as a bridging or crosslinking process and can also lead to the formation of bigger agglomerates.[96, 97]

In the study of complex formation in inorganic chemistry, the term “chelate” is frequently used. It explains how multiple ligands connected by a shared backbone bind to the same receptor, creating a bridge-like ligand framework.[98] The distance between the ligands and the backbone properties such as flexibility and spatial orientation both have a significant impact on the **chelate effect**. In general, an entropic effect from the first binding events favors the second as well as the following binding events.[96, 99]

**Steric shielding** occurs when the backbone, where ligands are present, prevents other ligands from further binding to the same receptor, resulting in a stabilizing effect for the receptor-ligand complex.[95, 100, 101]

It is challenging to investigate specific binding effects because of all these multivalency effects that occur during ligand receptor system interaction. It takes some sort of artificial system to deconstruct the complexity of these structures in order to gain a deeper understanding of these events occurring on a cell surface. Therefore, one method to look into these processes and

occurrences is to design and synthesize glycomimetic structures prior to performing lectin binding assays.

### 1.2.2 Carbohydrate conjugates and mimetics

Every eukaryotic cell has a complex layer of carbohydrates called the glycocalyx that is made up of several glycoconjugates, such as glycolipids and -proteins, generally known as glycans. It is difficult to follow individual interactions when multiple events occur simultaneously on the surface where another cell meets the glycocalyx. Glycomimetic systems are therefore ideal for "downsizing" these structures and focusing on individual interactions. Glycomimetics can therefore be constructed as simplified glycan structures which do not reflect the complete carbohydrate structure. Usually, the terminal monosaccharide motifs have the biggest influence on sufficient lectin binding which is the reason for being able to use the simplified carbohydrate motifs.

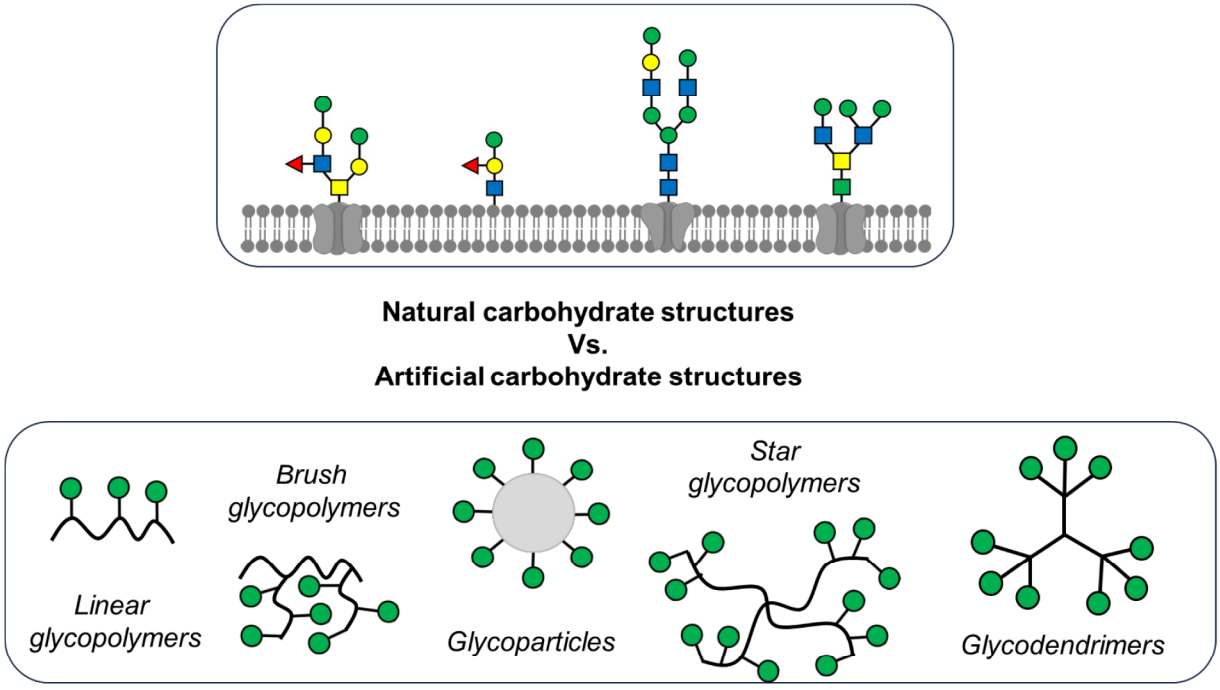


*Figure 9: Schematic Representation of the Glycocalyx structure compared to artificial carbohydrate structures for the use as glycomimetic.*[61]

The monosaccharides can be varied on different backbones. They can represent a monovalent system by presenting only binding ligands on the surface or create a hetero-multivalent system by combining binding and non-binding ligands. By using hetero-multivalent systems more than one protein receptor can be targeted here.[102-104] However, not only the presence of binding or non-binding ligands is decisive for the glycomimetic, but also the sequence and three-dimensional ligand arrangement. Starting with linear, polymeric backbones, branched dendrimers, micelles, nanoparticles, microgels, there are multiple possibilities to represent carbohydrates on particles or surfaces to enhance the protein-carbohydrate interaction.[94] In

the group of *Laura Hartmann* various numbers of different glycomimetics have been investigated, varying in their structure, valency, carbohydrate motif and the synthetic route.[105-109]

Application of glycoconjugates is not only important to investigate in the interaction but also to act as potential treatment to prevent bacterial or viral infections by inhibiting lectin attachment to the glycocalyx. An underestimated but equivalent variant of inhibitor is the use of polyelectrolytes and their phase forming complexes. The combined use of polyelectrolytes with conjugated carbohydrate ligands provides a new class of glycomimetics that could offer unprecedented possibilities and advantages.

As demonstrated in the previous chapters, it is important to look on both polyelectrolyte complexes and carbohydrate mimetics in order to gain a better understanding of the daily mechanisms that operate within the human organism. The majority of groups use solid-phase synthesis (SPS) to build up synthetically structures defined by a sequence. SPS is the simplest and most reliable method for creating sequence-defined oligomers and polymers.

## 1.3. Sequence defined structures

Sequence control is a fundamental prerequisite for many processes in nature to perform their functions, such as the linear assembly of a DNA sequence, a protein complex or carbohydrate structure. The best-known example of a natural, sequence-controlled macromolecule is the DNA. If only one nucleic acid is arranged differently, this can have enormous effects on the organism by leading to different protein translation as shown in the example of punctual mutation.[110] Thus, the primary amino acid sequence and its precise definition possess an important role. Nature has its own ways of achieving sequence control, but yielding defined synthetic structures is usually more challenging. Solid-phase synthesis can be used to synthesize approximate sequence-defined structures that can represent the naturally given sequence control.[111, 112]

### 1.3.1. Solid-phase synthesis

Solid-phase synthesis is a synthetic methodology to achieve sequence control. Solid-phase peptide synthesis was introduced by *Robert B. Merrifield*, who synthesized a tetrapeptide by using a solid-phase based on chloromethylated polystyrene resin.[113] Solid-phase synthesis is based on iterative coupling and deprotection processes that are applied step by step to provide sufficient control on monomer assembly.[114] The solid-phase resin is the starting point from which the peptide sequence is built up. The first amino acid is coupled to the reactive group of the resin bead using suitable coupling reagents. The reactive group of the resin can be adapted with appropriate functional linkers so that its cleavage conditions can be adjusted as required. It is important to ensure that the cleavage from the solid-phase is orthogonal to the deprotection

of the terminal amino acid. During SPS, in order to couple further amino acids step by step to the resin, the N-terminal amino acid attached must first be deprotected. Traditionally, the Fluorenylmethoxycarbonyl (Fmoc) or *tert*-Butyl (tBu) protection group strategy can be used for this purpose in SPS.[115, 116] After successful deprotection, the next amino acid can be coupled to the free amine group. This process is then repeated until the desired sequence has been build up and cleavage from the resin releases the final product. Since amino acids carry various side chains, that could also interfere with the coupling or deprotection reaction, orthogonal protecting groups must be used here to avoid possible side reactions. Especially primary amines of the amino acids must be adequately protected in order to be used for solid-phase synthesis. A wide range of different protecting groups, ensuring the desired orthogonality, are commercially available nowadays and do not have to be synthesized in the laboratory.[116]

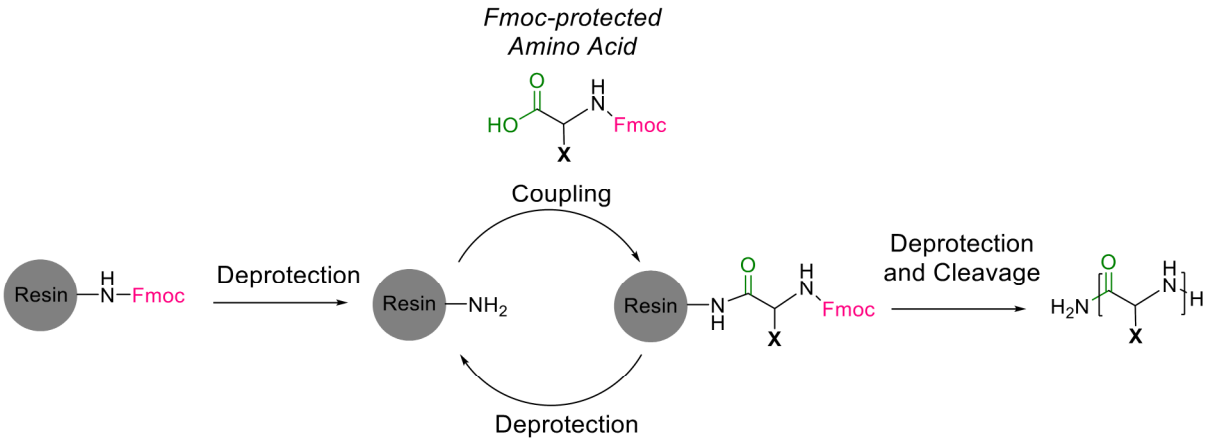


*Figure 10: Mechanism of solid-phase peptide synthesis showing an iterative coupling and deprotection approach.*

On the other hand, SPS is not limited to amino acids. The development and use of specially designed building blocks allows for the synthesis also of other sequence-defined macromolecules. The group of *Laura Hartmann* has developed a library of tailor-made building blocks that can be used for SPS giving access to non-natural oligoamidoamines. The variation here concerns the size, functionality and geometry of the macromolecules formed and also allows for conjugation of biomolecules such as carbohydrates.[114, 117-119] For example, azido-functionalized carbohydrates can be attached to the alkyne side chains introduced from one of the tailor-made building blocks by means of copper click reaction.[117, 120, 121] This has proven to be particularly useful to generate glycomimetics, as it allows the targeted synthesis of glycopolymer structures that can be varied in density, distribution, and functionality.

Alongside the advantages, solid-phase synthesis is also limited in some aspects. If the oligomers reach a certain size, it becomes more difficult to couple further building blocks and amino acids, as there is a much greater steric demand. This hinders the coupling efficiency,

which can lead to incorrect sequences and thus monodispersity and sequence definition are no longer maintained. Although this can be improved by a certain amount of repeated coupling or deprotection steps, this takes significantly more time. By using peptide synthesizers, the process can be mostly automated and made more efficient in terms of time, but still a limit is reached for the macromolecule above a certain size, due to different effects e.g. steric hindrance.[122-124]

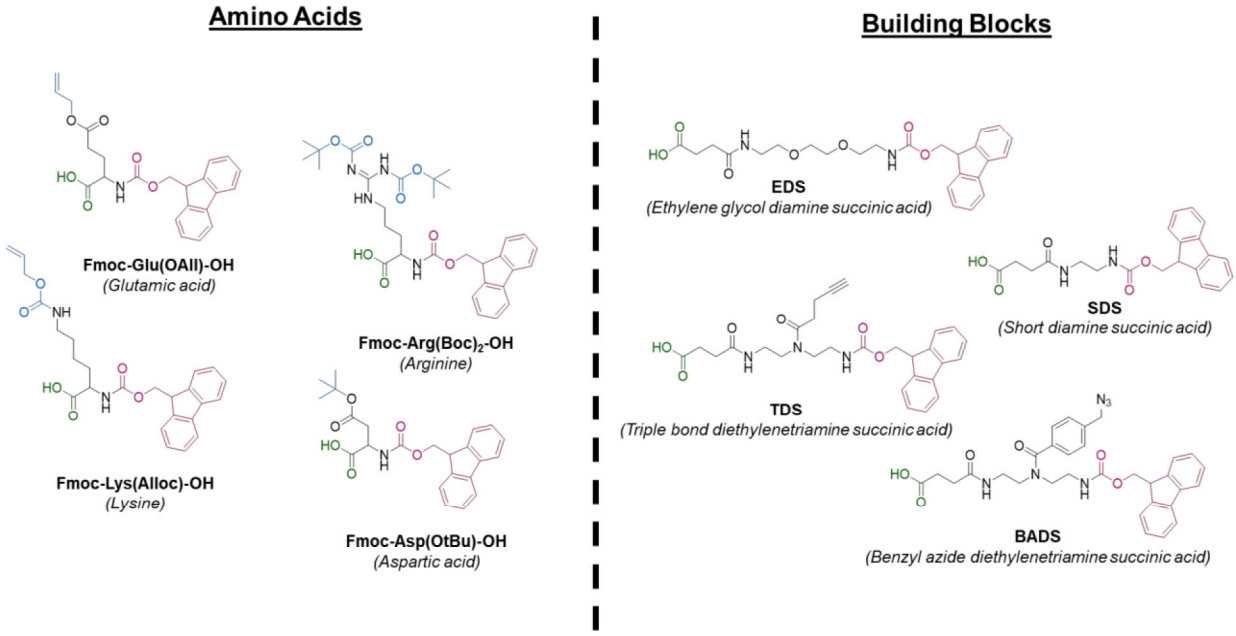


*Figure 11: A selection of amino acids and building blocks that can be used for Fmoc solid-phase synthesis. Fmoc protecting group (pink), free carboxyl group (green) and if necessary, protecting groups for the side chain (blue) are mandatory for an application in solid-phase synthesis.*

An approach to achieve larger polymer structures uses oligomers that have already been synthesized and can be further converted into brush-shaped polymers by means of the polymer analogous reaction on a pre-existing polymer backbone.

### 1.3.2. Polymer analogous reactions

Most linear polymers are produced by simple chain or step growth polymerization of monomers.[125] Besides the linear form of the polymer, polymer analogous reactions are a suitable way to synthesize so-called brush-shaped polymers. Already formed oligo- or polymers are used as an existing side chain or polymer backbone and further converted to larger and more complex macromolecules. In polymer analogous reactions, a classification is made between three different methods: grafting to, grafting from and grafting through.

In the **grafting from** method, an already formed polymer backbone serves as the basis of a macroinitiator. By adding further monomers, polymer growth can take place starting from the polymer backbone in order to form the brush side chains. The disadvantage of this technique is that it is difficult to control the length of the side chains.[126, 127]

By using the **grafting through** method, on the other hand, an already existing polymer forms the new side chain of the brush polymer instead of acting as a backbone. A suitable initiator can polymerize a terminal acrylate group, which forms the actual backbone of the brush polymer. The fact that the brush polymer's repeating units all carry the same side chain is advantageous, but it also has the biggest drawback because sterically demanding side chains severely restrict the number of repeating units that can be created.[128, 129]

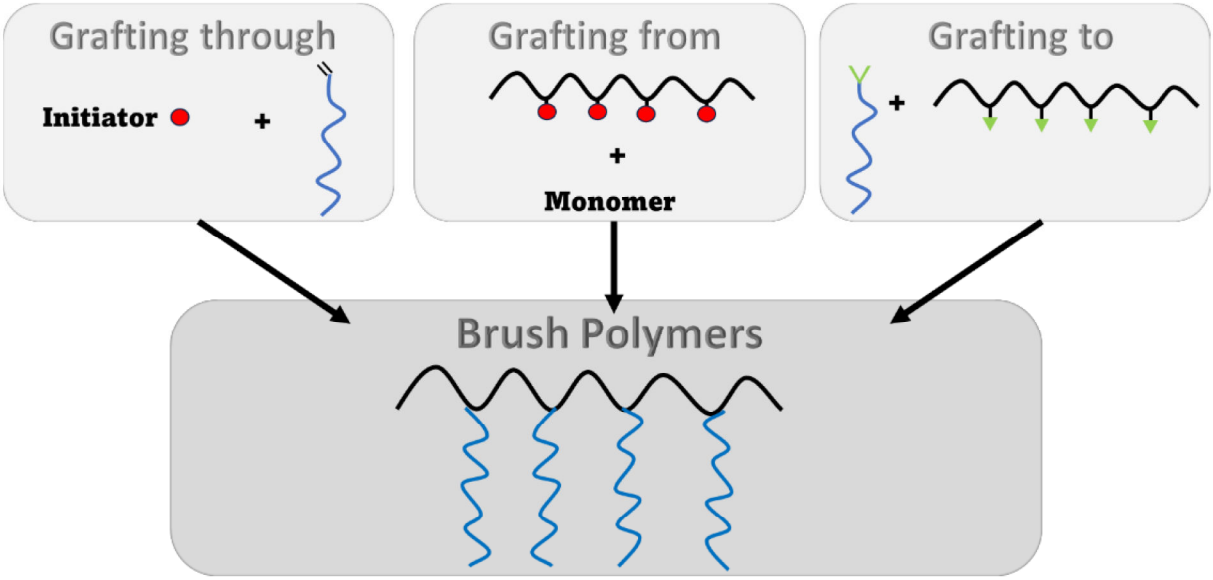


*Figure 12: Concept of polymer analogous reactions. The grafting to, grafting through and grafting from methods are shown.*

And finally, in the **grafting to** method, both the polymer backbone and the side chain already exist.[126, 127] The backbone contains reactive groups with which another polymer can react with a terminal reactive group. With the help of the grafting to method, polymers can be produced that have different side chains, but are all based on the same backbone and thus have the same size and dispersity, which contributes to the comparability of different effects of the side chains. The type of polymerization of the polymer backbone is particularly important. By choosing controlled radical polymerization, such as reversible-addition-fragmentation chain-transfer polymerization (RAFT), it is possible to specifically control the number of repeat units with a low dispersity.[130-132] Furthermore, the incorporation of the side chain can be controlled with the grafting to method, and a defined degree of functionalization can be aimed for, whereby the incorporation is also limited here by the steric size of the side chain.

There are various ways to synthesize sequence-defined and sequence-controlled structures. Each of these methods has certain advantages and disadvantages. However, if these methods are combined, new possibilities can be obtained to generate sequence-controlled structures.

# 2. Aims and Outlines

Nature creates some of the most complex structures in such a precise and defined way that the synthetic development of these systems seems almost unattainable. This precision is found, for example, on the surface of our cells in the form of complex carbohydrate layers or also within our cells as intrinsically disordered proteins. One of the greatest challenges is to understand the underlying mechanisms of such precise molecules interacting with each other and how their structure governs these interactions. Synthetically produced sequence-controlled polymers open new opportunities to be used as biomimetic structures and models to gain new structure-property correlations. In this work, special focus is on the creation of sequence-controlled polyelectrolytes in order to understand the phase behavior of coacervates. In Nature intrinsically disordered proteins and their orders disorder leads to the formation of coacervate phases, which is essential for the membraneless organelles. Based on the challenge to better understand this behavior, this thesis aims for the synthesis and investigation of sequence-controlled polyelectrolytes and polyampholytes. The influence of charge density, charge distribution, size of the polymer chain and the additional introduction of carbohydrates will be the focus for the investigation of the coacervate behavior.

The first part of this thesis focuses on the synthesis of sequence-controlled polyelectrolytes and polyampholytes. The aim is to obtain structures of varying length, charge density and charge sequence. A combination of classical solid-phase synthesis and polymer analogous reaction is applied to generate oligomers with different charge sequences. During solid-phase synthesis, lysine and glutamic acid are used as the positively and negatively charged amino acids. To enable larger polymer structures from these oligomeric electrolytes and ampholytes, polymer backbones are synthesized. RAFT polymerization is used here to ensure low dispersity and specific repeat units. A pentafluoro phenyl acrylate is polymerized to form an active ester polymer, which can then react in a subsequent process with free, primary amines of the oligomers synthesized to achieve brush-shaped polyelectrolytes. The aim in this part is to find an appropriate protecting group strategy, without unintended side reactions and to determine whether this combination of methods is suitable for the preparation of sequence-defined polyelectrolytes.

The second part deals with the investigation of the phase behavior of these sequence-controlled polyelectrolytes and polyampholytes. The focus is on drawing initial conclusions about the phase behavior and to investigate their salt resistance depending on the parameters, such as polymer length or charge sequence. Phase diagrams are created as a function of salt and polymer concentration, to determine the region where coacervation occurs. The whole investigation is examined by using optical light microscopy. The aim is also to identify the

relationship between the phase behavior of linear to brush-shaped polymers and to compare the results with existing literature.

The third and last part deals with the investigation of glycan-presenting coacervates as a new potential glycomimetic system. As in the first part of this work, polyelectrolytes are synthesized using solid-phase synthesis and the grafting to method of polymer analogous reaction. Using customized building blocks EDS and TDS, oligomers with sugar functionalities can be synthesized. Here the oligomers are functionalized with either mannose or galactose units, which serve as binding or non-binding units in the subsequent protein and bacteria assays. In addition, polyelectrolytes without any sugar functionality are also prepared to work as a second, but yet "non-specific" negative control. Before being used in protein and bacterial assays, the polyelectrolytes are first tested for their coacervation behavior to identify their salt resistance. Concanavalin A is used in the protein assays, whereby the uptake capacity of protein in the coacervates is analyzed regarding the specific binding units carried by them. This is analyzed using optical microscopy and UV-Vis spectroscopy. Furthermore, in bacterial assays, *E. coli* bacteria are used and analyzed with regard to their interaction with the coacervates.

# 3. Results and Discussion

The objective of this work is the synthesis of sequence-controlled polyelectrolytes and polyampholytes and the characterization of their phase behavior. The synthesis is accomplished by a combination of solid-phase synthesis and polymer analogous reactions. The amino acids glutamic acid and lysine were used as building blocks for the solid-phase synthesis to implement negative and positive charges within the macromolecule side chains. For the subsequent conversion of the sequence-defined oligomers to polymers, the polymer analogous reaction with poly active esters was chosen, using the "grafting to" method. Active ester polymers were prepared by RAFT polymerization, to achieve a low dispersity. After the conjugation with oligomers to receive brush-shaped polyelectrolytes and polyampholytes, phase diagrams were obtained in further investigation steps. Hence, liquid-liquid phase separations were observed and allowed to draw conclusions on the coacervation effect of charge sequence, density, and polymer length. Finally, comparable polyelectrolytes carrying carbohydrate moieties were prepared, investigated, and compared with the phase separation behavior or related polyelectrolytes and polyampholytes. Additionally, they were further analyzed on their selective binding properties towards lectins and bacteria.

## 3.1. Synthesis of sequence-controlled polyelectrolytes and polyampholytes

Variation in charge sequence, charge density and polymer length were reported in literature to significantly impact on the coacervation process.[21, 133-140] The first part of this thesis deals with the synthesis of sequence-controlled polyelectrolytes and polyampholytes, to investigate these aspects systematically. To this end, a library of charged structures was developed to determine how these factors were affecting the coacervation process. This library included parameters such as the incremental increase of charge density, to allow to interpret their effect on the phase separation process. An overview of the targeted structures for this type of library of polyelectrolyte structures and their classification into the investigated parameters is shown in Figure 13. Therefore, a suitable synthesis route was selected, which resulted in promising outcomes for many coacervation investigations. Solid-phase synthesis provides a suitable way to synthesize stepwise sequence-defined structures benefiting from the availability of many different commercial building blocks and aminos acid.[114] However, this synthesis is limited by the size of the targeted product structures, because above certain chain lengths, the coupling reaction of additional building blocks becomes less efficient and thus more challenging due to steric reasons.[114] To circumvent this kind of failure sequences, a different macromolecule architecture was used based on active ester polymers[141] which enabled larger, linear, and charged structures. But also by the combined application of polymer analogous reactions and solid-phase synthesis, non-linear brush polymers were synthesized, enabling the analysis of

charge distribution in a non-linear polyelectrolyte. For this reason, sequence-defined precursor for oligo-electrolytes and oligo-ampholytes were synthesized in the first step by using solid-phase synthesis, whereas in the second step, they are converted into polymers by polymer analogous reaction.

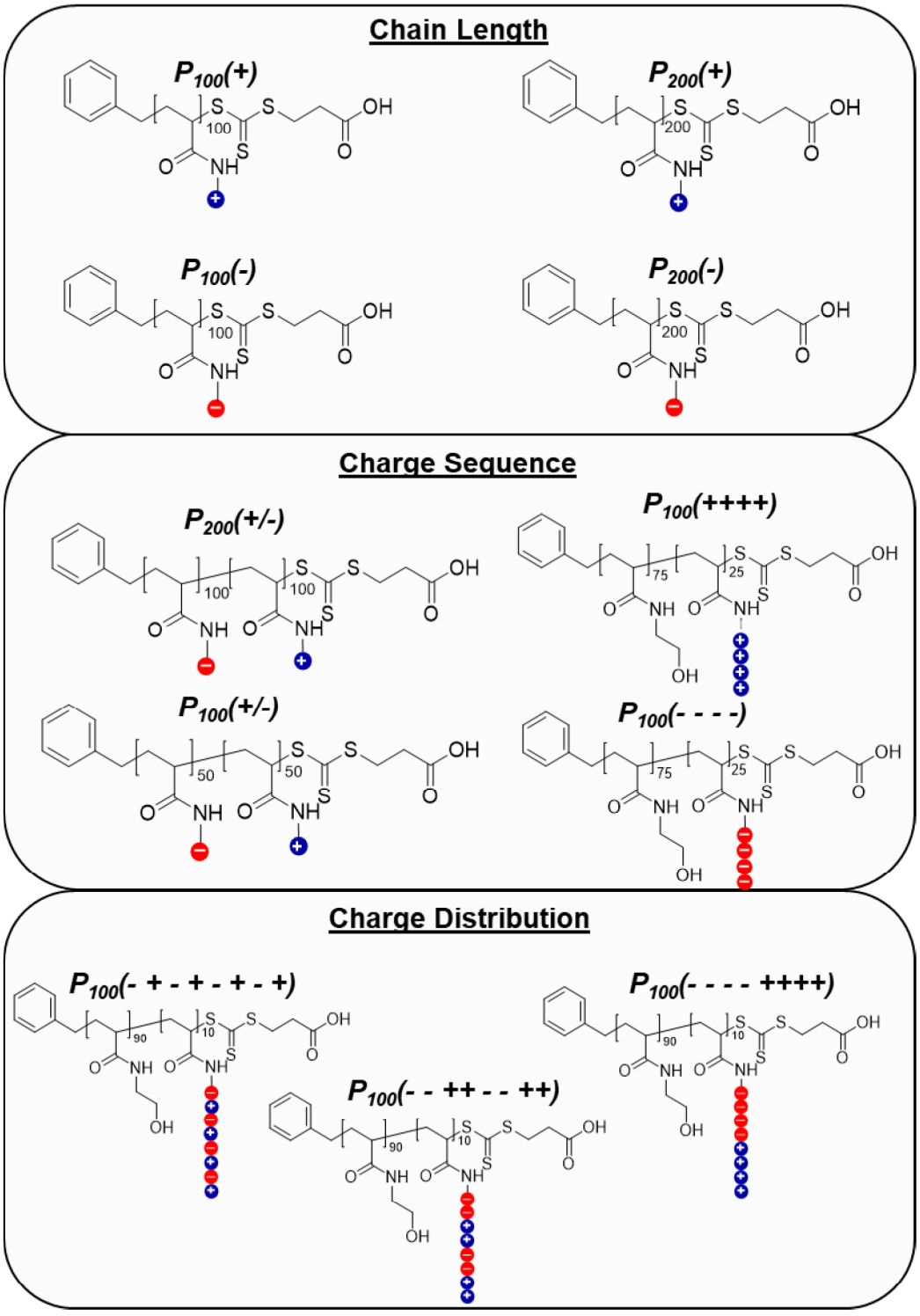


*Figure 13: Overview of polyelectrolyte and polyampholyte structures aimed in this thesis. The design was chosen so that the structures can be compared with each other based on their polymer length, the charge sequence, the charge distribution and the random charge arrangement.*

### 3.1.1. Synthesis of sequence-defined oligomers

During oligomer synthesis, it is necessary to ensure that a suitable protection group strategy is applied and to avoid unintended side reactions. Since solid-phase synthesis was used to assemble the oligomeric structures, a large selection of commercially available and synthetically established building blocks or amino acids can be used here. Especially natural amino acids with charged side chains e.g. lysine, arginine, histidine, asparagine or glutamic acid, are commonly used to generate polyelectrolyte via solid-phase synthesis.[142, 143] A tremendous advantage is the large selection of amino acids with various protection groups that are commercially available.[144] For the oligomers targeted here, the amino acids lysine and glutamic acid were selected to represent the positively and negatively charged units. For the solid-phase synthesis Fmoc protection strategy was selected.[114] The functional groups of these amino acids were orthogonally protected with “Allyl” and “Alloc” protection groups.[145, 146] As the synthesized oligomers were subsequently coupled to poly pentafluoro phenyl active esters, which react particularly well with primary amines,[147] appropriate protection of the amino acid side chain becomes crucial. Therefore, protection group of the lysine primary amine does not only need to be orthogonal to the operational protecting strategy during synthesis, but also stable against the resin cleavage process. So, the choice of the solid-phase resin is important for the overall synthetic strategy and every involved building block protecting group needed to be stable under basic and acidic conditions. Two different resins were used here, each with an acid labile linker. On the one hand, a Tentagel S-Ram resin (S-RAM) was used, which contains an acid-labile rink amid linker. The other is a chlorotrityl resin, which was additionally functionalized with an ethylene diamine linker (EDA) and is also cleaved acid-labile. The resins, amino acids, the coupling process, and the resulting oligomers are shown in Figure 14.

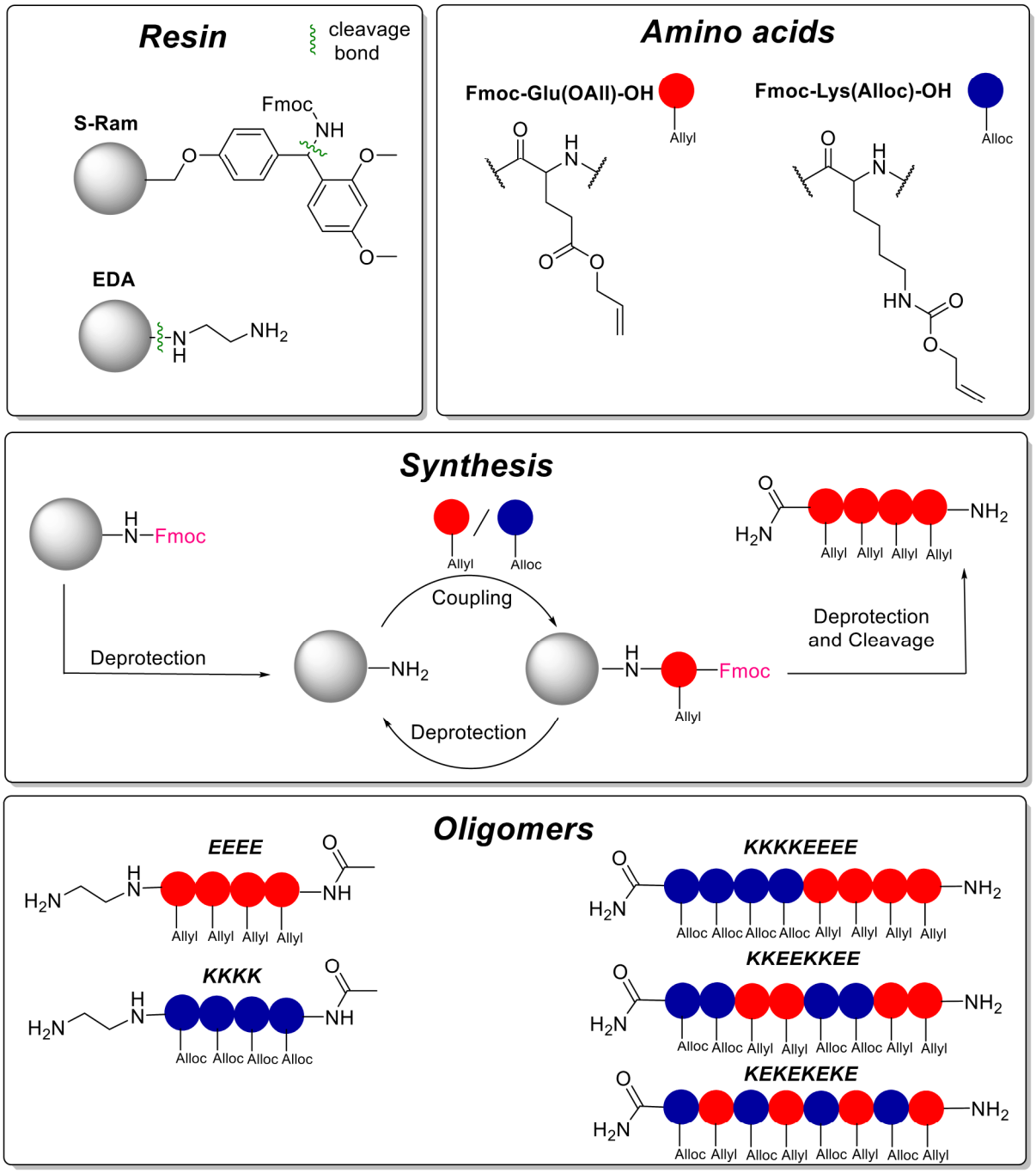


*Figure 14: Synthesis route of sequence-defined oligo-electrolytes and oligo-ampholytes via SPS. The resins used were S-Ram and an EDA-functionalized chlorotrityl resin and included the amino acids Fmoc-Lys(Alloc)-OH and Fmoc-Glu(All)-OH. After cleavage from the resin, the oligomers prepared still bear the side chain protection groups. The oligomeric sequence is abbreviated with the conventional amino acid abbreviations (here: K for lysine and E for glutamic acid.*

One of the more commonly used protecting groups, includes the Alloc group for primary amines and the Allyl group for carboxylic acids. These protection groups are stable under alkaline as well as acidic conditions and can only be removed under reductive conditions using a palladium catalyst and mild reaction conditions.[148] This good orthogonality towards the other reaction types was the reason for the decision of their favored use in this synthesis.[116]

For the first oligomer, Fmoc-Lys(Alloc)-OH was coupled four times to a chlorotrityl resin functionalized with an ethylene diamine linker (EDA-resin).[105] The resin with the EDA linker was chosen to yield an *N*-terminal primary amine group after cleavage from the resin. To reduce expected sterical issues that may occur later during the polymer analogous reaction, the choice was made for an EDA-resin. The oligomer synthesis was carried out on an automated peptide synthesizer. For the coupling process, a fivefold excess of the amino acid building block, the coupling reagent benzotriazol-1-yloxytripyrrolidinophosphonium hexafluorophosphate (PyBOP), and a tenfold excess of diisopropylethylamine (DIPEA) were employed. For the subsequent deprotection process, a 25% piperidine in DMF solution was used. After successfully completing the amino acid coupling sequence, a final deprotection step was carried out to remove residual *N*-Fmoc groups and to proceed with capping of the *N*-terminus by acetylation with acetic anhydride. Cleavage from the resin was carried out using a 95% trifluoroacetic acid (TFA) solution containing 2.5% dichloromethane (DCM) and 2.5% Triisopropyl silane (TIPS). The same procedure was repeated on a second oligomeric scaffold containing glutamic acid building blocks, also using the EDA resin. After isolation of the oligomer, the analysis was performed by RP-HPLC.

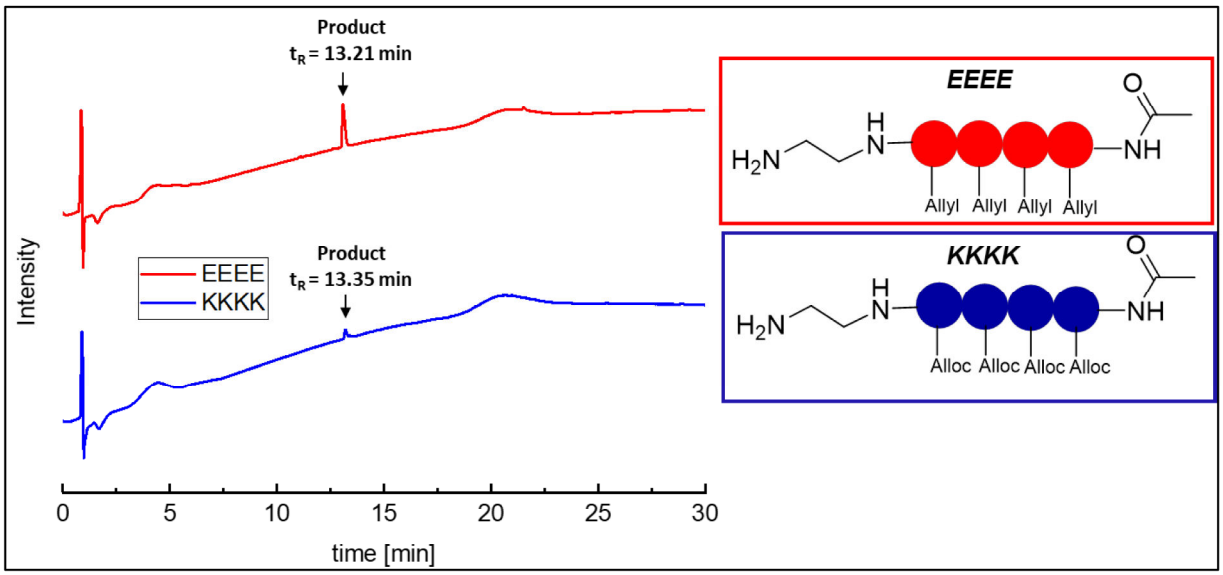


*Figure 15: RP-HPLC chromatograms of oligomers glutamic acid EEEE (top, red) and lysine KKKK (bottom, blue). Gradient from 95/5 $H_2O$/MeCN, 0.1% formic acid to 95/5 MeCN/$H_2O$, 0.1% formic acid over 30 min at 25°C using a Poroshell 120 EC-C18 1.8 µM (3.0x50 mm, 2.5 µM) column.*

The RP-HPLC-MS analysis data in Figure 15 indicates a relative purity of up to 99%, where the mass analysis of the glutamic acid oligomer (Figure E50) shows minor cleavage of the Allyl protecting group. This indicates that the Allyl protecting group was not completely stable against the coupling or cleavage conditions. Compared to the lysine oligomer, no cleavage products of the Alloc protecting group were found in mass spectrometry analysis (Figure E51). When comparing the two protecting groups with each other, Allyl groups ester bond might be more sensitive to hydrolysis effect and therefore easier to remove.[149] But since the absence

of the protective group here has no influence on the conversion of the polymers and results in a low level of impurities, the oligos were used without further purification. Only in the case of lysine oligomers is it important to ensure that all Alloc protecting groups are still present after cleavage from the resin so that no cross-linking reactions occur in the subsequent polymer analogous reaction.

For the synthesis of the ampholytic oligomers, the Alloc-protected amino acid lysine and the Allyl-protected glutamic acid were also used. The synthesis was carried out here using solid-phase according to the same peptide synthesizer protocol as the previously described oligo-electrolytes. The only adjustment is the exchange of solid-phase resin a Tentagel S-Ram resin, which is also cleavable under acidic conditions. However, under these circumstances no free amine would remain after cleavage from resin, but a *C*-terminal unreactive amide group. Therefore, in contrast to the oligo-electrolytes, no acetylation is carried out on solid-phase after the last deprotection to yield a deprotected terminal amine. Thus, the amine, which was used for the following polymer conjugation, was no longer at the *C*-terminal "resin end" but at the coupling end of the oligomer. After cleavage from resin, the relative purities of the oligomers achieved values between 93 and 97%, determined by RP-HPLC as shown in Figure 16.

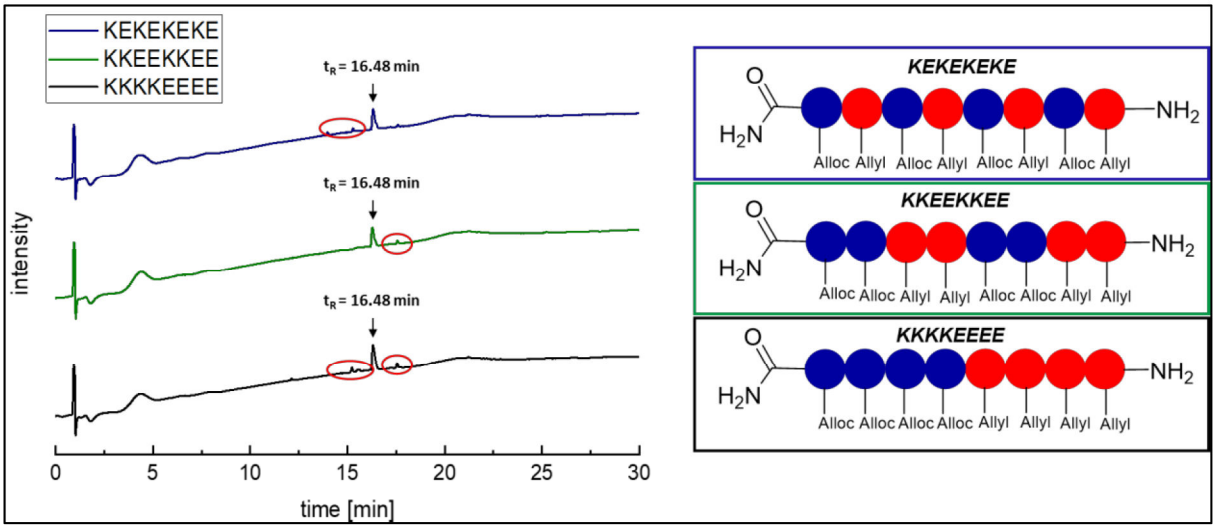


*Figure 16: HPLC chromatograms of ampholytic oligomers based on glutamic acid and lysine with different sequences. By-products and impurities were highlighted in red circles. Gradient from 95/5 $H_2O$/MeCN, 0.1% formic acid to 95/5 MeCN/$H_2O$, 0.1% formic acid over 30 min at 25°C using a Poroshell 120 EC-C18 1.8 µM (3.0x50 mm, 2.5 µM) column.*

All oligomers elute at the exact same retention time, are regioisomeric to each other and share the same, molecular weight because they only differ in their sequence. Smaller impurity peaks are also visible in Figure 16 (highlighted in red circles) and were associated with the masses of by-products, such as cleavage components that have lost one or more Allyl protecting groups. As described on the oligomer-electrolyte analysis, the Allyl protecting group was probably partially sensitive against the cleavage reaction. In this case of oligo-ampholyte

synthesis, these impurities did not affect the further conjugation reactions. These oligomers were also used for further conjugation reactions without further purification.

In conclusion, the oligomers could be synthesized without significant challenges. Minor impurities occurred but were negligible for the following process. In the following section, the active ester polymers for the polymer analogous reactions were prepared.

### 3.1.2. Synthesis of poly active ester precursor

Several approaches can be employed for the conversion of the obtained oligomeric structures towards polymers.[150-155] Polymer analogous reactions offer the possibility to convert already formed polymers or oligomers into brush-shaped polymers. This conversion can be realized using different routes such as the *grafting to, grafting from,* or *grafting through* method.[126-129] In this thesis, a reactive polymer backbone was formed where oligomers were conjugated onto the polymer side chain, whereby this approach is called "*grafting to*" method. Active ester polymers represent a commonly used class of polymers, since they can be easily substituted by strong nucleophiles, especially primary amines. Pentafluoro phenyl polymers (PPFPs) were already used in a wide range of studies.[141, 147, 156] Compared to other poly active esters such as those derived from N-(methacryloyloxy)succinimide, PPFP has good solubility in organic solvents, is very stable against hydrolysiss and offers the advantage that the substitution completion can be tracked by observing pentafluoro phenyl group signals on $^{19}$F-NMR. The monomer was prepared according to established literature; however the purification was performed by flash chromatography.[141] In order to enhance comparability of the structures, the polymers with different chain lengths were prepared via RAFT polymerization to achieve low dispersity. Here, Benzylsulfanylthiocarbonylsufanylpropionic acid (BSPA) was used as the RAFT reagent. The mechanism of the RAFT polymerization is shown in Figure 17.

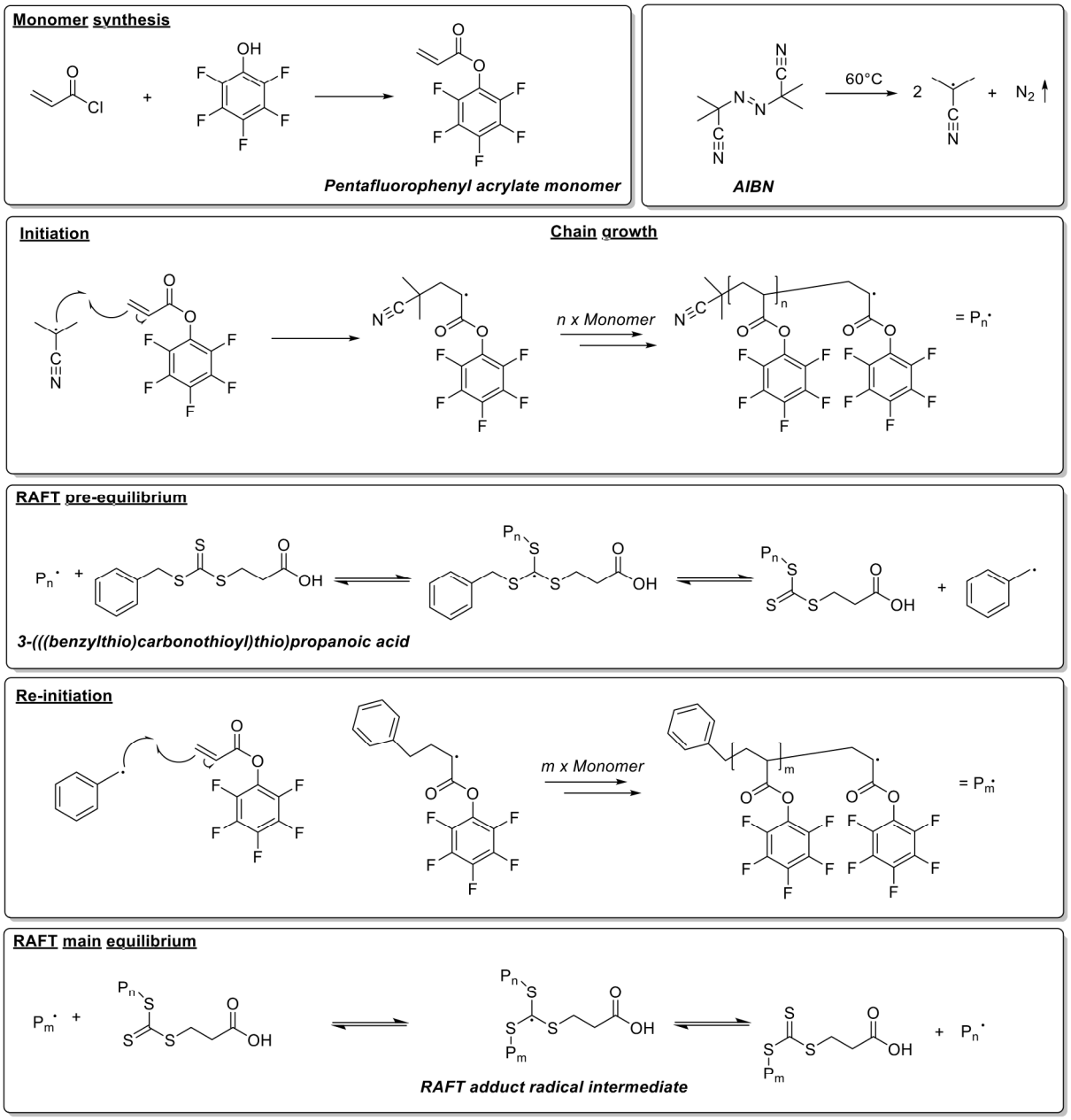


*Figure 17: Monomer synthesis and RAFT polymerization mechanism.*

The aim was to synthesize two different polymer chain lengths based on poly active ester precursors, one with 100 repeating units ($PPFP_{100}$) and the other with 200 units ($PPFP_{200}$). Benzene was used as a solvent, because it has already been shown in previous studies that this can result in very low dispersities.[147] The following reaction conditions are shown in Table 1.

*Table 1: Reaction conditions for RAFT polymerization.*

| Polymer | Monomer (PFA) | Initiator (AIBN) | RAFT agent (BSPA) | Time/Temp. |
|---|---|---|---|---|
| $PPFP_{100}$ | 1 eq. | 0.002 eq. | 0.01 eq. | 24h at 70°C |
| $PPFP_{200}$ | 1 eq. | 0.001 eq. | 0.005 eq. | 24h at 70°C |

The synthesis proceeded without any major challenges and the average repeating units of the polymers were determined by GPC and NMR after purification. For the evaluation by NMR, the ratio between BSPA-derived aromatic phenyl signals and backbone acrylate signals gave information about the amount of average repeating units.

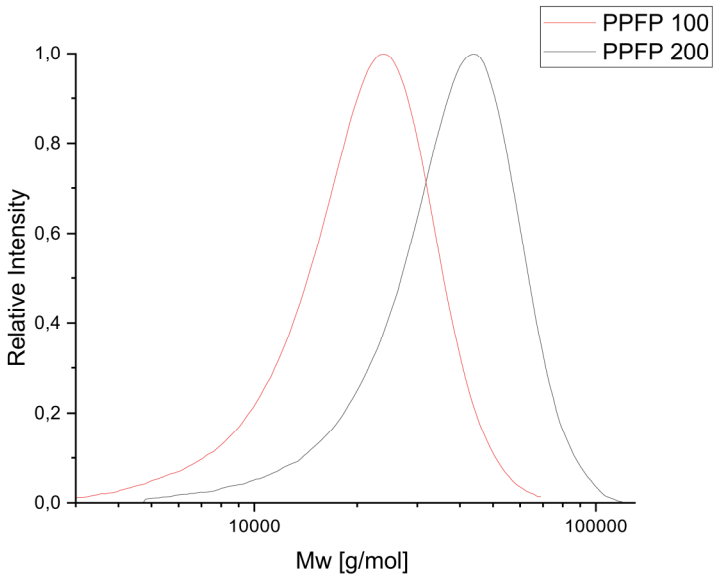


*Figure 18: GPC Analysis of PPFP with 100 and 200 repeating unit. Eluent: THF, Detector: RI*

*Table 2: Polymerization degree (Pn), dispersity (PDI), and molecular weight (MW) of PPFP polymers with 100 and 200 repeating units, determined via THF GPC and $^{1}$H-NMR.*

| Polymer | GPC MW [g/mol] | GPC Pn | GPC Đ | NMR Pn |
|---|---|---|---|---|
| $PPFP_{100}$ | 23278 | 96 | 1.28 | ~98 |
| $PPFP_{200}$ | 41598 | 175 | 1.26 | ~180 |

Compared to results known from the literature, the observed dispersities here are comparatively high. Dispersities between 1.05-1.15 would have been expected.[157] For the determination of the polymerization degree by NMR, the integral values of the signals were added and calculated by the corresponding number of protons of the repeating unit. The differences in the analysis of the GPC and the $^{1}$H-NMR resulted from the integration of the signals, as no accurate integration is possible due to the broad $^{1}$H-NMR signals. Overall, the synthesis of the polymer precursors was successful and further conversion to polyelectrolytes was proceeded with.

### 3.1.3. Polymer analogous synthesis of sequence-controlled polyelectrolytes.

After the successful preparation of oligomers and poly active ester precursors, the next step was the conversion of the polyelectrolytes. However, before conversion of oligomeric structures took place, linear charged structures were first prepared. For the synthesis of polyelectrolytes that only have a single charge per repeating unit without the presence of brush-shaped structural elements, poly active esters precursors were substituted in a different way. For polyanion synthesis, glycine was used, since the primary amine group was coupled with the reactive pentafluoro phenyl ester group. The free carboxylic group of glycine did not participate in this reaction and remained charged after being deprotonated.

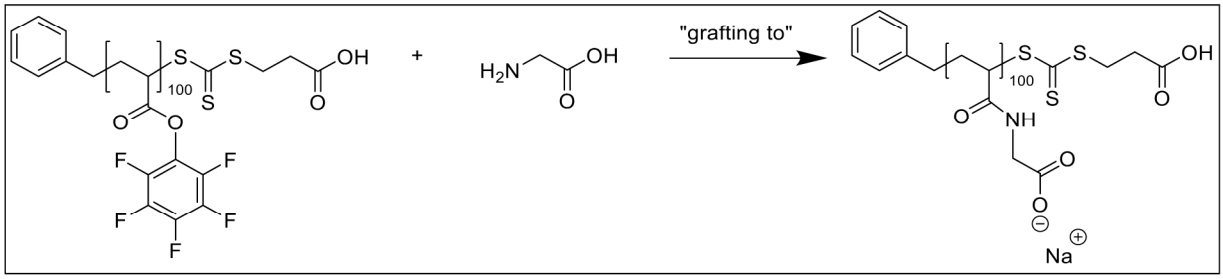


*Figure 19: Synthesis of polyanions using glycine and PPFP active esters via polymer analogous reaction.*

For the glycine coupling reaction, 2 eq. of glycine diluted in water were mixed with the PPFP in DMF and a catalytic amount of triethylamine (TEA). In contrast to known literature on the conversion of poly active esters, the converted product was not precipitated in organic solvents, but directly diluted and transferred into an appropriate dialysis tube. The underlying reason is that previous experiments showed a large yield loss associated with the precipitation. Thus, purification was carried out by dialysis and pH were adjusted to 7 by using 1 M HCl and 1 M NaOH solution. The procedure for pH value adjustment turned out to be an important aspect. The order in which the acid and base were added as well as the washing process by dialysis were decisive factors, as otherwise there was no exchange of counterions, and triethylamine remained in the solution. The complete TEA removal was detected by $^1$H-NMR and thus indicated whether the washing process had been completed.

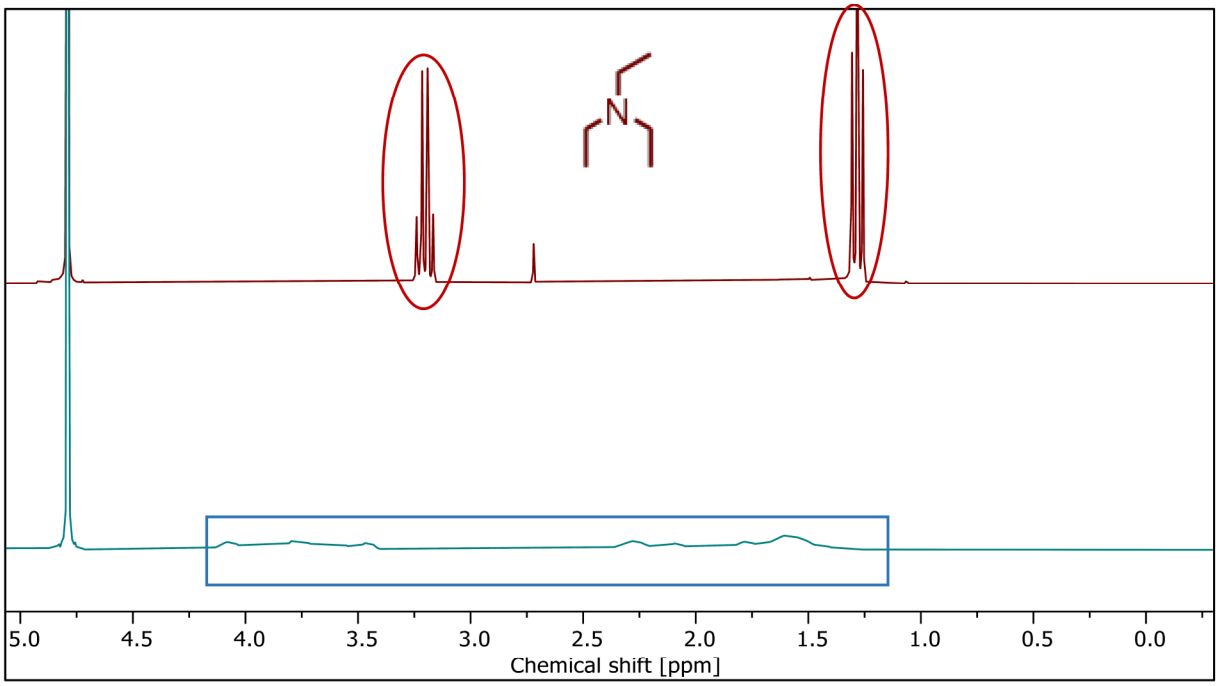


*Figure 20: Comparison of the NMR spectra of $P_{100}$(-) before (red graph, top) and after (blue graph, bottom) sufficient dialysis. The signals of the triethylamine are highlighted in red circles. The polymer signals were hardly detectable, due to the high intensities of the triethylamine signals. After successful dialysis, the polymer signals were clearly visible (highlighted in blue).*

Further analysis was carried out with $^{1}$H-NMR and $^{19}$F-NMR. The latter showed no signals here, which indicates a complete replacement of the pentafluoro phenyl groups and thus a complete conjugation with glycine.

Further, for linear charged polycation structures a single sided trityl-protected ethylene diamine (EDA-Trt) was prepared according to the synthesis demonstrated in Figure 21.

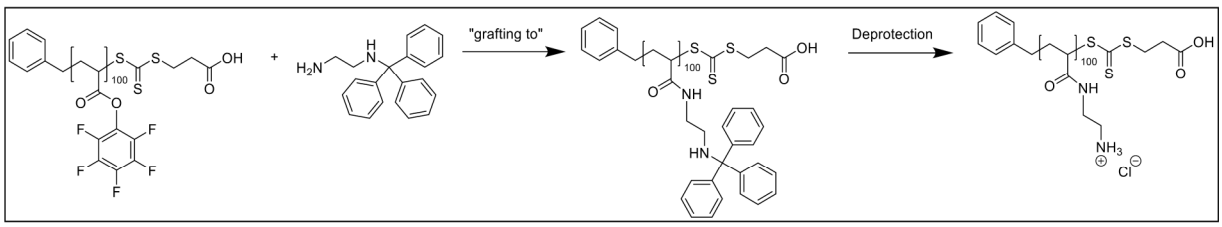


*Figure 21: Designed synthesis of $PPFP_{100}$ to polycation using single Trt-protected EDA*

While the synthesis of the single-sided protected EDA proceeded without further complications, the polymer analogous reaction was not successful. $^{19}$F-NMR demonstrated that no full conversion of poly active esters precursors with EDA-Trt occured. A reason for this finding could be, that the trityl-protection group was sterically demanding which did not allow for the complete substitution of all pentafluoro phenyl groups of the poly active ester.

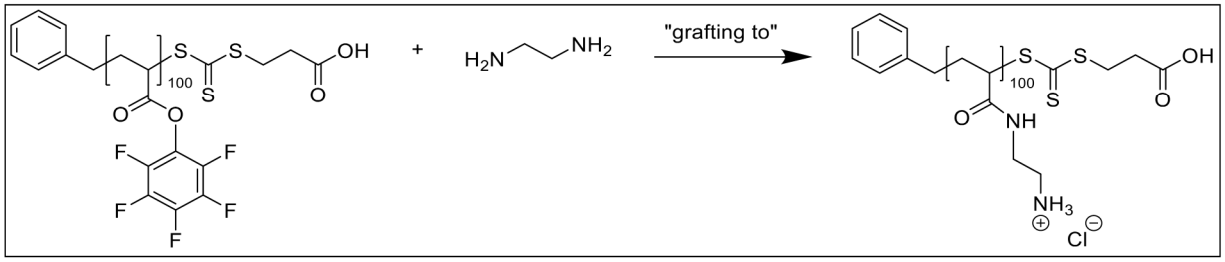


*Figure 22: Alternative conversion of $PPFP_{100}$ with a high excess of unprotected EDA.*

As an alternative route, as shown in Figure 22, the reaction of the polymers was carried out with unprotected EDA. However, to minimize cross-linking of the second primary amine group, the EDA was used in 50-fold excess. The remaining purification was adapted from the previous polyanion synthesis.

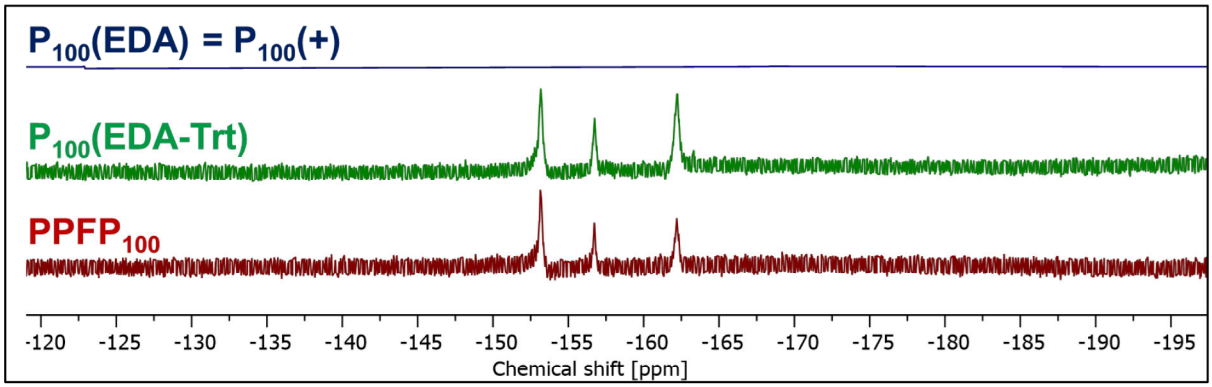


*Figure 23: Comparison of the $^{19}$F-NMRs of the poly active ester precursor $PPFP_{100}$ (bottom), after polymer analogous reaction with EDA-Trt (middle) and after reaction with unprotected EDA in 50 eq. excess (top).*

The $^{19}$F-NMR graphs in Figure 23 confirm that after replacement with the unprotected EDA, all pentafluoro phenyl groups have been removed. Once a suitable synthesis route was found for both the polyanions and the polycations, the reactions were transferred to the related $PPFP_{200}$ precursors. The results of all linear charged polyanion and polycation synthesis are summarized in the following Table 3.

*Table 3: Overview of reactions and yields for the synthesis of linear charged polyelectrolytes using polymer analogous reactions.*

| Polyelectrolyte | Precursor | Reaction compound | After conversion $^{19}$F-NMR | Yield |
|---|---|---|---|---|
| $P_{100}(+)$ | $PPFP_{100}$ | 50 eq. EDA | No signals | ***86 mg (68%)*** |
| $P_{100}(-)$ | $PPFP_{100}$ | 2 eq. Glycine | No signals | ***100 mg (79%)*** |
| $P_{200}(+)$ | $PPFP_{200}$ | 50 eq. EDA | No signals | ***80 mg (63%)*** |
| $P_{200}(-)$ | $PPFP_{200}$ | 2 eq. Glycine | No signals | ***96 mg (77%)*** |

After a successful synthesis improvement of the linear charged polyelectrolyte structures, polyampholyte structures were also approached. For this purpose, the oligomeric

intermediated described in section 3.1.1 had already been synthesized, but also linear charged polyampholytes could arise from this approach using polymer analogous reaction. The target is to investigate the random arrangement of charges in the same polymer precursor.

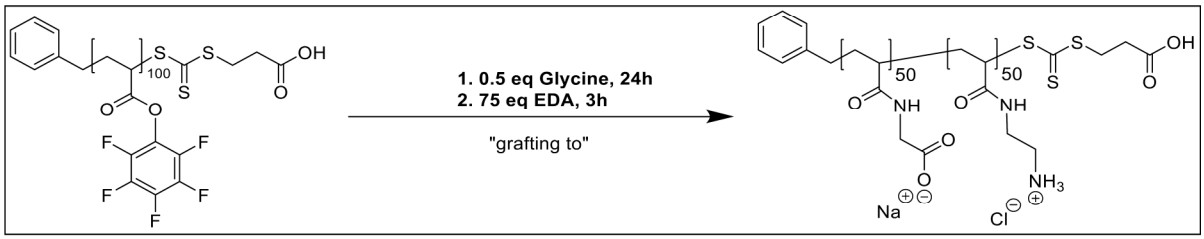


*Figure 24: Conversion of $PPFP_{100}$ to linear charged polyampholytes using glycine and a high excess of EDA.*

Glycine and EDA were used here as well, whereby the amount of glycine was reduced to 0.5 eq. and the EDA was added to the synthesis after 24h, to make sure all glycine groups had reacted. The idea was to synthesize a polyampholyte structure that contains equal amounts of negative and positive charges, which are randomly distributed within the polymer. The purification was conducted by dialysis and involved the adjustment of the pH value.

*Table 4: Overview of reactions and yields for the synthesis of linear charged polyampholytes using polymer analogous reactions.*

| Polyelectrolyte | Precursor | Reaction compound | After conversion $^{19}$F-NMR | Yield |
|---|---|---|---|---|
| $P_{100}$(+/-) | $PPFP_{100}$ | 0,5 eq Glycine (24h)<br>75 eq EDA (3h) | No signals | ***136 mg***<br>***86%*** |
| $P_{200}$(+/-) | $PPFP_{200}$ | 0,5 eq Glycine (24h)<br>75 eq EDA (3h) | No signals | ***122 mg***<br>***77%*** |

After successful synthesis of the linear charged polymers, the conversion of the oligomers was continued, which, however, could not follow the same synthetic route as the linear structures. Due to different side chain sizes, a complete substitution of the PPFP side chains with the oligomers is very unlikely or even impossible, analogous to the previous attempts with the EDA-Trt precursors. Since the focus of this work was not on the complete conversion of the polymers, but rather the investigation of different charge distributions, only a defined percentage of the group substitution was aimed. The remaining PFP groups were replaced with smaller, non-charged molecules. For the fourfold charged oligo-grafted polyelectrolytes, an incorporation of 25% was aimed for. Polymers should have the same number of charges but distributed differently within the polymer chain, in this case brush-shaped. This allows a better comparison of the phase behavior at a later stage with the linear charged polyelectrolytes. For the ampholytic structures, a reduced functionalization degree of 10% was targeted due to the higher sterically demand.

The synthesis and analysis of the oligomer structures has already been discussed in chapter 3.1.1. Hence, it was focused on maintaining the protection group on the primary amines to avoid undesired crosslinking reactions of the polymer side chains. The cleavage reaction from the solid-phase needed to be orthogonal to the protection group chemistry to prevent crosslinking during polymer analogous reaction. The only unprotected and reactive amines were the *N*-terminal amines of the oligomer backbone, which were used as a conjugation site for the active ester.

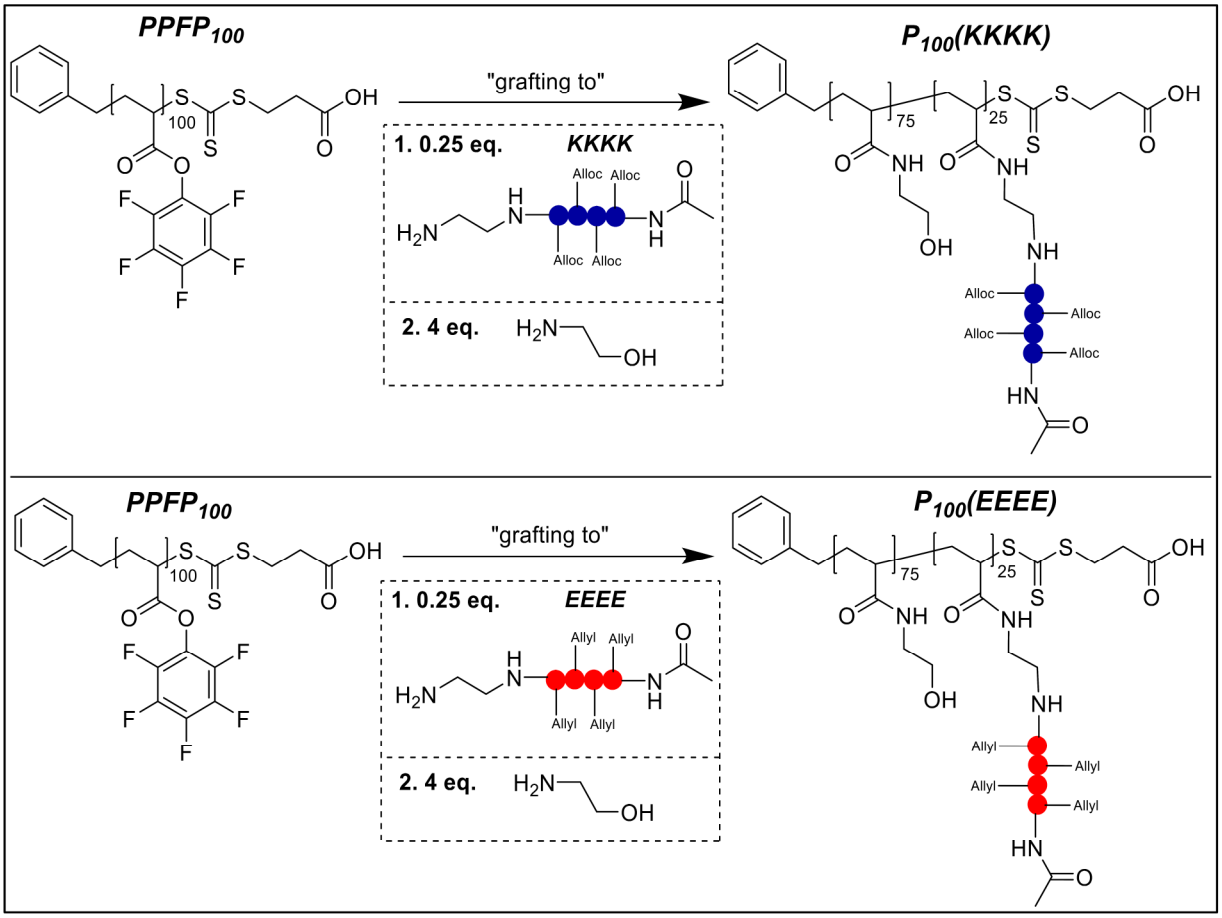


*Figure 25: Conversion to the $P_{100}$ oligomer-grafted polyelectrolytes using previous synthesized oligo-electrolytes in 0.25 eq. and 4 eq. ethanolamine.*

The “grafting to” method was applied similarly to the conversion of the single charged polyampholytes as described previously. Oligomers were dissolved in DMF and coupling reaction with the poly active ester was performed for 24h, before remaining PFP groups were substituted by the addition of ethanolamine to the proceeding reaction. Here, ethanolamine was chosen for substitution, because of its small molecule size and its low steric demand compared to the oligomers. After successful conjugation of ethanolamine, the free hydroxyl group did not contribute to the overall charge of the polymer. Purification and ion exchange was performed by dialysis and pH adjustment as already mentioned above. The conversion completion of the PFP groups was confirmed by $^{1}$H- and $^{19}$F-NMR. Figure 26 shows how the

conversion of the $P_{100}$(EEEE) is traced using an $^{1}$H-NMR comparison of the oligomer and the final oligomer-polymer hybrid structure. In the polymer structure, the Allyl signals were clearly detectable and broadened which is typical for polymers. In addition, the protons of the phenyl ring of the polymer backbone can be clearly identified downfield in the NMR spectrum.

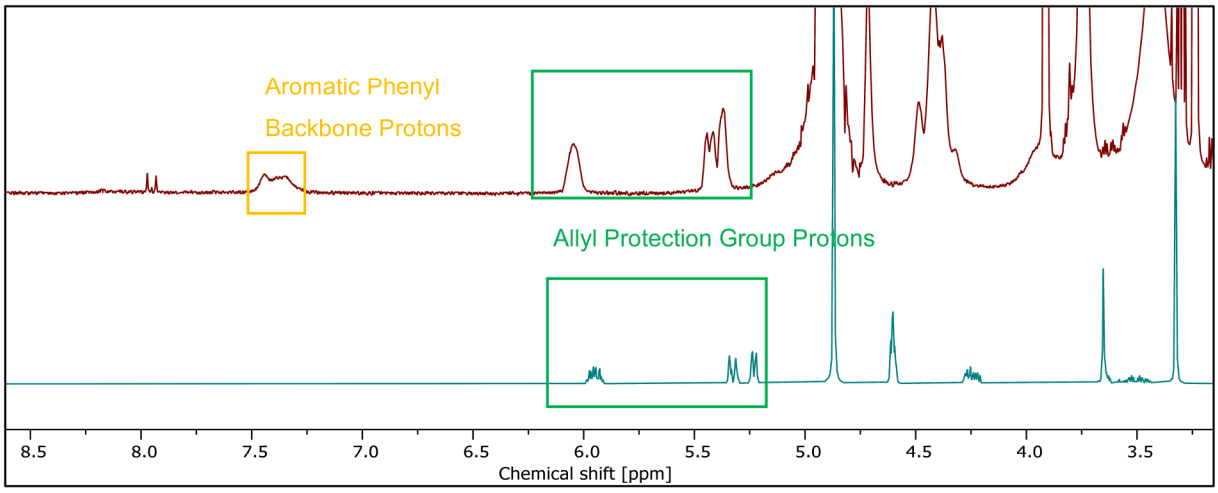


*Figure 26: Comparison of the $^{1}$H-NMR spectra of the EEEE oligomer (bottom) and the conjugated oligomer-grafted polymer hybrid structure (top). The signals of the Allyl protecting group were highlighted in green. The final incorporation of the oligomer is determined by the integral ratio of the aromatic polymer backbones (highlighted in yellow) and the Allyl protecting groups.*

Purification of the pure lysine oligomer KKKK has been observed to be much more intricate in contrast to the other Polymer $P_{100}$(EEEE). Dialysis in water could not be used as a purification method. Due to a high amount of protection groups per oligomer/polymer, the polymer appeared to have a significantly higher hydrophobicity, which caused an insolubility in water. This effect made it more difficult to adequately analyze and purify the polymers directly after the conjugation process. Since degree of functionalization was determined before the removal of the side protection groups, incorporation of $P_{100}$(KKKK) was not determinable.

The conversion of the oligomer-grafted polyampholytes, on the other hand, could be carried out without complications as well, as their dialysis purification. Oligomers were used in 0.1 eq. and reacted for 24h until ethanolamine was added to the reaction solution (see Figure 27).

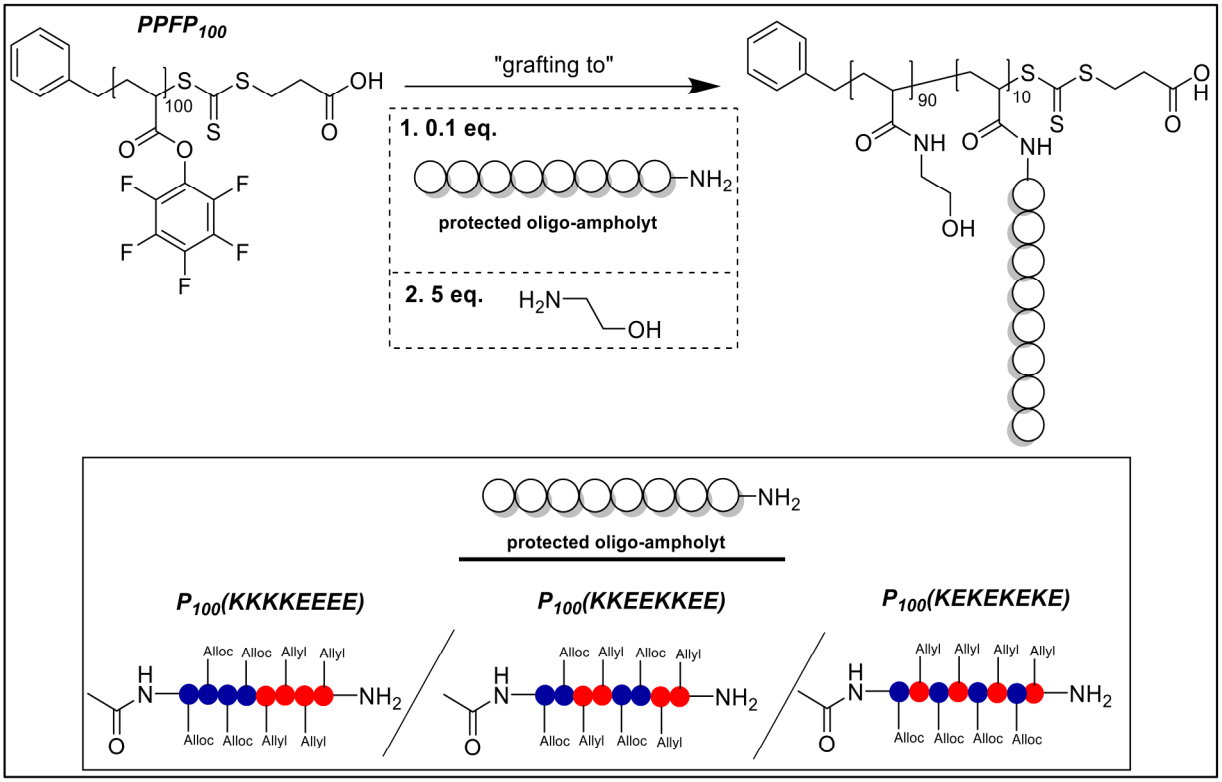


*Figure 27: Conversion of PPFP$_{100}$ to oligomer-grafted polyampholyte using previous synthesized oligomers in 0.1 eq. and 5 eq. ethanolamine (top) and the different conjugated oligomers (bottom).*

The results of the polymer analogous reactions with the oligomers were summarized in the following Table 5.

*Table 5: Overview of the targeted functionalization degrees of the oligomer-grafted polymer structures and the calculated incorporation in the polymer.*

| Polymer | Yield | Target Func. Degree | Calculated Func. Degree |
|---|---|---|---|
| P$_{100}$(EEEE) | 70 mg (60%) | 25% | 10% |
| P$_{100}$(KKKK) | 84 mg (59%) | 25% | not determinable |
| P$_{100}$(KEKEKEKE) | 50 mg (59%) | 10% | 4.5% |
| P$_{100}$(KKEEKKEE) | 52 mg (61%) | 10% | 4.8% |
| P$_{100}$(KKKKEEEE) | 45 mg (53%) | 10% | 4.3% |

The incorporation was determined using $^{1}$H-NMR. As explained above, the aromatic phenyl polymer backbone signals were compared with the Alloc and Allyl protecting group signals. The underlying problem involved two aspects: First, it was shown during the oligomer cleavage from solid-phase that the protecting groups of the Allyl protecting group were partially removed before the deprotection procedure. Although this effect was relatively small, unfortunately, no precise assumption of the final functionalization degree could take place after the partial protection group removal during polymer analogous reactions. Also other polymer signals could not be clearly assigned in the $^{1}$H-NMR, due to the large overlapping of the individual

signals. Therefore, with the given signals of $P_{100}$(EEEE) an functionalization of ca. 10% could be determined. The second problem was the insufficient purification of the $P_{100}$(KKKK), which made it impossible to determine the functionalization degree here. Nevertheless, the NMRs for all polyelectrolytes and polyampholytes which showed clearly assignable signals were analyzed and summarized in Table 5.

In general, different polyelectrolytes and polyampholytes were successfully obtained, purified and characterized. Only $P_{100}$(KKKK) was not purified according to the standard protocol but was remedied directly after the deprotection reaction.

Proceeding to the deprotection of the amino acid side chain, the choice of the Alloc and Allyl protecting group was previously justified as described in section 3.1.1 and is associated with the orthogonality of the Fmoc-deprotection conditions to the solid-phase synthesis process and the subsequent cleavage process from the resin. In many examples from literature, Alloc and Allyl protection groups are often used for solid-phase synthesis and are usually removed before cleavage from the resin[158, 159], which showed differences to the synthesis strategy applied in this work. In this process, cleavage of the protection groups should only take place after completion of the polymer analogous reaction and therefore needed to be performed in solution. For this purpose, a standard Alloc deprotection protocol was transferred from solid-phase conditions to a solution-based approach, using barbituric acid and Palladium(0) catalyst under inert conditions. In a first approach, the polymers $P_{100}$(EEEE) and $P_{100}$(KKKK) were treated with the modified cleavage protocol. Therefore, the polymers were dissolved in DMF and purged with argon, before tetrakis(triphenylphosphine)palladium(0) and barbituric acid were added. After 2h, polymer was precipitated in cold diethyl ether and dialyzed. Deprotection was confirmed by $^1$H-NMR, but even after two attempts, only the cleavage of the Allyl protection groups of glutamic acid was accomplished, while cleavage of the Alloc protection groups could not be reported under described conditions. Although this Alloc deprotection was described in literature on many examples for solid-phase, a method transfer in solution remained unsuccessful. The successful deprotection of the Allyl protecting group might be explained by the significantly higher acid-lability of the ester bond compared to the Alloc group. This explanation is consistent with the previously established assumption from chapter 3.1.1, whereby part of the Allyl protection groups were removed during oligomer cleavage from the resin.

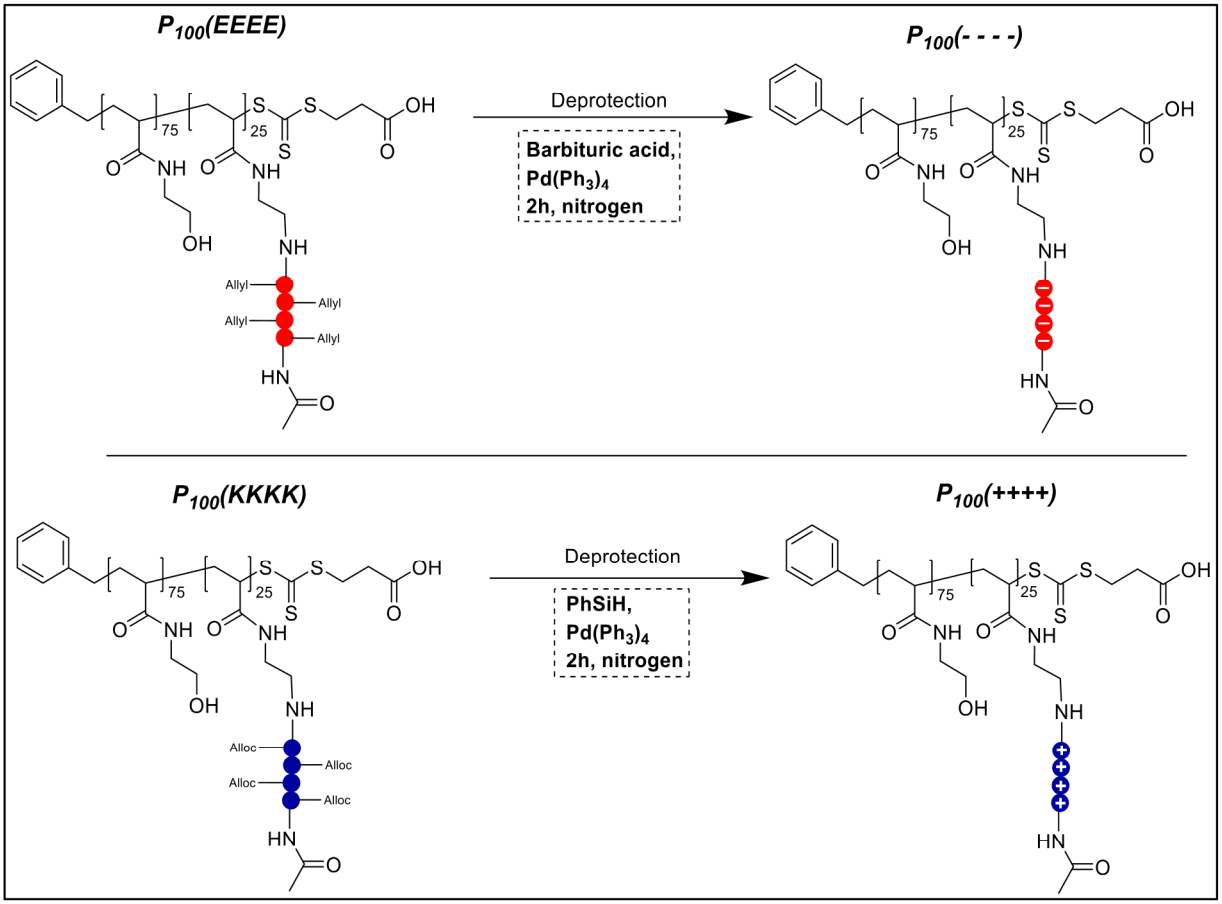


*Figure 28: Deprotection step of $P_{100}$(EEEE) to $P_{100}$(- - - -) and $P_{100}$(KKKK) to $P_{100}$(++++) using two different cleavage protocols.*

Hence, an alternative deprotection protocol, also based on deprotection on solid-phase, was transferred to the reaction in solution. Here, an exchange of barbituric acid with phenyl silane was performed.[160] These deprotection conditions allowed for cleavage of Alloc protection groups, but required repetition to achieve full deprotection. The incomplete deprotection reaction after the first phenyl silane treatment was determined via $^{1}$H-NMR (see Figure 29). The deprotection process was repeated, but it still did not lead to a complete removal of the protection groups.

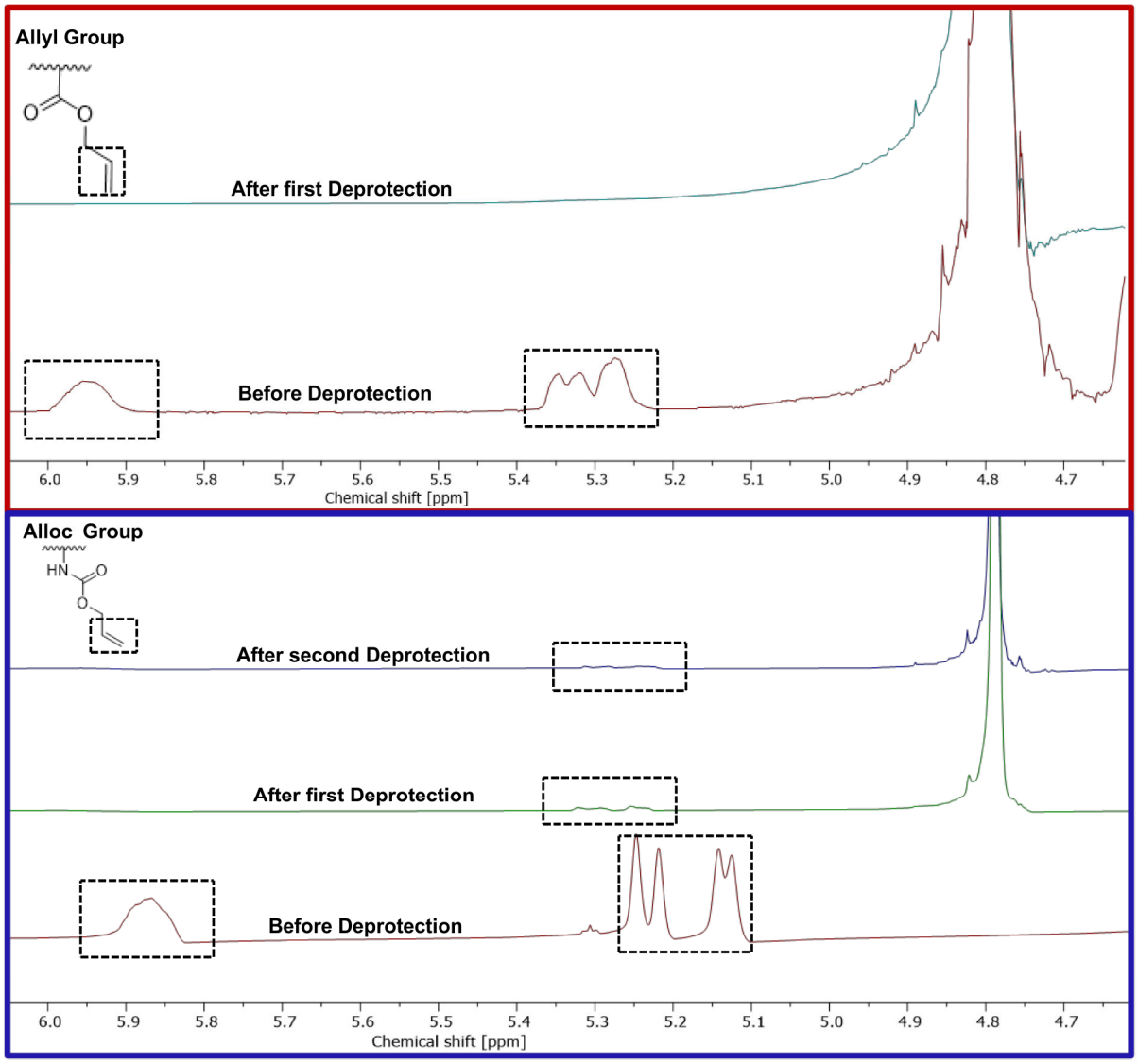


*Figure 29: Comparison of $^{1}$H-NMR of Protected and Deprotected Polyelectrolytes $P_{100}$(- - - -) (red) and $P_{100}$(++++) (blue).*

After the deprotection process for the oligomer-grafted polyelectrolytes was accomplished, the synthetic approach was transferred to the oligomer-grafted polyampholytes. Here, after the treatment with phenyl silane, no further residues of the protecting groups were found.

In summary, the methods of solid-phase synthesis and polymer analogous reaction were successfully combined to give access to sequence-controlled polyelectrolytes and polyampholytes. There were certain limitations in terms of control over the degree of functionalization and the position within the polymer, but there is precise control of the side chain sequence and thus targeted brush-shaped polyelectrolytes were constructed. In addition to the difficulty of the complete cleavage of the Alloc protection group, the $^{1}$H-NMR analysis was shown to be challenging. There were no significant signals that indicated the degree of incorporation from oligomer to polymer. Additionally, the partial loss of Allyl protecting groups during oligomer cleavage made the analysis more difficult. Therefore, it is not advisable to

determine the degree of incorporation by reference to the Allyl protons, although these are the most clearly assignable in the spectrum. In the future, it would be advisable to consider new ways of analysis to determine the degree of functionalization more clearly. This opens the possibility of creating larger controlled structures for investigating the polyelectrolyte phase behavior in aqueous solution to acquire more profound knowledge of the impact of sequence, charge density and distribution within the polyelectrolytes. First studies on this phase behavior are discussed in the following chapter.

## 3.2. Phase behavior investigation of polyelectrolytes and polyampholytes

The interaction of differently charged polyelectrolytes or polyampholytes in solution leads to the formation of polyelectrolyte complexes. Coacervation is one type of polyelectrolyte complexes, which describes a liquid-liquid phase separation that occurs through the interaction of the charged polymers. The mixture separates into a polymer-rich and a dilute phase. As already outlined in chapter 1.1.1, coacervates fulfill a major role in nature[38, 50, 51, 54, 161, 162] and synthetically prepared coacervates are also used in pharmaceutical industry. However, the influence of external factors such as temperature, salt or polymer concentration on the coacervation process is still not fully understood. The impact of charge sequence and charge distribution were also investigated and published in initial studies, but in this work, a modified synthesis procedure of such sequence-controlled polyelectrolytes was chosen. These structures were investigated in the following chapter, focusing on an initial observation of the charge sequence as a function of the salt and polymer concentration of the solution. An initial indication that coacervate formation is occurring is the turbidity of the solution caused by the formation of tiny coacervate droplets. These solutions were analyzed using optical microscopy to confirm the formation of these two-phase systems.

### 3.2.1 Phase behavior - polyelectrolytes

First, the investigation of linear-charged polymers was started. A phase diagram was generated, which shows the dependency between polymer and salt concentration. The formation of the polyelectrolyte complexes, and particularly, the coacervates, was analyzed using optical microscopy. The phase diagram was used to visualize the area in which phase separation occurs and where the limits of the two-phase system exist. To create a phase diagram, different polymer and salt concentrations of the polyelectrolytes were prepared in solution and analyzed for coacervate droplets. Only the formation of coacervate droplets was considered here, regardless of their number and size.

For the preparation of the measurement stock solutions of the respective polyelectrolytes and a salt solution were prepared. In this instance monovalent salt ions were used, specifically sodium chloride. Polymer concentrations from 0.1 mM to 100 mM and salt concentrations from 0 mM to 2000 mM were investigated to obtain a complete phase diagram and to identify the point at which coacervates are no longer formed. The concentration of the polymer stock solutions was calculated based on the molecular weight of the polymer repeating unit. An equimolar ratio of polycations and polyanions was used for the polyelectrolytes to ensure the same amount of positive and negative charges.

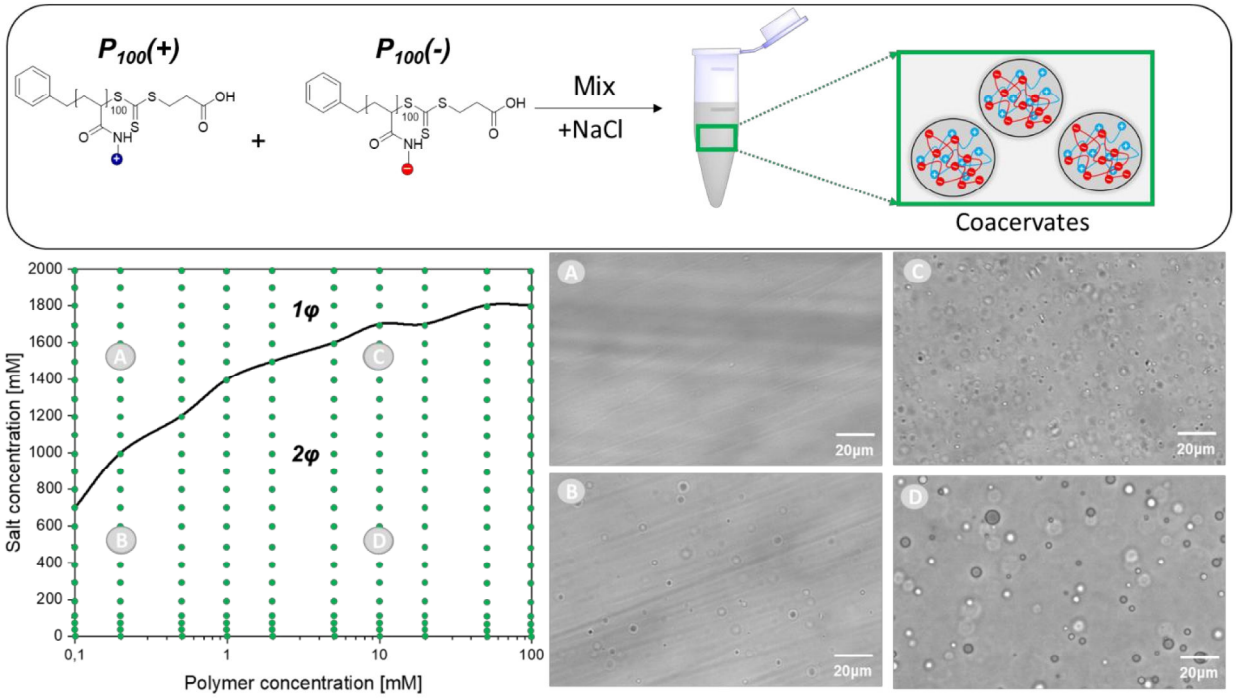


*Figure 30:* ***Top****: Scheme of polyelectrolyte mixture and coacervate droplets.* ***Left:*** *Phase diagram of $P_{100}$(+) and $P_{100}$(-) mixture with correlation of salt and polymer concentration. Black line marks the measured critical salt concentration (CSC) of the coacervate phase at corresponding polymer concentration, separating the one phase (1φ) area and two-phase area (2φ).Green dots are marking the data points (this was perfromed with every fowllowing phase diagram).* ***Right:*** *Microscope images of coacervate droplets at different salt and polymer concentrations* ***A****: Polymer conc. 0.2 mM, salt conc. 1500 mM;* ***B****: Polymer conc. 0.2 mM, salt conc. 500 mM;* ***C****: Polymer conc. 10 mM, salt conc. 1500 mM;* ***D****: Polymer conc. 10 mM, salt conc. 500 mM;*

Figure 30 depicts the phase diagram of the mixture of $P_{100}$(+) and $P_{100}$(-). The curve represents the limit between the two-phase liquid-liquid phase separation and a single-phase solution. Below the curve, the polyelectrolytes are assembled in coacervate droplets, which is shown in microscope images (Images B-D). Depending on polymer and salt concentration, these may vary in both size and number, but also time is also a factor that should not be neglected. Observations have shown that over time the droplets coalesce and merge into larger droplets. Clearly discernible is that at higher polymer concentrations and low salt concentrations, the coacervates were particularly easy to identify. Compared to the other regions, they form significantly larger coacervate droplets in the same time. Looking at the image A of the phase diagram, low polymer concentration and high salt concentration, there were no droplets to be found and the polymers were completely dissolved. Due to the high proportion of dissolved ions, the side chains of the polyelectrolyte were "blocked" with the salt counterions and could no longer interact with other polyelectrolytes. The first results of the phase diagram were as expected from the literature and can therefore be used as a reference standard for the other polyelectrolytes structures.[31, 32] The same procedure was performed with the linear charged polyelectrolyte with approximately 200 repeating units. Again, a phase diagram was generated as a function of salt and polymer concentration, which is shown in Figure 31.

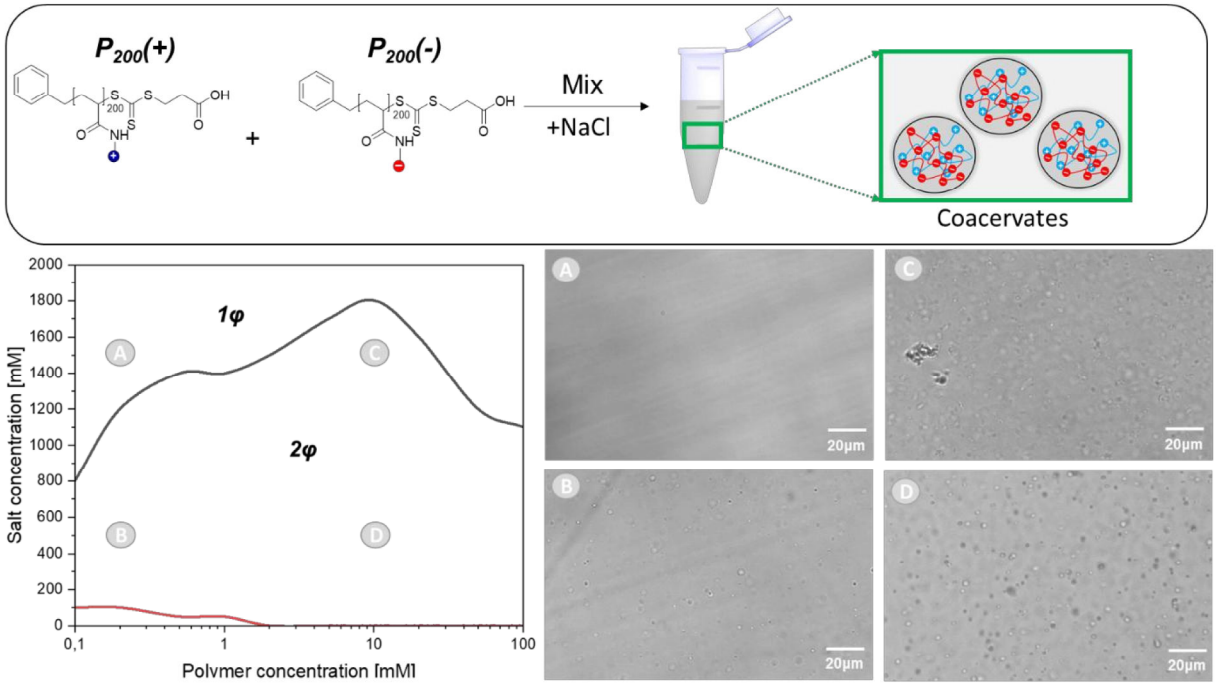


*Figure 31:* ***Top****: Scheme of polyelectrolyte mixture and coacervate droplets.* ***Left:*** *Phase diagram of $P_{200}$(+) and $P_{200}$(-) mixture with correlation of salt and polymer concentration. Black line marks the measured critical salt concentration (CSC) of the coacervate phase at corresponding polymer concentration, separating the one-phase (1φ) area and two-phase-area (2φ). The area below the red line marks the area in which no coacervates were found* ***Right:*** *Microscope images of coacervate droplets at different salt and polymer concentrations* ***A****: Polymer conc. 0.2 mM, salt conc. 1500 mM;* ***B****: Polymer conc. 0.2 mM, salt conc. 500 mM;* ***C****: Polymer conc. 10 mM, salt conc. 1500 mM;* ***D****: Polymer conc. 10 mM, salt conc. 500 mM;*

The coacervation droplets were also clearly visible for the $P_{200}$ polyelectrolyte mixture, but here a shift of the coacervation area was present. Compared to the previous $P_{100}$ mixture, a second transition state in the phase diagram, marked in red, was observed here. This marks the area, where coacervates could not be clearly verified. It appears that the polyelectrolytes had not yet been able to interact sufficiently with each other. Even if the salt concentration in the solution leads to a dissolution of the coacervate phase at too high concentrations, it could be beneficial to support the coacervate formation.[23, 163, 164] The drop in the critical salt concentration, above a polymer concentration of 10 mM, was also remarkable. The range in which the coacervates were stable decreases rapidly and critical salt concentration lowers to just 1100 mM at the maximum polymer concentration of 100 mM.

By comparing the images from Figure 30 and Figure 31, which compare the same polymer architecture and salt concentrations with different overall polymer lengths, the same trend can be seen in both examples. Figures B-D all show coacervate droplets, whereby in Figure D these are particularly clearly visible (see Figure 32).

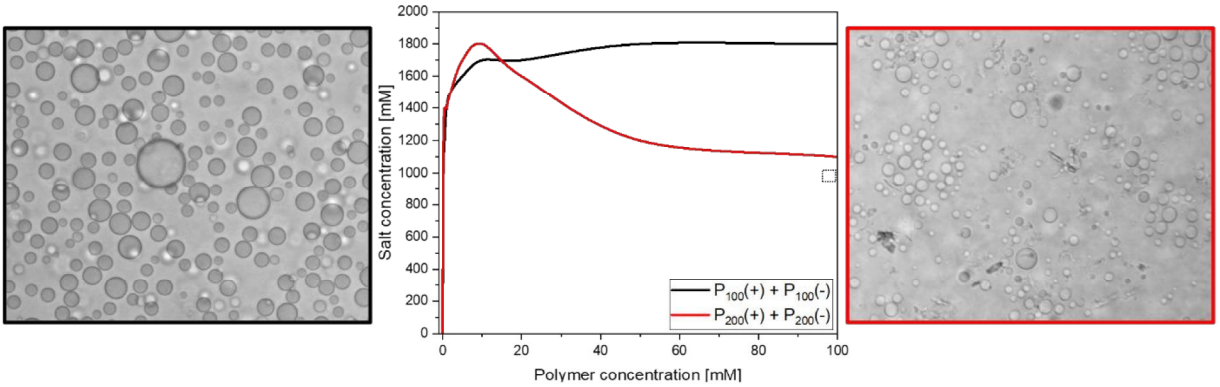


*Figure 32:* ***Middle****: Comparison of the salt resistance of the coacervate phases of $P_{100}$(+) + $P_{100}$(-) and $P_{200}$(+) + $P_{200}$(-). Microscope images show the polymer and salt concentration of the marked area in the diagram of corresponding polyelectrolytes.* ***Left:*** *$P_{100}$(+) + $P_{100}$(-), polymer conc. 100 mM, salt conc. 1000 mM;* ***Right:*** *$P_{200}$(+) + $P_{200}$(-), polymer conc. 100 mM, salt conc. 1000 mM*

Since the calculated polymer concentration of the solution is based on the polymer repeating, the same number of charges is present in the mixture, only the length of the polymers varies. A direct comparison of the two-phase diagrams reveals that although the longer polymer backbone leads to an overall higher CSC, at higher polymer concentrations it switches to a single-phase system much more rapidly. While the coacervates of the $P_{100}$ polyelectrolytes are clearly visible and well defined, there are still noticeable droplets in the $P_{200}$ polyelectrolytes, but they are considerably reduced and smaller in size. In addition, they become increasingly blurred in the background, which indicates that the limit of the CSC is getting gradually closer at this point.

Continuing with the next phase diagram, a comparison of the polymers based on the charge distribution in the polymer was aimed for. For this purpose, a phase diagram of $P_{100}$(++++) and $P_{100}$(----) was recorded. Here too, the polymer concentration was calculated based on the polymer repeating unit, but since there were two different repeating units, the molecular weight of the monomer unit was calculated proportionally, depending on the planed incorporation of the side chain. The equation below shows the calculation with reference to the $P_{100}$(++++) polymer.

$$Mw(Oligomer) * \%\ in\ Polymer + Mw(Ethanolamine) * \%\ in\ Polymer = Mw\ (Repeating\ unit) \quad \textbf{(1)}$$

$$760.58\frac{g}{mol} * 25\% + 115.13\frac{g}{mol} * 75\% \ = 276{,}49\frac{g}{mol} \quad \textbf{(2)}$$

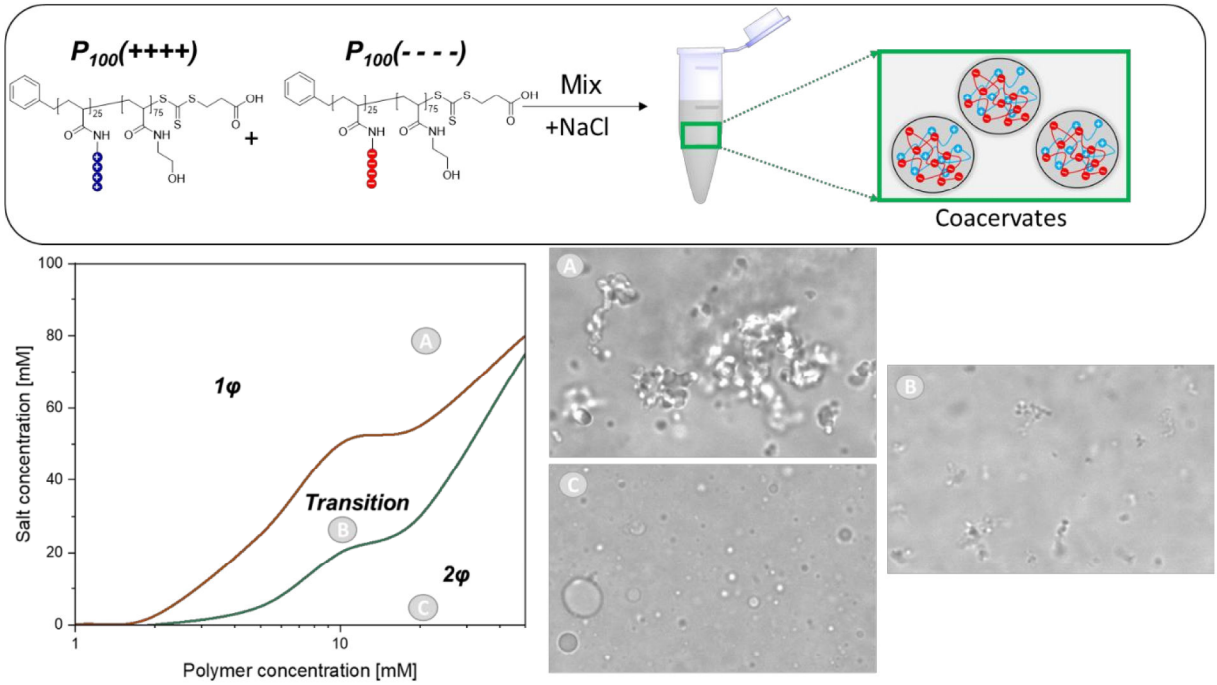


*Figure 33:* ***Top****: Scheme of polyelectrolyte mixture and coacervate droplets.* ***Left:*** *Phase diagram of fourfold charged oligomer-grafted polyelectrolytes $P_{100}$(++++) and $P_{100}$(- - - -) mixture with correlation of salt and polymer concentration. Red line marks the maximum salt resistance of the transition phase at corresponding polymer concentration. Green line marks the area in which coacervates are going over into transition state between liquid-liquid phase separation and precipitate* ***Right: A****: Polymer conc. 20 mM, salt conc. 80 mM;* ***B****: Polymer conc. 10 mM, salt conc. 25 mM;* ***C****: Polymer conc. 20 mM, salt conc. 0 mM.*

There are two things that highlight the phase behavior of the brush-shaped polymers: No coacervate formation at lower polymer concentrations and significantly lower salt resistance of the two-phase system. The range in which coacervate droplets can be located is limited to a range of up to 50 mM polymer concentration. Higher polymer densities could not be measured due to the decreased polymer solubility. The first coacervate droplets are formed at a polymer concentration of 2 mM and above, whereby the droplets are not yet clearly noticeable, but appear more like a transitional state between coacervate formation and the dissolved form and/or aggregate formation (Figure 33,B). Above the transition state, especially at high polymer densities, the polymers are not completely dissolved but are clustered in aggregates, which may be related to the low solubility of the polymers. Within the transition state, the polymers are in a form which they are partially discernible as droplets, but they showed tendencies towards forming aggregates. No clear droplets can be detected as with lower concentrations, only at higher polymer densities droplets are clearly visible, as shown in Figure 33,C. The comparison with the linear polyelectrolytes is summarized in Figure 34.

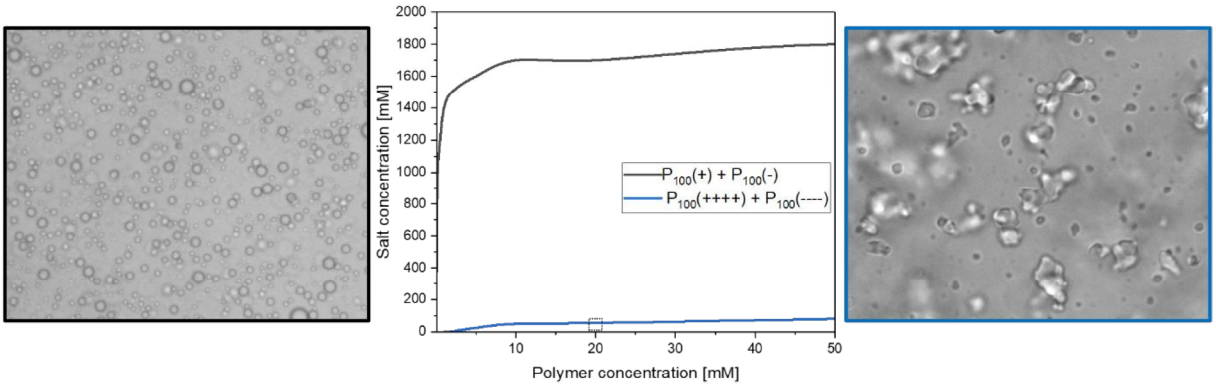


*Figure 34:* ***Middle****: Comparison of the salt resistance of the coacervate phases of $P_{100}$(+) + $P_{100}$(-) and $P_{100}$(++++) + $P_{100}$(- - - -), Microscope images show the polymer and salt concentration of the marked area in the diagram of corresponding polyelectrolytes.* ***Left:*** *$P_{100}$(+) + $P_{100}$(-), polymer conc. 20 mM, salt conc. 50 mM;* ***Right:*** *$P_{100}$(++++) + $P_{100}$(- - - -), polymer conc. 20 mM, salt conc. 50 mM.*

The direct comparison illustrates the significant low salt resistance of the brush-shaped polyelectrolytes compared to the linear polymers. This could be due to the lower flexibility of the polyelectrolytes, which leads to less interaction between the charged side chains. Not considered here is the option of an imbalance in the charge ratio within the polymer mixture. The incorporation of the charged oligomers was finally determined by $^{1}$H-NMR, which was already discussed in the previous chapter. It is conceivable that inaccuracies may occur, and the actual incorporation may be lower. This would in turn lead to an inaccurate charge ratio and thus affect the coacervate behavior. As further analysis of the polymers to ascertain the degree of incorporation could not be carried out, this hypothesis could be tested in further experiments by adjusting the polymer content of the individual polyelectrolytes.

### 3.2.2 Phase behavior - polyampholytes

Since polyampholytes contain both negative and positive charges, they are able to undergo coacervate formation on their own, which is referred to as self-coacervation or simple coacervation. The dependence of the charge sequence on their coacervate behavior has already been investigated in previous studies with linear polyampholyte structures. It has been shown that the coacervate behavior is favored with an increased density of consecutive identical charges.[32] The following section investigates the previously prepared polyampholytes. One type of ampholyte has a linear structure, whereby the arrangement of the charges is completely random in the polymer. The other polyampholytes are defined in their sequence but do not have a linear structure, instead, they follow a brush-shaped arrangement.

Firstly, the behavior of the randomly assembled, linear sequence with variable polymer length was investigated. For the preparation of a phase diagram, the molecular weight of the polymer repeating unit and therefore the polymer concentration was determined here, analogous to the previous oligomer-grafted polyelectrolytes. It was assumed that the negative and positive side

chains have been incorporated in equal parts, whereby the calculation of a repeating unit was calculated as follows:

$$Mw(Glycine) * \%\ in\ Polymer + Mw(Ethylenediamine) * \%\ in\ Polymer = Mw\ (Repeating\ unit) \quad \textbf{(3)}$$

$$151.10\frac{g}{mol} * 50\% + 150.61\frac{g}{mol} * 50\% \ = 150.86\frac{g}{mol} \quad \textbf{(4)}$$

The previous phase diagrams of linear charged polyelectrolytes have shown that coacervation is most favorable at especially high polymer concentrations and low salt concentrations, which is the reason for using an initial polymer concentration of 100 mM for these structures.

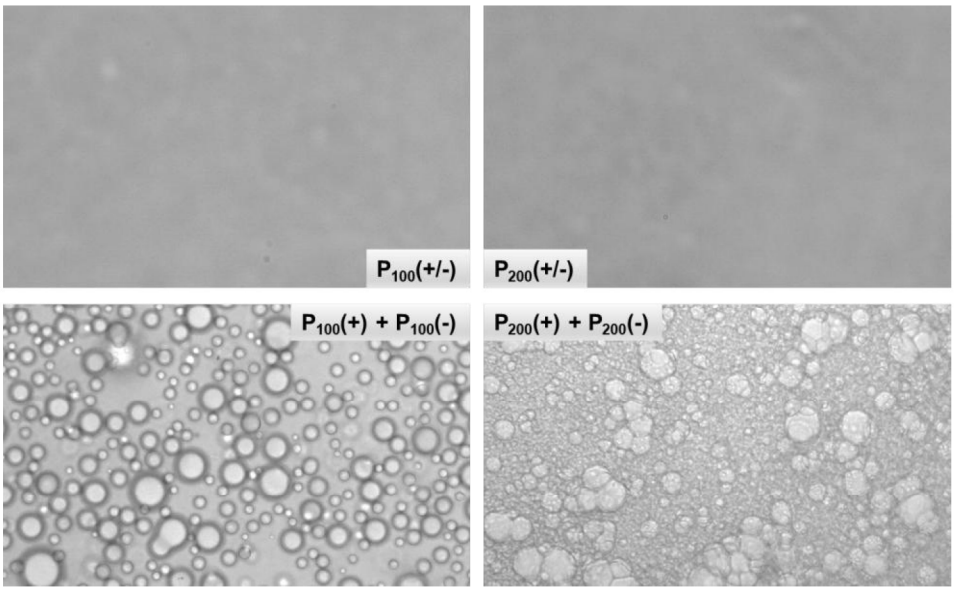


*Figure 35: Comparison of $P_{100}$ and $P_{200}$ polyampholyte phase behavior to $P_{100}$ and $P_{200}$ polyelectrolyte phase behavior. Polymer conc. 100 mM, salt conc. 100 mM.*

Figure 35 depicts the phase behavior of the polyampholytes of different lengths in comparison to the corresponding polyelectrolyte compounds. At the highest polymer concentration, no phase separation behavior could be observed neither for the $P_{100}$(+/-) polyampholyte nor the longer $P_{200}$(+/-). Higher polymer concentrations could not be tested due to limited polymer solubility. A completely random arrangement within the polymer does not appear to lead to coacervate formation even with adequate polymer lengths and concentration. *Perry et al*. investigated linear polyampholytes in various chain lengths and sequences and showed that at least eight consecutive units of the same charge must follow each other to allow coacervate formation.[32] This does not seem to be the case here. Compared to the polyelectrolytes, which already show well-defined coacervate droplets, the randomly arranged polyampholytes were unable to phase separate. An ordered sequence could not be achieved here for the linear polyampholytes with the chosen method of polymer analogous reaction, whereas other studies have already provided good findings here. In these studies, similar polyampholyte structures were prepared using solid-phase synthesis only without any subsequent active esters coupling

reactions.[31, 32, 140] However, the aim of synthesizing these structures was to investigate if such randomly ordered polyampholytes structures were able to undergo coacervation, which could not be confirmed with this experiment.

For a comparison with sequence-controlled polyampholytes, the oligomer-grafted polyampholytes were analyzed in aqueous solution. For the preparation of a phase diagram, the polymer concentration was determined here as a function of the molecular weight of the monomer unit, which was calculated using the same method as described above for the polyelectrolytes (see equation (1)). The highest possible polymer concentration of 50 mM was tested here as well, initially without the addition of any salt.

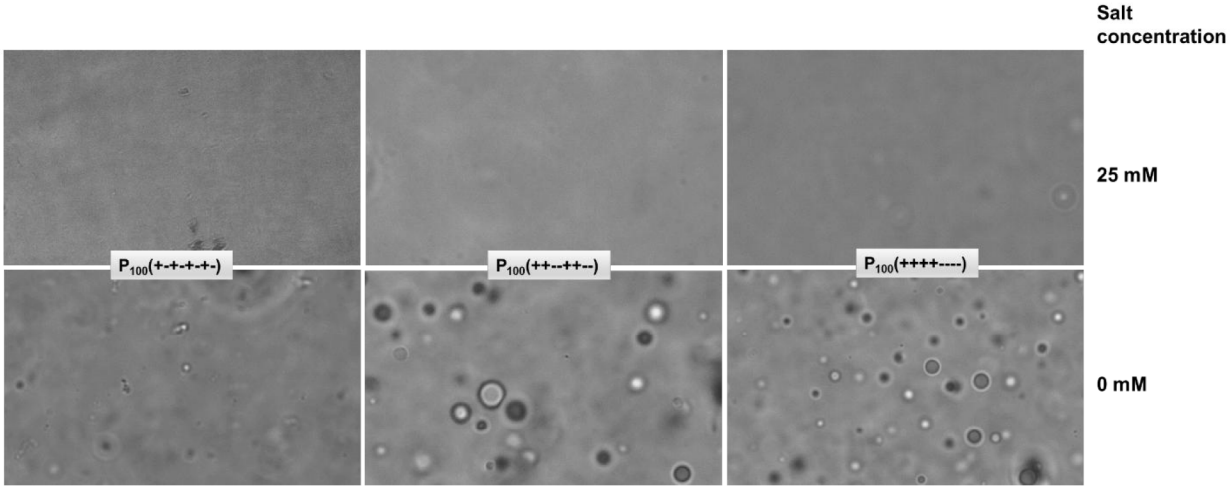


*Figure 36: Phase behavior comparison of oligomer-grafted polyampholytes $P_{100}$(+-+-+-+-), $P_{100}$(++--++--) and $P_{100}$(++++----) at 0 mM and 25 mM salt conc, polymer conc. 100 mM.*

In contrast to other studies with linear polyampholytes, in the present experiments, it was shown on the example of brush-shaped polyampholytes that coacervates are already formed consisting of two consecutive charges (see Figure 36). The different arrangement within the overall polymer structure seems to lead to a lowering of the successive charges. The polymers that have only one consecutive charge, on the other hand, did not lead to coacervate formation, as the charge density does not seem to be sufficient. Subsequently, the salt resistance of the formed coacervates was tested. By increasing the salt concentration to 25 mM, the two-phase systems immediately dissolved again. Compared to the linear structures, this is a significant drop in the CSC. To clearly differentiate the polymeric structures in their salt resistance, the measurement points were obtained in smaller steps. The results are shown in Table 6.

*Table 6: Overview of salt resistance for polyampholytes at 50 mM polymer concentration and linear charged polyelectrolyte structures.*

| Polymer | $P_{100}$(+-+-+-+-) | $P_{100}$(++--++--) | $P_{100}$(++++----) | $P_{100}$(+/-) | $P_{100}$(+) + $P_{100}$(-) |
|---|---|---|---|---|---|
| **Salt resistance** | *No Coacervation* | *12 mM* | *18 mM* | *No Coacervation* | *1800 mM* |

Although the polyampholytes showed initial phase separation behavior at a lower number of consecutive charges, they were again significantly less resistant to the addition of salt. The same effect was also observed with brush-shaped polyelectrolytes and may be related to a lower mobility of the polymer chains. However, a comparison of the salt resistance with the results of other studies of linear polyampholytes showed a similarly low concentration.[32] Furthermore, an effect could be confirmed that an increase in salt resistance occurred with an increased blockiness of the charges. What could not be confirmed is that, in theory, the salt resistance of ampholytic polymers is higher than that of their comparable homolytic structures. Neither the linear charged polyelectrolytes nor the brush-shaped polyelectrolytes showed a higher salt resistance compared to the ampholytic polymers. This could also be due to the brush-shaped structure of the polymers since the polymer chains and especially the side chain charges were less flexible and therefore interaction between different charges was hindered.

In summary, through a combination of solid-phase synthesis and the "grafting to" method, via polymer analogous reaction, access to sequence-controlled polyelectrolytes and polyampholytes was provided. This allowed good comparability using the same polymer backbone to investigate the phase behavior in initial studies. Based on this synthesis, further structures can be built up in a controlled procedure using further extensions such as tailor-made building blocks. The polyelectrolyte structures obtained showed unambiguous coacervate behavior and the salt resistance could be determined by creating a phase diagram. If the polyelectrolytes are compared with each other depending on their length, the longer polymers show a slightly higher CSC, but are significantly more affected by the ions of the salt at higher polymer concentrations, which leads to a faster dissolution of the previously formed coacervates. However, if the arrangement of the charges inside the polymer is changed to a brush-shaped configuration, the coacervate area will drop drastically. It has not been finally ascertained whether the exact number of conjugated charges is present, as the incorporation of the oligomer could not be clearly determined. Therefore, there is the possibility of a lower number of charges present, which contributes to the lower salt resistance. An unbalanced charge ratio could also contribute to this effect of decrease in salt resistance, as it can strongly influence the coacervate behavior by preventing formation in the first place.[134, 165, 166] However, as droplet formation occurs here, the influence here is estimated to be significantly low. Furthermore, for the ampholytic structures presented in this study, linear, randomly arranged charges within the polymer chain could not lead to coacervation formation. This confirms the assumption that a certain number of consecutive identical charges must be present for phase separation to occur. However, if the arrangement of the charges is converted into brush-shaped polymers, phase separation already takes place with two consecutive charges, whereas in comparable studies this was only observed after eight consecutive charges.[32] But here, too, the area of the coacervate phase is relatively small compared to the polyelectrolyte

structures. However, linear and in some cases shorter polymers were considered here, whereas only polymers with at least 100 repeating units were investigated in this work.

The following chapter will present the published work on glycan containing coacervates.[167] The preparation by solid-phase synthesis and polymer analogous reactions and the investigation of their phase behavior and lectin/bacteria capture will be discussed.

## 3.3. Glycan-presenting coacervates derived from charged poly(active esters): preparation, phase behavior and lectin capture

Authors: M.Illmann, L.Schäfl, F.Drees, L.Hartmann and S.Schmidt

Journal: Biomacromolecules

DOI: 10.1021

Impact Factor: 6.978 (2023)

Own contributions:

Collaborative synthesis of sequence-defined oligomers containing mannose and galactose moieties, as well as an AIE Dye. Collaborative synthesis of polyelectrolytes containing glyco-oligomers via polymer analogous reaction. Investigation of their phase behavior by variation of polymer and salt concentration. Investigation of incorporation of Concanavalin A within glycan coacervates. Determination of capture effectivity. Collaborative manuscript writing.

pubs.acs.org/Biomac

Article

# Glycan-Presenting Coacervates Derived from Charged Poly(active esters): Preparation, Phase Behavior, and Lectin Capture

Michele Denise Illmann, Lea Schäfl, Felicitas Drees, Laura Hartmann,* and Stephan Schmidt*

Cite This: *Biomacromolecules* 2023, 24, 2532−2540

Read Online

ACCESS | Metrics & More | Article Recommendations | Supporting Information

**ABSTRACT:** This study presents the preparation and phase behavior of glycan-functionalized polyelectrolytes for capturing carbohydrate-binding proteins and bacteria in liquid condensate droplets. The droplets are formed by complex coacervation of poly(active ester)-derived polyanions and polycations. This approach allows for a straightforward modular introduction of charged motifs and specifically interacting units; mannose and galactose oligomers are used here as first examples. The introduction of carbohydrates has a notable effect on the phase separation and the critical salt concentration, potentially by reducing the charge density. Two mannose binding species, concanavalin A (ConA) and *Escherichia coli*, are shown to not only specifically bind to mannose-functionalized coacervates but also to some degree to unfunctionalized, carbohydrate-free coacervates. This suggests non-carbohydrate-specific charge−charge interactions between the protein/bacteria and the droplets. However, when mannose interactions are inhibited or when non-binding galactose-functionalized polymers are used, interactions are significantly weakened. This confirms specific mannose-mediated binding functionalization and suggests that introducing carbohydrates reduces non-specific charge−charge interactions by a so far unidentified mechanism. Overall, the presented route toward glycan-presenting polyelectrolytes enables new functional liquid condensate droplets with specific biomolecular interactions.

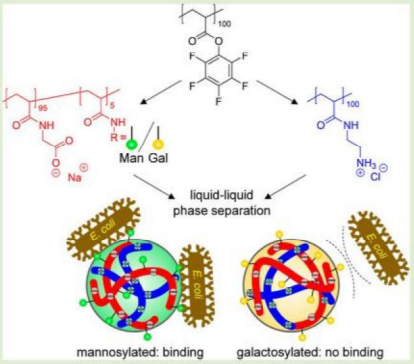


## 1. INTRODUCTION

Carbohydrate-mediated interactions dictate many biological processes on the cellular level, for example, adhesion, communication, signal transduction, or fertilization.[1,2] Lectins, an important class of carbohydrate-binding proteins, decorate the surface of pathogens and enable adhesion to the cell's glycocalyx, which is a critical step in infection processes.[3−5] Since the interaction of a single carbohydrate ligand with a protein is rather weak, nature employs multivalency to increase the binding affinity and selectivity.[6,7] Multivalent synthetic carbohydrate-presenting scaffolds such as linear glycopolymers, branched scaffolds, or particle-based glycocalyx mimetics via gold nanoparticles, micelles, vesicles, or microgels were developed to acquire insights into the molecular mechanisms of multivalent carbohydrate interactions.[8−15] At a high density of carbohydrate units, these scaffolds can achieve a lectin-binding avidity that is an order of magnitude larger in comparison to a single unit.[16,17] A potential application of such glycoconjugates is the treatment and prevention of infections by binding and blocking pathogenic lectins and their attachment to the glycocalyx.[18−23] Furthermore, responsive glycopolymers allow controlling the avidity by triggering an increase or decrease of the carbohydrate density or accessibility.[24−30] Mostly so far, thermoresponsive polymers with uncharged polar repeat units are used to form dense solid phase-separated aggregates upon a temperature change. In addition, some work was done on solid carbohydrate-presenting scaffolds that are held together and self-assemble by electrostatic interactions.[31,32]

Rather than such solid phase-separated systems, here we pursue liquid−liquid phase-separated glycopolymers. On the cellular scale, such liquid−liquid phase-separated systems, also known as coacervates, play an important role in the formation of protein-based intracellular membraneless organelles. Also, the biosynthesis of tough biomaterials such as silks or marine adhesives is partially based on coacervates.[33−36] These natural coacervate systems combine quite ideal functional properties such as molecular recognition, partitioning of bioactive molecules, self-assembly, processability, good wetting, low viscosity, and many more. Therefore, in recent years, synthetic polymer-based coacervates have attracted renewed interest in different areas, including food formulations, cosmetics, or as a means of drug delivery and improving drug stability.[37−39] The involved macromolecules are typically charged and phase-separated via multivalent, electrostatic interactions between polyanionic and polycationic segments. There is a large body

**Received:** January 12, 2023
**Revised:** April 17, 2023
**Published:** May 3, 2023

**Table 1. Synthesis Details of the PPFP-Derived Polyelectrolytes and Glyco-polyelectrolytes, Composition of the Reaction Mixture, and Reaction Conditions**

| sample | reaction mixture | reaction conditions |
|---|---|---|
| $P_{100}$+ | PPFP (0.84 mmol), triethylamine (2.9 mmol), and ethylenediamine (63 mmol) | add all reactants to 4 mL of DMF and react at 40°C for 2.5 h |
| $P_{100}$− | PPFP (0.84 mmol), triethylamine (2.9 mmol), and glycine (1.7 mmol) | mix PPFP and TEA in 4 mL of DMF, then add pre-dissolved glycine in 1 mL of water, and react at 40°C for 2.5 h |
| $P_{100}$−Man/$P_{100}$−Gal | PPFP (0.84 mmol), triethylamine (2.9 mmol), mannose (Man) or galactose (Gal) oligomer (0.042 mmol), and glycine (1.7 mmol) | mix PPFP, TEA, and Man/Gal oligomer in 5 mL of DMF, react at 40 °C for 18 h, then add pre-dissolved glycine in 1 mL of water, and react at 40 °C for 2.5 h |

**Scheme 1. Synthesis of Polyelectrolyte Structures**

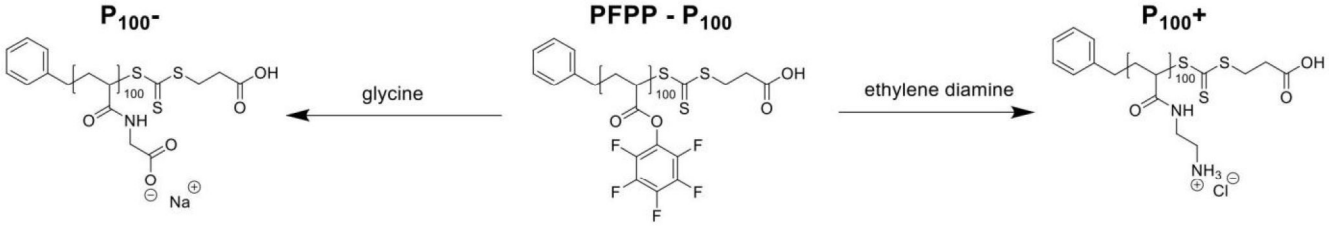


of work describing the phase behavior of polyanion and polycation mixtures that form so-called complex coacervates. More recent work has focused on emulating the functional properties of protein-based coacervates using polyelectrolytes.[40−44] Further recent examples are the phase separation into multiple stable subphases,[45−48] alteration and control of protein functions in liquid condensates,[49] partitioning of bioactive compounds,[50,51] as well as the conservation or killing of pathogens.[52−55]

Here, we present glycan-functionalized polyelectrolytes with the ability to form dense coacervate phases. Thus, we introduce molecular recognition motifs to macromolecules with well-established liquid−liquid phase-separation behavior. The charged glycopolymers are derived from poly(active esters) to enable readily tunable carbohydrate functionalization and labeling. Next, the coacervates as a new class of high-avidity glyco-material will be tested regarding specific binding with a carbohydrate-binding protein and bacteria. Furthermore, the effect of formulating the coacervates and the role of ionic interactions in carbohydrate-mediated binding will be discussed.

## 2. EXPERIMENTAL SECTION

**2.1. Synthesis of Glyco-oligomers.** The oligomer scaffolds were prepared via solid phase assembly of tailor-made building blocks employing the Fmoc strategy using an automated peptide synthesizer (CSBio, USA), as established previously.[56] Building blocks and carbohydrate azides were synthesized based on the literature,[57−59] Fmoc-Lys(Boc)-OH and 1-ethynyl-4-(1,2,2-triphenylethenyl) benezene (TPE) dyes were acquired from BLD Pharmatech GmbH, Germany. As a solid support, a Tentagel SRAM resin (Rapp Polymere, Gemany) was used. Boc deprotection, TPE dye coupling, and copper click reactions were performed manually after peptide synthesis (further details, see Supporting Information Section 2.1). Oligomers were analyzed via $^1$H NMR and RP-HPLC-MS (see Figures S1−S8).

**2.2. Synthesis of Polyelectrolytes and Glyco-polyelectrolytes.** Pentafluorophenyl acrylate (PFPA) was synthesized according to the literature.[60] Briefly, RAFT polymerization was performed by mixing PFPA (21 mmol), 3-(((benzylthio)carbonothioyl)thio)-propanoic acid (RAFT agent) (0.2 mmol), and AIBN (0.042 mmol) in 20 mL of benzene. The mixture was purged by nitrogen and heated to 70 °C for 24 h. The polymerization was stopped by using liquid nitrogen, followed by precipitating the polymer in *n*-hexane. Poly(pentafluorophenyl) active ester (PPFP) was analyzed via GPC, $^1$H NMR, and $^{19}$F NMR (see Figures S9−S13, Tables S2, and S3).

Next, polyelectrolytes were synthesized via polymer analogous reactions. For polycations, PPFP was reacted with ethylenediamine for polyanions with glycine (Sigma-Aldrich, Germany). To obtain the carbohydrate-containing polyanions, 5 mol % of mannose or galactose oligomer was added to PPFP before the remaining active ester groups were replaced with glycine, see Table 1 for details. For cleanup, reaction solutions were adjusted to pH 7 using HCl and NaOH and purified by VivaSpin (MWCO 3 kDa, Fisher Scientific, Germany). The structures of the final glyco-polyelectrolytes and carbohydrate functionalization degrees were determined by $^1$H and $^{19}$F NMR (see Figures S14−S21).

**2.3. Coacervation Assays.** Stock solutions of $P_{100}$− and $P_{100}$+ were prepared with the following concentrations: 200, 100, 40, 20, 10, 4, and 2 mM (based on the repeat unit average molecular weight). Stock solutions of sodium chloride with concentrations between 400 and 4000 mM in 200 mM steps and 100 and 50 mM were prepared. For each measurement, 12.5 μL NaCl solution, 6.75 μL $P_{100}$−, and 6.75 μL $P_{100}$+ were added and mixed. Mixtures were transferred into 384-well plates (Greiner, Germany) and observed under a microscope after 30 min of equilibration at room temperature.

**2.4. Lectin-Binding Assay.** For the ConA-binding assays, the preparation was performed according to previous work.[50] Polyelectrolyte stock solutions of 10 mM (based on the average repeat unit weight) and a lectin-binding buffer (LBB, 0.25 M HEPES, 1.25 M NaCl, 25 mM $CaCl_2$, 25 mM $MnCl_2$, pH 7.4) were prepared. A stock solution containing 2 mg mL$^{-1}$ of ConA labeled with Alexa 647 (Thermo-Fisher, Germany) in 4× diluted LBB was prepared. For the measurement, 23.5 μL of MilliQ and 4 μL of LBB were prepared. Then 35 μL of each of the polyelectrolytes and 2.5 μL of ConA were added. The order of polyanion/polycation/ConA addition for preparing the mixtures was varied. Between each addition, the solution was shaken. Afterward, the samples were examined by fluorescence microscopy. Subsequently, the coacervate phases were separated by centrifugation (10,000 RCF for 15 min, cooled at 20 °C), and the supernatant was analyzed via microplate reading at 665 nm on a 384 clear bottom well plate to quantify residual ConA in the continuous phase.

**2.5. Bacterial Binding Assays.** *Escherichia coli* (PKL1162) were prepared and cultivated as described previously.[28] Bacteria were separated from growth media by centrifugation (3000 RCF for 5 min) and washed three times with 4× diluted LBB to obtain a clean dispersion (4 mg/mL). 0.5 μL ultra-pure water, 0.75 μL of LBB, 8.75 μL of each polyelectrolyte (10 mM) and 6.25 μL of the *E. coli*


https://doi.org/10.1021/acs.biomac.3c00046
Biomacromolecules 2023, 24, 2532−2540

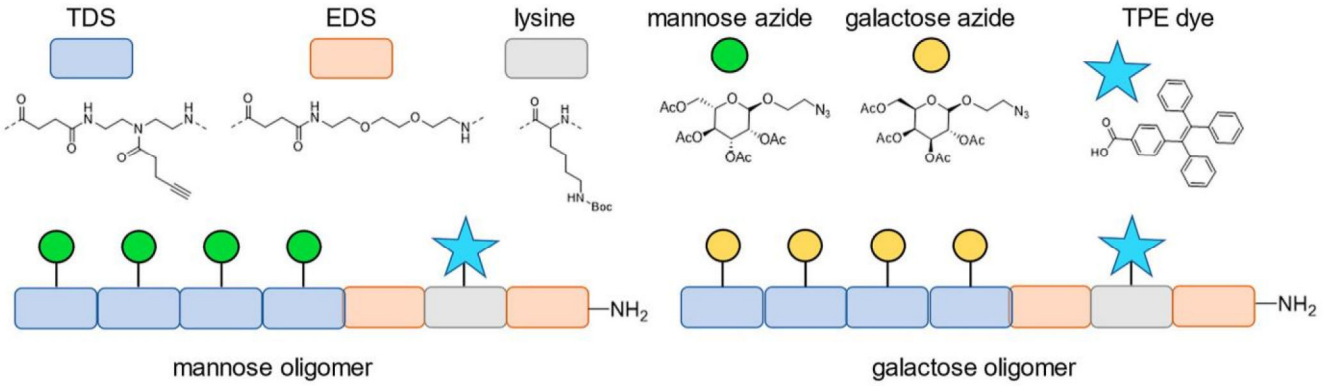


**Figure 1.** Overview of the utilized building blocks, amino acids, TPE dye, and synthesized glyco-oligomers. TDS: triple bond-functionalized diethylenetriamine coupled with the succinic anhydride building block and EDS ethylenedioxy building block.

**Scheme 2. Synthesis of Glyco-polyelectrolyte Structures**

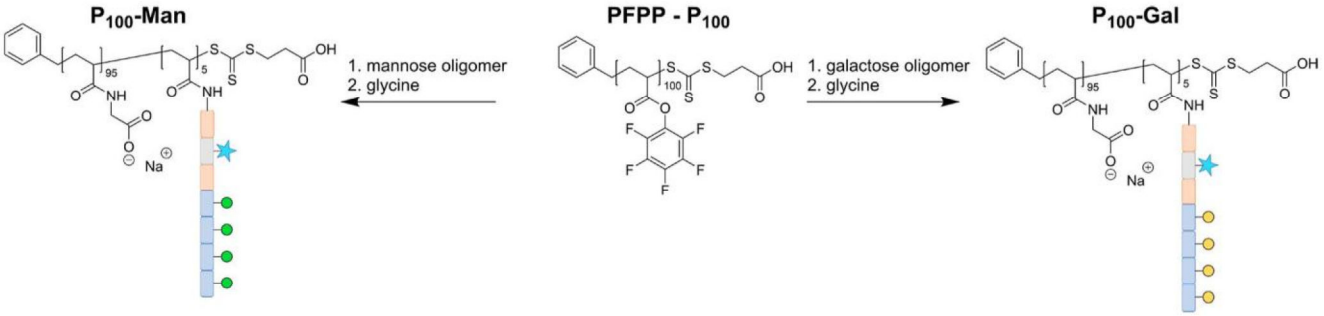


solution were mixed in an Eppendorf tube before examination under the microscope.

## 3. RESULTS

**3.1. Synthesis of Polyelectrolytes.** We started out by preparing the polymeric active ester PFPP via RAFT polymerization to achieve a low dispersity of 1.1 at a polymerization degree of 100 (see Supporting Information S11 for GPC analysis). Next, to obtain polyanions and polycations, the PFP groups were substituted with glycine or with ethylenediamine via polymer analogue reactions, giving the polyanion ($P_{100}-$) and, respectively, the polycation ($P_{100+}$), see Scheme 1. Using this approach, all PFP groups were converted into charged residues, as confirmed by $^{19}F$ NMR and by analyzing the number of repeating units via $^{1}H$ NMR (Supporting Information Figures S14–S17).

To be able to prepare carbohydrate-containing polyelectrolytes, mannose and galactose-bearing oligomers were prepared by solid phase synthesis (Figure 1). The solid phase synthesis approach was chosen to obtain multivalent, more strongly binding carbohydrate ligands. Additionally, the luminophore TPE was introduced to test the molecular flexibility in the coacervate phases. TPE undergoes aggregation-induced emission, i.e., light emission is increased when the molecular mobility is impaired. The building blocks EDS (red, Figure 1), TDS (blue), and Fmoc-Lys(Boc)-OH (gray) were coupled using standard Fmoc peptide coupling chemistry on an automated peptide synthesizer until the oligomer backbone was completed. Afterward, the Boc protective group on the lysine residue was selectively removed on support, and TPE was coupled to the lysine side chain.

To introduce the glyco-oligomers, the batch was divided, and via copper click reaction, one part was conjugated with mannose azide and the other with galactose azide via the alkyne bearing TDS building block. To avoid side reactions, carbohydrate azide building blocks were acetylated. The substitution of PFP groups with the terminal amine group of the glyco-oligomers was similar to the preparation of the pure polyelectrolytes $P_{100}+$ and $P_{100}-$. The mannose and galactose oligomers were incorporated in a 5% ratio with respect to the glycine units with the goal to obtain polyelectrolytes $P_{100}-$Man and $P_{100}-$Gal at a glycine/carbohydrate ratio of 95/5. The reason for functionalizing the polyanion rather than the polycation is that the mannosylated polyanions bind more specifically to the negatively charged targets, *E. coli* bacteria, and ConA (isoelectric point 4.5–5.5). The polycation already binds electrostatically to the negatively charged bacteria and protein surfaces and is thus not suitable for carbohydrate-mediated binding. Complete conversion of the PFP groups was shown via $^{19}F$ NMR, while incorporation of the oligomer into the polymer could be quantified by $^{1}H$ NMR. The final substitution for $P_{100}-$Man was determined to be about 3% for $P_{100}-$Gal to about 4%, which is reasonable, considering 5% would signify a complete incorporation of all added glycooligomers. The final carbohydrate-functionalized polymers $P_{100}-$Man and $P_{100}-$Gal are shown in Scheme 2.

**3.2. Phase Separation and Carbohydrate Binding.** *3.2.1. Phase Separation as a Function of Polymer and Salt Concentration.* For a first insight into the phase behavior of the prepared polymers, solutions of $P_{100}+$ and $P_{100}-$ were mixed under the variation of the polymer concentration and ionic strength and studied by optical microscopy. Combining the polyanions and polycations at identical concentrations


https://doi.org/10.1021/acs.biomac.3c00046
Biomacromolecules 2023, 24, 2532−2540

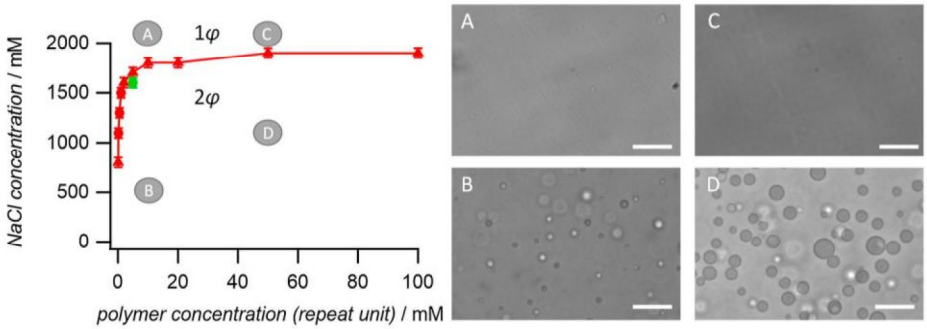


**Figure 2.** Coacervation is affected by the salt and polymer concentrations. Left: Plot of the polymer-dilute part of the phase diagram of the complex coacervate forming polyelectrolytes $P_{100}-$ and $P_{100}+$. The single green data point was determined from $P_{100}-$Gal and $P_{100}+$ mixtures (5 mM) at varying NaCl concentrations. Right: A selection of microscopy images showing the solutions in the one-phase (A,C) and two-phase regime (B,D). Scale bars: 20 $\mu$m.

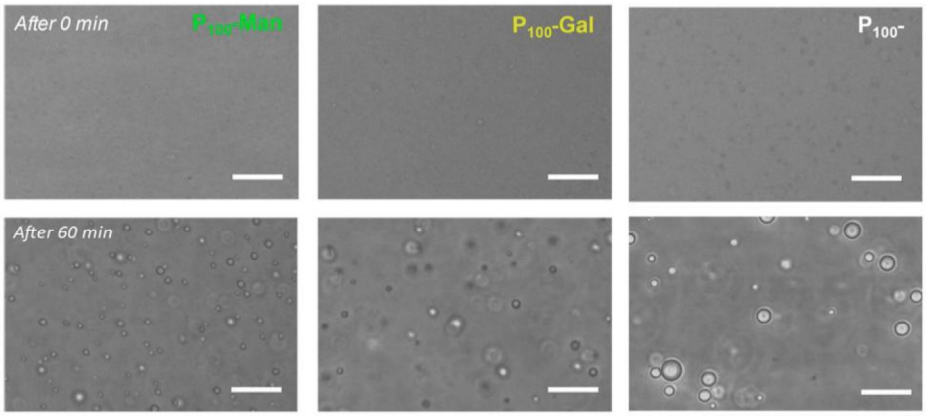


**Figure 3.** Complex coacervation of $P_{100}+$ and the polyanions with carbohydrates ($P_{100}-$Man, $P_{100}-$Gal) results in slower droplet growth compared to coacervation with the full polyanion $P_{100}-$. Scale bars: 20 $\mu$m.

from 0.2 to 100 mM and varying the concentration of added NaCl between 0 and 2 M allowed us to construct the dilute branch of the phase diagram. In the range of very low salt concentrations, liquid–liquid phase separation was present, even at the lowest polymer concentration tested. The addition of salt led to a smaller number of coacervate droplets. Above 1800 mM NaCl for the highest polymer concentrations, phase separation was absent, giving an estimate of the critical salt concentration.

The complex coacervation behavior of $P_{100}+$ and $P_{100}-$ (Figure 2) implies that droplets will also be formed in physiological buffers with an ionic strength in the 150 mM range. This was confirmed by the droplet formation of $P_{100}+$ and $P_{100}-$Man/Gal in lectin-binding buffer (LBB), see Figure 3. However, the addition of a carbohydrate unit to the polyanionic led to a slower droplet growth and a slightly lower estimated critical salt concentration when compared to the unmodified polyanion (Figure 2, green datapoint).

As a side note, the TPE group introduced as a fluorescent label undergoes aggregation-induced emission and was supposed to show a potential restriction of molecular flexibility in the phase-separated state of the polymers. The emission remained very low in the coacervate droplets (data not shown), signifying the absence of TPE and high molecular flexibility and confirming the liquid-like nature of the condensates.

*3.2.2. ConA-Binding Assay.* After studying the phase separation behavior, we tested if the carbohydrate-modified polyelectrolytes were able to bind and enrich carbohydrate-binding species in the coacervate droplets. As a carbohydrate-binding protein, we used ConA, a well-established mannose-binding lectin that does not bind to Gal. ConA was fluorescently labeled, and the formed coacervate droplets were studied by fluorescence microscopy to detect a potential enrichment of ConA in the polymer-rich phase because of carbohydrate binding (Figure 4). The polyelectrolytes and ConA were mixed, varying the order of addition. This allowed testing for potential differences in binding when ConA first encounters the already formed coacervate droplets (Figure 4A) or in homogeneous solution before the coacervate formation. the polycation (Figure 4B), or polyanion with Man or Gal (Figure 4C). Indeed, ConA was enriched in droplets containing the mannose-functionalized polyanion $P_{100}-$Man, as observed by an increase in fluorescence. The droplets containing the Gal-functionalized polymer $P_{100}-$Gal showed only a very weak ConA enrichment in the droplets. On the other hand, carbohydrate-free droplets formed by the polyanion $P_{100}$ also showed readily detectable ConA absorption. However, here ConA is detected only at the periphery of the droplets. The fluorescence intensity at the periphery was not as strong as for the mannose-containing coacervates, which appear to have taken up significantly more ConA due to the mannose motif. Similar results were obtained when changing the addition order of the three components—a polyanion, a polycation, and ConA (Figure S22).



https://doi.org/10.1021/acs.biomac.3c00046
Biomacromolecules 2023, 24, 2532−2540

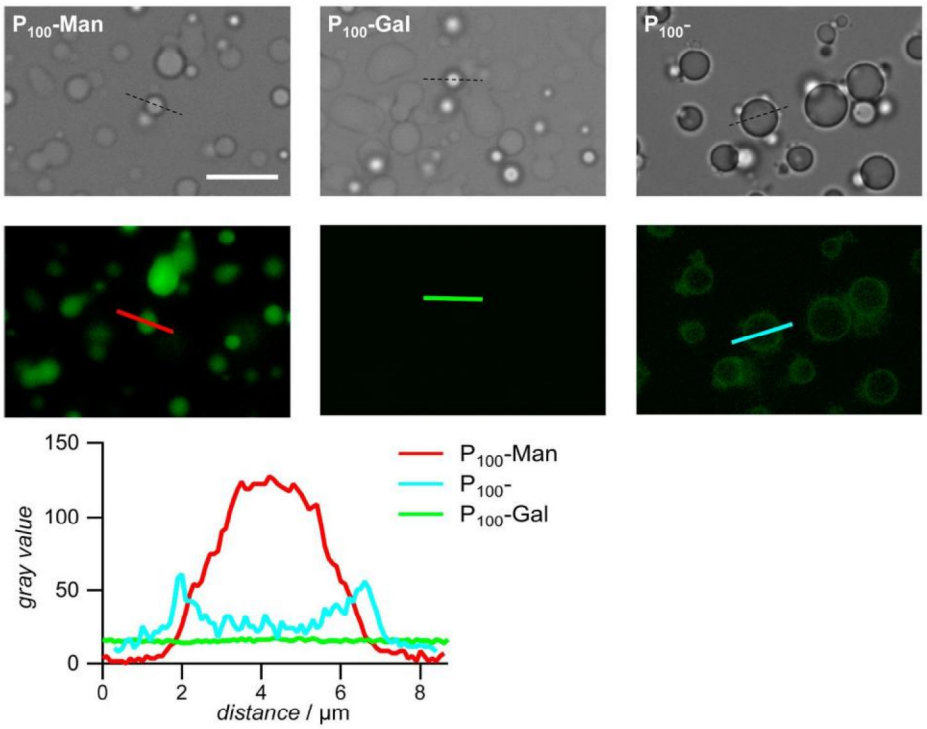


**Figure 4.** Micrographs of the droplets formed by $P_{100}$+ and the polyanions $P_{100}$−Man, $P_{100}$−Gal, and $P_{100}$− in the presence of fluorescently labeled ConA: the upper images in each group were taken by transmission microscopy and the bottom images by fluorescence microscopy detecting ConA emission (false coloring). Scalebar: 10 $\mu$m (see the top left image, applies to all images).

To quantify the amount of coacervate-associated ConA, the polymer-rich phase was separated from the polymer-depleted phase by centrifugation, and the supernatant was analyzed to detect non-bound ConA (Figure 5). In line with microscopy results, the smallest amount of non-bound ConA was found for mannose-containing complex coacervates. In addition, coacervate phases formed with no carbohydrates were able to bind more ConA when compared to Gal-containing phases. Again, the order of polymer and ConA addition did not seem to affect the ConA capture strongly (Figure S22). Thus, it could be determined that the mannose-containing coacervates bound most ConA due to specific carbohydrate interactions. Coacervates without glycans also bound substantial amounts of ConA non-specifically to a much larger degree when compared to the galactose-containing system.

*3.2.3. Bacterial Binding Assays.* Next, the interaction of mannose-binding *E. coli* bacteria with the coacervate droplets was tested. Here, we assessed the possibility of using liquid−liquid phase-separated materials to specifically capture or engulf bacteria, which could lead to new concepts in the fight against infections. *E. coli* binds to mannose units via the lectin FimH positioned at hair-like fimbriae coating the bacteria.[61] With FimH, we could expect a ConA-like binding behavior to coacervate droplets since FimH also does not bind to galactose. The bacteria express the GFP-tag to make them visible under the fluorescence microscope in the presence of pre-formed coacervate droplets (Figure 6). Binding of *E. coli* to coacervate droplets was present in the case of using $P_{100}$−Man or $P_{100}$− as a polyanion. No binding was seen in the case of $P_{100}$−Gal, even if the bacteria swim into direct contact with the coacervate droplets (Figure 7), see the Supporting Information for videos). Upon inhibition with methyl $\alpha$-D-mannose (MeMan), a well-known FimH binding molecule, the mannose-binding sites are blocked and *E. coli* cannot bind to mannosylated surfaces anymore.[28] Indeed, when MeMan was added, *E. coli* did not bind to $P_{100}$−Man containing coacervate droplets, but binding to $P_{100}$− containing coacervates without mannose units was still possible (Figure 6b). We further noted that the bacteria were bound independently of the coacervate droplet size. The droplet size increased over time, as was seen already when analyzing the phase behavior (Figure 4). As the droplets grow and form a sediment, wetting and droplet spreading on the glass surface of the fluid cell occur. The bacteria were also immobilized by this coacervate surface layer containing $P_{100}$−, $P_{100}$−Man but not in the case of $P_{100}$−Gal.

Thus, *E. coli* attachment to the surface of the coacervates can be attributed on the one hand to the mannose-mediated binding and on the other hand to the charge−charge interactions. Such charge−charge interactions are very likely due to the negatively charged surface of the bacteria and the presence of the polycation $P_{100}$+. Zeta potential measurements showed a reversal of *E. coli* surface charge when treating the bacteria in a solution of the $P_{100}$+ (Table 2, Supporting Information Section 3.2). Of note, by exposing the bacteria to solutions containing the polyanions before the zeta potential measurements, the negative surface charge was increased further. This suggests that *E. coli* always binds to the polycation $P_{100}$+, which was permanently present to a certain extent in the continuous phase of the droplet solutions. Consequently, binding to polycations also implies that *E. coli* binds to polyanions, so the bacteria should attach to any polyelectrolyte coacervate droplets. However, this was not the case for the carbohydrate-containing coacervates when including the non-binding galactose or when inhibiting the mannose-FimH interaction.



https://doi.org/10.1021/acs.biomac.3c00046
Biomacromolecules 2023, 24, 2532−2540

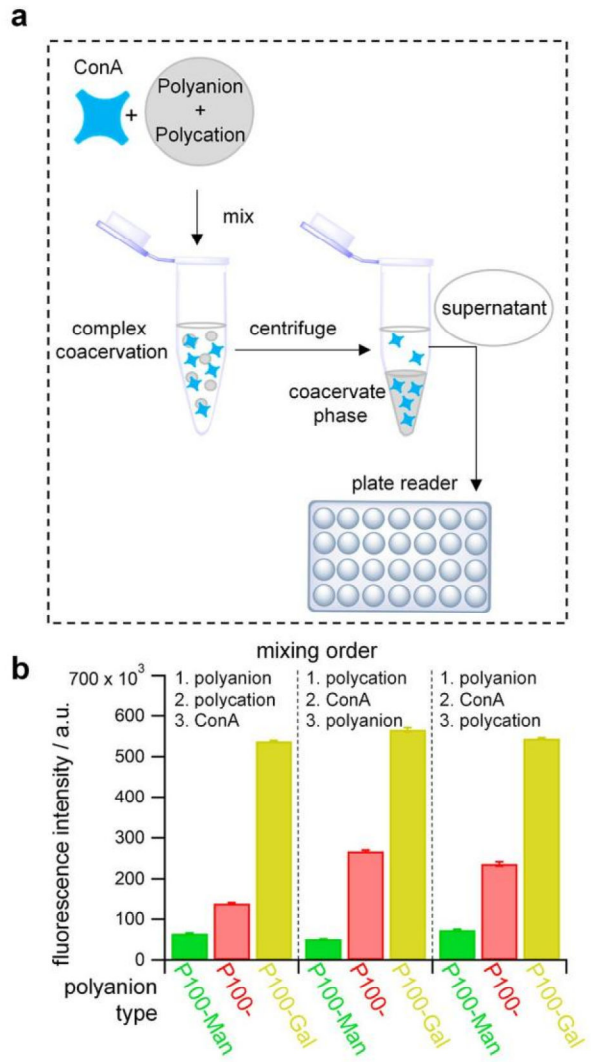


**Figure 5.** Quantification of the ConA binding to the coacervate droplets by detecting unbound ConA in the supernatant. (A) Sketch of the experiment; (B) relative amount of the residual, non-captured ConA in the supernatant. The data represent averages over five measurements.

## 4. DISCUSSION

The phase diagram of the pure polycation $P_{100}$+ and polyanion $P_{100}$− mixture gave a critical salt concentration of around 1.8 M, which appears to be consistent with the literature with respect to the charge density and the presence of additional motifs such as amide groups in the polymer.[62] The addition of carbohydrate units on the polyanion resulted only in a minor decrease in the critical salt concentration. This is to be expected since replacing ∼4% charged residues with carbohydrate units resulted only in a small decrease of the charge density. Furthermore, the observed slower droplet growth for the carbohydrate-functionalized systems could hint at a lower surface tension or a higher viscosity of the droplets. Both parameters were not measured here, but it could be argued that the additional hydrophilic and uncharged sugar units lower the surface tension by enriching at the periphery of the droplets to maximize the charge−charge interactions in the droplet interior.

Studying the droplets in the presence of the mannose-binding species ConA and *E. coli* showed that polyelectrolyte-derived coacervates can be used as a new type of material with specific carbohydrate interactions. First, it was found that the mannose-containing coacervates bound most ConA, while pure polyelectrolyte-coacervates without glycan units bound ConA to a much lower degree and only at the periphery of the droplets. Droplets with the non-binding sugar galactose showed an even lower take-up of ConA. This agrees with *E. coli*-binding studies that also showed no binding in the case of the galactose droplets but for mannose- and pure polyelectrolyte droplets. The binding of ConA and *E. coli* to the pure polyelectrolyte droplets without sugars is most likely driven by charge−charge interactions, as was observed also for other polyelectrolyte/protein coacervates.[38,51] For the mannose-containing droplets, the stronger ConA uptake and the fact that the *E. coli* immobilization could be inhibited by the addition of MeMan show that specific carbohydrate interactions were involved. Moreover, binding of ConA to mannose units at the droplet interface appears to form $P_{100}$−Man/ConA complexes that are taken-up entirely, leading to a homogeneous distribution of ConA in the droplets.

The galactose-containing droplets or mannose droplets under inhibiting conditions by the addition of MeMan showed strongly reduced binding. It could be argued that their overall lower charge density compared to the pure polyanions results in a reduced charge−charge-binding capability. Nevertheless, the glycan-presenting polyanions are still highly charged considering the low functionalization degree of 4% and taking into account the only minor decrease in the critical salt concentration compared to the pure polyelectrolyte. Thus, the strongly reduced binding of the galactose and inhibited mannose systems was likely not caused by this slightly reduced charge density. Alternatively, the galactose and mannose units were likely positioned at the interface of the droplets due to the lower interaction potential of the uncharged carbohydrates compared to the charged residues in the droplet interior. The non-binding carbohydrate layer leads to steric shielding of charge−charge interactions with the protein and bacteria at the droplet surface, which lowers their uptake. Such steric repulsion effects of glycans are quite common, for example, at the cell glycocalyx and are used for the design of antiviral/antibacterial glycopolymer drugs.[5,23] Also, the enrichment of ConA at the periphery of the pure glycan-free polyelectrolyte droplets (Figure 4, right) suggests such surface effects. Similar protein surface enrichment was found in different complex coacervate/protein systems[49,63] and explained by either a net surface charge of the droplets or partitioning of non-charged residues at the interface. In addition, electrostatically self-assembled block copolymers with uncharged carbohydrate segments were also shown to present the carbohydrates at the periphery.[31] Overall, it appears that introducing non-binding glycans leads to a strong reduction in charge-based interactions, potentially because of the enrichment of uncharged sugar units at the droplet interface. However, a direct confirmation of surface enrichment and a quantification of related effects such as the reduction of droplet surface tension and charge density could not be given at this stage.

## 5. CONCLUSIONS

Here, we established phase-separating glycan-functionalized polyelectrolytes and confirmed that the formed liquid condensates can undergo specific interactions with carbohy-


https://doi.org/10.1021/acs.biomac.3c00046
Biomacromolecules 2023, 24, 2532−2540

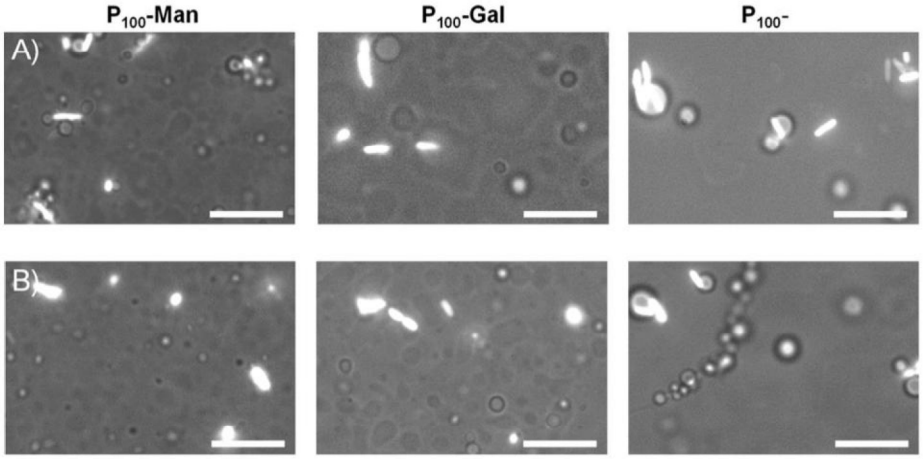


**Figure 6.** Coacervate droplets with *E. coli* bacteria observed under the fluorescence microscope. The coacervate phases were formed with different polyanions: $P_{100}$−Man (left), $P_{100}$−Gal (middle), and $P_{100}$− (right). (A) *E. coli* in the presence of coacervates without inhibitor. The bacteria stick to $P_{100}$−Man and $P_{100}$− containing droplets but not to $P_{100}$−Gal. (B) In the presence of MeMan as an inhibitor, *E. coli* do not stick to $P_{100}$−Man droplets but still bind to $P_{100}$− droplets. Scale bars: 10 $\mu$m.

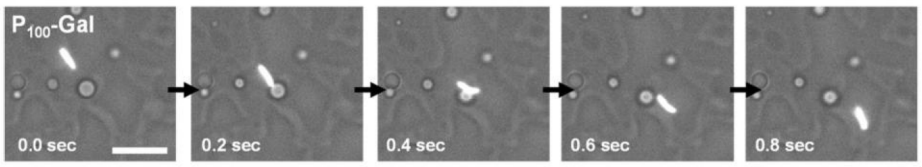


**Figure 7.** Fluorescence microscope time series of a bacterium making contact with a $P_{100}$−Gal-containing droplet while remaining motile within the coacervate solution. Videos shown in the Supporting Information give a more distinct impression of the bound or motile state of *E. coli*. Scale bar: 10 $\mu$m.

**Table 2. Zeta Potential of *E. coli* and the Effect of Treatment with the Polyelectrolytes Prior to the Measurement**

| | *E. coli*/$H_2O$ | *E. coli*/$P_{100}$− | *E. coli*/$P_{100}$−Man | *E. coli*/$P_{100}$−Gal | *E. coli*/$P_{100}$+ |
|---|---|---|---|---|---|
| zeta potential | −53 ± 2 mV | −77 ± 1 mV | −63 ± 1 mV | −50 ± 4 mV | 42 ± 3 mV |

drate-binding proteins or bacteria. Mannose-binding *E. coli* and ConA were shown to interact more strongly with mannose-functionalized coacervate droplets, whereas no binding was found under inhibiting conditions and for galactose functionalization. These species were also bound to unfunctionalized, glycan free polyelectrolyte coacervates, likely due to charge−charge interactions. The degree of specific binding of the carbohydrate-functionalized, but still highly charged, polyelectrolyte droplets was quite surprising. An explanation could not yet be given here, but future work will look at a possible surface enrichment of carbohydrate units at the droplet surface and other explanations. Lastly, the polymer analogous reactions of a poly(active ester) proved to be quite advantageous to combine the charged groups and carbohydrate units. This approach might be easily adapted to introduce other specifically interacting residues, cross-linkers, labels, etc. to investigate the molecular mechanism of liquid−liquid phase separation or to design new functional materials.

## ■ ASSOCIATED CONTENT

### Supporting Information

The Supporting Information is available free of charge at https://pubs.acs.org/doi/10.1021/acs.biomac.3c00046.

Details on synthesis, analytical data, materials, and instruments (PDF)

Motility of *E. coli* in the case of $P_{100}$− (MP4)

Motility of *E. coli* in the case of $P_{100}$−Man (MP4)

Non-motility of *E. coli* in the case of $P_{100}$−Gal (MP4)

## ■ AUTHOR INFORMATION


### Corresponding Authors

**Stephan Schmidt** − *Institute of Organic Chemistry and Macromolecular Chemistry, Heinrich-Heine-Universität Düsseldorf, 40225 Düsseldorf, Germany; Institute of Macromolecular Chemistry, Albert-Ludwigs-Universität Freiburg, 79104 Freiburg, Germany;* orcid.org/0000-0002-4357-304X; Email: stephan.schmidt@makro.uni-freiburg.de

**Laura Hartmann** − *Institute of Organic Chemistry and Macromolecular Chemistry, Heinrich-Heine-Universität Düsseldorf, 40225 Düsseldorf, Germany; Institute of Macromolecular Chemistry, Albert-Ludwigs-Universität Freiburg, 79104 Freiburg, Germany;* orcid.org/0000-0003-0115-6405; Email: laura.hartmann@makro.uni-freiburg.de

### Authors

**Michele Denise Illmann** − *Institute of Organic Chemistry and Macromolecular Chemistry, Heinrich-Heine-Universität Düsseldorf, 40225 Düsseldorf, Germany;* orcid.org/0000-0003-4249-5155

**Lea Schäfl** − *Institute of Organic Chemistry and Macromolecular Chemistry, Heinrich-Heine-Universität*




https://doi.org/10.1021/acs.biomac.3c00046
Biomacromolecules 2023, 24, 2532−2540

*Düsseldorf, 40225 Düsseldorf, Germany;* orcid.org/0000-0002-6055-7893

**Felicitas Drees** − *Institute of Organic Chemistry and Macromolecular Chemistry, Heinrich-Heine-Universität Düsseldorf, 40225 Düsseldorf, Germany; Institute of Macromolecular Chemistry, Albert-Ludwigs-Universität Freiburg, 79104 Freiburg, Germany*

Complete contact information is available at: https://pubs.acs.org/10.1021/acs.biomac.3c00046

### Notes

The authors declare no competing financial interest.

## ■ ACKNOWLEDGMENTS

The authors acknowledge funding by the German Research foundation (DFG) in the projects SCHM 2748/7-1 and SCHM 2748/8-1.

## ■ REFERENCES

(1) Varki, A. *Essentials of Glycobiology*; Cold Spring Harbor Laboratory Press, 2017.

(2) Dwek, R. A. Glycobiology: Toward Understanding the Function of Sugars. *Chem. Rev.* **1996**, *96*, 683−720.

(3) Ofek, I.; Mirelman, D.; Sharon, N. Adherence of Escherichia coli to human mucosal cells mediated by mannose receptors. *Nature* **1977**, *265*, 623−625.

(4) Imberty, A.; Varrot, A. Microbial recognition of human cell surface glycoconjugates. *Curr. Opin. Struct. Biol.* **2008**, *18*, 567−576.

(5) Gerling-Driessen, U. I. M.; Hoffmann, M.; Schmidt, S.; Snyder, N. L.; Hartmann, L. Glycopolymers against pathogen infection. *Chem. Soc. Rev.* **2023**, *52*, 2617−2642, DOI: 10.1039/D2CS00912A.

(6) Lee, R. T.; Lee, Y. C. Affinity enhancement by multivalent lectin−carbohydrate interaction. *Glycoconjugate J.* **2000**, *17*, 543−551.

(7) Mammen, M.; Choi, S. K.; Whitesides, G. M. Polyvalent interactions in biological systems: implications for design and use of multivalent ligands and inhibitors. *Angew. Chem., Int. Ed. Engl.* **1998**, *37*, 2754−2794.

(8) Zhao, T.; Terracciano, R.; Becker, J.; Monaco, A.; Yilmaz, G.; Becer, C. R. Hierarchy of Complex Glycomacromolecules: From Controlled Topologies to Biomedical Applications. *Biomacromolecules* **2022**, *23*, 543−575.

(9) Cecioni, S.; Imberty, A.; Vidal, S. Glycomimetics versus Multivalent Glycoconjugates for the Design of High Affinity Lectin Ligands. *Chem. Rev.* **2015**, *115*, 525−561.

(10) Bhattacharya, K.; Kalita, U.; Singha, N. K. Tailor-made glycopolymers via reversible deactivation radical polymerization: design, properties and applications. *Polym. Chem.* **2022**, *13*, 1458−1483.

(11) Kim, Y.; Hyun, J. Y.; Shin, I. Multivalent glycans for biological and biomedical applications. *Chem. Soc. Rev.* **2021**, *50*, 10567−10593.

(12) Bojarova, P.; Kren, V. Sugared biomaterial binding lectins: achievements and perspectives. *Biomater. Sci.* **2016**, *4*, 1142−1160.

(13) Thalji, M. R.; Ibrahim, A. A.; Chong, K. F.; Soldatov, A. V.; Ali, G. A. M. Glycopolymer-Based Materials: Synthesis, Properties, and Biosensing Applications. *Top. Curr. Chem.* **2022**, *380*, 45.

(14) Behren, S.; Westerlind, U. Novel Approaches To Design Glycan-Based Antibacterial Inhibitors. *Eur. J. Org. Chem.* **2022**, *26*, No. e202200795.

(15) Yilmaz, G.; Becer, C. R. Glycopolymer code based on well-defined glycopolymers or glyconanomaterials and their biomolecular recognition. *Front. Bioeng. Biotechnol.* **2014**, *2*, 39.

(16) Gestwicki, J. E.; Cairo, C. W.; Strong, L. E.; Oetjen, K. A.; Kiessling, L. L. Influencing Receptor−Ligand Binding Mechanisms with Multivalent Ligand Architecture. *J. Am. Chem. Soc.* **2002**, *124*, 14922−14933.

(17) Kiessling, L. L.; Grim, J. C. Glycopolymer probes of signal transduction. *Chem. Soc. Rev.* **2013**, *42*, 4476−4491.

(18) Bernardi, A.; Jiménez-Barbero, J.; Casnati, A.; De Castro, C.; Darbre, T.; Fieschi, F.; Finne, J.; Funken, H.; Jaeger, K.-E.; Lahmann, M.; et al. Multivalent glycoconjugates as anti-pathogenic agents. *Chem. Soc. Rev.* **2013**, *42*, 4709−4727.

(19) Bhatia, S.; Dimde, M.; Haag, R. Multivalent glycoconjugates as vaccines and potential drug candidates. *Medchemcomm* **2014**, *5*, 862−878.

(20) Muller, C.; Despras, G.; Lindhorst, T. K. Organizing multivalency in carbohydrate recognition. *Chem. Soc. Rev.* **2016**, *45*, 3275−3302.

(21) Hudak, J. E.; Bertozzi, C. R. Glycotherapy: new advances inspire a reemergence of glycans in medicine. *Chem. Biol.* **2014**, *21*, 16−37.

(22) Soria-Martinez, L.; Bauer, S.; Giesler, M.; Schelhaas, S.; Materlik, J.; Janus, K.; Pierzyna, P.; Becker, M.; Snyder, N. L.; Hartmann, L.; et al. Prophylactic Antiviral Activity of Sulfated Glycomimetic Oligomers and Polymers. *J. Am. Chem. Soc.* **2020**, *142*, 5252−5265.

(23) Jacobi, F.; Wilms, D.; Seiler, T.; Queckborner, T.; Tabatabai, M.; Hartmann, L.; Schmidt, S. Effect of PEGylation on Receptor Anchoring and Steric Shielding at Interfaces: An Adhesion and Surface Plasmon Resonance Study with Precision Polymers. *Biomacromolecules* **2020**, *21*, 4850−4856.

(24) Wang, Y.; Kotsuchibashi, Y.; Liu, Y.; Narain, R. Study of Bacterial Adhesion on Biomimetic Temperature Responsive Glycopolymer Surfaces. *ACS Appl. Mater. Interfaces* **2015**, *7*, 1652−1661.

(25) Tang, J. S. J.; Rosencrantz, S.; Tepper, L.; Chea, S.; Klopzig, S.; Kruger-Genge, A.; Storsberg, J.; Rosencrantz, R. R. Functional Glyco-Nanogels for Multivalent Interaction with Lectins. *Molecules* **2019**, *24*, 1865.

(26) von der Ehe, C.; Bus, T.; Weber, C.; Stumpf, S.; Bellstedt, P.; Hartlieb, M.; Schubert, U. S.; Gottschaldt, M. Glycopolymer-Functionalized Cryogels as Catch and Release Devices for the Pre-Enrichment of Pathogens. *ACS Macro Lett.* **2016**, *5*, 326−331.

(27) Schmidt, S.; Paul, T. J.; Strzelczyk, A. K. Interactive Polymer Gels as Biomimetic Sensors for Carbohydrate Interactions and Capture-Release Devices for Pathogens. *Macromol. Chem. Phys.* **2019**, *220*, 1900323.

(28) Paul, T. J.; Strzelczyk, A. K.; Feldhof, M. I.; Schmidt, S. Temperature-Switchable Glycopolymers and Their Conformation-Dependent Binding to Receptor Targets. *Biomacromolecules* **2020**, *21*, 2913−2921.

(29) Wilms, D.; Muller, J.; Urach, A.; Schroer, F.; Schmidt, S. Specific Binding of Ligand-Functionalized Thermoresponsive Microgels: Effect of Architecture, Ligand Density, and Hydrophobicity. *Biomacromolecules* **2022**, *23*, 3899−3908.

(30) Siirila, J.; Hietala, S.; Ekholm, F. S.; Tenhu, H. Glucose and Maltose Surface-Functionalized Thermoresponsive Poly(N-Vinylcaprolactam) Nanogels. *Biomacromolecules* **2020**, *21*, 955−965.

(31) Yuan, F.; Wang, S.; Lu, W.; Chen, G.; Tu, K.; Jiang, H.; Wang, L.-Q. Facile preparation of cancer-specific polyelectrolyte nanogels from natural and synthetic sugar polymers. *J. Mater. Chem. B* **2015**, *3*, 4546−4554.

(32) Chen, K.; Bao, M.; Muñoz Bonilla, A.; Zhang, W.; Chen, G. A biomimicking and electrostatic self-assembly strategy for the preparation of glycopolymer decorated photoactive nanoparticles. *Polym. Chem.* **2016**, *7*, 2565−2572.

(33) Malay, A. D.; Suzuki, T.; Katashima, T.; Kono, N.; Arakawa, K.; Numata, K. Spider silk self-assembly via modular liquid-liquid phase separation and nanofibrillation. *Sci. Adv.* **2020**, *6*, No. eabb6030.

(34) Hofman, A. H.; van Hees, I. A.; Yang, J.; Kamperman, M. Bioinspired Underwater Adhesives by Using the Supramolecular Toolbox. *Adv. Mater.* **2018**, *30*, 1704640.

(35) Baer, A.; Schmidt, S.; Haensch, S.; Eder, M.; Mayer, G.; Harrington, M. J. Mechanoresponsive lipid-protein nanoglobules facilitate reversible fibre formation in velvet worm slime. *Nat. Commun.* **2017**, *8*, 974.

(36) Baer, A.; Hansch, S.; Mayer, G.; Harrington, M. J.; Schmidt, S. Reversible Supramolecular Assembly of Velvet Worm Adhesive Fibers

via Electrostatic Interactions of Charged Phosphoproteins. *Biomacromolecules* **2018**, *19*, 4034−4043.
(37) Johnson, N. R.; Wang, Y. D. Coacervate delivery systems for proteins and small molecule drugs. *Expert Opin. Drug Delivery* **2014**, *11*, 1829−1832.
(38) Black, K. A.; Priftis, D.; Perry, S. L.; Yip, J.; Byun, W. Y.; Tirrell, M. Protein Encapsulation via Polypeptide Complex Coacervation. *ACS Macro Lett.* **2014**, *3*, 1088−1091.
(39) Eghbal, N.; Choudhary, R. Complex coacervation: Encapsulation and controlled release of active agents in food systems. *LWT* **2018**, *90*, 254−264.
(40) Larson, R. G.; Liu, Y.; Li, H. L. Linear viscoelasticity and time-temperature-salt and other superpositions in polyelectrolyte coacervates. *J. Rheol.* **2021**, *65*, 77−102.
(41) Manoj Lalwani, S.; Eneh, C. I.; Lutkenhaus, J. L. Emerging trends in the dynamics of polyelectrolyte complexes. *Phys. Chem. Chem. Phys.* **2020**, *22*, 24157−24177.
(42) Blocher, W. C.; Perry, S. L. Complex coacervate-based materials for biomedicine. *Wiley Interdiscip. Rev.: Nanomed. Nanobiotechnol.* **2017**, *9*, 28.
(43) Sing, C. E.; Perry, S. L. Recent progress in the science of complex coacervation. *Soft Matter* **2020**, *16*, 2885−2914.
(44) Yewdall, N. A.; Andre, A. A. M.; Lu, T. M.; Spruijt, E. Coacervates as models of membraneless organelles. *Curr. Opin. Colloid Interface Sci.* **2021**, *52*, 101416.
(45) Lu, T.; Spruijt, E. Multiphase Complex Coacervate Droplets. *J. Am. Chem. Soc.* **2020**, *142*, 2905−2914.
(46) Mountain, G. A.; Keating, C. D. Formation of Multiphase Complex Coacervates and Partitioning of Biomolecules within them. *Biomacromolecules* **2020**, *21*, 630−640.
(47) Fisher, R. S.; Elbaum-Garfinkle, S. Tunable multiphase dynamics of arginine and lysine liquid condensates. *Nat. Commun.* **2020**, *11*, 4628.
(48) Donau, C.; Späth, F.; Stasi, M.; Bergmann, A. M.; Boekhoven, J. Phase Transitions in Chemically Fueled, Multiphase Complex Coacervate Droplets. *Angew. Chem., Int. Ed. Engl.* **2022**, *61*, No. e202211905.
(49) McCall, P. M.; Srivastava, S.; Perry, S. L.; Kovar, D. R.; Gardel, M. L.; Tirrell, M. V. Partitioning and Enhanced Self-Assembly of Actin in Polypeptide Coacervates. *Biophys. J.* **2018**, *114*, 1636−1645.
(50) Blocher McTigue, W. C.; Perry, S. L. Incorporation of proteins into complex coacervates. *Methods Enzymol.* **2021**, *646*, 277−306.
(51) Lindhoud, S.; Claessens, M. M. A. E. Accumulation of small protein molecules in a macroscopic complex coacervate. *Soft Matter* **2016**, *12*, 408−413.
(52) Mi, X.; Blocher McTigue, W. C.; Joshi, P. U.; Bunker, M. K.; Heldt, C. L.; Perry, S. L. Thermostabilization of viruses via complex coacervation. *Biomater. Sci.* **2020**, *8*, 7082−7092.
(53) Nikolaou, A.; Felipe-Sotelo, M.; Dorey, R.; Gutierrez-Merino, J.; Carta, D. Silver-doped phosphate coacervates to inhibit pathogenic bacteria associated with wound infections: an in vitro study. *Sci. Rep.* **2022**, *12*, 10778.
(54) Peng, Q.; Wu, Q.; Chen, J.; Wang, T.; Wu, M.; Yang, D.; Peng, X.; Liu, J.; Zhang, H.; Zeng, H. Coacervate-Based Instant and Repeatable Underwater Adhesive with Anticancer and Antibacterial Properties. *ACS Appl. Mater. Interfaces* **2021**, *13*, 48239−48251.
(55) Nallamilli, T.; Ketomaeki, M.; Prozeller, D.; Mars, J.; Morsbach, S.; Mezger, M.; Vilgis, T. Complex coacervation of food grade antimicrobial lauric arginate with lambda carrageenan. *Curr. Res. Food Sci.* **2021**, *4*, 53−62.
(56) Shamout, F.; Fischer, L.; Snyder, N. L.; Hartmann, L. Recovery, Purification, and Reusability of Building Blocks for Solid Phase Synthesis. *Macromol. Rapid Commun.* **2020**, *41*, 1900473.
(57) Ponader, D.; Wojcik, F.; Beceren-Braun, F.; Dernedde, J.; Hartmann, L. Sequence-Defined Glycopolymer Segments Presenting Mannose: Synthesis and Lectin Binding Affinity. *Biomacromolecules* **2012**, *13*, 1845−1852.
(58) Ebbesen, M. F.; Gerke, C.; Hartwig, P.; Hartmann, L. Biodegradable poly(amidoamine)s with uniform degradation fragments via sequence-controlled macromonomers. *Polym. Chem.* **2016**, *7*, 7086−7093.
(59) Chen, G.; Tao, L.; Mantovani, G.; Geng, J.; Nyström, D.; Haddleton, D. M. A Modular Click Approach to Glycosylated Polymeric Beads: Design, Synthesis and Preliminary Lectin Recognition Studies. *Macromolecules* **2007**, *40*, 7513−7520.
(60) Boyer, C.; Davis, T. P. One- pot synthesis and biofunctionalization of glycopolymersviaRAFT polymerization and thiol−ene reactions. *Chem. Commun.* **2009**, *40*, 6029−6031.
(61) Wilms, D.; Schroer, F.; Paul, T. J.; Schmidt, S. Switchable Adhesion of E. coli to Thermosensitive Carbohydrate-Presenting Microgel Layers: A Single-Cell Force Spectroscopy Study. *Langmuir* **2020**, *36*, 12555−12562.
(62) Perry, S. L.; Leon, L.; Hoffmann, K. Q.; Kade, M. J.; Priftis, D.; Black, K. A.; Wong, D.; Klein, R. A.; Pierce, C. F., III; Margossian, K. O.; et al. Chirality-selected phase behaviour in ionic polypeptide complexes. *Nat. Commun.* **2015**, *6*, 6052.
(63) Martin, N.; Li, M.; Mann, S. Selective Uptake and Refolding of Globular Proteins in Coacervate Microdroplets. *Langmuir* **2016**, *32*, 5881−5889.


https://doi.org/10.1021/acs.biomac.3c00046
*Biomacromolecules* 2023, 24, 2532−2540

# Supporting information

# Glycan-presenting coacervates derived from charged poly(active esters): preparation, phase behavior and lectin capture

*Michele Denise Illmann*[1], *Lea Schäfl*[1], *Felicitas Drees*[1,2], *Laura Hartmann*[1,2] *and Stephan Schmidt*[1,2*]

[1] Institute of Organic Chemistry and Macromolecular Chemistry, Heinrich-Heine-Universität Düsseldorf, Universitätsstr. 1, 40225 Düsseldorf, Germany

[2] Institute of Macromolecular Chemistry, Albert-Ludwigs-Universität Freiburg, Stefan-Meier-Str. 31, 79104 Freiburg, Germany

*Email: stephan.schmidt@makro.uni-freiburg.de

Contents

## 1. Experimental

### 1.1. Materials

All reagents were used without further purification.
3-(((benzylthio)carbonothioyl)thio)propanoic acid (>98%) was purchased from TCI chemicals. Toluol-4-Sulfonic acid monohydrate (>99%) and acryloyl chloride (≥97%) were purchased from Merck. Benzene (99.5%), potassium carbonate (99%) and calcium chloride (96%) were purchased from PanReac AppliChem. Triethylsilane (99%), pentaflurophenol (99%) and D-Galactose pentaacetate (95%) were purchased from Fluorochem. Diethyl ether (99.5%) was purchased from Honeywell Riedel de Haen. Succinicanhydride (>99%) was purchased from Carbolution Chemicals GmbH. Acetic anhydride (99.5%), methanol (≥99.8%), Amberlite® IR120 H hydrogen form, chloramphenicol (≥98%), ampicillin sodium salt (BioReagent), diethylentriamine (>98%), ethylenedioxybisethylamine (98%), acetone (≥99.5%), tetrahydrofuran (≥99.9%), 2,2′-Azobis(2-methylpropionitrile) (AIBN) (≥98%), sodium sulfate (≥99%), sodium bicarbonate (≥99.7%), manganese(II) chloride (≥96%), sodium ascorbate (≥98%) and VivaSpin (MWCO: 3.000 Mw) were purchased from Sigma-Aldrich. Acetonitrile (≥99.9%), ethylacetate (≥99%), n-hexane (≥95%), 1,4-dioxane (≥99.5%), citric acid (≥99%), glycine (≥99%), trifluoroacetic acid (≥99%), hydrochloric acid, toluene (≥99.7%), triethylamine (≥99%), dichloromethane (≥99.5%) and Cytiva Vivaspin™ 20 (MWCO 3 kDa) were purchased from Fisher Scientific. N,N-Dimethylformamide (≥99.9%) was purchased from Biosolve. Ethyl trifluoracetate (≥99%) was purchased from Apollo Scientific. 4-pentynoic acid (≥95%), bromethanole (≥97%), magnesium sulfate (99%), sodium azide (≥99%), triphenylmethyl chloride (98%) and oxalyl chloride (98%) were purchased from Acros Organics. Sodium hydroxide (≥99.5%) was purchased from Chemsolute. HEPES (≥99.5%) was purchased from Fischer BioReagents. AIE TPE Dye (98%) , Fmoc-Lys(Boc)-OH (≥98%) and Fmoc-choride (≥98%) were purchased from BLD Pharmatech GmbH. ConA labeled with Alexa-647 was purchased from Thermo Fisher. TentaGel®S RAM resin was purchased from Rapp Polymere with a loading of 0.26 mmol/g. Benzotriazol-1-yl-oxytripyrrolidinophosphonium hexafluorophosphate (PyBOP) (≥98%) was purchased from Iris Biotech. DIPEA (99%), D-Mannose (≥99%), ethylenediamine (≥99,5%) and sodium chloride (≥99,5%) were purchased from Carl Roth. Sodium diethyldithiocarbamate (99 %) and boron trifluoride diethyl etherate (≥98%) were purchased from Alfa Aesar. Copper(II) sulfate pentahydrate (98%), piperidine (99%),

sodium methoxide (95%) and triisopropysilane (TIPS) (98%) were purchased from Acros Organics.

### 1.2. Instrumentation

Nuclear Magnetic Resonance Spectroscopy (NMR)

$^{1}$H-NMR and $^{19}$F-NMRwere recorded on a Bruker Avance III 300 or a Bruker Avance III 600. Chemical shifts were reported as delta (δ) in parts per million (ppm) and coupling constants as J in Hertz (Hz). Multiplicities are stated as follows: s = singlet, d = doublet, t = triplet, q = quartet, m = multiplet, br = broad/wide.

Reversed Phase – High Pressure Liquid Chromatography (RP-HPLC)

Analytical RP-HPLC-MS measurements were performed on Agilent Technologies 6120 series coupled with an Agilent quadrupole mass spectrometer with an Electrospray Ionization (ESI) source operating in a m/z range of 200 to 2000. All spectra were measured with solvents A: 95% H2O, 5% ACN, +0.1% formic acid and B: 5% H2O, 95% ACN, +0.1% formic acid. As a column, a Poroshell 120 EC-C18 1.8 µM (3.0x50 mm, 2.5 µM) reversed phase column was used. Indicated purities were determined by integration of the UV-signal detected by a wavelength detector set to 214 nm with the OpenLab ChemStation software for LC/MS from Agilent Technologies.

Lyophilization

Lyophilization of the final structures was conducted on an Alpha 1-4 LD plus instrument from Martin Christ Freeze Dryers GmbH. The lyophilization was done at -42°C and a pressure of 0.1 mbar.

MilliQ Water

The MilliQ water (ultra-pure water) was purified using a Thermo Scientific "Barnstead Micropure ST". The conductivity was 18.20 MΩ*cm.

Peptide synthesizer

The CS136XT peptide synthesizer from CS Bio Co. was used for the synthesis of the oligomer backbone. Used protocols are listed below.

Centrifuges

For the Eppendorf tubes, a "Mini-Centrifuge Rotilabo®" from Carl Roth was used. For samples with larger volumes, the "Centrifuge 5702" from Eppendorf was used. For polymer purification by Viva-Spin, a "Heraeus Megafuge 8R Centrifuge" from Thermo Scientific was used.

Gel permeation chromatography

Gel permeation chromatography was performed on a Viscotek GPCmax VE-2001 with a HPLC pump, two Malvern Viscotek T columns (styrene-divinylbenzene-copolymer, pore size 500 Å and 5000 Å) and a Viscotek RI detector. The molecular weight was determined according to polystyrene calibration in the range of 1300 g $mol^{-1}$ to 1373000 g $mol^{-1}$.

Microplate Reader

A "CLARIOstar" from BMG LABTECH was used for absorbance and fluorescence measurements. 384 well microliter plates from Greiner Bio-One were used, into each of which 30 µL and 25 µL of the samples were added, respectively.

Microscope

Optical analysis of the coacervates was performed on an "Olympus IX73" microscope using a 60x oil objective.

Zetasizer

Zetasizer measurements were performed on a “Zetasizer Nano ZS” from Malvern Panalytical.

### 1.3. Abbrevations

| | |
|---|---|
| ACN | Acetonitrile |
| AIE | Aggregation Induced Emission |
| DIPEA | N,N-Diisopropylethylamine |

| | |
|---|---|
| EDS | Ethylene glycol-Diamine-Succinic acid |
| PyBOP | Benzotriazol-1-yloxytripyrrolidinophosphonium hexafluorophosphate |
| RI | Refractive index |
| TDS | Triple bond-Diethylenetriamine-Succinic acid |
| TFA | Trifluoroacetic acid |
| TIPS | Triisopropysilane |
| TPE | Tetraphenylethane |
| UV | Ultraviolet |

## 2. Synthesis and analytical data

### 2.1. Synthesis procedures

*Building block and sugar azide synthesis*

Building block EDS and TDS and sugar azides Mannose and Galactose were synthesized based on literature.[1-3]

*Standard synthesizer protocol*

Oligomer backbone was synthesized using a peptide synthesizer. Following protocols refer to 0.3 mmol resin.

*Swelling protocol*

The resin was swollen twice in 15 mL DCM for 15 minutes each. It was then washed three times with 15 mL DMF for one minute each.

*Deprotection/coupling protocol*

The resin was washed three times for 10 min with 15 mL each of a 25% piperidine in DMF solution. Between the deprotection steps, the resin was washed three times with 15 mL DMF for 1 min each. After the last deprotection step, the resin was washed ten times with 15 mL DMF for 1 min each. For the coupling, 4 mL of the amino acid (AA) or building block (BB) solution (5eq in 4 mL), 4 mL of 1 molar DIPEA in DMF solution and 4 mL of PyBOP solution (5eq in 4 mL) were premixed and shaken with the resin for 90 minutes. The resin was then washed ten times for one minute each with 15 mL DMF.

This protocol was repeated for every amino acid and building block until the desired structure was synthesized

*Swelling protocol after coupling*

After coupling of the last AA or BB resin was swelled twice with 15 mL DCM for 15 minutes each. It was then washed three times with 15 mL DMF for one minute each.

*AIE TPE coupling*

First, the Boc protecting group on the side chain of the lysine was removed. A solution of 4M HCl in dioxane was added, and the mixture was shaken for 30 min. The resin was washed several times with DMF. For coupling the dye, PyBOP (1.35 mmol) and TPE (1.35 mmol) were dissolved in 5 mL DCM and DIPEA (10.8 mmol) was added. The solution was shaken for 1 h. Afterwards, the resin was washed thoroughly with DMF several times.

*Copper-click reaction*

Oligomer backbone batch was divided into three smaller batches of 0.1 mmol. One batch was functionalized with α-D-mannose azide, the other with galactose azide.

Sugar azide (1 mmol) was dissolved in 3 mL DMF. CuSO4 (0.5 mmol) and sodium ascorbate (0.5 mmol were each dissolved in approximately 10 drops of ultra-pure water. The solutions were added to the resin and mixtures were shaken for 17 h. Then, the resin was repeatedly washed with DMF, sodium diethyldithiocarbamate solution and DCM until the wash solution became clear.

*Capping*

Fmoc protecting group was removed from both batches, by using 5 ml of 25 vol% piperidine in DMF. The mixtures were shaken for 15 min. The resin was washed with DMF and the process was repeated. Afterwards, resin was washed several times with DMF and 7 mL acetic anhydride were added. Mixture was shaken for 1h and resin was washed again with DMF.

*Cleavage*

Resin was mixed with 4 mL of a cleavage solution consisting of 95 vol% TFA, 2.5 vol% TIPS, and 2.5 vol% DCM and were shaken for 1 h. The products were then precipitated in cold diethyl ether and centrifuged off. The diethyl ether was decanted off, and the residues were dissolved in approximately 8 mL of MilliQ water and lyophilized.

*Determination of functionalization degree of $P_{100}$-Man and $P_{100}$-Gal*

The determination of the functionalization degree of $P_{100}$-Man and $P_{100}$-Gal was calculated by using NMR. The NMR integrals are normalized to the number of triazole protons of the sugar oligomer. Therefore, the remaining aromatic protons in the NMR represent the remaining TPE and

aromatic polymer backbone protons. For this purpose, the number of aromatic protons of a polymer backbone (5 protons) was divided by the value of the difference between the number of aromatic protons in the NMR and the number of protons of a TPE unit (19 protons). The following calculation demonstrates it using the example of $P_{100}$-Man (Figure S18)

$$Function.Degree = \frac{Aromatic\ protons\ of\ one\ polymerbackbone}{Aromatic\ protons\ from\ NMR - TPE\ protons} = \frac{5}{20{,}7 - 19} = 2.94\%$$

## 2.2. Analytical data

*Oligomer backbone (**1**)*

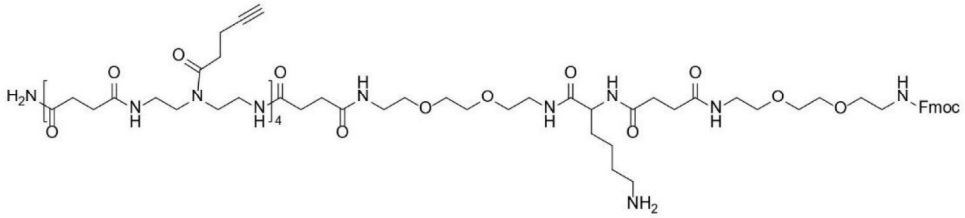


After synthesis of oligomer backbone, a first analysis by RP-HPLC and ESI-MS was made, before it was further reacted. The Boc protecting group was not considered here because it is cleaved during the cleavage process with TFA for analysis.

**RP-HPLC-MS**: $t_R$ = 12.5 min, >97% relative purity (UV), from 95/5 to 5/95 Vol. % Water/acetonitrile with 0,1% formic acid in 30 min at 25 °C

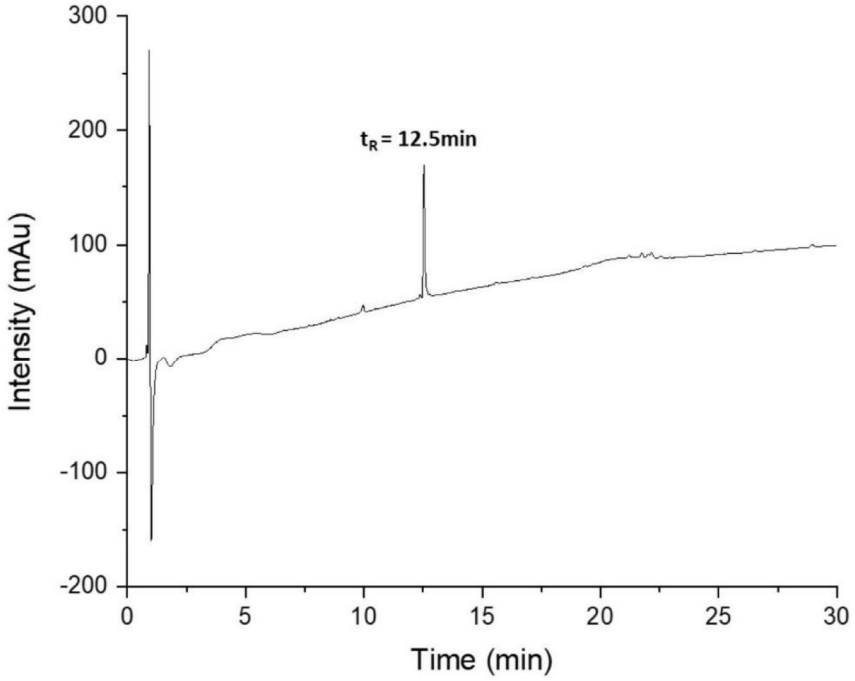


**Figure S1: RP-HPLC-MS chromatogram of (from 95/5 to 5/95 Vol. % Water/acetonitrile with 0,1% formic acid in 30 min at 25 °C) of compound (1).**

**ESI-MS** calc. for $C_{93}H_{137}N_{19}O_{23}$: $[M+4H]^{4+}$ 473, $[M+3H]^{3+}$ 630.34, $[M+2H]^{2+}$ 945.01; found $[M+4H]^{4+}$ 473.2, $[M+3H]^{3+}$ 630.6, $[M+2H]^{2+}$ 945.2

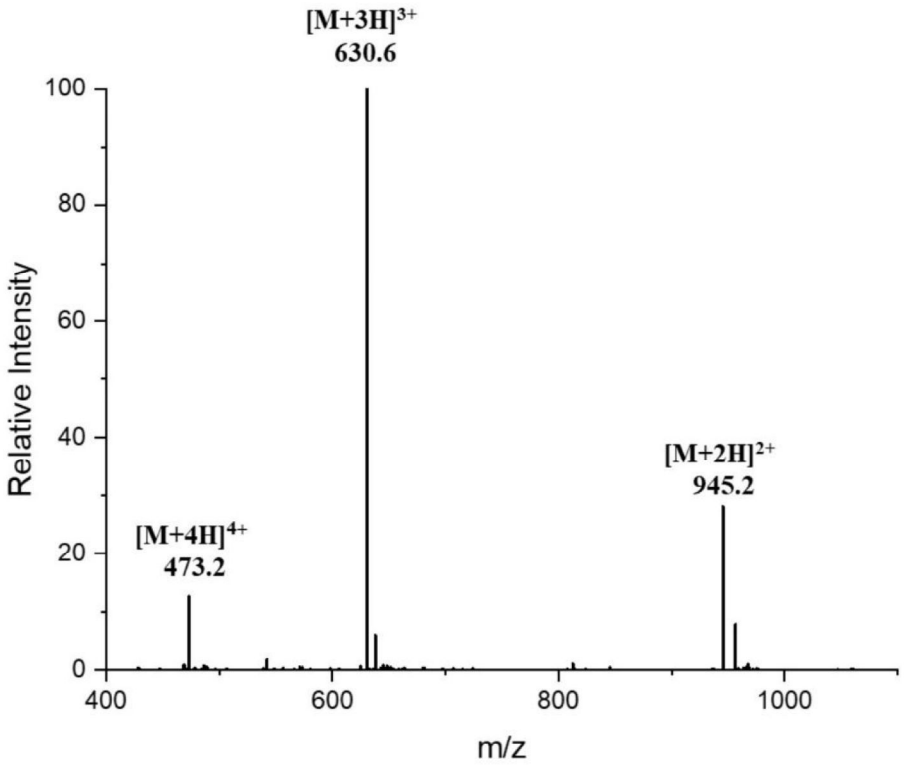


**Figure S2: ESI-MS spectrum of oligomer backbone (1) (positive mode)**

*Mannose oligomer (acetylated) (2)*

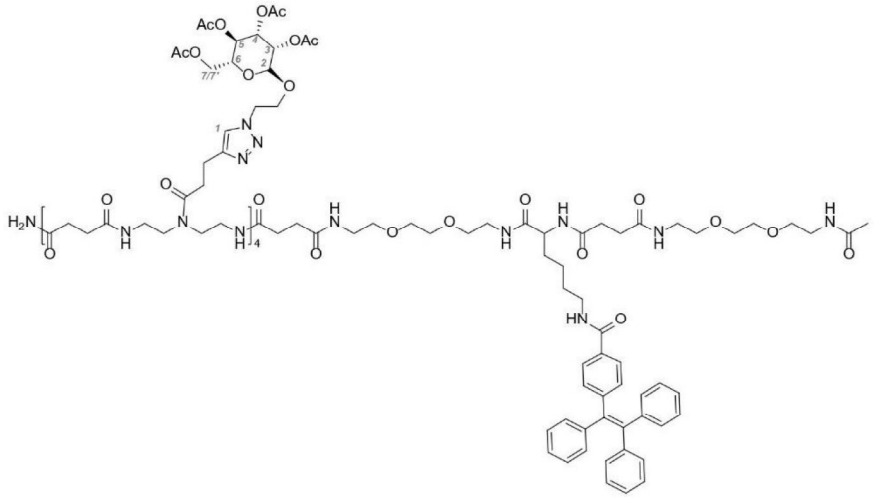

**$^1$H-NMR** (600 MHz, MeOD-$d_4$): δ (ppm) = 7.90 (s, 4H, *H-1*), 7.59–7.54 (m, 1H, *aromatic protons TPE*), 7.14–7.07 (m, 8H, *aromatic protons TPE*), 7.04–6.97 (m, 4H, *aromatic protons TPE*), 5.23–5.12 (m, 13H, *H-3, H-4, H-5*), 4.84 (s, 4H, *H-2*), 4.67 (s, 9H, -C(O)NHC*H*$_2$C*H*$_2$–(TDS and EDS)), 4.18–4.14 (m, 4H, *H-6*), 4.03 (br.d, 4H, *H-7*), 3.94 (t, $^3$J=6.47 Hz, 4H, *H-7'*), 3.77 – 3.28 (m, 87H, -C(O)NHC*H*$_2$C*H*$_2$–(TDS and EDS)), 3.20 – 2.75 (m, 24H, -C(O)NHC*H*$_2$C*H*$_2$–(TDS and EDS)), 2.56 – 2.42 (m, 26H, -C(O)NHC*H*$_2$C*H*$_2$–(TDS and EDS)), 2.18–2.10 (m, 12H, -C(O)C*H*$_3$), 2.09–2.00 (m, 24H, -(C(O)C*H*$_3$)$_2$), 1.95 (d,12H, -C(O)C*H*$_3$).

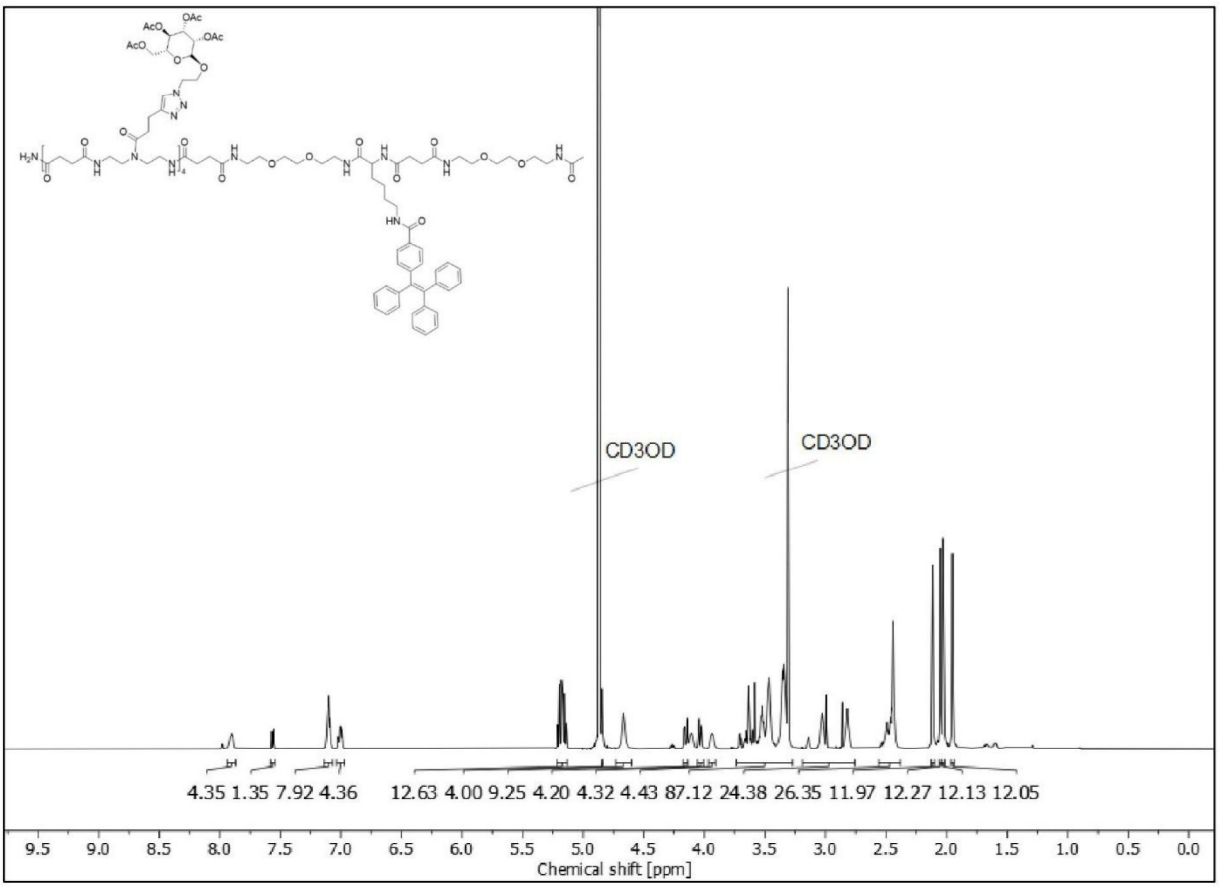


**Figure S3: $^{1}$H-NMR of Mannose oligomer (acetylated) (2)**

*Mannose oligomer (deacetylated)* ***(3)***

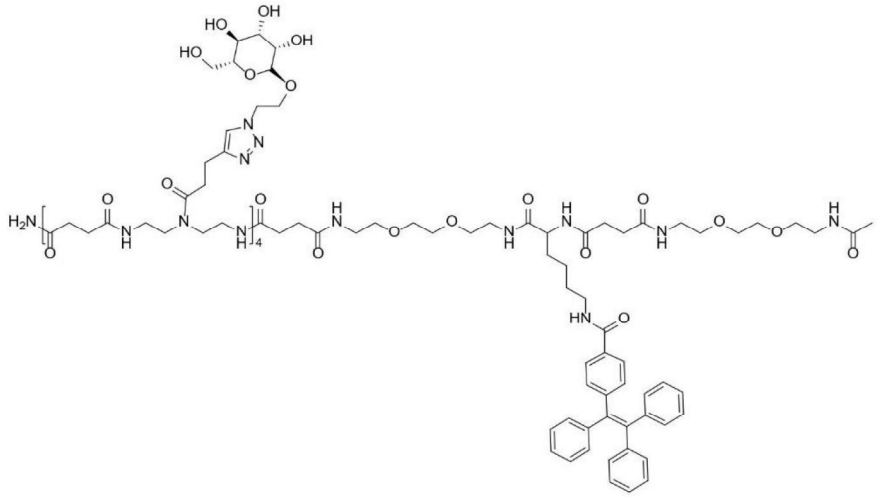

**RP-HPLC-MS**: $t_R$ = 14.87 min, >98% relative purity (UV), from 95/5 to 5/95 Vol. % Water/acetonitrile with 0,1% formic acid in 30 min at 25 °C

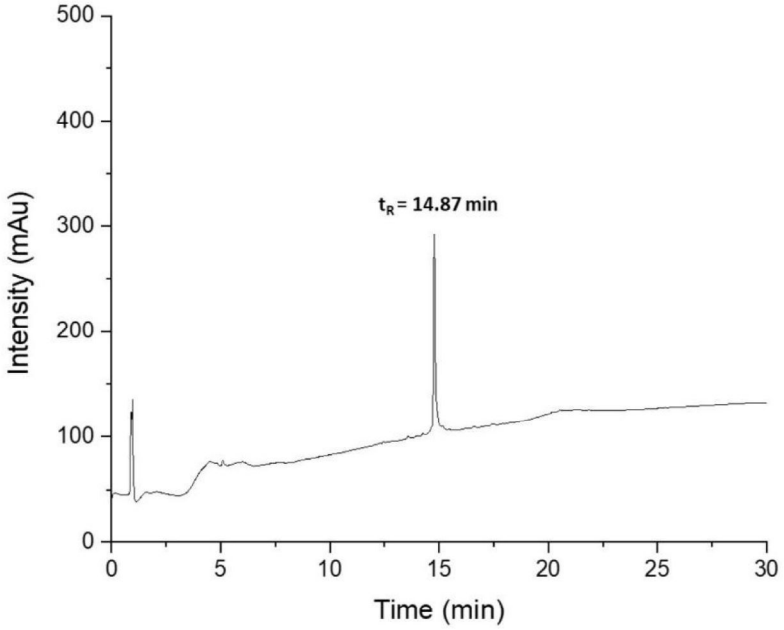


**Figure S4: RP-HPLC-MS chromatogram of (from 95/5 to 5/95 Vol. % Water/acetonitrile with 0,1% formic acid in 30 min at 25 °C) of compound 3.**

**ESI-MS** calc. for $C_{139}H_{212}N_{31}O_{47}$:$[M+5H]^{5+}$ 613.7, $[M+4H]^{4+}$ 766.88, $[M+3H]^{3+}$ 1022.17; found 613.8 $[M+5H]^{5+}$, 767 $[M+4H]^{4+}$, 1022.2 $[M+3H]^{3+}$

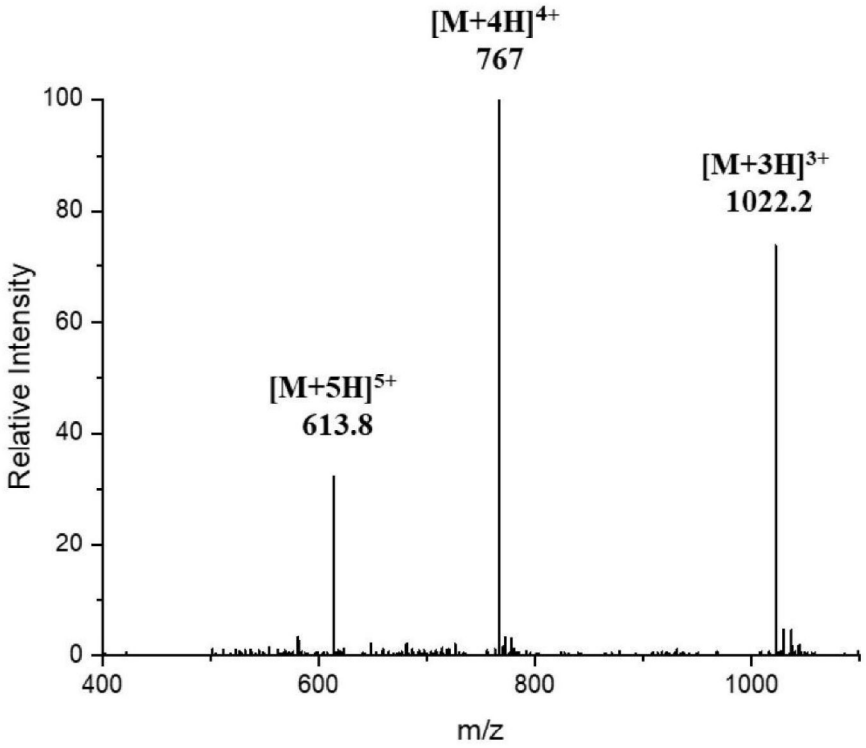


**Figure S5: ESI-MS spectrum of Mannose oligomer (deacetylated) (3) (positive mode)**

*Galactose oligomer (acetylated)* ***(4)***

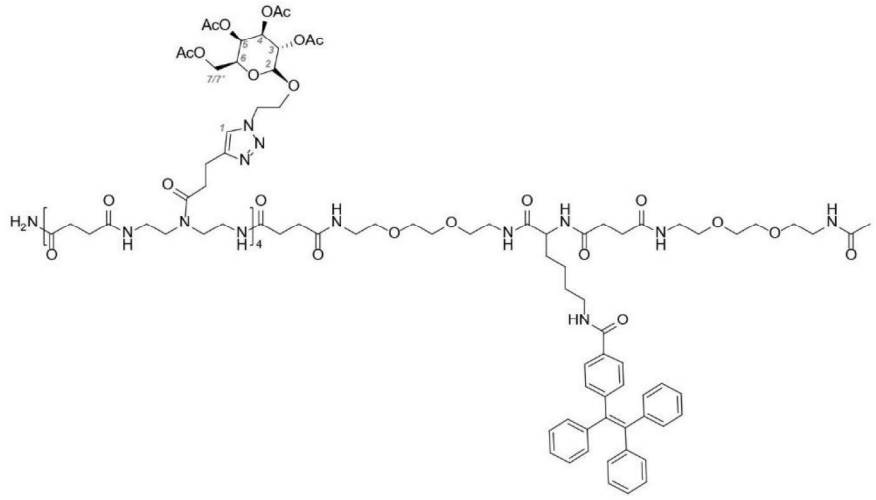

**$^{1}$H-NMR** (600 MHz, MeOD-$d_4$): δ (ppm) = 7.79 (m, 4H, *H-1*), 7.56 (d, $^{3}$J=8.33 Hz, 1.5H, *aromatic protons TPE*), 7.10 (m, 9H, *aromatic protons TPE*), 7.04–6.97 (m, 5H, *aromatic protons TPE*), 5.38 (d, $^{3}$J=3.42 Hz, 4H, (TDS and EDS)), 5.14 - 4.99 (m, 9H, *H-3, H-4, H-5*), 4.66 (dd, $^{3}$J=7.84 Hz, $^{4}$J=2.52 Hz, 5H, *H-2*), 4.59 (s, 9H, (TDS and EDS)), 4.24 – 4.18 (m, 4H, *H-6*), 4.16 – 4.10 (m, 13H, *H-7*), 4.00 (s, 5H, *H-7´*), 3.74 – 3.26 (m, 98H, (TDS and EDS)), 3.19 – 2.73 (m, 30H, (TDS and EDS)), 2.15 – 2.11 (m, 12H, -C(O)C*H*$_3$), 2.05 – 1.99 (m, 14H, -C(O)C*H*$_3$), 1.98 – 1.95 (m, 12H, -C(O)C*H*$_3$), 1.94 – 1.91 (m, 12H, -C(O)C*H*$_3$).

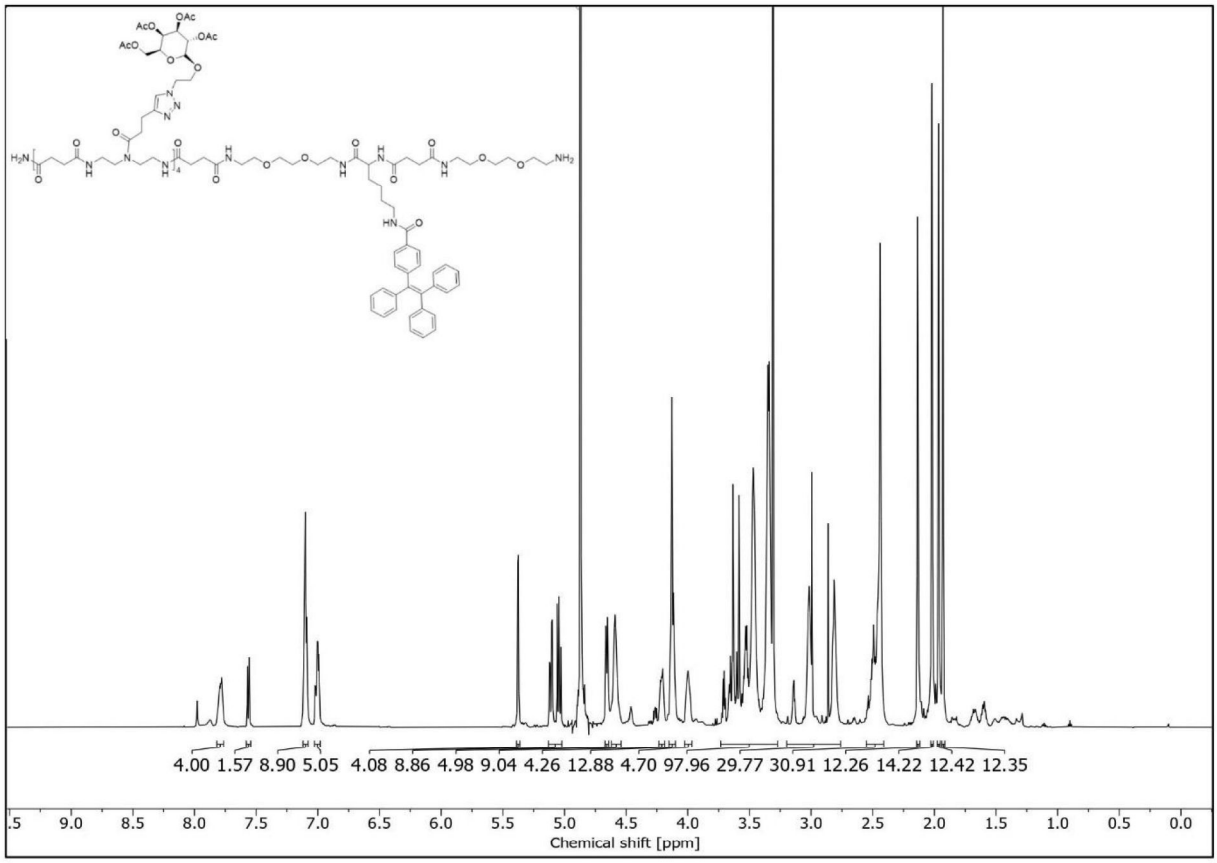


**Figure S6: $^{1}$H-NMR of galactose oligomer (acetylated) (4)**

*Galactose oligomer (deacetylated)* ***(5)***

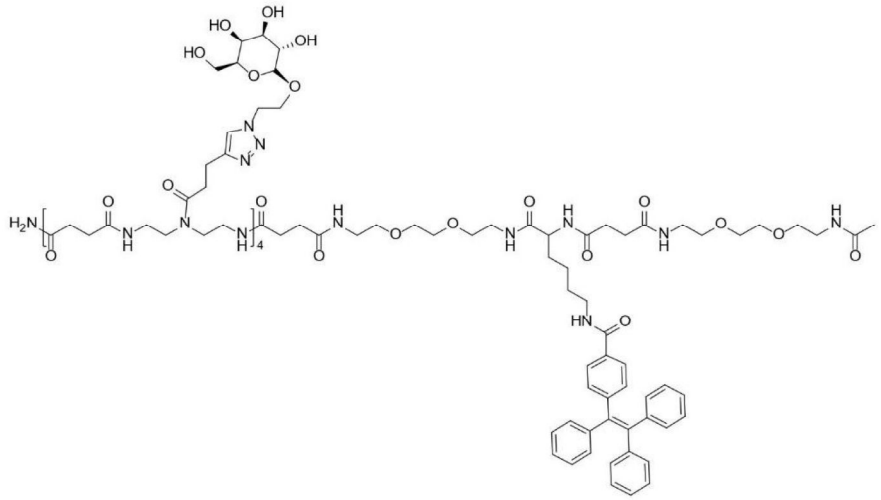

**RP-HPLC-MS**: $t_R$ = 14.81 min, >96% relative purity (UV), from 95/5 to 5/95 Vol. % Water/acetonitrile with 0,1% formic acid in 30 min at 25 °C

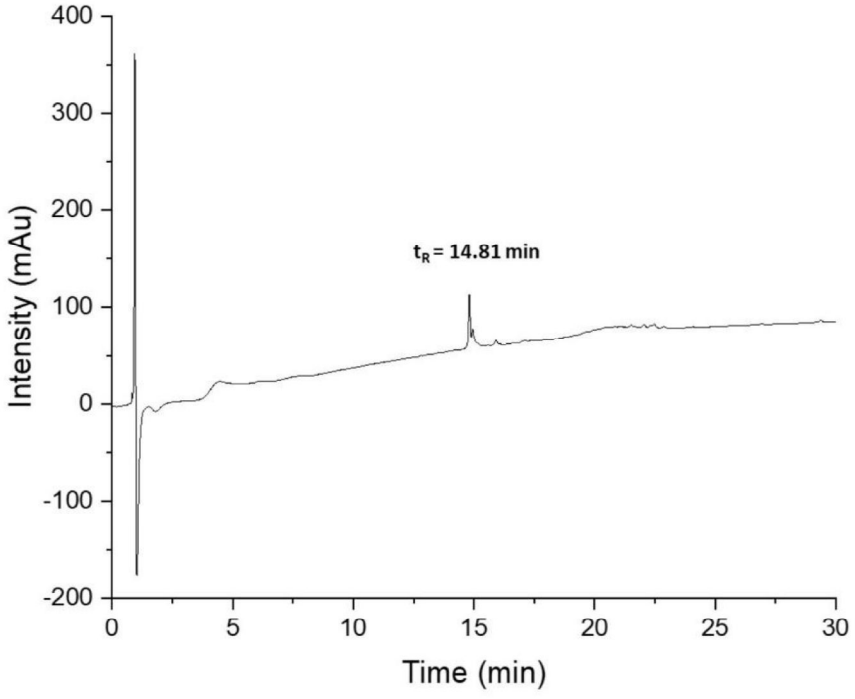


**Figure S7: RP-HPLC-MS chromatogram of (from 95/5 to 5/95 Vol. % Water/acetonitrile with 0,1% formic acid in 30 min at 25 °C) of compound 5.**

**ESI-MS** calc. for $C_{139}H_{212}N_{31}O_{47}$:$[M+5H]^{5+}$ 613.7, $[M+4H]^{4+}$ 766.88, $[M+3H]^{3+}$ 1022.17; found 613.8 $[M+5H]^{5+}$, 767 $[M+4H]^{4+}$, 1022.2 $[M+3H]^{3+}$

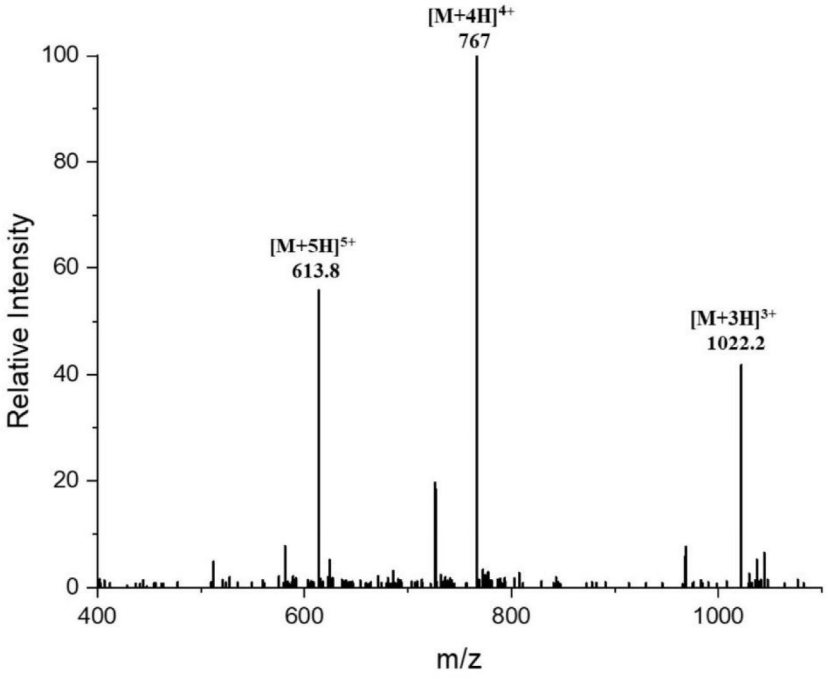


**Figure S8: ESI-MS spectrum of Galactose oligomer (deacetylated) (3) (positive mode)**

*Pentafluorophenyl acrylate monomer (**6**)*

**$^1$H-NMR** (600 MHz, $CDCl_3$): δ (ppm) = 6.72 (dd, *J* = 17.3, 0.9 Hz, 1H, $CH_2$=CH-), 6.37 (dd, *J* = 17.3, 10.6 Hz, 1H, $CH_2$=C*H*-), 6.18 (dd, *J* = 10.5, 0.9 Hz, 1H, $CH_2$=CH-).

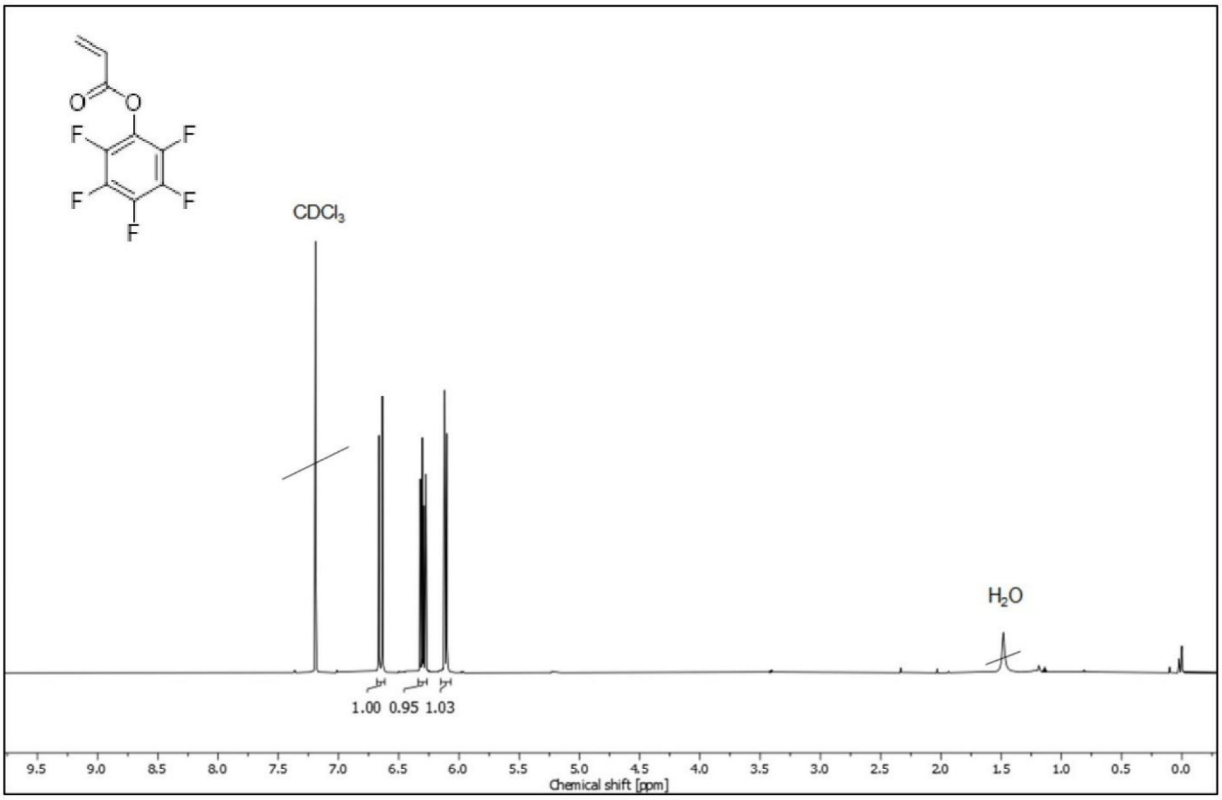


**Figure S9: $^1$H-NMR of Pentafluorophenyl acrylate monomer (6)**

**$^{19}$F-NMR** (600 MHz, $CDCl_3$): δ (ppm) = -152.54 (m, 2F), -157.92 (t, 1F), -162.32 (m, 2F)

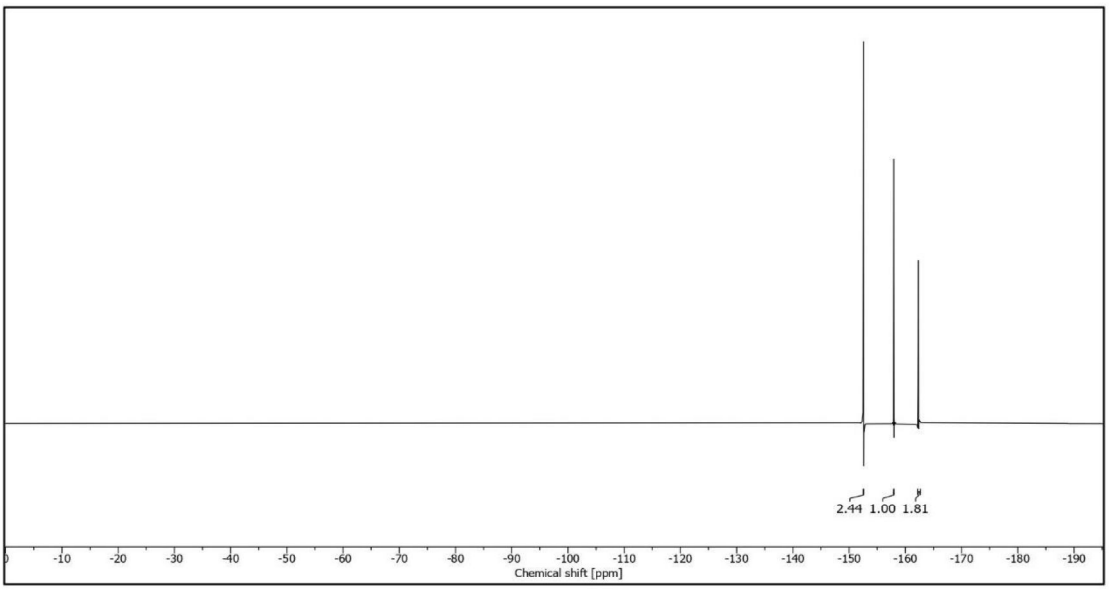


**Figure S10: $^{19}$F-NMR of Pentafluorophenyl acrylate monomer (6)**

*Poly(pentafluorophenyl acrylate) 100 (7)*

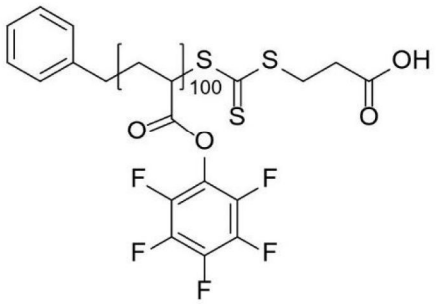


Polymerization degree was determined by Gel permeation chromatography (GPC) and $^{1}$H-NMR analysis.

**Table S1: Average Polymerization degree determined by GPC and $^{1}$H-NMR of Poly(pentafluoro-phenyl acrylate) 100 (7)**

| Method | Pn |
|---|---|
| $^{1}$H-NMR | ~ 98 |

**Table S2: GPC analysis of Poly(pentafluorophenyl acrylate) 100 (7)**

| **Detector** | UV | RI |
|---|---|---|
| **Mw** | 22619 | 23278 |
| **Mn** | 17228 | 18140 |
| **D** | 1.31 | 1.28 |

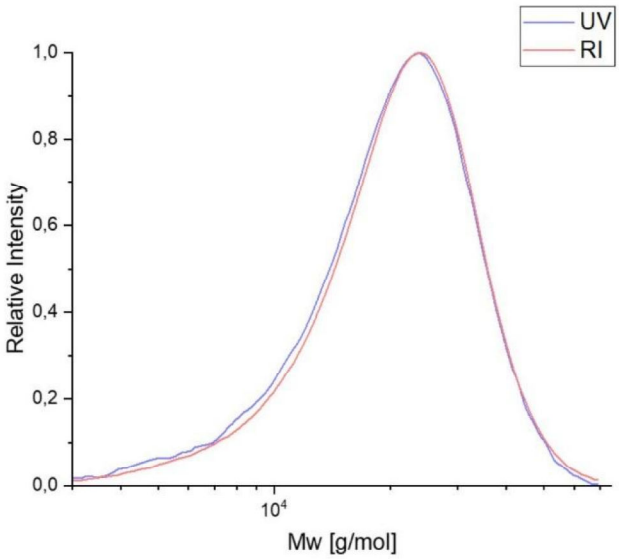


**Figure S11: GPC measurement (Eluent:THF) of compound (7)**

**$^1$H NMR** (600 MHz, $CDCl_3$): δ (ppm) = 7.18 (d, *J* = 7.6 Hz, 4H), 3.64 (s, 2H), 3.08 (m, 90H), 2.88 – 2.72 (m, 17H), 2.50 (bs, 40H), 2.11 (m, 151H).

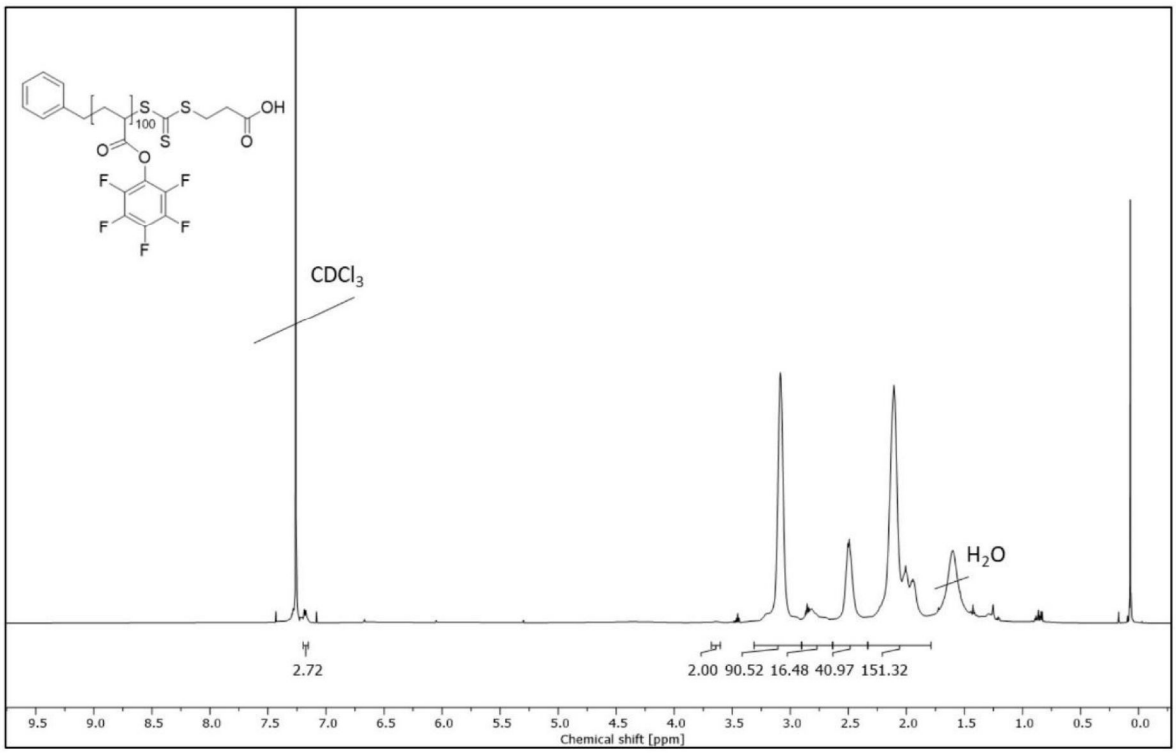


**Figure S12: $^1$H-NMR of Poly(pentafluorophenyl acrylate) 100 (7)**

**$^{19}$F-NMR** (600 MHz, $CDCl_3$): δ (ppm) = -153.21 (m, 2F), -156.7 (m, 1F), -162.16 (m, 2F)

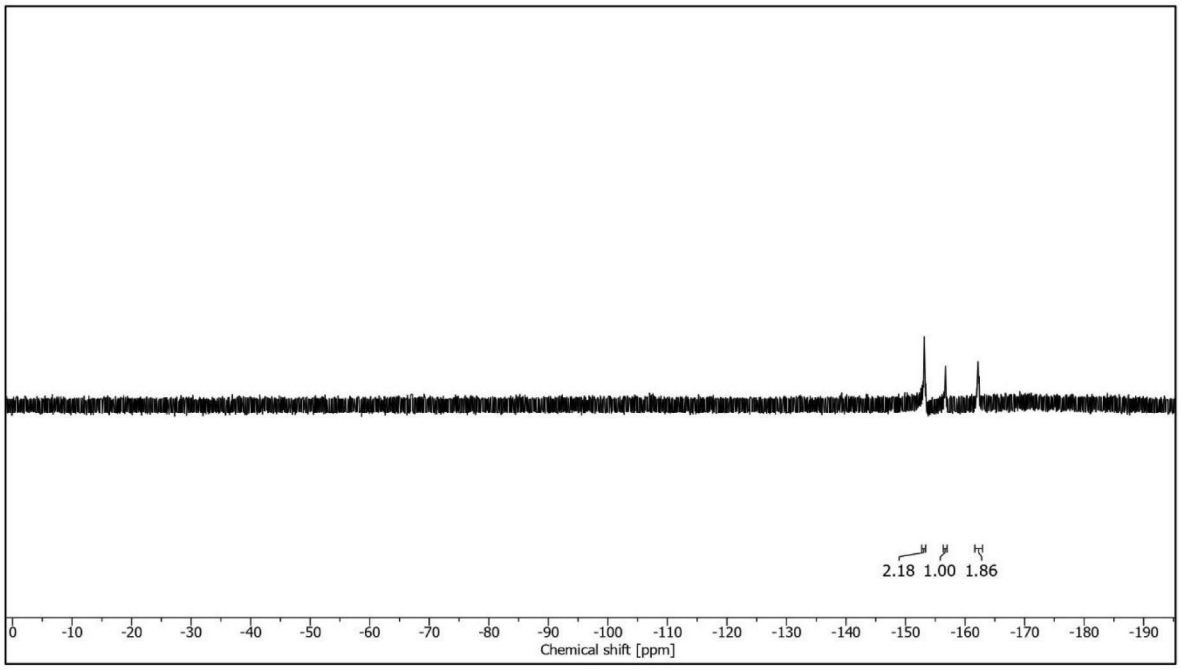


**Figure S13: $^{19}$F-NMR of Poly(pentafluorophenyl acrylate) 100 (7)**

*$P_{100}$- **(8)***

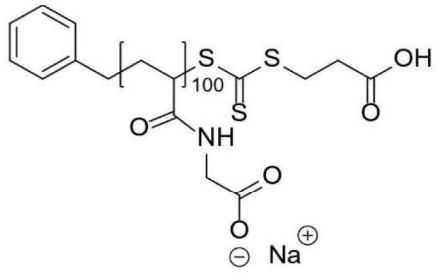


**$^1$H-NMR** (600 MHz, $D_2O$): δ (ppm) = 9.67 – 9.10 (m, 12H), 7.47 – 7.16 (m, 5H, $H_{aromatic}$), 4.36 – 3.29 (m, 190H,-NHC$H_2$COO-), 3.07 – 1.01 (m, 300H, C$H_{2\ Backbone}$)

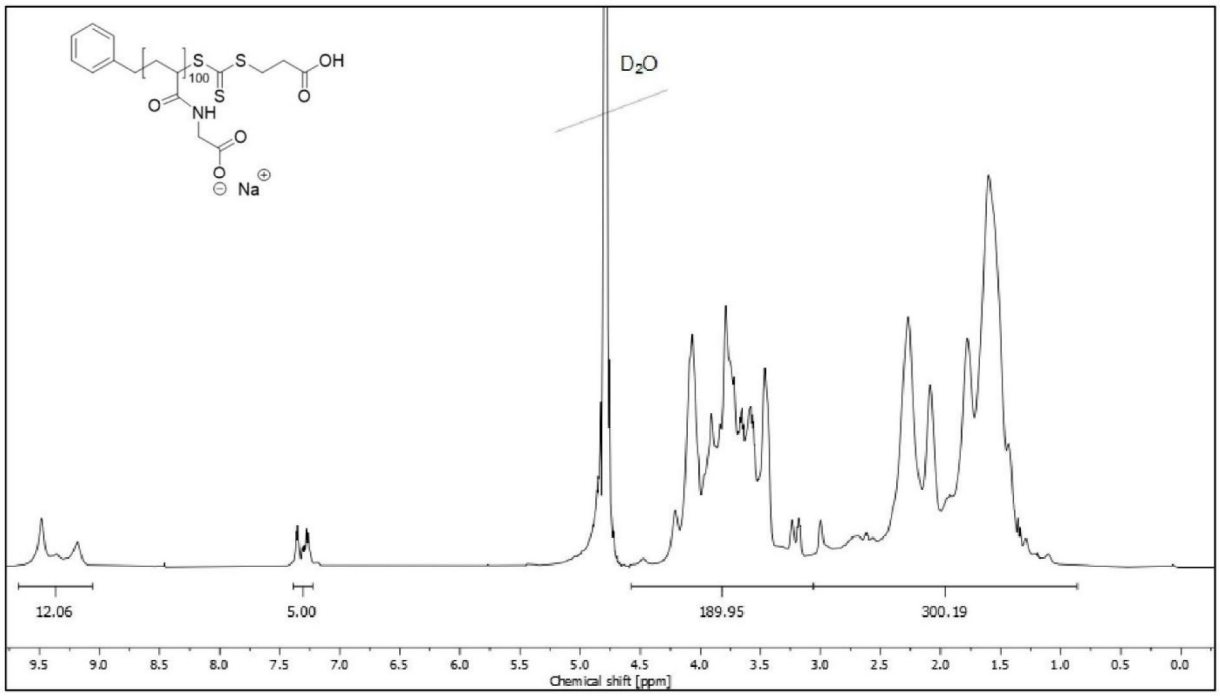


**Figure S14: $^1$H-NMR of $P_{100}$(-) (8)**

**$^{19}$F-NMR** (600 MHz, $CDCl_3$): δ (ppm) = -no signals

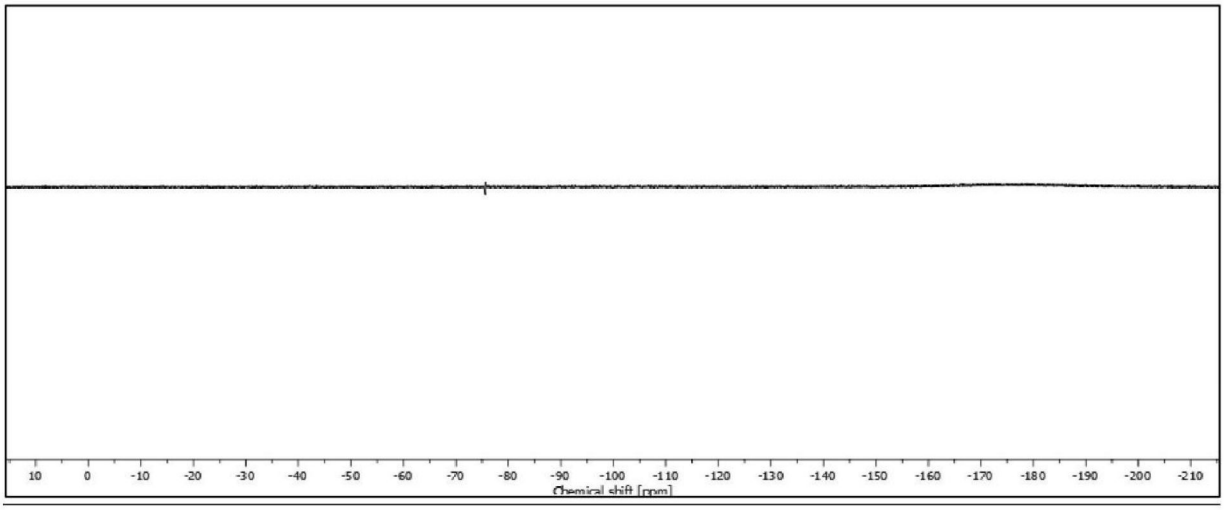


**Figure S15: $^{19}$F-NMR of $P_{100}$(-) (8)**

*$P_{100}$+* ***(9)***

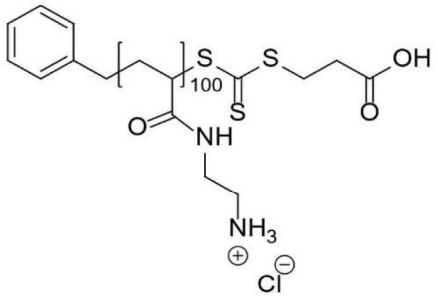


**$^1$H NMR** (600 MHz, $D_2O$): δ (ppm) = 7.45 – 7.19 (m, 5H, $H_{aromatic}$), 3.71 – 3.00 (m, 402H, NHC$H_2$C$H_2$N$H_2$), 2.39 – 1.11 (m, 335H, C$H_2$ Backbone).

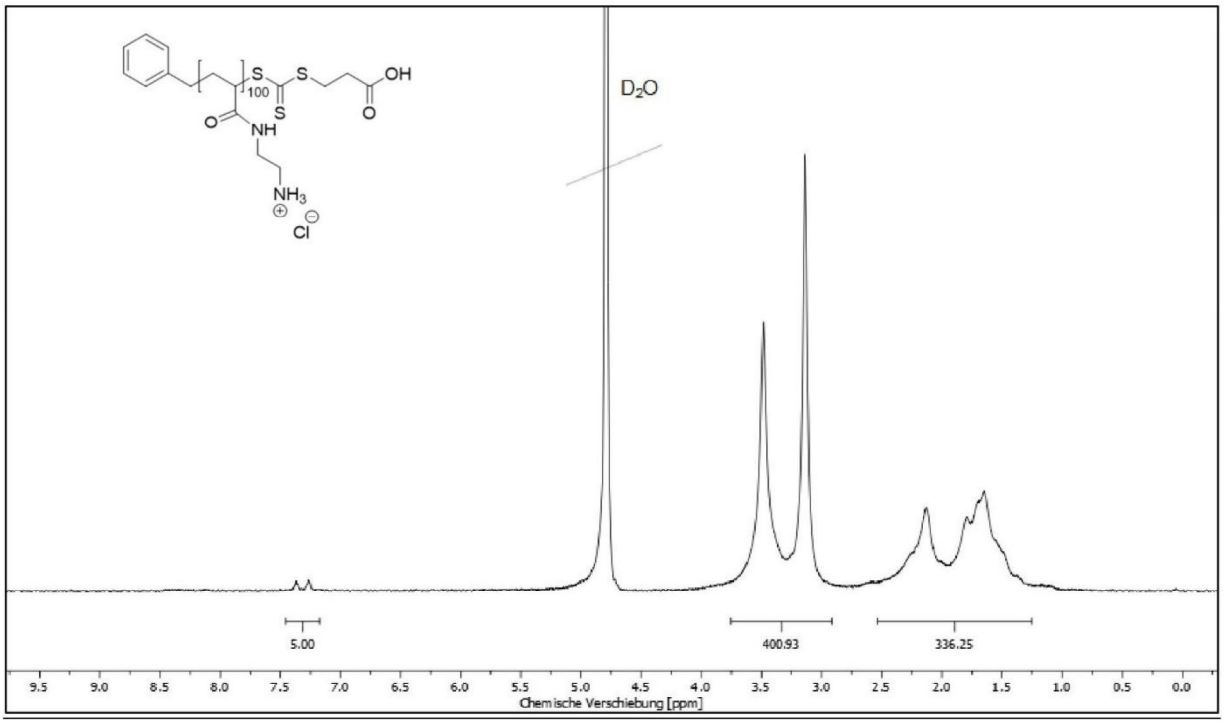


**Figure S16: $^1$H-NMR $P_{100}$(+) (9)**

**$^{19}$F-NMR** (600 MHz, $CDCl_3$): δ (ppm) = -no signals

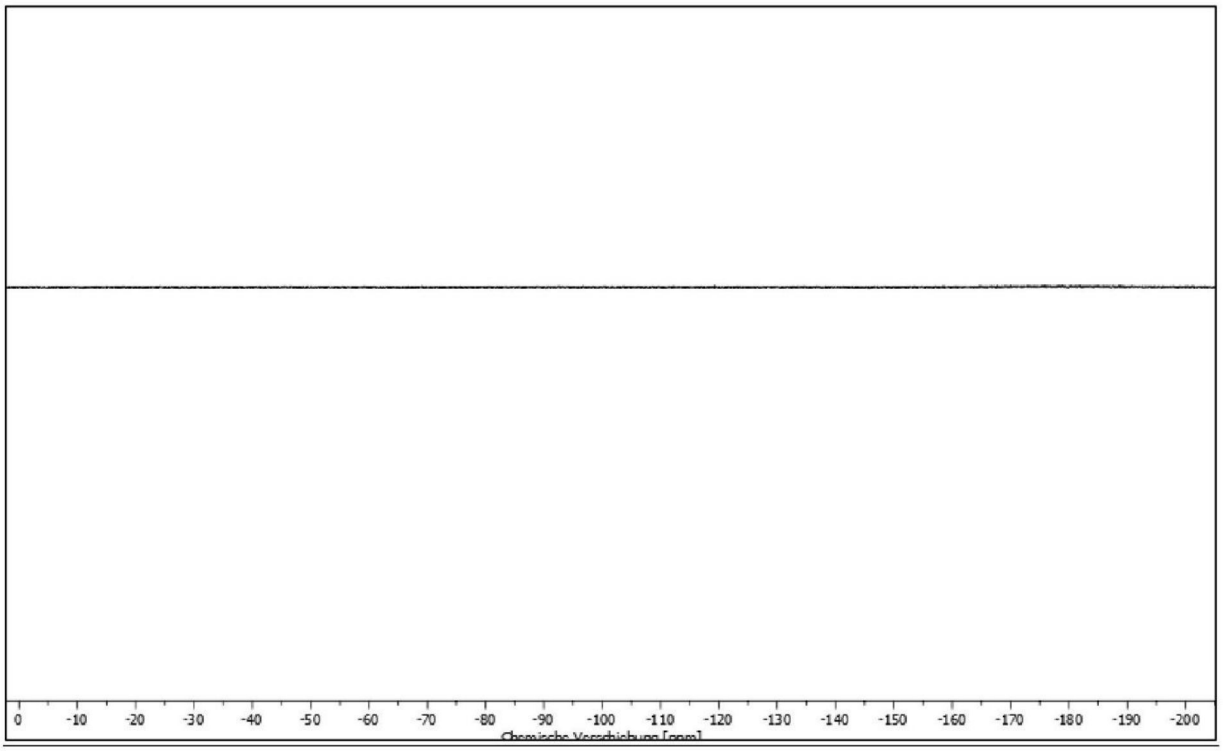


**Figure S17: $^{19}$F-NMR $P_{100}$(+) (9)**

*$P_{100}$-Man (acetylated) (**10**)*

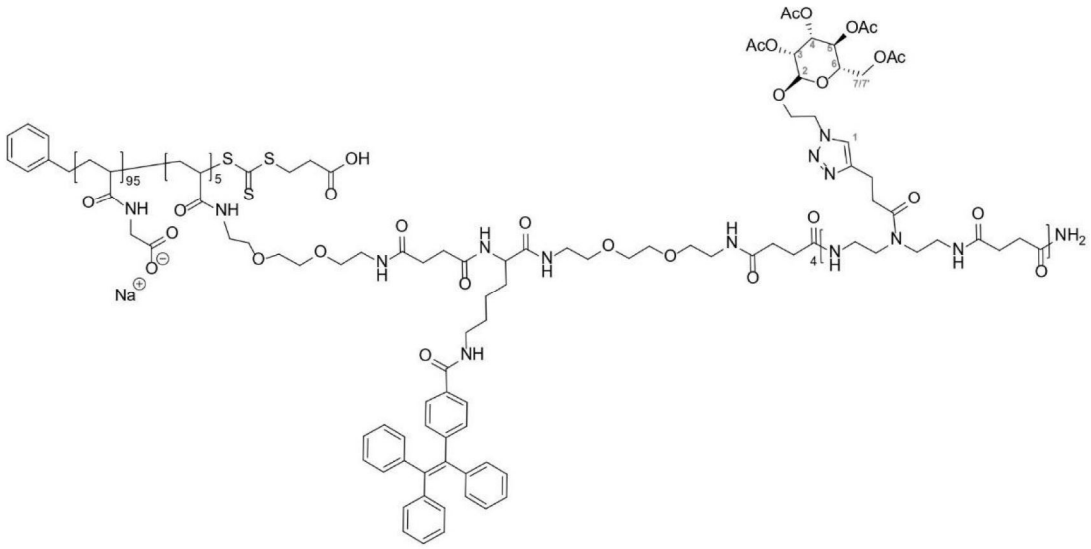

**$^1$H-NMR** (600 MHz, $D_2O$): δ (ppm) = 7.99 – 7.78 (m, *H-1*), 7.57-6.96 (m, aromatic protons), 5.30-5.05 (m, *H-3, H-4, H-5*), 4.74 – 4.55 (m, *H-2*, protons of oligomer and polymer backbones), 4.22 (s, *H-6*), 4.10-3.89 (m, *H-7, H-7´*), 3.87 – 2.27 (m, protons of oligomer and polymer backbones), 2.19-1.89 (m, *H-8*), 1.86 – 1.03 (m, protons of oligomer and polymer backbones).

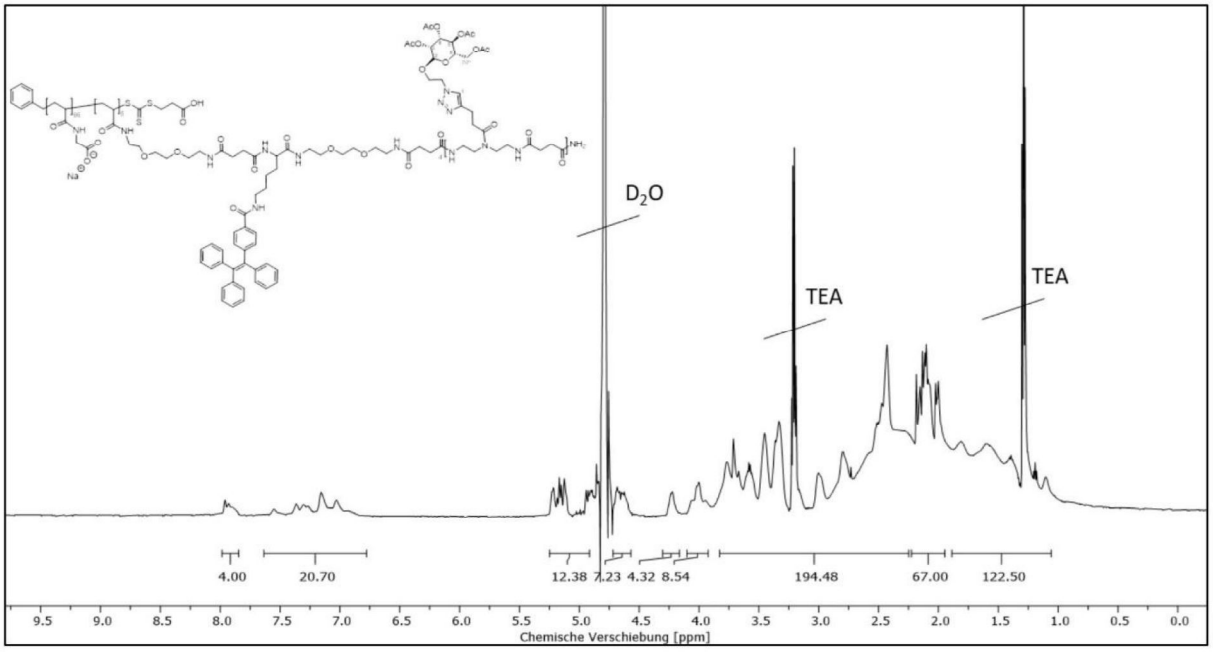


**Figure S18: $^1$H-NMR of $P_{100}$(-)Man (acetylated) (10)**

**$^{19}$F-NMR** (600 MHz, $CDCl_3$): δ (ppm) = -no signals

*$P_{100}$-Man (deacetylated)* ***(11)***

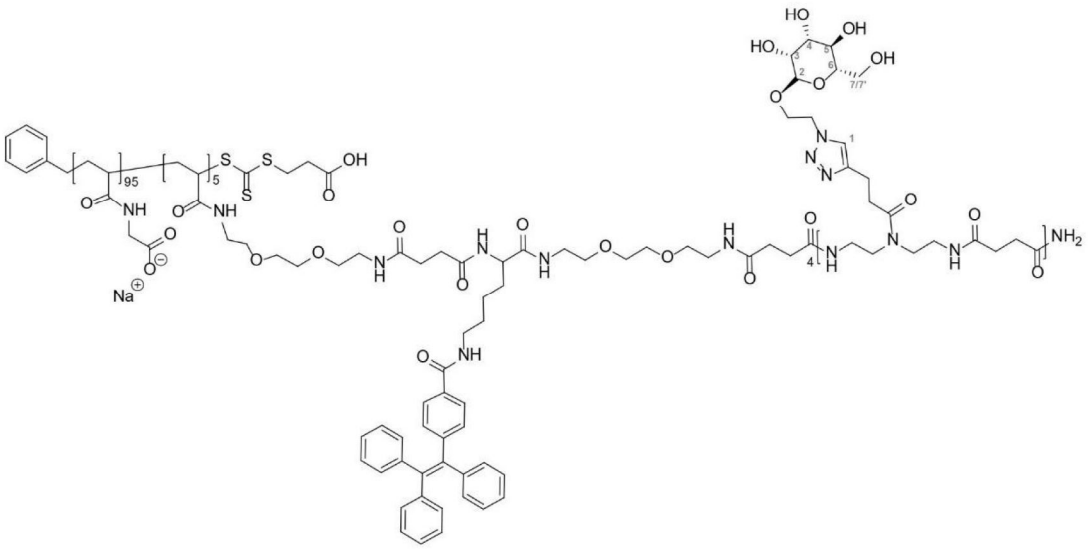

**$^{1}$H-NMR** (600 MHz, $D_2O$): δ (ppm) = 7.91 – 7.78 (m, *H-1*), 7.60 – 6.94 (m, aromatic protons), 4.62 (s, *H-2*), 4.22 (s, *H-6*), 4.06 (s, *H-7*, *H-7´*), 3.93 – 0.83 (m, *H-3*, *H-4*, *H-5*, protons of oligomer and polymer backbones).

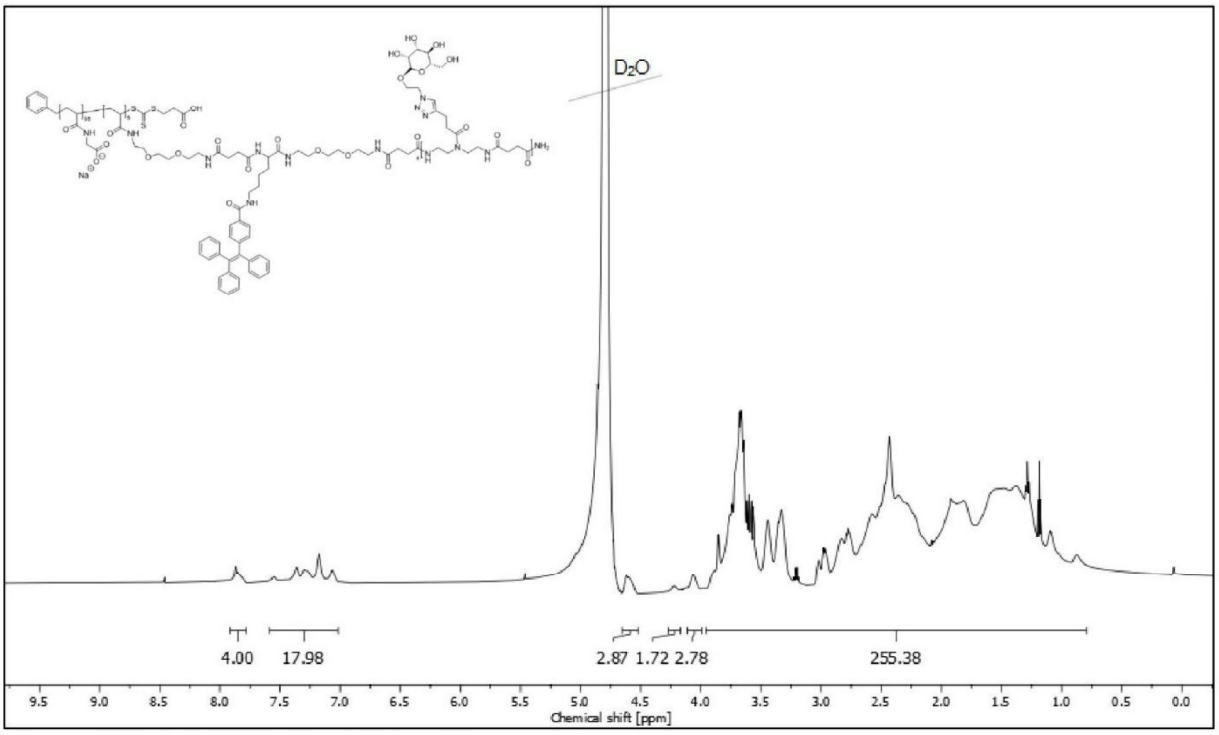


**Figure S19: $^{1}$H-NMR $P_{100}$(-)Man (deacetylated) (11)**

**$^{19}$F-NMR** (600 MHz, $CDCl_3$): δ (ppm) = -no signals

*$P_{100}$-Gal (acetylated)* ***(12)***

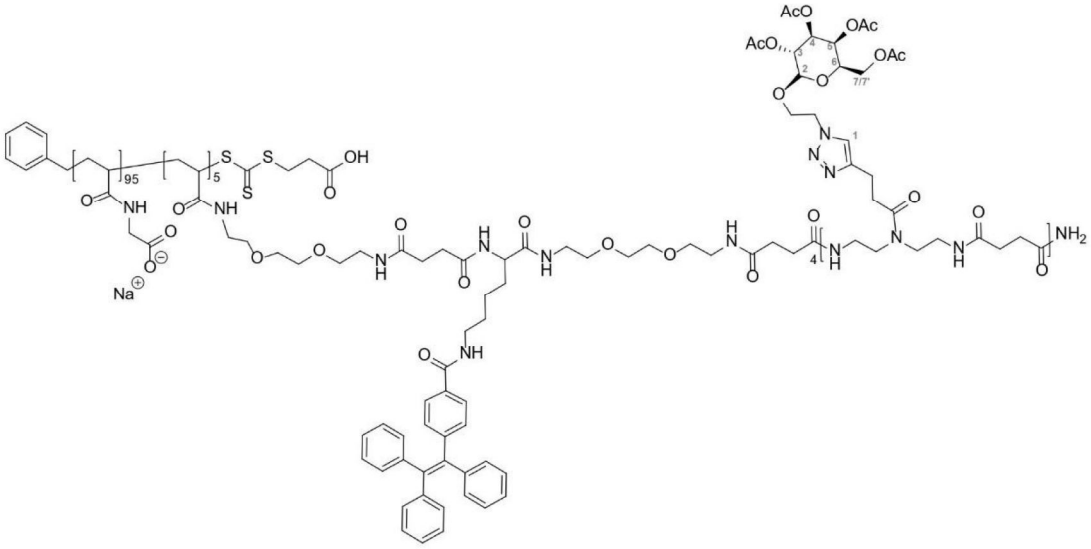

**$^{1}$H-NMR** (600 MHz, $D_2O$): δ (ppm) = 7.84-7.66 (m, *H-1*), 7.58-6.71 (m, aromatic protons), 5.42 (s, *H-3*), 5.15 (s, *H-4*), 4.99 (s, *H-5*), 4.59 (s, *H-2*, protons of oligomer and polymer backbones), 4.31-4.08 (m, *H-6*, *H-7*, *H-7´*), 3.85 – 2.29 (m, protons of oligomer and polymer backbones), 2.26-1.85 (m, *H-8*), 1.75 – 1.03 (m, protons of oligomer and polymer backbones).

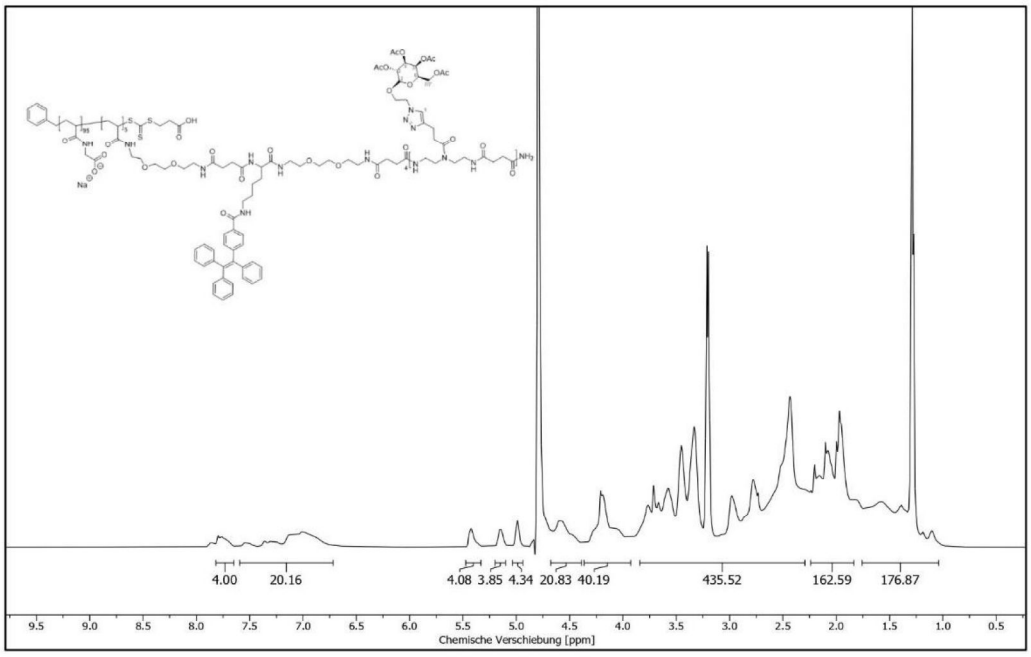


**Figure S20: $^{1}$H-NMR $P_{100}$(-)Gal (acetylated) (12)**

**$^{19}$F-NMR** (600 MHz, $CDCl_3$): δ (ppm) = -no signals

*$P_{100}$-Gal (deacetylated)* ***(13)***

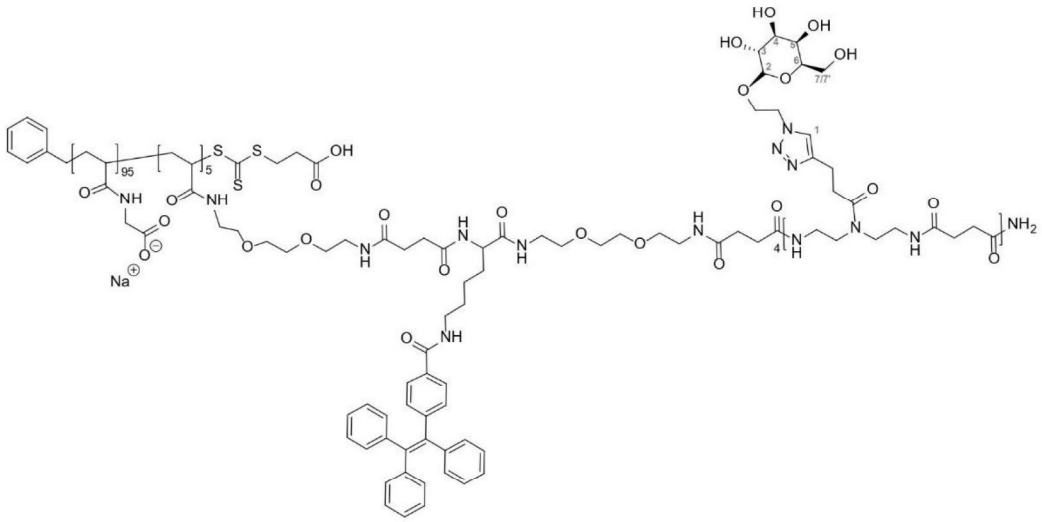

**$^{1}$H-NMR** (600 MHz, $D_2O$): δ (ppm) = 7.89 (s, *H-1*), 7.66 – 6.92 (m, aromatic protons), 4.07 – 0.76 (m, *H-2*, *H-3*, *H-4*, *H-5*, *H-6*, *H-7*, *H-7´*, protons of oligomer and polymer backbones).

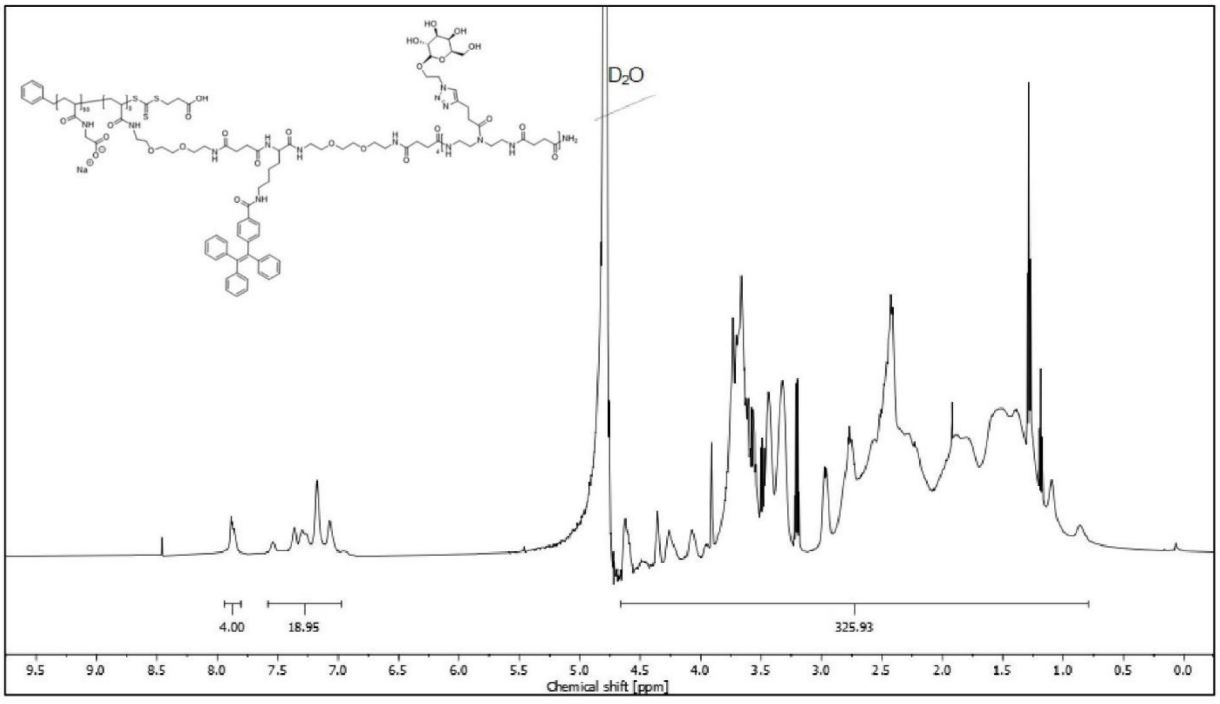


**Figure S21: $^{1}$H-NMR $P_{100}$(-)Gal (deacetylated) (13)**

**$^{19}$F-NMR** (600 MHz, $CDCl_3$): δ (ppm) = -no signals

## 3. Measurements

### 3.1 ConA uptake under variation of addition order

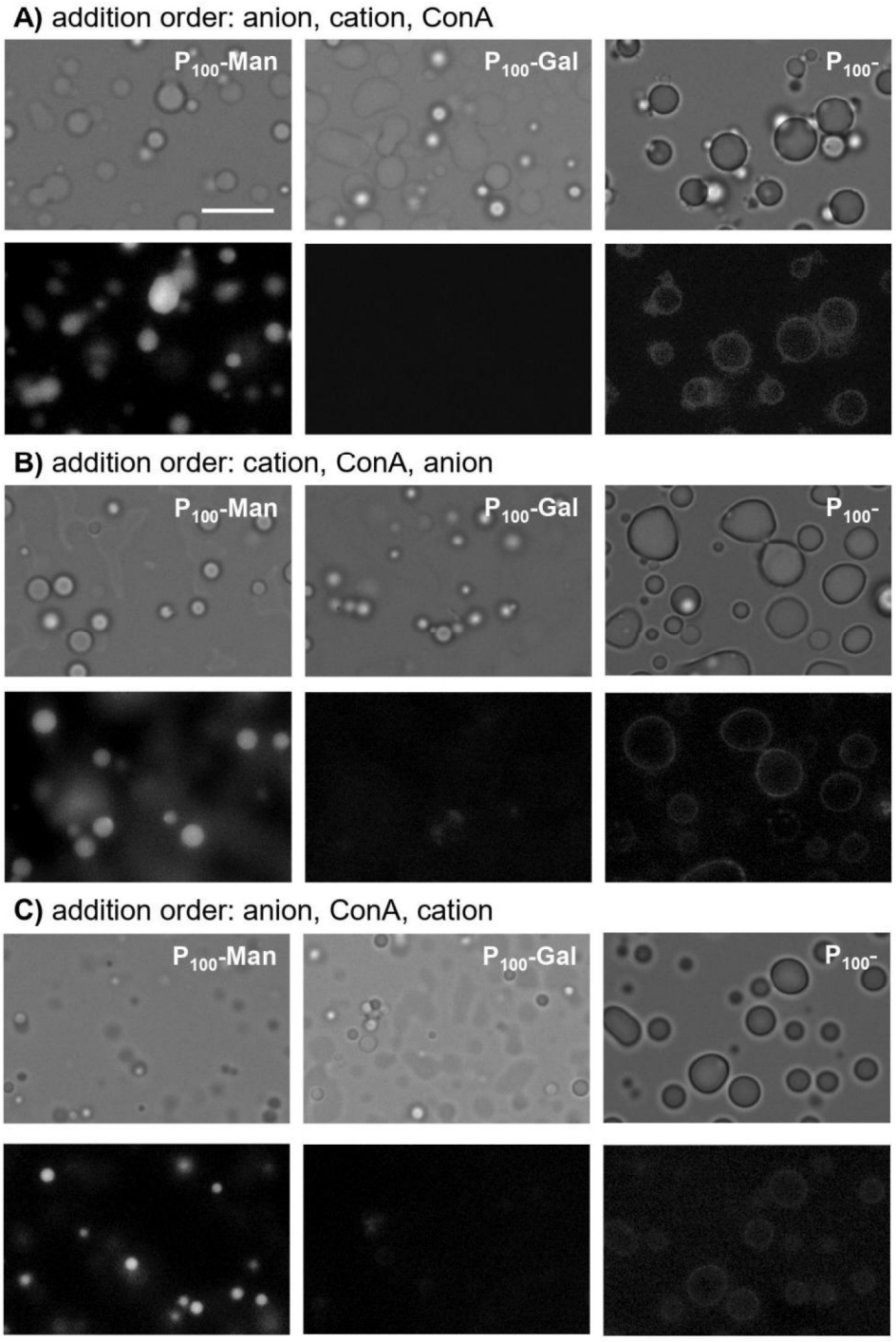


**Figure S22:** Micrographs of the droplets formed by $P_{100}$+ and the polyanions $P_{100}$-Man, $P_{100}$-Gal and $P_{100}$- in the presence of fluorescently labeled ConA and under variation of the addition order. The top images were taken by transmission microscopy, the bottom images by fluorescence microscopy. Scalebar: 10 µm (applies to all images).

### 3.2. Protein assays

**Table S3 Final concentrations in solution for protein assays**

| Polyanion [mM] | Polycation [mM] | ConA [µg/mL] | Order of Addition |
|---|---|---|---|
| 3.5 | 3.5 | 50 | Anion -> Cation -> ConA |
| 3.5 | 3.5 | 50 | Anion -> ConA -> Cation |
| 3.5 | 3.5 | 50 | Cation -> ConA -> Anion |

### 3.3. Zeta potential

**Table S4: Zetapotential results of E.coli bacteria with differnet polyelectrolytes**

| | *E. coli* | *E. coli* / $P_{100}$- | *E. coli* / $P_{100}$-Man | *E. coli* / $P_{100}$-Gal | *E. coli* / $P_{100}$+ |
|---|---|---|---|---|---|
| Zeta potential | -53 ± 2 mV | -77 ± 1 mV | -63 ± 1 mV | -50 ± 4 mV | 42 ± 3 mV |

For zetapotential measurements 35µL of Polyelectrolyte (Stocksolution 10mM) were mixed with 25µL *E. coli* solution (Stock solution 4mg/mL in milliQ water) and 940µL milliQ water. The mixture was allowed to stand for 5 minutes before measurement.

### Supporting references

(1) Ponader, D.; Wojcik, F.; Beceren-Braun, F.; Dernedde, J.; Hartmann, L. Sequence-Defined Glycopolymer Segments Presenting Mannose: Synthesis and Lectin Binding Affinity. *Biomacromolecules* **2012**, *13* (6), 1845-1852. DOI: 10.1021/bm300331z.
(2) Geng, J. M., G. Tao, L. Nicolas, J. Chen, G. Wallis, R. Mitchell, D. Johnson, B. Evans, S. Haddleton, D. Site-Directed Conjugation of "Clicked" Glycopolymers To Form Glycoprotein Mimics: Binding to Mammalian Lectin and Induction of Immunological Function. *JACS* **2007**, *129* (49), 15156-15163. DOI: 10.1021/ja072999x.
(3) Ebbesen, M. F.; Gerke, C.; Hartwig, P.; Hartmann, L. Biodegradable poly(amidoamine)s with uniform degradation fragments via sequence-controlled macromonomers. *Polymer Chemistry* **2016**, *7* (46), 7086-7093. DOI: 10.1039/c6py01700b.

# 4. Conclusion and Outlook

Polyelectrolytes and their phase change behavior are of major importance, as they are the natural drivers of several phenomena and mechanisms such as the formation of membraneless organelles or the fiber formation from the slime of the red velvet worm. Since these modes of operation have not yet been fully understood, the studies conducted here were aimed at identifying a new synthesis route to gain access to sequence-controlled polyelectrolytes and polyampholytes. These systems were then investigated for their coacervation behavior in order to gain further insights into the mechanism of this class of liquid-liquid phase separation. Furthermore, new possibilities should be investigated to consider coacervates as potential glycomimetics and to further analyze their behavior in lectin and bacterial assays.

The first part of this thesis focused on the establishment of a new synthesis route for sequence-controlled polyelectrolytes. Therefore, solid-phase synthesis further developed in the *Hartmann* group, based on a Fmoc protection strategy, was used to build up sequence-defined oligomers. The charge sequences of the oligomers were constructed using amino acids lysine and glutamic acid. The challenge here was to find a suitable protecting group strategy that would keep the amino acid side chains protected even after cleavage from the solid-phase. This described protection group stability is crucial for the subsequent process, ensuring that they remain unreactive in further conversion reactions. For this purpose, the Alloc and Allyl protecting groups were used, which are both stable under basic conditions during solid-phase synthesis and are not affected by the acidic cleavage conditions of the resin. The synthesis of the oligomers showed no major challenges; only a small amount of by-product was found with partial Allyl protecting group removal. However, this part only consisted of a relatively small amount, which allowed the structures to be used without further purification steps. As an innovation for the controlled synthesis of polyelectrolytes, in the next step oligomers were converted into brush-shaped polymers by using polymer analogous reaction. For this purpose, a pentafluoro phenyl acrylate was converted by RAFT polymerization to an active ester polymer, which could then be converted to larger polymer structures in a subsequent reaction with the free amines of the oligomers. Protection groups of oligomers were remained during polymer analogous reaction so that no cross-linking occurred during the polymer conjugation. The complete conversion was observed using $^{19}$F-NMR. When converting the polycations, an one-sided trityl-protected EDA building block was initially used, which did not lead to full conversion of the active esters due to the excessive steric requirement of the protection group. By using unprotected EDA building blocks in high excess, this problem could be circumvented and crosslinking reactions could be avoided. When incorporating the protected oligo-electrolytes, there was a complication with the lysine structures during purification, as the high

proportion of Alloc protecting groups decreased the water solubility and therefore dialysis could not take place. Hence, the determination of lysine incorporation into the oligomer was difficult, as $^{1}$H-NMR interpretation was not possible due to signal overlapping. The use of optimized dialysis methods using alternative solvents, could be considered for purifying structures in the future. Meanwhile, the synthesis of the polyampholytes, both the linear and the protected brush-shaped polymers, proceeded without further problems. For the brush-shaped polymers, initial assumptions could be made about the final incorporation of the oligomers based on the ratio of the protecting group signals to the polymer backbone protons in the $^{1}$H-NMR. The challenge in the next step was the removal of the Alloc and Allyl protecting groups to expose the charges of the amino acids. A solid-phase based deprotection protocol using phenyl silane was successfully transferred to a solution-based deprotection reaction and was used in this synthesis. Only for the polyelectrolytes with the fourfold charged lysine residues of the Alloc protecting group could be detected in the $^{1}$H-NMR. While the amount of the remaining protection group is relatively small, there is still scope for optimization here for more efficient future processes in order to maximize deprotection efficiency and minimize the loss of yield due to the need for multiple deprotection steps. Nevertheless, a precise determination of the incorporation degree for the brush-shaped polymers could not be achieved with the analytical methods chosen. GPC and MALDI TOF provided no reliable results and the clear identification of the polymer backbone or the oligo side chain signals in $^{1}$H-NMR turned out to be a significant challenge. However, initial assumptions could also be made here and further methods of analysis, such as titration, should be considered here when being used in subsequent investigations. Despite this, polyelectrolytes and polyampholytes were successfully produced and were analyzed in the further course of the thesis.

The second part of this thesis was therefore dedicated to the investigation of the phase behavior of the synthesized polyelectrolytes and polyampholytes. The structures were analyzed regarding their length and charge distribution, in terms of their charge density and sequence. To compare the structures with each other, phase diagrams were recorded in aqueous solution as a function of salt and polymer concentration using optical microscopy. The linear charged polyelectrolytes showed successful coacervate formation even at low polymer and salt concentrations. Increasing polyelectrolyte chain length had the effect of partially increasing salt resistance, but significantly decreased the possible polymer concentrations. When comparing the brush-shaped polyelectrolytes, there was an even greater reduction of the coacervate phase salt resistance. This effect could be explained by the limited flexibility of the polymer chains or by the presence of partially unbalanced charge ratios within the structures. This could be investigated in future studies by setting a charge balance through the verification of the final incoporation of charged oligomers or the variation of the proportions of polycations to polyanions. In contrast, no phase separation effects could

be observed when analyzing the linear polyampholytes, which leads to the assumption that the number of consecutive identical charges is lower than required for coacervation formation. The brush-shaped polyampholytes, on the other hand, have a defined charge sequence in the side chain and lead to a phase separation, albeit not a remarkably stable formation, even with two consecutive, identical charges. Even with the smallest amounts of additional salt ions, coacervates could be dissolved. However, the salt resistance increases with the length of the successive charges. Finally, the newly synthesized polyelectrolyte and polyampholyte structures provided initial insights into the coacervate behavior of brush-shaped polymers and the potential of the newly applied method of production for future structures.

The combined use of solid-phase synthesis and polymer analogous reactions gave access to brush-shaped polyelectrolyte structures and allowed for the investigation of their coacervation behavior. This synthesis strategy also offers the potential to build further, more complex structures for the future. For instance, an entirely new class of carbohydrate containing polyelectrolyte structures could be generated through a combination with tailor-made building blocks, such as those introduced in the *Hartmann* group.

Carbohydrate-containing oligomers were produced using customized building blocks EDS and TDS, which served both as spacers and as conjugation sites for carbohydrates. Oligomers containing mannose and galactose were synthesized, which were used in binding studies on ConA. Whereas mannose structures showed binding towards ConA, the galactose-functionalized compounds served as negative controls. The oligomers were converted into brush-shaped polyelectrolytes via a polymer analogous reaction. Previous studies with the single-charged polyelectrolytes have shown that they exhibit high salt resistance. This effect allowed studies on protein binding assays which usually required stability in buffered media. A significantly slower progression of coalescence was observed in the phase separation of the carbohydrate-containing polyelectrolytes. The carbohydrate-containing coacervates were then examined for interaction with the lectin ConA, which can specifically bind mannose but not galactose. By using fluorescence microscopy, it was observed that both the mannose-containing coacervates and the non-functionalized coacervates were able to partially incorporate the lectin. On the other hand, the galactose-containing coacervates showed no uptake of ConA. The captured portion of ConA was also quantitatively determined and showed that the mannose-containing coacervates were also able to bind the largest amount of ConA. Finally, the carbohydrate structures were investigated with *E. coli* bacteria, which are also able to specifically bind mannose due to their cell surface protein FimH. Here, the behavior was again investigated using fluorescence microscopy. While the mannose-containing and non-functionalized coacervates were able to capture and immobilize the bacteria, the bacteria repelled after contact with the galactose-containing coacervates. If the FimH binding sites were

blocked with alpha methyl mannose, the mannose containing coacervates did not bind to the bacteria, whereas the non-functionalized coacervates continued their interaction with the bacteria. This can be explained by the charged surface of the bacteria, which continues to interact with the polyelectrolytes of the coacervates in an unspecific manner. The lectin and bacterial assays have shown that glycan-presenting coacervates can be used as a new material in the study of specific carbohydrate binding structures and therefore open new possibilities in the development of biomimetic systems.

Overall, in this work, a successful synthesis of sequence-controlled polyelectrolytes and polyampholytes has been achieved. The extended synthesis route can be used to gain improved access to new and more complex polyelectrolyte structures and thus further investigate the coacervate behavior as a function of charge density sequences and polymer size. In addition, initial investigations of coacervates as glycan presenting coacervate droplets were performed, which showed the potential of this new method and thus paves the way for further investigations of specific biological processes.

# 5. Experimental Part

## 5.1. Materials

All reagents were used without further purification.

3-(((benzylthio)carbonothioyl)thio)propanoic acid (>98%) was purchased from TCI chemicals. Acryloyl chloride (≥97%) were purchased from Merck. Benzene (99.5%), potassium carbonate (99%) and calcium chloride (96%) were purchased from PanReac AppliChem. Triethylsilane (99%), pentafluoro phenol (99%) and D-Galactose pentaacetate (95%) were purchased from Fluorochem. Diethyl ether (99.5%) was purchased from Honeywell Riedel de Haen. Succinicanhydride (>99%) and Fmoc-Lys(Alloc)-OH (99%) was purchased from Carbolution Chemicals GmbH. Acetic anhydride (99.5%), methanol (≥99.8%), Amberlite® IR120 H hydrogen form, chloramphenicol (≥98%) and ampicillin sodium salt (BioReagent), diethylentriamine (>98%), ethylenedioxybisethylamine (98%), acetone (≥99.5%), tetrahydrofuran (≥99.9%), 2,2′-Azobis(2-methylpropionitrile) (AIBN) (≥98%), barbituric acid (99%), phenylsilane (97%), sodium sulfate (≥99%), sodium bicarbonate (≥99.7%), manganese(II) chloride (≥96%), sodium ascorbate (≥98%) and VivaSpin (MWCO: 3.000 Mw) were purchased from Sigma-Aldrich. Acetonitrile (≥99.9%), ethylacetate (≥99%), n-hexane (≥95%), 1,4-dioxane (≥99.5%), citric acid (≥99%), glycine (≥99%), trifluoroacetic acid (≥99%), hydrochloric acid, toluene (≥99.7%), triethylamine (≥99%), dichloromethane (≥99.5%) and Cytiva Vivaspin™ 20 (MWCO 3 kDa) were purchased from Fisher Scientific. N,N-Dimethylformamide (≥99.9%) was purchased from Biosolve. Ethyl trifluoracetate (≥99%) was purchased from Apollo Scientific. 4-pentynoic acid (≥95%), bromethanole (≥97%), magnesium sulfate (99%), sodium azide (≥99%), triphenylmethyl chloride (98%), trityl chloride (98%) and oxalyl chloride (98%) were purchased from Acros Organics. Sodium hydroxide (≥99.5%) was purchased from Chemsolute. Fmoc-choride (≥98%) were purchased from BLD Pharmatech GmbH. TentaGel®S RAM resin (Loading of 0.28 mmol/g) and Tentalgel® chlorotrityl resin (0.22 mmol/g) were purchased from Rapp Polymere. Benzotriazol-1-yl-oxytripyrrolidinophosphonium hexafluorophosphate (PyBOP) (≥98%) and Fmoc-Glu(OAll)-OH (99%) was purchased from Iris Biotech. DIPEA (99%), ethylenediamine (≥99,5%) and sodium chloride (≥99,5%) were purchased from Carl Roth. Sodium diethyldithiocarbamate (99%) and boron trifluoride diethyl etherate (≥98%) were purchased from Alfa Aesar. Copper(II) sulfate pentahydrate (98%), piperidine (99%), sodium methoxide (95%), triisopropysilane (TIPS) (98%) were purchased from Acros Organics.

## 5.2. Instrumentation

***Centrifuges***

For the Eppendorf tubes, a "Mini-Centrifuge Rotilabo®" from Carl Roth was used. Samples with larger volumes, the "Centrifuge 5702" from Eppendorf was used. For polymer purification by Viva-Spin, a "Heraeus Megafuge 8R Centrifuge" from Thermo ScientificI was used.

***Gel permeation chromatography***

Gel permeation chromatography was performed on a Viscotek GPCmax VE-2001 with a HPLC pump, two Malvern Viscotek T columns (styrol-divinylbenzene-copolymer, pore size 500 Å and 5000 Å) and a Sykam S3250 UV/Vis detector.

***Lyophilization***

Lyophilization was conducted on an Alpha 1-4 LD plus instrument from Martin Christ Freeze Dryers GmbH. It was performed at -42°C and a pressure of 0.1 mbar.

***Microplate Reader***

For absorbance and fluorescence measurements a "CLARIOstar" from BMG LABTECH was used. 384 well microliter plates from Greiner Bio-One were used, into each of which 30 µL and 25 µL of the samples were added, respectively.

***Microscope***

Optical analysis of the coacervates was performed on an "Olympus IX73" microscope using a 60x oil objective. 384 well microliter plates from Greiner Bio-One were used, into each of which 30 µL of the samples were added, respectively.

***MilliQ Water***

The MilliQ water (ultra-pure water) was purified using a Thermo Scientific "Barnstead Micropure ST". The conductivity was 18.20 MΩ*cm.

***Nuclear Magnetic Resonance Spectroscopy (NMR)***

$^{1}$H-NMR and $^{19}$F-NMR were recorded on a Bruker Avance III 300 or a Bruker Avance III 600. Chemical shifts were reported as delta (δ) in parts per million (ppm) and coupling constants as J in Hertz (Hz). Multiplicities are stated as follows: s = singulet, d = doublet, t = triplet, q = quartet, m = multiplett, br = broad/wide.

***Peptide synthesizer***

The CS136XT peptide synthesizer from CS Bio Co. was used for the synthesis of the oligomer backbone. The used protocols are listed below.

***Reversed Phase – High Pressure Liquid Chromatography (RP-HPLC)***

Analytical RP-HPLC-MS measurements were performed on Agilent Technologies 6120 series coupled with an Agilent quadrupole mass spectrometer with an Electrospray Ionization (ESI) source operating in a m/z range of 200 to 2000. All spectra were measured with solvents A: 95% H2O, 5% MeCN, +0.1% formic acid and B: 5% H2O, 95% MeCN, +0.1% formic acid. As a column, a Poroshell 120 EC-C18 1.8 µM (3.0x50 mm, 2.5 µM) reversed phase column was used. Indicated purities were determined by integration of the UV-signal detected by a wavelength detector set to 214 nm with the OpenLab ChemStation software for LC/MS from Agilent Technologies.

## 5.3. General Methods

***Standard synthesizer protocol***

Oligomer backbones were synthesized using a peptide synthesizer. Following protocols refer to 0.3 mmol resin.

***Swelling protocol***

The resin was swollen twice in 15 mL DCM for 15 minutes each. It was then washed three times with 15 mL DMF for one minute each.

***Deprotection/coupling protocol***

The resin was washed three times for 10 min with 15 mL each of a 25% piperidine in DMF solution. Between the deprotection steps, the resin was washed three times with 15 mL DMF for 1 min each. After the last deprotection step, the resin was washed ten times with 15 mL DMF for 1 min each. For the coupling, 4 mL of the amino acid (AA) or building block (BB) solution (5 eq. in 4 mL), 4 mL of 1 molar DIPEA in DMF solution and 4 mL of PyBOP solution (5 eq. in 4 mL) were premixed and shaken with the resin for 90 minutes. The resin was then washed ten times for one minute each with 15 mL DMF.

This protocol was repeated for every amino acid and building block until the desired structure was synthesized.

***Swelling protocol after coupling***

After coupling of the last AA or BB resin was swelled twice with 15 mL DCM for 15 minutes each. It was then washed three times with 15 mL DMF for one minute each.

***Capping***

Fmoc protecting group was removed from both batches, by using 5 ml of 25 vol% piperidine in DMF. The mixtures were shaken for 15 min. The resin was washed with DMF and the process was repeated. Afterwards, resin was washed several times with DMF and 7 mL acetic anhydride were added. Mixture was shaken for 1h and resin was washed again with DMF.

***Cleavage***

Resin was mixed with 4 mL of a cleavage solution consisting of 95 vol% TFA, 2.5 vol% TIPS, and 2.5 vol% DCM and were shaken for 1h. The products were then precipitated in cold diethyl ether and centrifuged off. The diethyl ether was decanted off, and the residues were dissolved in approximately 8 mL of MilliQ water and lyophilized.

***Determination of functionalization degree***

The determination of the functionalization degree was calculated by using $^{1}$H-NMR. The aromatic protons in the NMR represent aromatic polymer backbone protons. For this purpose, the number of aromatic protons of a polymer backbone was set to five protons to represent one polymer molecule. The signal of the protection group at 5.7-6 ppm was integrated and divided by the number of protection groups present (four for the oligo-electrolytes and eight for the oligo-ampholytes). A calculation example for the $P_{100}$(EEEE) is shown below:

$$Function.Degree = \frac{Protons\ of\ PG\ at\ 5.7-6\ ppm}{Number\ of\ protecting\ groups} = \frac{40}{4} = 10\%$$

An overview of the calculated functionalization is shown in Table 5.

***Coacervation of linear charged polyelectrolytes and ampholytes***

The general coacervate formation of the linear polyelectrolytes was performed according to the following protocol. 200 mM stock solutions of the anionic and cationic polymers were prepared with respect to the molecular weight of the polymer repeating unit. A 4 M NaCl solution was prepared. For the microscope measurement, 50 µL of the salt solution was prepared in a 0.5 mL reaction tube and mixed with 25 µL of the anionic polymer for 10 seconds. Next, 25 µL of the cationic polymer was added and mixed again. The concentration of the salt and the polymers in the final solution was therefore half the concentration of the stock solution. The finished coacervate solution was then analyzed under a microscope. For the ampholytic structures, the measurement was carried out as described above with the exception that 50 µL of salt solution was first added and then 50 µL of the ampholytic polymer solution was added and mixed.

***Coacervation of brush-shaped polyelectrolytes and -ampholytes***

To measure the brush-shaped polymers, the molecular weight of the repeating unit was first determined. Since the polymer was made up of two different repeating units, the molecular weight was calculated as a percentage of the targeted incorporation of the side chains.

$$Mw\ of\ repeating\ unit =$$

$$\%\ in\ Polymer * Mw\ of\ Ethanolamine + \%\ in\ Polymer * Mw\ of\ Oligomer =$$

$$0.75 * 115{,}13\frac{g}{mol} + 0{,}25 * 668{,}62\frac{g}{mol} =$$

$$276{,}49\frac{g}{mol}$$

The coacervate measurement was then carried out as described above for the linear polymers.

## 5.4. Syntheses

### 5.4.1. Oligomers

All Oligomers were synthesized using the standard protocol described in Chapter 5.3. The solid support was either TentaGel® S RAM resin with a capacity of 0.28 mml/g or TentaGel® S TRT-Cl resin functionalized with an EDA linker according to literature[111] with a subsequent capacity of 0.2 mmol/g.

***Oligomer: EEEE***

The oligomer was synthesized on an EDA functionalized chlorotrityl resin according to the standard synthesizer protocol and was obtained with a yield of 84% and a relative purity of 98%.

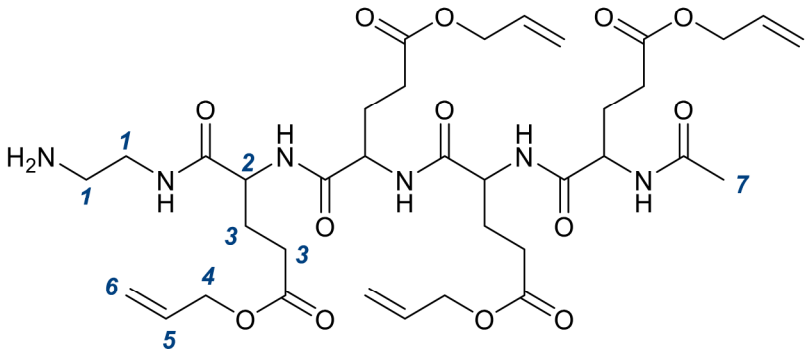

**$^1$H-NMR** (600 MHz, MeOD-d4): δ (ppm) = 6.01 – 5.86 (m, 4H, ***H5***), 5.31 (m, 4H, ***H6***) 5.22 (m, 4H, ***H6***), 4.59 (m, 8H, ***H4***), 4.30 – 4.12 (m, 4H, ***H2***), 3.58 – 3.36 (m, 2H, ***H1***), 3.16 – 2.97 (m, 2H, ***H1***), 2.62 – 2.37 (m, 8H, ***H3***), 2.25 – 1.90 (m, 12H, ***H3, H7***).

**RP-HPLC-MS:** $t_R$ = 13.21 min, >98% relative purity (UV), from 95/5 to 5/95 Vol. % Water/acetonitrile with 0,1% formic acid in 30 min at 25 °C.

**ESI-MS:** calc. for $C_{36}H_{54}N_6O_{13}$: $[M+2H]^{2+}$ 390.19, $[M+H]^+$ 779.38; found 390.0 $[M+2H]^{2+}$, 779.2 $[M+H]^+$.

***Oligomer: KKKK***

The oligomer was synthesized on an EDA functionalized chlorotrityl resin according to the standard synthesizer protocol and was obtained with a yield of 79% and a relative purity of 99%.

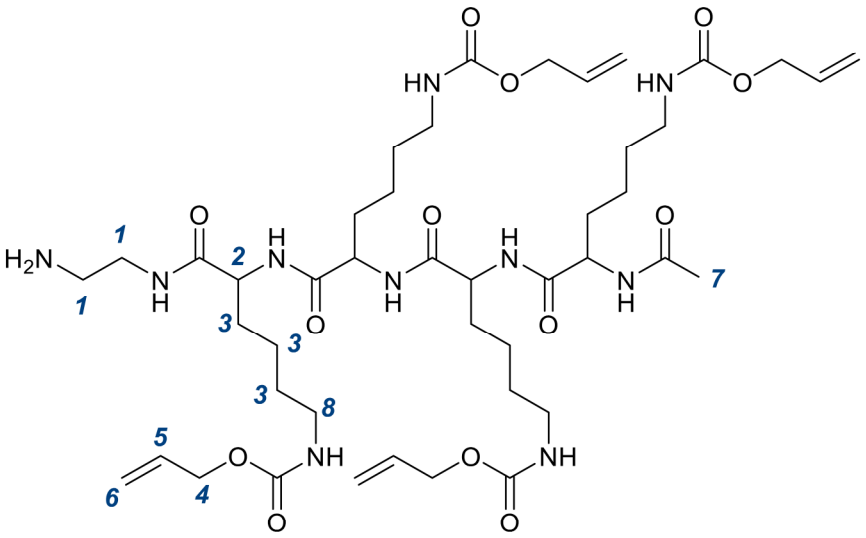

**$^1$H-NMR** (600 MHz, MeOD-d4): δ (ppm) = 5.94 (m, 4H, ***H5***), 5.30 (m, 4H, ***H6***), 5.19 (m, 4H, ***H6***), 4.53 (m, 8H, ***H4***), 4.26 – 4.12 (m, 4H, ***H2***), 3.61 – 3.41 (m, 2H, ***H1***), 3.12 (m, 10H, ***H1, H8***), 2.04 (s, 3H, ***H7***), 1.92 – 1.68 (m, 8H, ***H3***), 1.63 – 1.50 (m, 8H, ***H3***), 1.49 – 1.35 (m, 9H, ***H3***) .

**RP-HPLC-MS:** $t_R$ = 13.35 min, >99% relative purity (UV), from 95/5 to 5/95 Vol. % Water/acetonitrile with 0,1% formic acid in 30 min at 25 °C.

**ESI-MS:** calc. for $C_{44}H_{74}N_{10}O_{13}$: $[M+2H]^{2+}$ 476.28, $[M+H]^+$ 951.55; found 476.4 $[M+2H]^{2+}$, 951.6 $[M+H]^+$.

***Oligomer: KEKEKEKE***

The oligomer was synthesized on Tentagel S-RAM resin according to the standard synthesizer protocol and was obtained with a yield of 65% and a relative purity of 95%

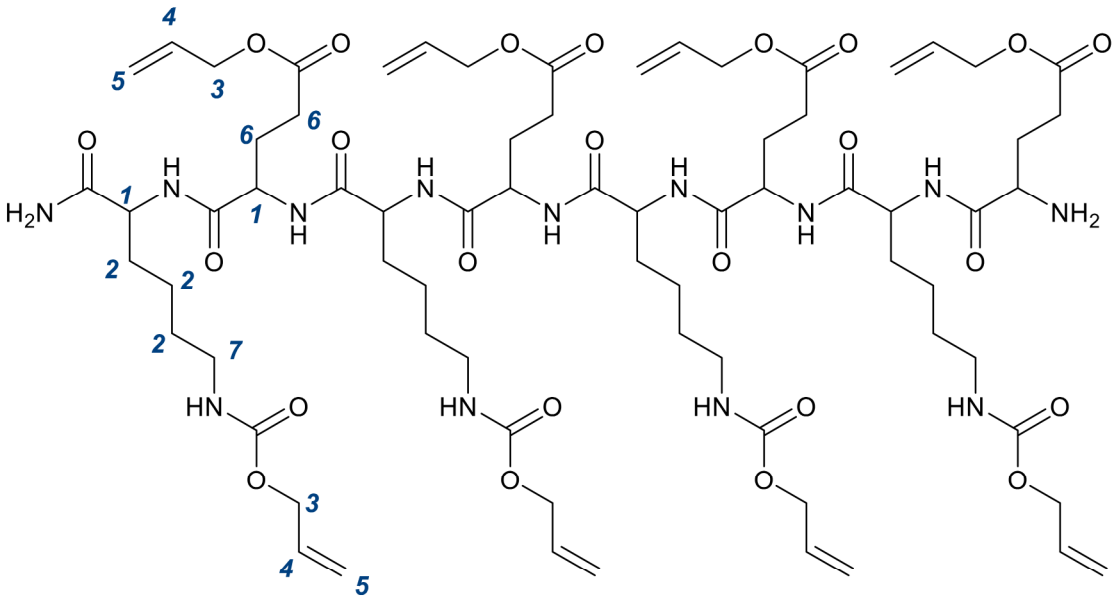

**$^1$H-NMR** (600 MHz, $D_2O$/MeCN-d3): δ (ppm) = 5.86 (m, 8H, ***H4***), 5.33 – 5.03 (m, 16H, ***H5***), 4.61 – 4.38 (m, 16H, ***H3***), 2.99 (m, 9H, ***H7***), 2.51 – 2.31 (m, 9H, ***H6***), 2.16 – 1.97 (m, 9H, ***H6***), 1.78 – 1.17 (m, 34H, ***H2***).

**RP-HPLC-MS:** $t_R$ = 16.48 min, >95% relative purity (UV), from 95/5 to 5/95 Vol. % Water/acetonitrile with 0,1% formic acid in 30 min at 25 °C.

**ESI-MS:** calc. for $C_{72}H_{111}N_{13}O_{24}$: $[M+2H]^{2+}$ 771.9, $[M+H]^+$ 1542.79; found 772.0 $[M+2H]^{2+}$, 1544.6 $[M+H]^+$.

***Oligomer: KKEEKKEE***

The oligomer was synthesized on Tentagel S-RAM resin according to the standard synthesizer protocol and was obtained with a yield of 70% and a relative purity of 97%

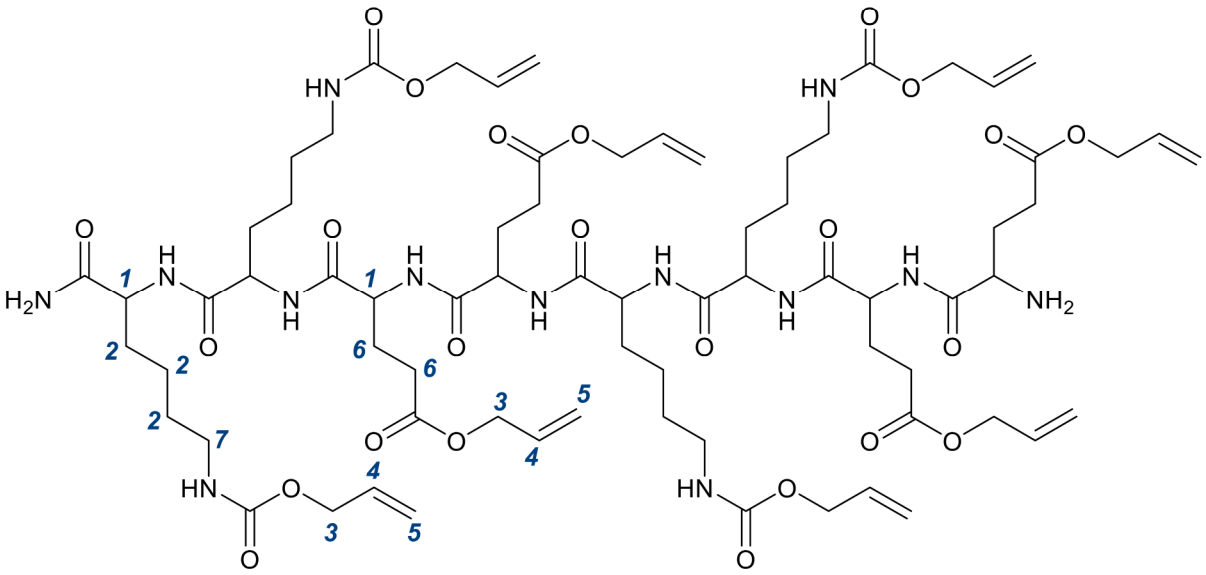

**$^1$H-NMR** (600 MHz, $D_2O$/MeCN-d3): δ (ppm) = 6.00 – 5.74 (m, 8H, ***H4***), 5.34 – 5.04 (m, 16H, ***H5***), 4.57 – 4.40 (m, 16H, ***H3***), 4.10 (m, 9H, ***H1***), 2.99 (m, 8H, ***H7***), 2.52 – 2.34 (m, 8H, ***H6***), 2.17 – 1.99 (m, 9H, ***H6***), 1.79 – 1.10 (m, 29H, ***H2***).

**RP-HPLC-MS:** $t_R$ = 16.48 min, >97% relative purity (UV), from 95/5 to 5/95 Vol. % Water/acetonitrile with 0,1% formic acid in 30 min at 25 °C.

**ESI-MS:** calc. for $C_{72}H_{111}N_{13}O_{24}$: $[M+2H]^{2+}$ 771.9, $[M+H]^+$ 1542.79; found 772.0 $[M+2H]^{2+}$, 1543.8 $[M+H]^+$.

***Oligomer: KKKKEEEE***

The oligomer was synthesized on Tentagel S-RAM resin according to the standard synthesizer protocol and was obtained with a yield of 86% and a relative purity of 93%.

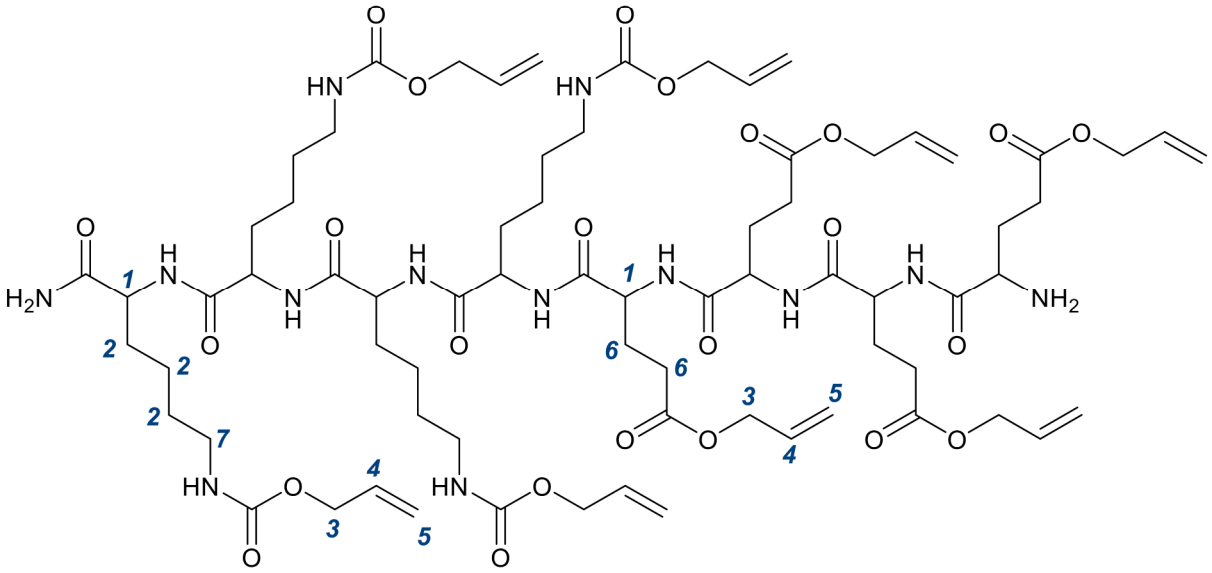

**$^1$H-NMR** (600 MHz, $D_2O$/MeCN-d3): δ (ppm) = 5.97 – 5.75 (m, 8H, ***H4***), 5.30 – 5.06 (m, 16H, ***H5***), 4.55 – 4.37 (m, 17H, ***H3***), 4.14 – 4.00 (m, 8H, ***H1***), 2.98 (m, 9H, ***H7***), 2.58 – 2.31 (m, 8H, ***H6***), 2.13 – 1.99 (m, 8H, ***H6***), 1.81 – 1.14 (m, 32H, ***H2***).

**RP-HPLC-MS:** $t_R$ = 16.48 min, >93% relative purity (UV), from 95/5 to 5/95 Vol. % Water/acetonitrile with 0,1% formic acid in 30 min at 25 °C.

**ESI-MS:** calc. for $C_{72}H_{111}N_{13}O_{24}$: $[M+2H]^{2+}$ 771.9, $[M+H]^+$ 1542.79; found 772.0 $[M+2H]^{2+}$, 1543.8 $[M+H]^+$.

### 5.4.2. Polymers

***Pentafluoro phenyl acrylate monomer – PFPA***

The monomer was synthesized according to literature and was obtained with a yield of 58%.[109]

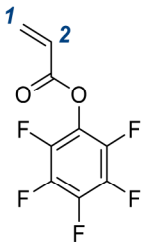


**$^{1}$H-NMR** (600 MHz, $CDCl_3$): δ (ppm) = 6.72 (dd, *J* = 17.3, 0.9 Hz, 1H, ***H1***), 6.37 (dd, *J* = 17.3, 10.6 Hz, 1H, ***H2***), 6.18 (dd, *J* = 10.5, 0.9 Hz, 1H, ***H1***).

**$^{19}$F-NMR** (600 MHz, $CDCl_3$): δ (ppm) = -152.54 (m, 2F), -157.92 (t, 1F), -162.32 (m, 2F).

***Poly(pentafluoro phenyl acrylate) 100 - PPFP$_{100}$***

The polymer was synthesized with reference to the literature.[109] PFPA (21 mmol, 1 eq.), BSPA (0.21 mmol, 0.01 eq.) and AIBN (0.042 mol, 0.002 eq.) were dissolved in 20 mL benzene. The mixture was in an ice bath and flushed with nitrogen for 30 min. Afterwards the mixture got heated in an oil bath to 70°C for 24h. The reaction is terminated by purging the mixture with air and freezing it with liquid nitrogen. The polymer was precipitated in hexane, centrifuged and dried under vacuum. The polymer was obtained with a yield of 65%.

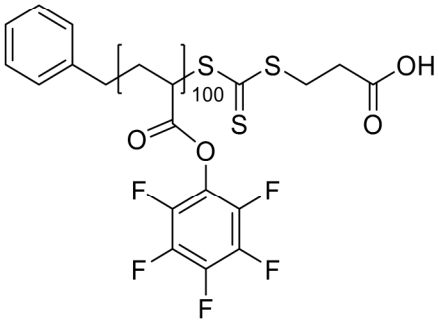


**$^{1}$H-NMR** (600 MHz, $CDCl_3$): δ (ppm) = 7.18 (m, 4H), 3.64 (s, 2H), 3.08 (m, 90H), 2.88 – 2.72 (m, 17H), 2.50 (bs, 40H), 2.11 (m, 151H).

**$^{19}$F-NMR** (600 MHz, $CDCl_3$): δ (ppm) = -153.21 (m, 2F), -156.7 (m, 1F), -162.16 (m, 2F).

**GPC analysis**

*Table E1: GPC analysis of Poly(pentafluoro phenyl acrylate) 100 (PPFP$_{100}$)*

| **Detector** | UV | RI |
|---|---|---|
| **Mw** | 22619 | 23278 |
| **Mn** | 17228 | 18140 |
| **Đ** | 1.31 | 1.28 |

***Poly(pentafluoro phenyl acrylate) 200 – PPFP$_{200}$***

The polymer was synthesized with reference to the literature.[109] PFPA (21 mmol, 1 eq.), BSPA (0.105 mol, 0.005 eq.) and AIBN (0.021 mol, 0.001 eq.) were dissolved in 20 mL benzene. The mixture was in an ice bath and flushed with nitrogen for 30 min. Afterwards the mixture got heated in an oil bath to 70°C for 24h. The reaction is terminated by purging the mixture with air and freezing it with liquid nitrogen. The polymer was precipitated in hexane, centrifuged and dried under vacuum. The polymer was obtained with a yield of 68%.

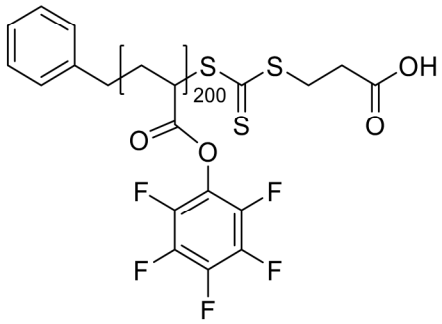


**$^{1}$H-NMR** (600 MHz, $CDCl_3$): δ (ppm) = 7.18 (m, 4H), 3.67 (m, 2H), 3.26 – 2.63 (m, 218H), 2.60 – 1.77 (m, 405H).

**$^{19}$F-NMR** (600 MHz, $CDCl_3$): δ (ppm) = -153.20 (m, 2F), -156.77 (m, 1F), -162.29 (m, 2F).

**GPC analysis**

*Table E2: GPC analysis of Poly(pentafluoro phenyl acrylate) 200 (PPFP$_{200}$)*

| **Detector** | UV | RI |
|---|---|---|
| **Mw** | 40896 | 41598 |
| **Mn** | 31680 | 32981 |
| **Đ** | 1.29 | 1.26 |

***Ethylene diamine-Trt (EDA-Trt)***

EDA (0.08 mmol, 4 eq.) was dissolved in 150 mL DCM and cooled in an ice bath. Triphenylmethyl chloride (0.02 mmol, 1 eq.) was dissolved in 90 mL DCM and dropwise added to the EDA mixture. After the addition, the ice bath got removed and the reaction solution was stirred for 16h at room temperature. The solution was concentrated to approximately 50 mL using a rotary evaporator and washed three times with saturated $NaHCO_3$ solution. Organic phase was dried using $MgSO_4$ and solvent was removed. Product was obtained with a yield of 85%.

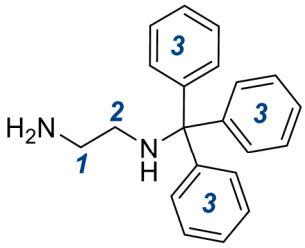


**$^1$H-NMR** (300 MHz, $CDCl_3$): δ (ppm) = 9.50 – 9.44 (m, 6H, ***H3***), 9.29 – 9.21 (m, 7H, ***H3***), 9.18 – 9.08 (m, 3H, ***H3***), 4.78 (t, J = 6.0 Hz, 2H, ***H2***), 4.19 (t, J = 6.0 Hz, 2H, ***H1***).

***$P_{100}$(+)***

The polymer analogous reaction was performed by dissolving $PPFP_{100}$ (0.84 mmol, 1 eq.) in 4 mL DMF. TEA (2.8 mmol, 3.4 eq.) and EDA (42 mmol, 50 eq.) were added to the reaction mixture and stirred for 3h at 40°C. Afterwards the polymer was diluted with distilled water and purified by Viva Spin (MWCO 3 kDa, Fischer Scientific, Germany). PH was adjusted to 7 by using 1 M NaOH and 1 M HCl, purified by Vivaspin and lyophilized. It was obtained with a yield of 68%.

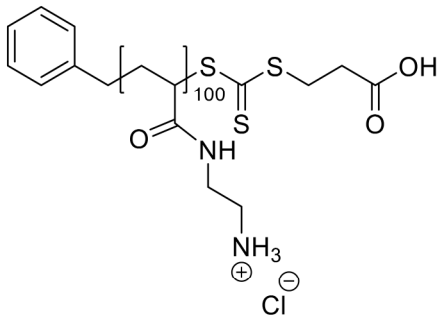


**$^{1}$H-NMR** (600 MHz, $D_2O$): δ (ppm) = 7.45 – 7.19 (m, 5H, $H_{aromatic}$), 3.71 – 3.00 (m, 402H, -NHC$H_2$C$H_2$$NH_3^+$), 2.39 – 1.11 (m, 335H, C$H_{2\ Backbone}$).

**$^{19}$F-NMR** (600 MHz, $D_2O$): δ (ppm) = no signals.

***$P_{100}$(-)***

The polymer analogous reaction was performed by dissolving $PPFP_{100}$ (0.84 mmol, 1 eq.) in 4 mL DMF. TEA (2.8 mmol, 3.4 eq.) was added to the reaction mixture. Glycine (1.68 mmol, 2 eq.) was dissolved in 1 mL MilliQ water, added to the reaction mixture and stirred for 3h at 40°C. Afterwards the polymer was diluted with distilled water and purified by Viva Spin (MWCO 3 kDa, Fischer Scientific, Germany). PH was adjusted to 7 by using 1 M NaOH and 1 M HCl, purified by Vivaspin and lyophilized. It was obtained with a yield of 79%.

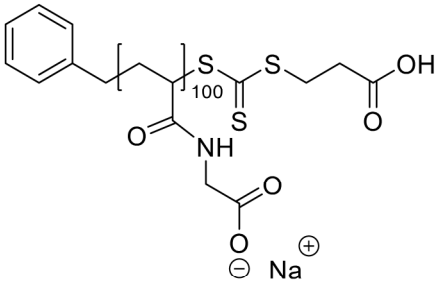


**$^{1}$H-NMR** (600 MHz, $D_2O$): δ (ppm) = 9.67 – 9.10 (m, 12H), 7.47 – 7.16 (m, 5H, $H_{aromatic}$), 4.36 – 3.29 (m, 190H, -NHC$H_2$COO$^-$), 3.07 – 1.01 (m, 300H, C$H_{2\ Backbone}$).

**$^{19}$F-NMR** (600 MHz, $D_2O$): δ (ppm) = no signals.

***$P_{200}$(+)***

The polymer analogous reaction was performed by dissolving $PPFP_{200}$ (0.84 mmol, 1 eq.) in 4 mL DMF. TEA (2.8 mmol, 3.4 eq.) and EDA (42 mmol, 50 eq.) were added to the reaction mixture and stirred for 3h at 40°C. Afterwards the polymer was diluted with distilled water and purified by Viva Spin (MWCO 3 kDa, Fischer Scientific, Germany). PH was adjusted to 7 by using 1 M NaOH and 1 M HCl, purified by Vivaspin and lyophilized. It was obtained with a yield of 63%.

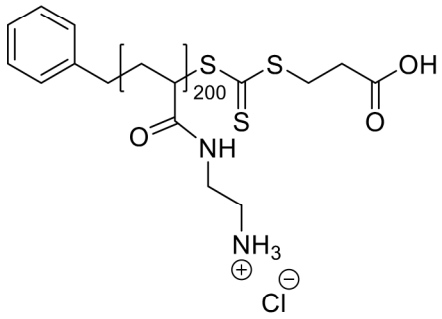


**$^{1}$H-NMR** (600 MHz, $D_2O$): δ (ppm) = 7.46 – 7.22 (m, 5H, $H_{aromatic}$), 3.67 – 2.95 (m, 752H, -NHC$H_2$C$H_2$$NH_3^+$), 2.57 – 0.93 (m, 590H, C$H_{2\ Backbone}$).

**$^{19}$F-NMR** (600 MHz, $D_2O$): δ (ppm) = no signals.

***$P_{200}$(-)***

The polymer analogous reaction was performed by dissolving $PPFP_{200}$ (0.84 mmol, 1 eq.) in 4 mL DMF. TEA (2.8 mmol, 3.4 eq.) was added to the reaction mixture. Glycine (1.68 mmol, 2 eq.) was dissolved in 1 mL MilliQ water, added to the reaction mixture and stirred for 3h at 40°C. Afterwards the polymer was diluted with distilled water and purified by Viva Spin (MWCO 3 kDa, Fischer Scientific, Germany). PH was adjusted to 7 by using 1 M NaOH and 1 M HCl, purified by Vivaspin and lyophilized. It was obtained with a yield of 77%.

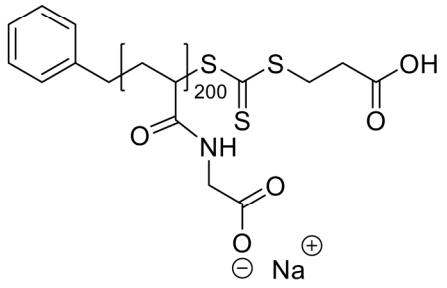


**$^{1}$H-NMR** (600 MHz, $D_2O$): δ (ppm) = 7.43 – 7.15 (m, 5H, $H_{aromatic}$), 4.30 – 3.29 (m, 373H, -NHC$H_2$COO$^-$), 2.52 – 1.08 (m, 619H, C$H_{2\ Backbone}$).

**$^{19}$F-NMR** (600 MHz, $D_2O$): δ (ppm) = no signals.

***$P_{100}$(+/-)***

The polymer analogous reaction was performed by dissolving $PPFP_{100}$ (1.05 mmol, 1eq.) in 5 mL DMF. TEA (3.5 mmol, 8.5 eq.) was added to the reaction mixture. Glycine (0.5 mmol, 0.5 eq.) was dissolved in 0.5 mL MilliQ water, added to the reaction mixture and stirred for 24h at 40°C. Afterwards EDA (75 mmol, 78.75 eq.) was added to the reaction mixture and stirred for 3h at 40°C. The polymer was diluted with distilled water and purified by Viva Spin (MWCO 3 kDa, Fischer Scientific, Germany). PH was adjusted to 7 by using 1 M NaOH and 1 M HCl, purified by Vivaspin and lyophilized. It was obtained with a yield of 86%.

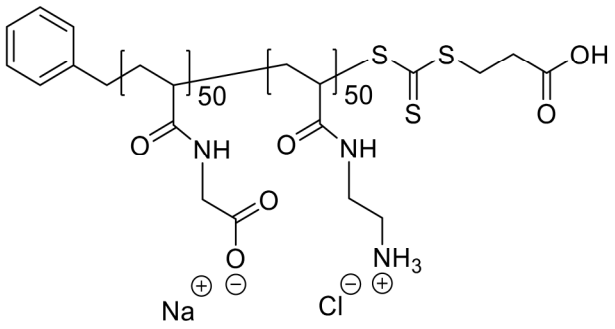


**$^{1}$H-NMR** (600 MHz, $D_2O$): δ (ppm) = 7.40 – 7.21 (m, 5H, $H_{aromatic}$), 4.26 – 3.01 (m, 198H, -NHC$H_2$COO-, -NHC$H_2$C$H_2$$NH_3^+$), 2.52 – 1.08 (m, 329H, C$H_{2\ Backbone}$).

**$^{19}$F-NMR** (600 MHz, $D_2O$): δ (ppm) = no signals.

***$P_{200}$(+/-)***

The polymer analogous reaction was performed by dissolving $PPFP_{200}$ (1.05 mmol, 1eq.) in 5 mL DMF. TEA (3.5 mmol, 8.5 eq.) was added to the reaction mixture. Glycine (0.5 mmol, 0.5 eq.) was dissolved in 0.5 mL MilliQ water, added to the reaction mixture and stirred for 24h at 40°C. Afterwards EDA (75 mmol, 78.75 eq.) was added to the reaction mixture and stirred for 3h at 40°C. The polymer was diluted with distilled water and purified by Viva Spin (MWCO 3 kDa, Fischer Scientific, Germany). PH was adjusted to 7 by using 1 M NaOH and 1 M HCl, purified by Vivaspin and lyophilized. It was obtained with a yield of 77%.

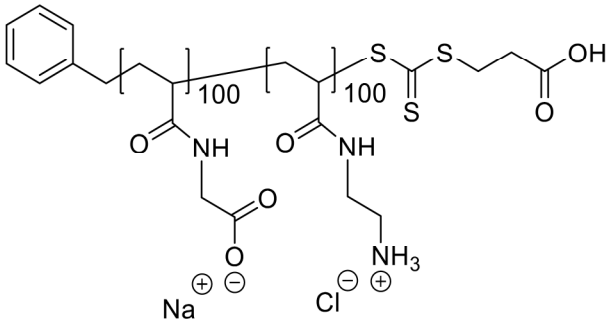


**$^{1}$H-NMR** (600 MHz, $D_2O$): δ (ppm) = 7.40 – 7.21 (m, 5H, $H_{aromatic}$), 4.46 – 2.93 (m, 421H, -NHC$H_2$COO-, -NHC$H_2$C$H_2$$NH_3^+$), 2.86 – 1.03 (m, 672H, C$H_{2\ Backbone}$).

**$^{19}$F-NMR** (600 MHz, $D_2O$): δ (ppm) = no signals.

***$P_{100}$(++++)***

The polymer analogous reaction was performed by dissolving $PPFP_{100}$ (0.42 mmol, 1 eq.) in 2 mL DMF. TEA (0.71 mmol, 1.7 eq.) was added to the reaction mixture. The oligomer KKKK (0.11 mmol, 0.25 eq.) was dissolved in 5 mL DMF, added to the reaction mixture and stirred for 24h at 40°C. Afterwards ethanolamine (1.65 mmol, 3.9 eq.) was added to the reaction mixture and stirred for 3h at 40°C. The polymer was lyophilized without further purification. For the deprotection of Alloc protection groups, the molecular weight was set equal to the mass of the oligomer. Deprotection was performed by dissolving the obtained $P_{100}$(KKKK) (0.025 mmol, 1 eq.) in 2 mL DMF. Phenyl silane (1.2 mmol, 48 eq.) and Tetrakis-(triphenylphosphine)-palladium(0) (0.02 mmol, 0.8 eq.) dissolved in 1 mL DMF were added to the reaction mixture and stirred for 15 min under nitrogen atmosphere. The reaction mixture was precipitated in diethyl ether, centrifuged and dissolved in MilliQ water. PH was adjusted to 7 by using 1 M NaOH and 1 M HCl. The polyelectrolyte was purified by Vivaspin (MWCO 5 kDa, Fischer Scientific, Germany) and lyophilized. It was obtained with an overall yield of 45%.

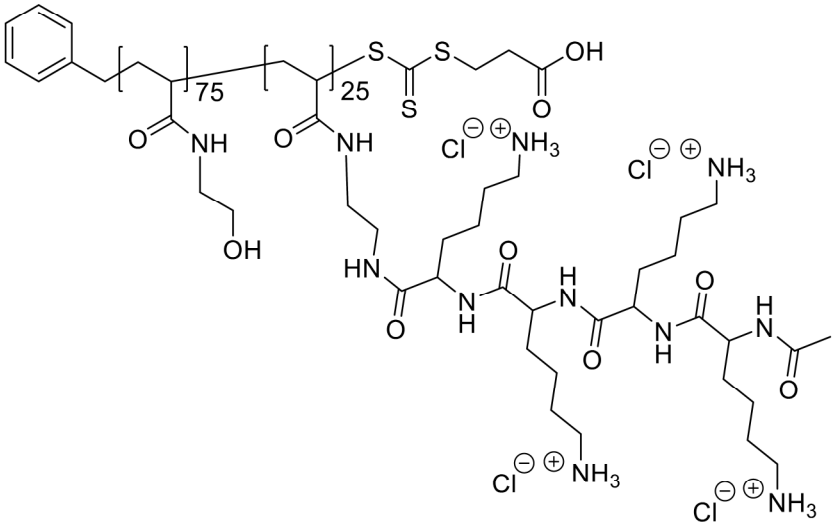


Functionalization degree was not determinable, because no purification could be performed after polymer analogous reaction.

**$^{19}$F-NMR** (600 MHz, $D_2O$): δ (ppm) = no signals.

***$P_{100}$(----)***

The polymer analogous reaction was performed by dissolving $PPFP_{100}$ (0.42 mmol, 1 eq.) in 2 mL DMF. TEA (0.71 mmol, 1.7 eq.) was added to the reaction mixture. The oligomer EEEE (0.11 mmol, 0.25 eq.) was dissolved in 5 mL DMF, added to the reaction mixture and stirred for 24h at 40°C. Afterwards ethanolamine (1.65 mmol, 3.9 eq.) was added to the reaction mixture and stirred for 3h at 40°C. The polymer was diluted with MilliQ water, purified by Viva Spin (MWCO 3 kDa, Fischer Scientific, Germany) and lyophilized. Functionalization degree was determined by $^1$H-NMR. For the deprotection of Allyl protection groups, the molecular weight was set equal to the mass of the oligomer EEEE. Deprotection of Allyl protection groups was performed by dissolving the obtained $P_{100}$(EEEE) (0.025 mmol, 1 eq.) in 2 mL DMF. barbituric acid (1.2 mmol, 48 eq.) and Tetrakis-(triphenylphosphine)palladium(0) (0.02 mmol, 0.8 eq.) dissolved in 1 mL DMF were added to the reaction mixture and stirred for 15 min under nitrogen atmosphere. The reaction mixture was precipitated in diethyl ether, centrifuged and dissolved in MilliQ water. PH was adjusted to 7 by using 1 M NaOH and 1 M HCl. The polyelectrolyte was purified by Vivaspin (MWCO 5 kDa, Fischer Scientific, Germany) and lyophilized. It was obtained with an overall yield of 57%.

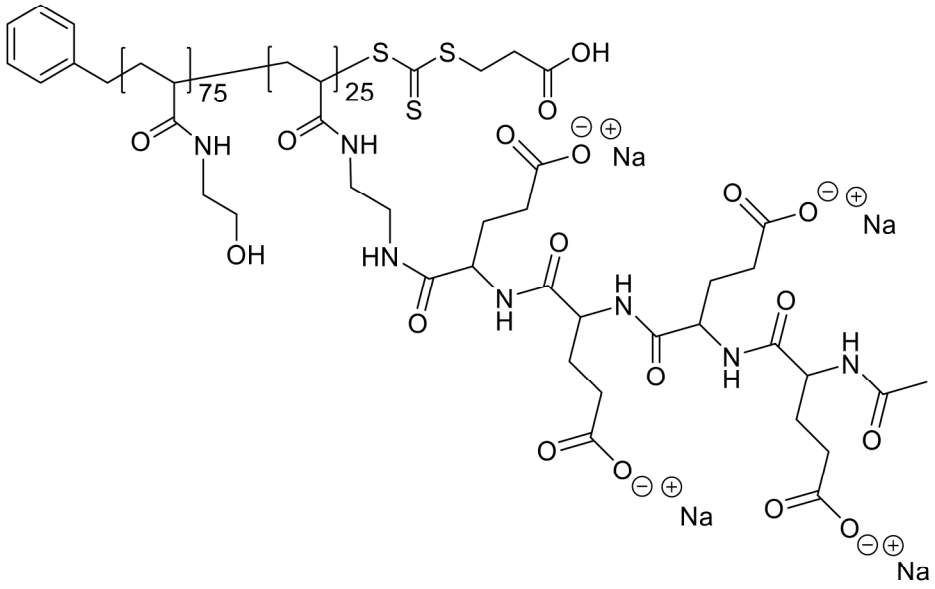


Only aromatic and protection group signals were integrated in $^1$H-NMR to calculate functionalization degree. Final functionalization degree: 10%

**$^1$H-NMR** (600 MHz, $D_2O$): Signals were used to calculate functionalization degree.

**$^{19}$F-NMR** (600 MHz, $D_2O$): δ (ppm) = no signals.

***$P_{100}$(+-+-+-+)***

The polymer analogous reaction was performed by dissolving $PPFP_{100}$ (0.32 mmol, 1 eq.) in 1.5 mL DMF. TEA (1.07 mmol, 2.6 eq.) was added to the reaction mixture. The oligomer KEKEKEKE (0.032 mmol, 0.1 eq.) was dissolved in 1 mL DMF, added to the reaction mixture and stirred for 16h at 40°C. Afterwards ethanolamine (1.6 mmol, 5 eq.) was added to the reaction mixture and stirred for 2h at 40°C. The polymer was diluted with MilliQ water, purified by Viva Spin (MWCO 5 kDa, Fischer Scientific, Germany) and lyophilized. Functionalization degree was determined by $^1$H-NMR. For the deprotection of Alloc and Allyl protection groups, the molecular weight was set equal to the mass of the oligomer KEKEKEKE. Deprotection of Allyl protection groups was performed by dissolving the obtained $P_{100}$(KEKEKEKE) (0.025 mmol, 1 eq.) in 2 mL DMF. Phenyl silane (0.72 mmol, 29 eq.) and Tetrakis-(triphenylphosphine)palladium(0) (0.012 mmol, 0.5 eq.) dissolved in 1 mL DMF were added to the reaction mixture and stirred for 15 min under nitrogen atmosphere. The reaction mixture was precipitated in diethyl ether, centrifuged and dissolved in MilliQ water. PH was adjusted to 7 by using 1 M NaOH and 1 M HCl. The polyampholyte was purified by Vivaspin (MWCO 5 kDa, Fischer Scientific, Germany) and lyophilized. It was obtained with an overall yield of 52%.

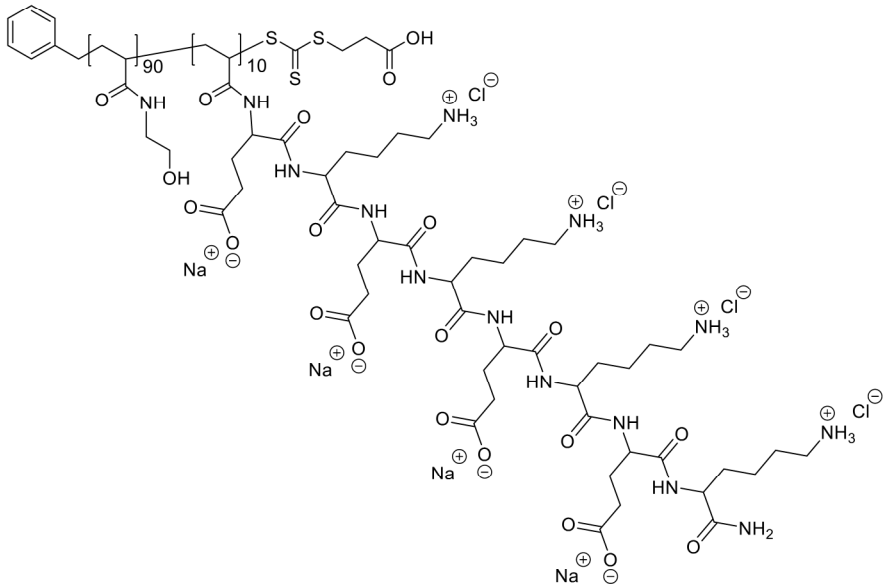

Only aromatic and protection group signals were integrated in $^1$H-NMR to calculate functionalization degree. Final functionalization degree: 4.5%

**$^1$H-NMR** (600 MHz, $D_2O$): Signals were used to calculate functionalization degree.

**$^{19}$F-NMR** (600 MHz, $D_2O$): δ (ppm) = no signals.

***$P_{100}$(++--++--)***

The polymer analogous reaction was performed by dissolving $PPFP_{100}$ (0.32 mmol, 1 eq.) in 1.5 mL DMF. TEA (1.07 mmol, 2.6 eq.) was added to the reaction mixture. The oligomer KKEEKKEE (0.032 mmol, 0.1 eq.) was dissolved in 1 mL DMF, added to the reaction mixture and stirred for 16h at 40°C. Afterwards ethanolamine (1.6 mmol, 5 eq.) was added to the reaction mixture and stirred for 2h at 40°C. The polymer was diluted with MilliQ water, purified by Viva Spin (MWCO 5 kDa, Fischer Scientific, Germany) and lyophilized. Functionalization degree was determined by $^1$H-NMR. For the deprotection of Alloc and Allyl protection groups, the molecular weight was set equal to the mass of the oligomer KKEEKKEE. Deprotection of Allyl protection groups was performed by dissolving the obtained $P_{100}$(KKEEKKEE) (0.025 mmol, 1 eq.) in 2 mL DMF. Phenyl silane (0.72 mmol, 29 eq.) and Tetrakis-(triphenylphosphine)palladium(0) (0.012 mmol, 0.5 eq.) dissolved in 1 mL DMF were added to the reaction mixture and stirred for 15 min under nitrogen atmosphere. The reaction mixture was precipitated in diethyl ether, centrifuged and dissolved in MilliQ water. PH was adjusted to 7 by using 1 M NaOH and 1 M HCl. The polyampholyte was purified by Vivaspin (MWCO 5 kDa, Fischer Scientific, Germany) and lyophilized. It was obtained with an overall yield of 42%.

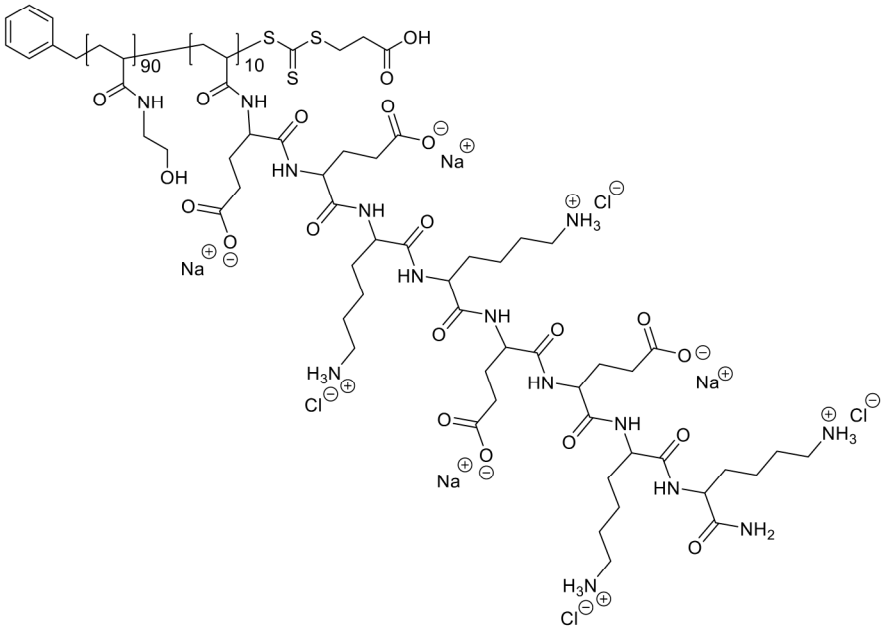

Only aromatic and protection group signals were integrated in $^1$H-NMR to calculate functionalization degree. Final functionalization degree: 4.8%

**$^1$H-NMR** (600 MHz, $D_2O$): Signals were used to calculate functionalization degree.

**$^{19}$F-NMR** (600 MHz, $D_2O$): δ (ppm) = no signals.

***$P_{100}$(++++----)***

The polymer analogous reaction was performed by dissolving $PPFP_{100}$ (0.32 mmol, 1 eq.) in 1.5 mL DMF. TEA (1.07 mmol, 2.6 eq.) was added to the reaction mixture. The oligomer KKKKEEEE (0.032 mmol, 0.1 eq.) was dissolved in 1 mL DMF, added to the reaction mixture and stirred for 16h at 40°C. Afterwards ethanolamine (1.6 mmol, 5 eq.) was added to the reaction mixture and stirred for 2h at 40°C. The polymer was diluted with MilliQ water, purified by Viva Spin (MWCO 5 kDa, Fischer Scientific, Germany) and lyophilized. Functionalization degree was determined by $^1$H-NMR. For the deprotection of Alloc and Allyl protection groups, the molecular weight was set equal to the mass of the oligomer KKKKEEEE. Deprotection of Allyl protection groups was performed by dissolving the obtained $P_{100}$(KKKKEEEE) (0.025 mmol, 1 eq.) in 2 mL DMF. Phenyl silane (0.72 mmol, 29 eq.) and Tetrakis-(triphenylphosphine)palladium(0) (0.012 mmol, 0.5 eq.) dissolved in 1 mL DMF were added to the reaction mixture and stirred for 15 min under nitrogen atmosphere. The reaction mixture was precipitated in diethyl ether, centrifuged and dissolved in MilliQ water. PH was adjusted to 7 by using 1 M NaOH and 1 M HCl. The polyampholyte was purified by Vivaspin (MWCO 5 kDa, Fischer Scientific, Germany) and lyophilized. It was obtained with an overall yield of 38%.

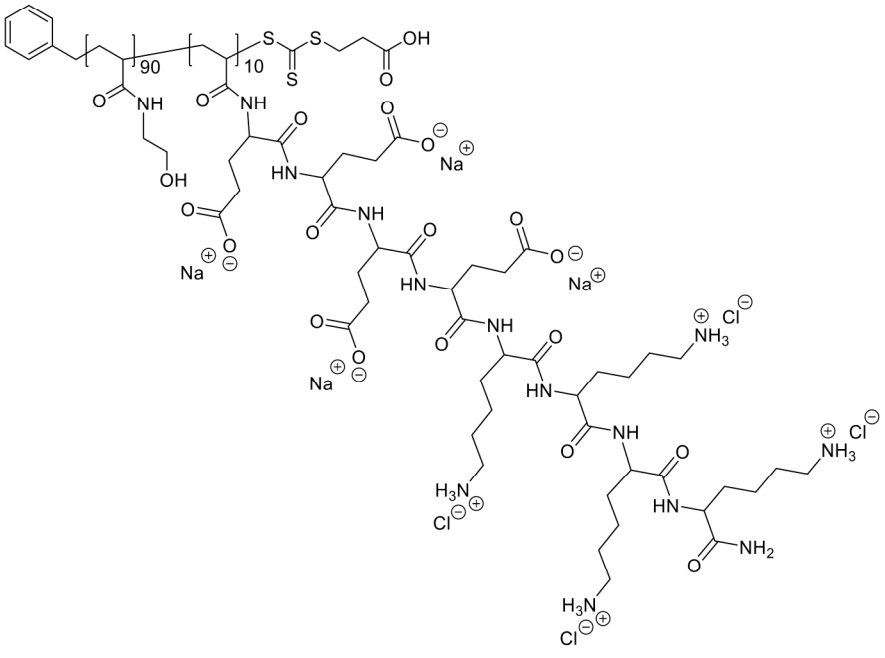

Only aromatic and protection group signals were integrated in $^1$H-NMR to calculate functionalization degree. Final functionalization degree: 4.3%

**$^1$H-NMR** (600 MHz, $D_2O$): Signals were used to calculate functionalization degree.

**$^{19}$F-NMR** (600 MHz, $D_2O$): δ (ppm) = no signals.

# 6. Appendix

## 6.1. NMR

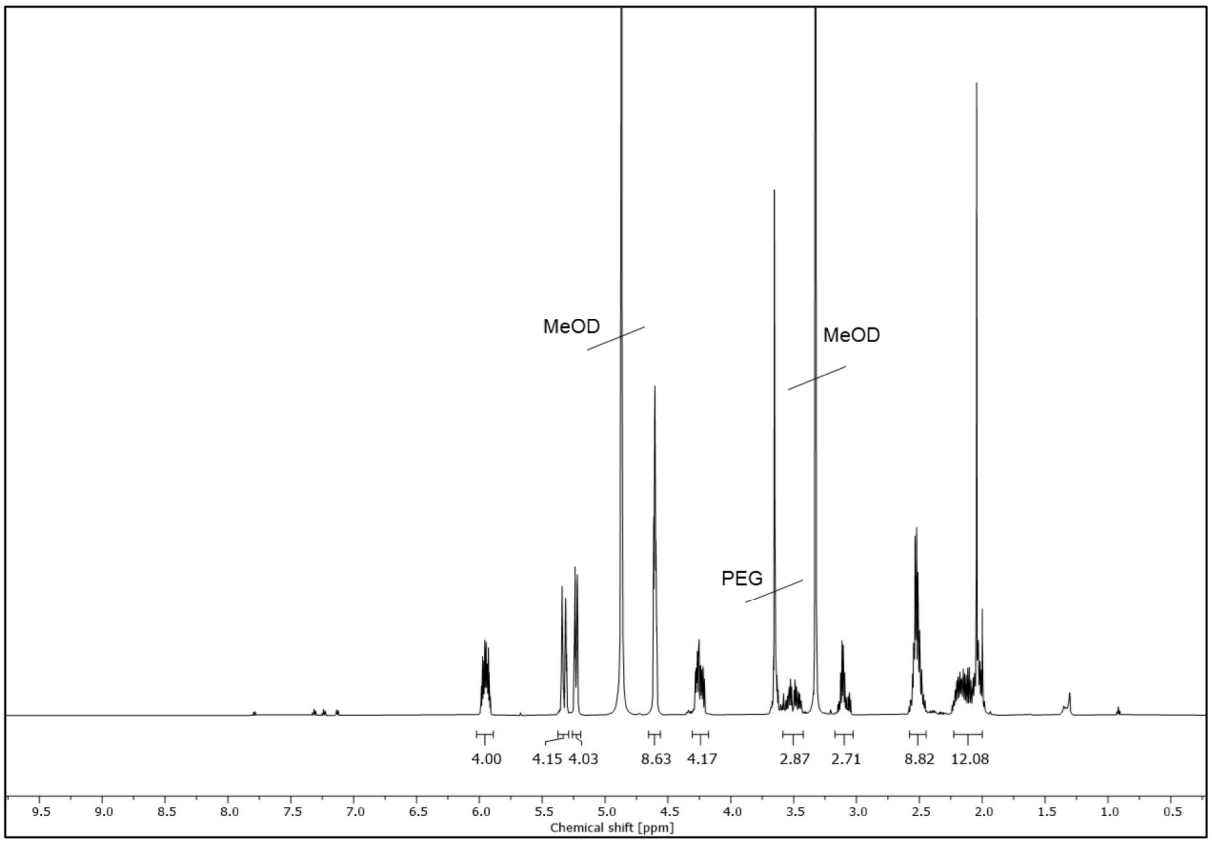


*Figure E1: $^{1}$H-NMR spectrum of Oligomer EEEE (600 MHz, MeOD-d4)*

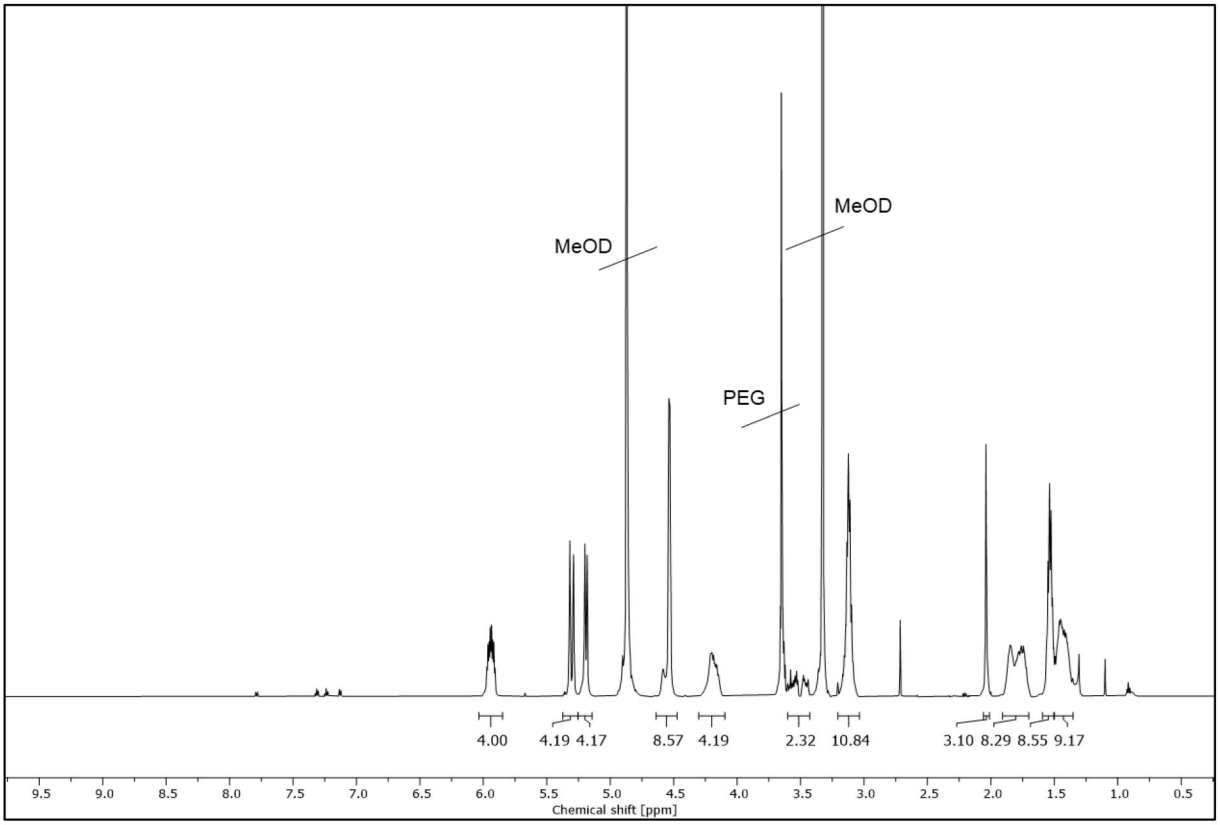


*Figure E2: [1]H-NMR spectrum of Oligomer KKKK (600 MHz, MeOD-d4)*

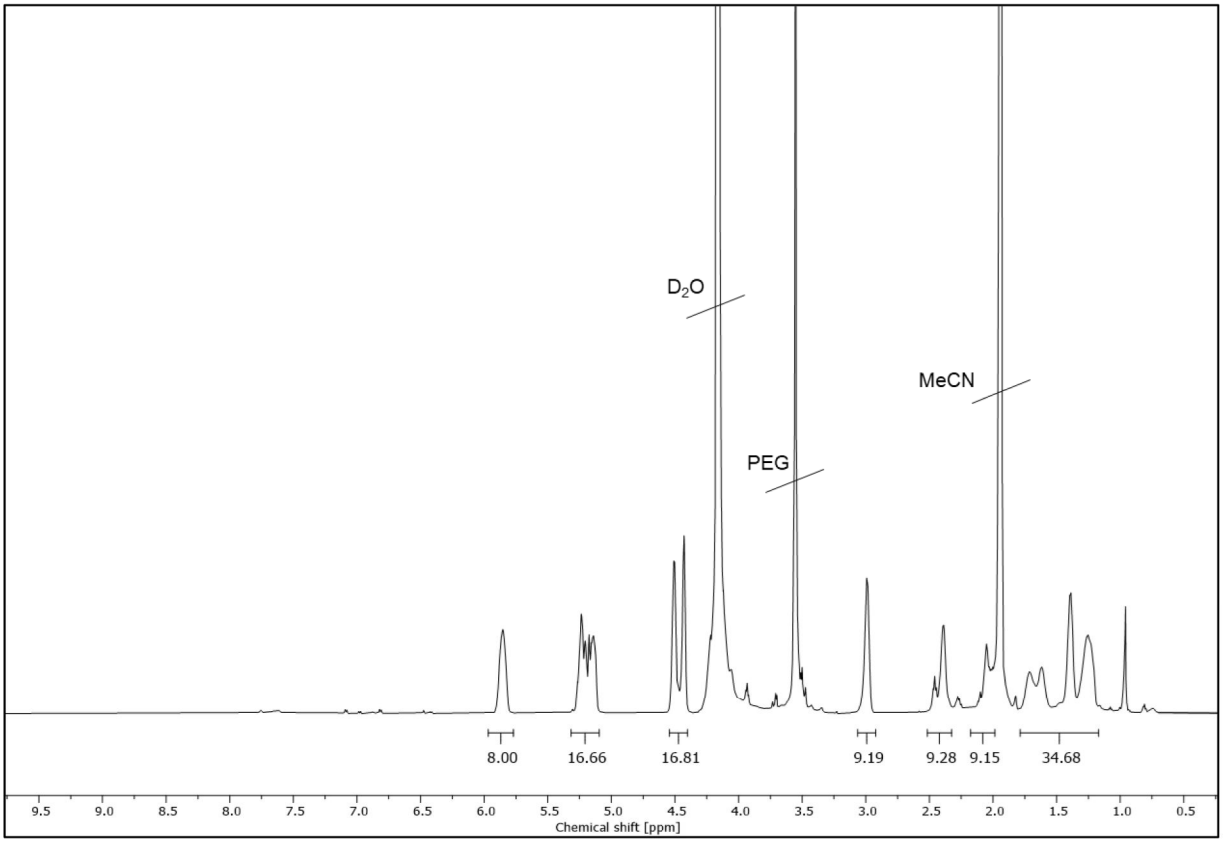


*Figure E3: [1]H-NMR spectrum of Oligomer KEKEKEKE (600 MHz, $D_2O$/MeCN-d3)*

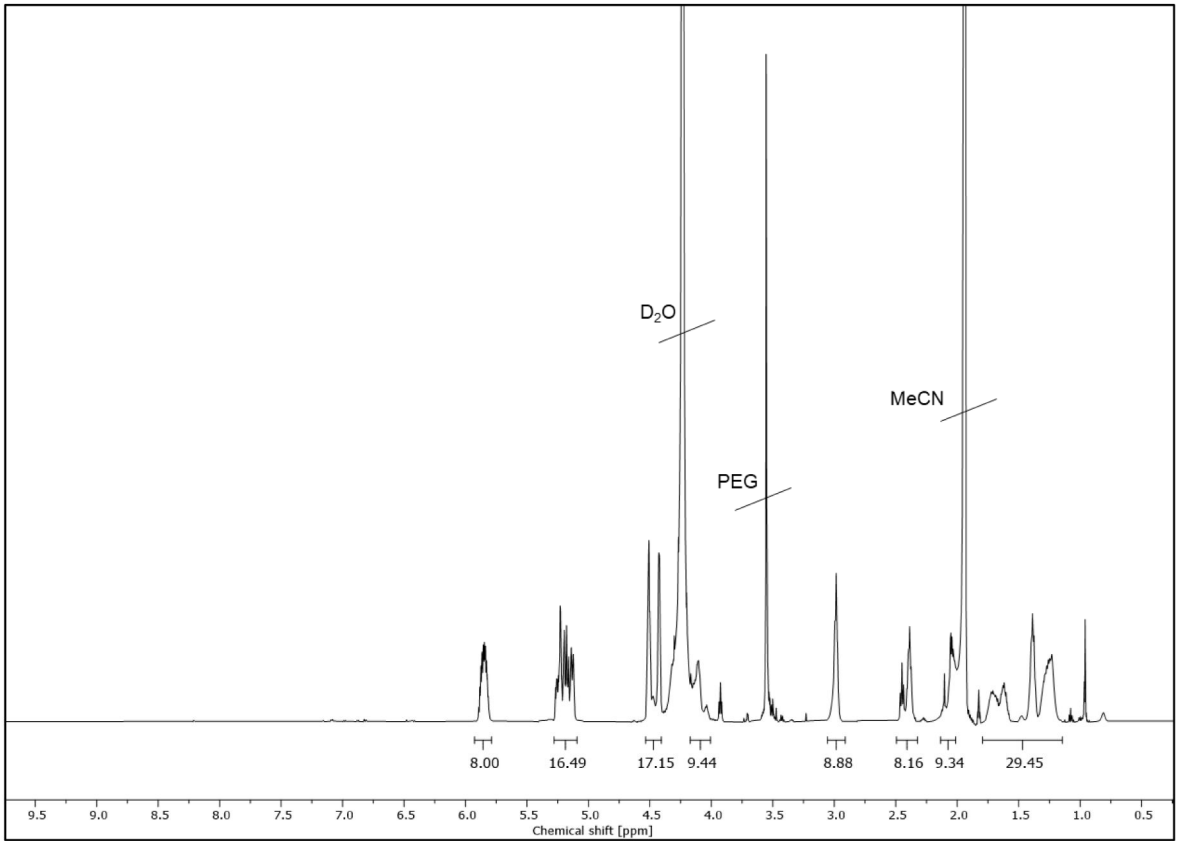


*Figure E4: $^{1}$H-NMR spectrum of Oligomer KKEEKKEE (600 MHz, $D_2O$/MeCN-d3)*

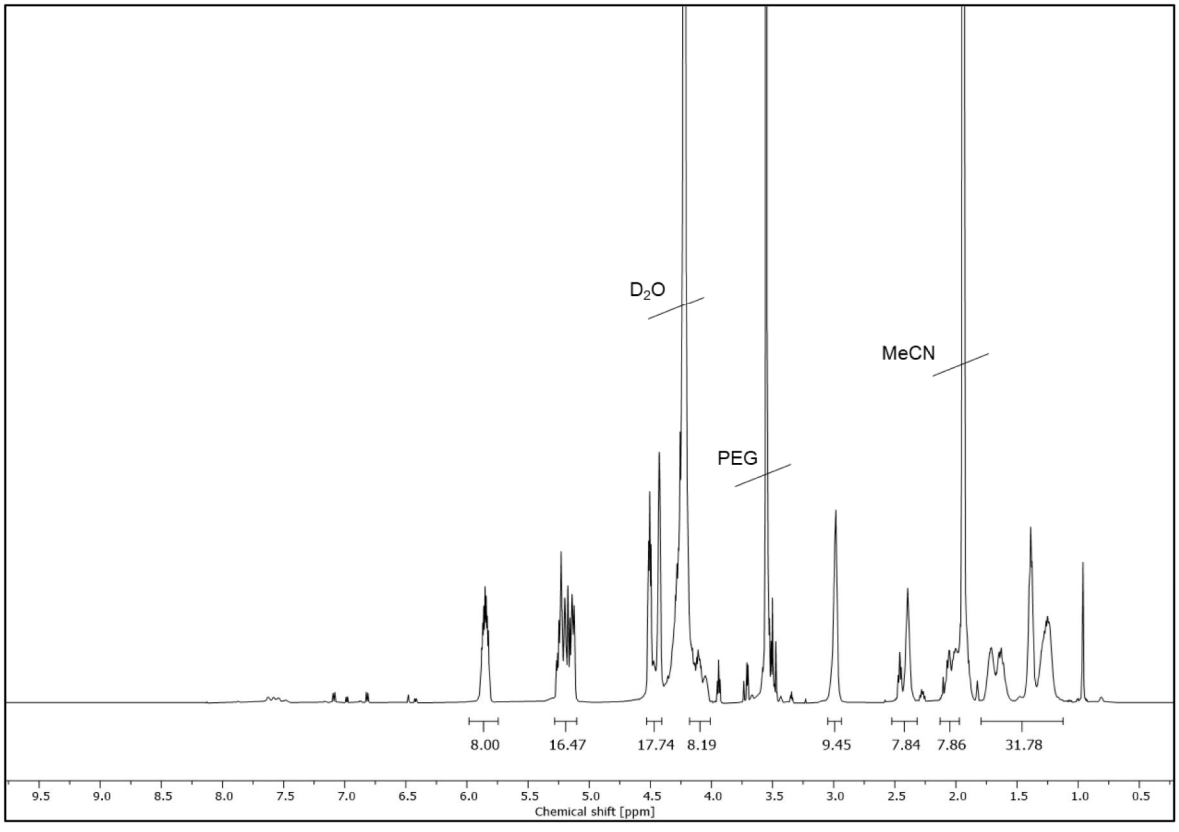


*Figure E5: $^{1}$H-NMR spectrum of Oligomer KKKKEEEE (600 MHz, $D_2O$/MeCN-d3)*

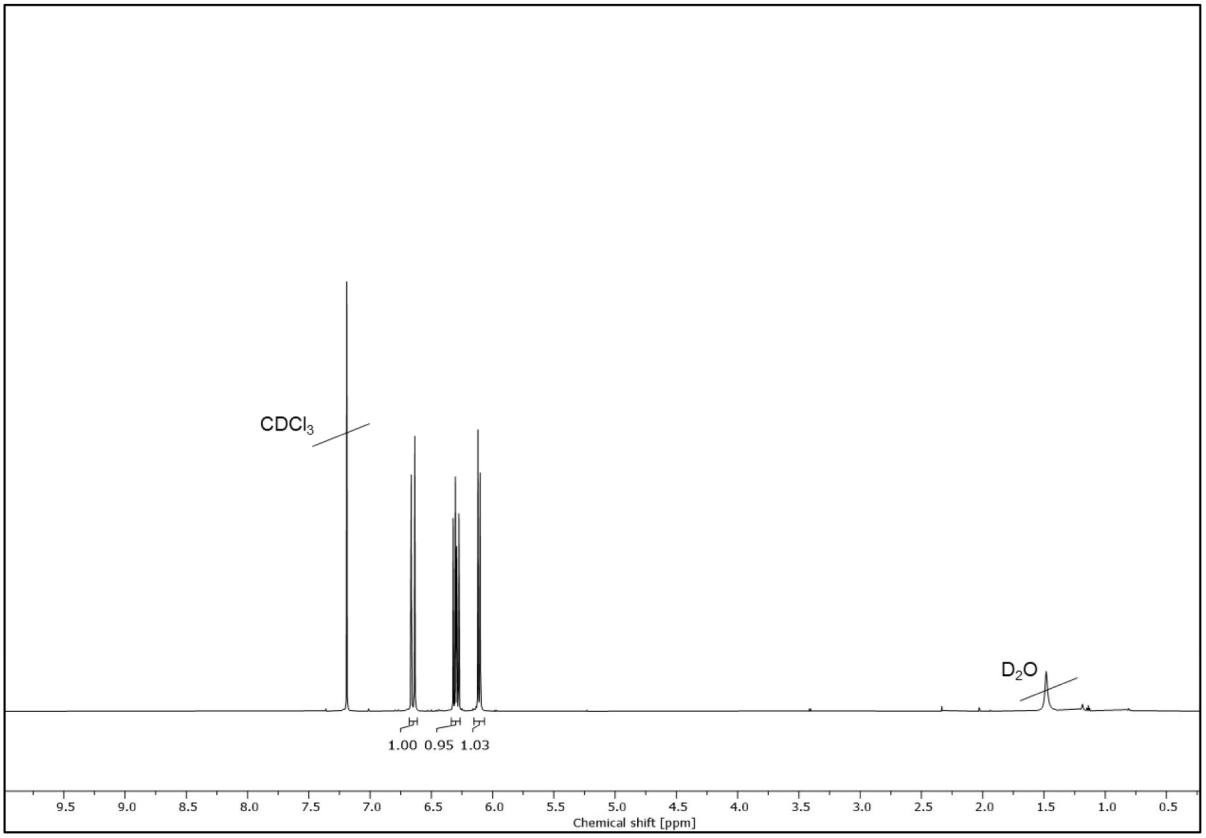


*Figure E6: $^{1}$H-NMR spectrum of Pentafluoro phenyl acrylate monomer (600 MHz, $CDCl_3$)*

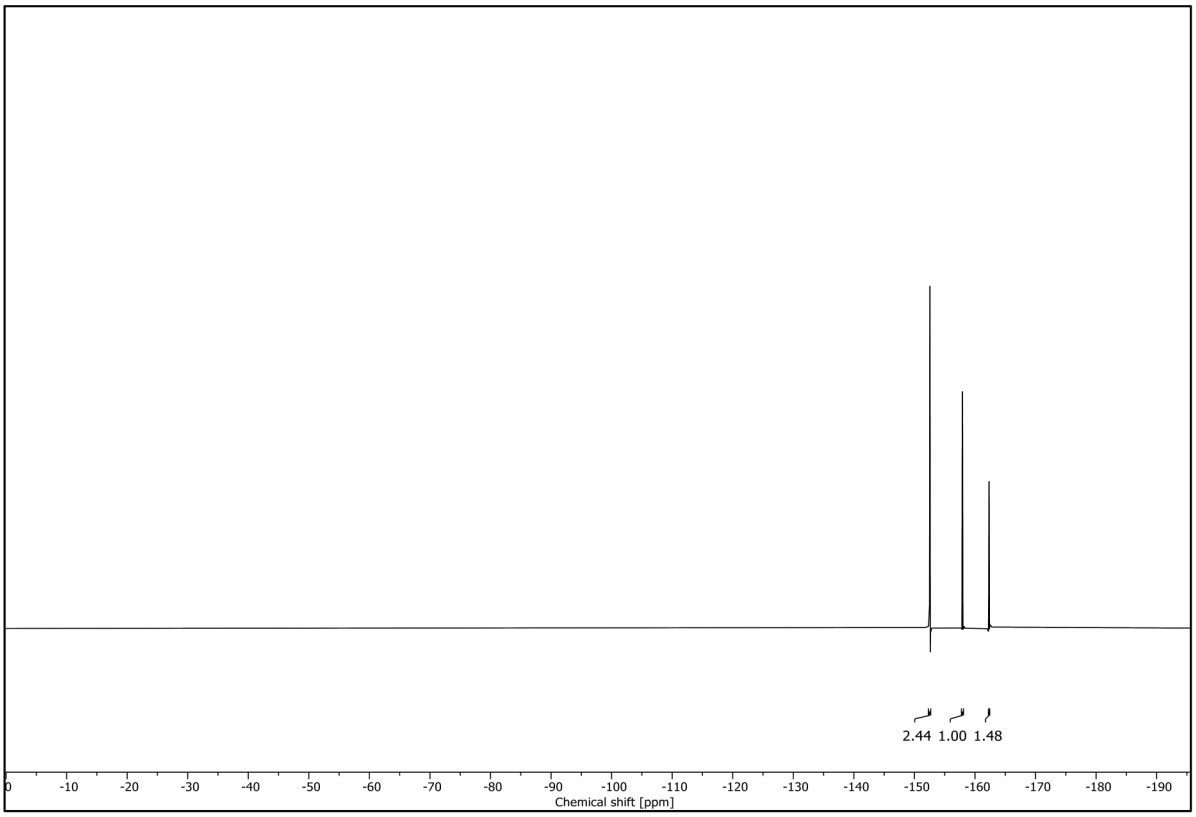


*Figure E7: $^{19}$F-NMR spectrum of Pentafluoro phenyl acrylate monomer (600 MHz, $CDCl_3$)*

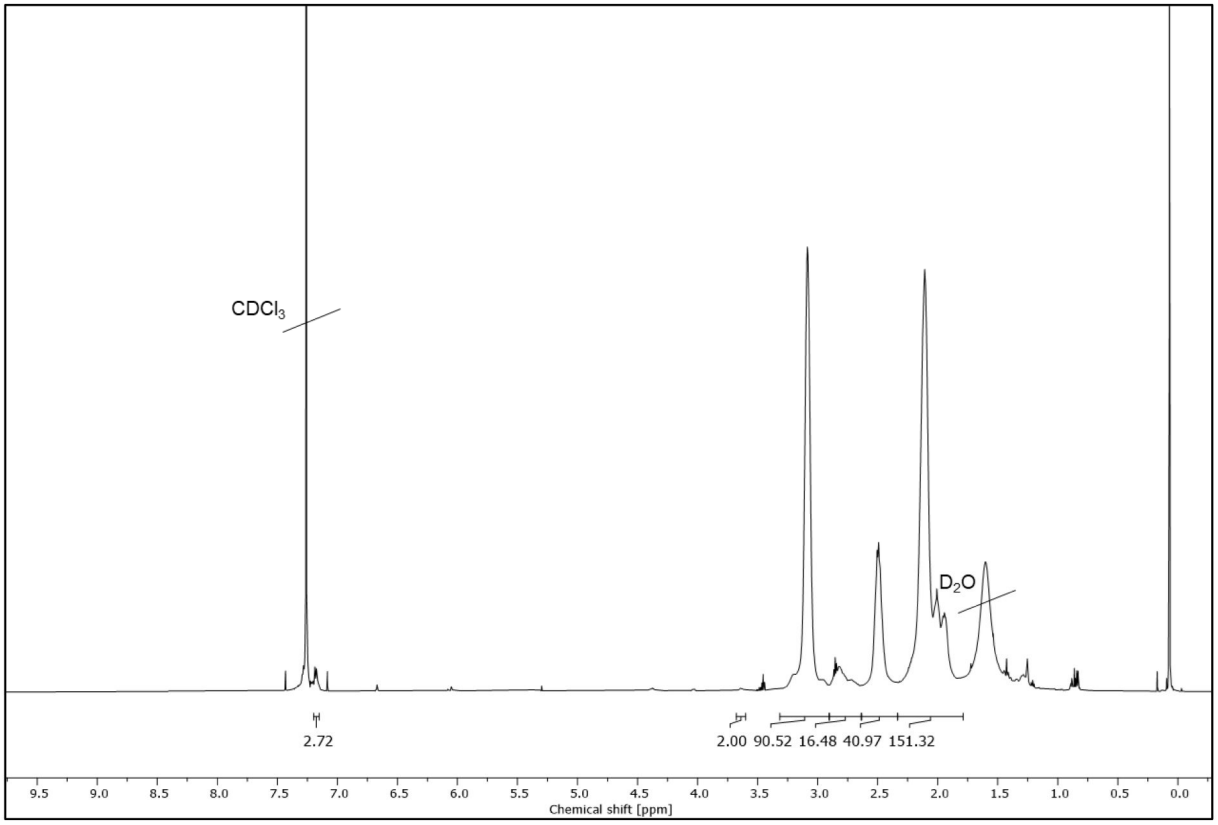


*Figure E8: $^{1}$H-NMR spectrum of Poly(Pentafluoro phenyl acrylate) 100 ($PPFP_{100}$) (600 MHz, $CDCl_3$)*

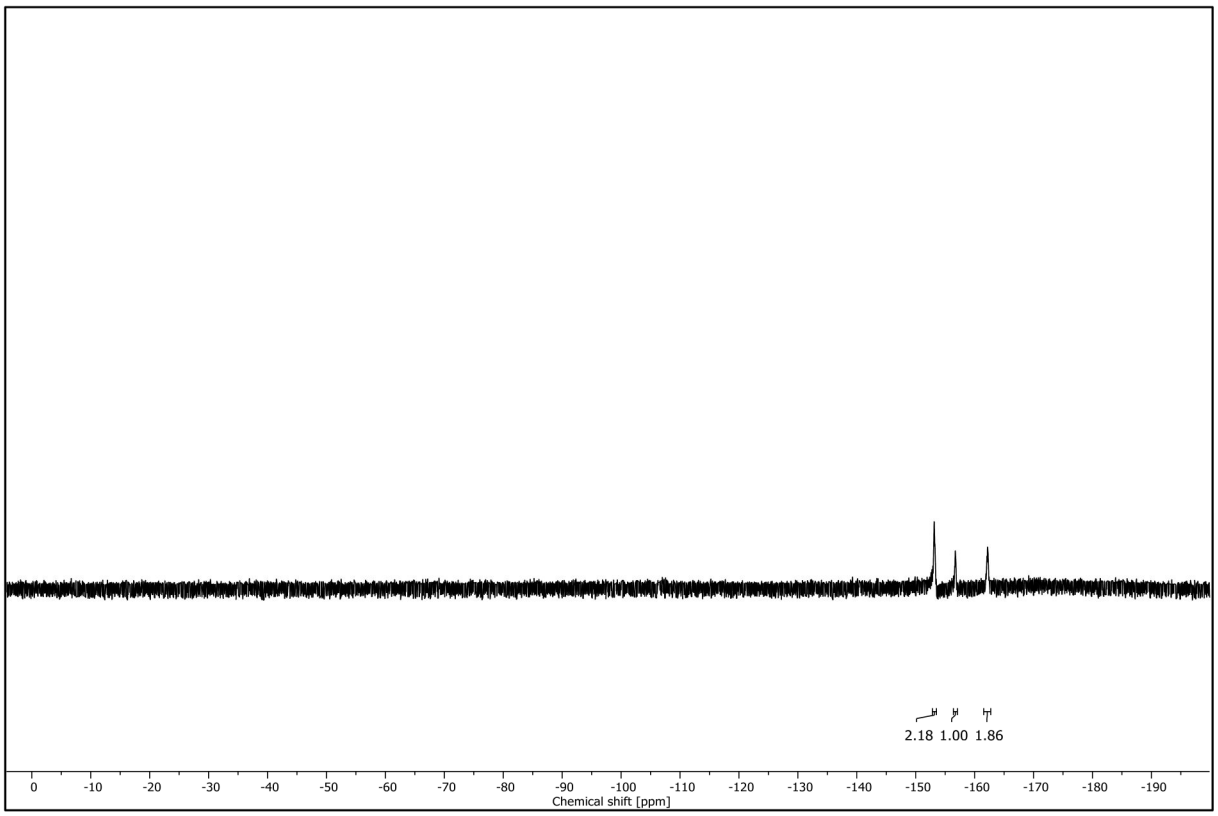


*Figure E9: $^{19}$F-NMR spectrum of Poly(Pentafluoro phenyl acrylate) 100 ($PPFP_{100}$) (600 MHz, $CDCl_3$)*

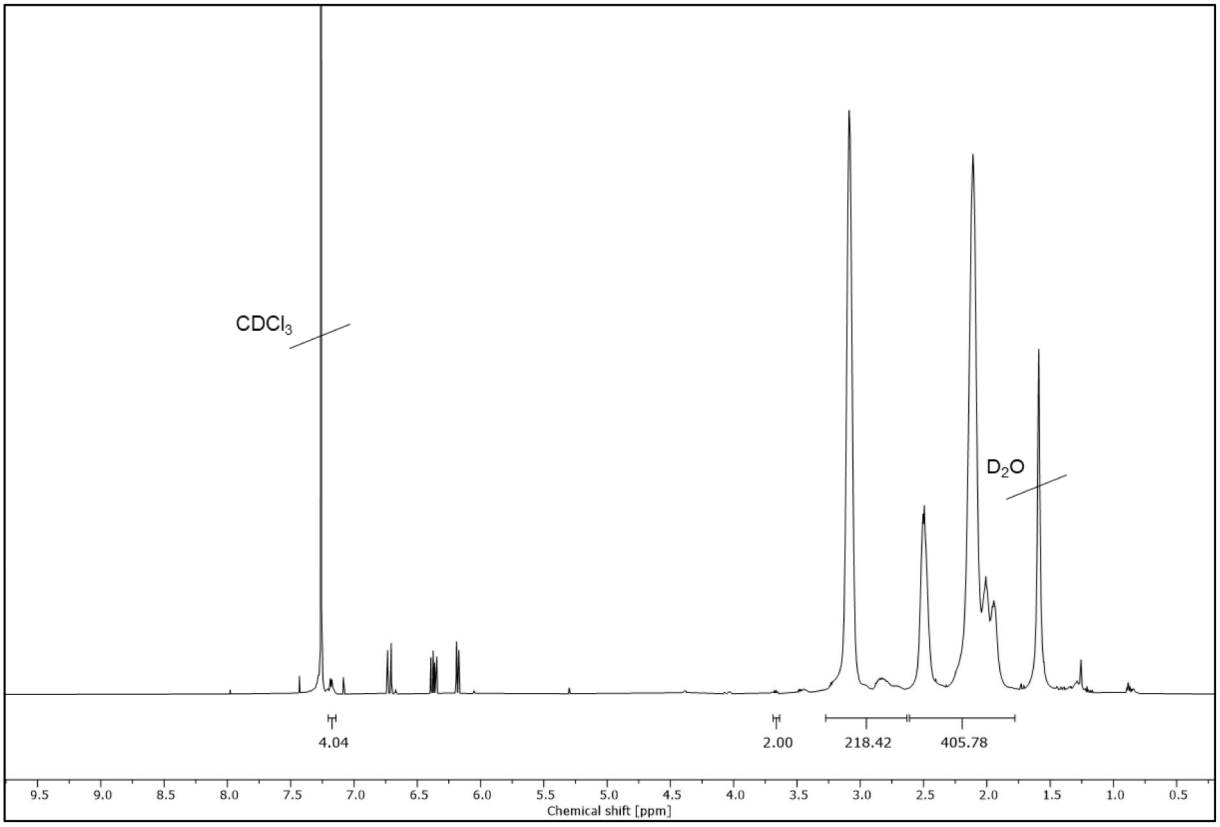


*Figure E10: $^{1}$H-NMR spectrum of Poly(Pentafluoro phenyl acrylate) 200 ($PPFP_{200}$) (600 MHz, $CDCl_3$)*

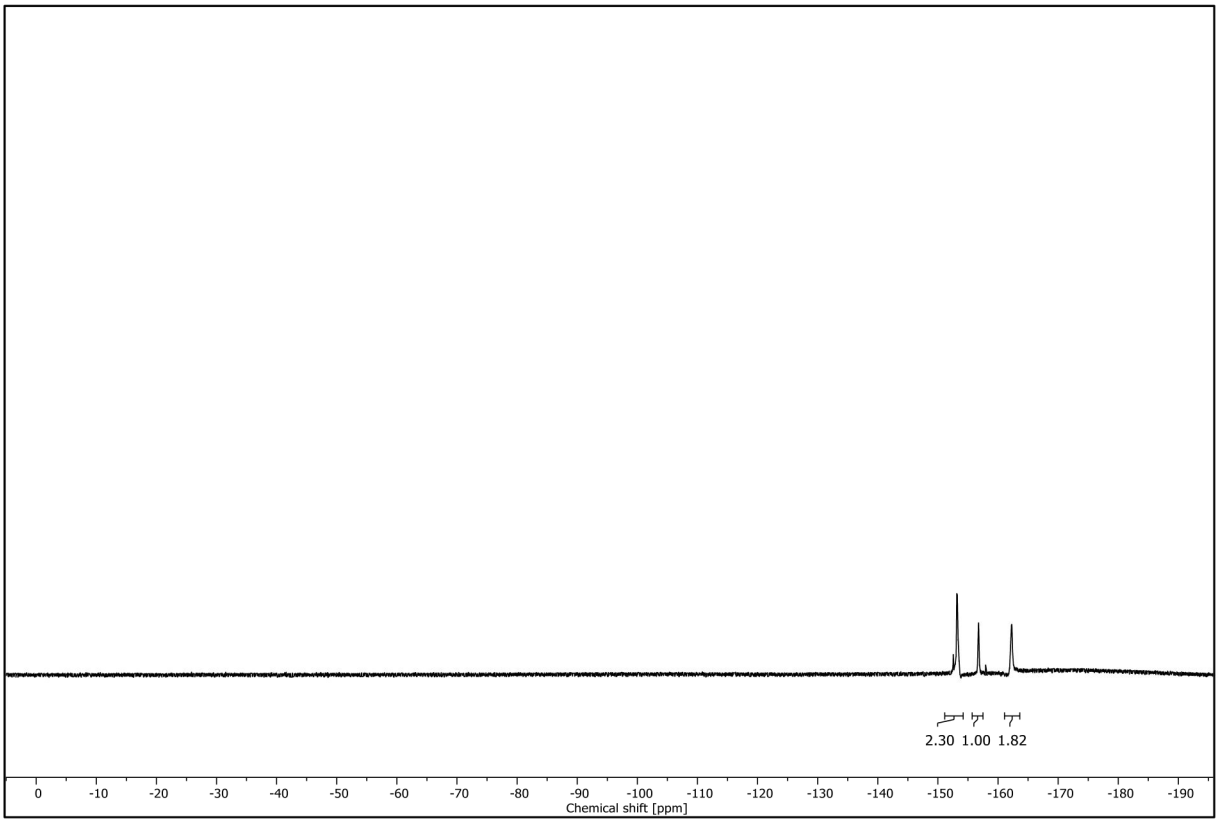


*Figure E11: $^{1}$H-NMR spectrum of Poly(Pentafluoro phenyl acrylate) 200 ($PPFP_{200}$) (600 MHz, $CDCl_3$)*

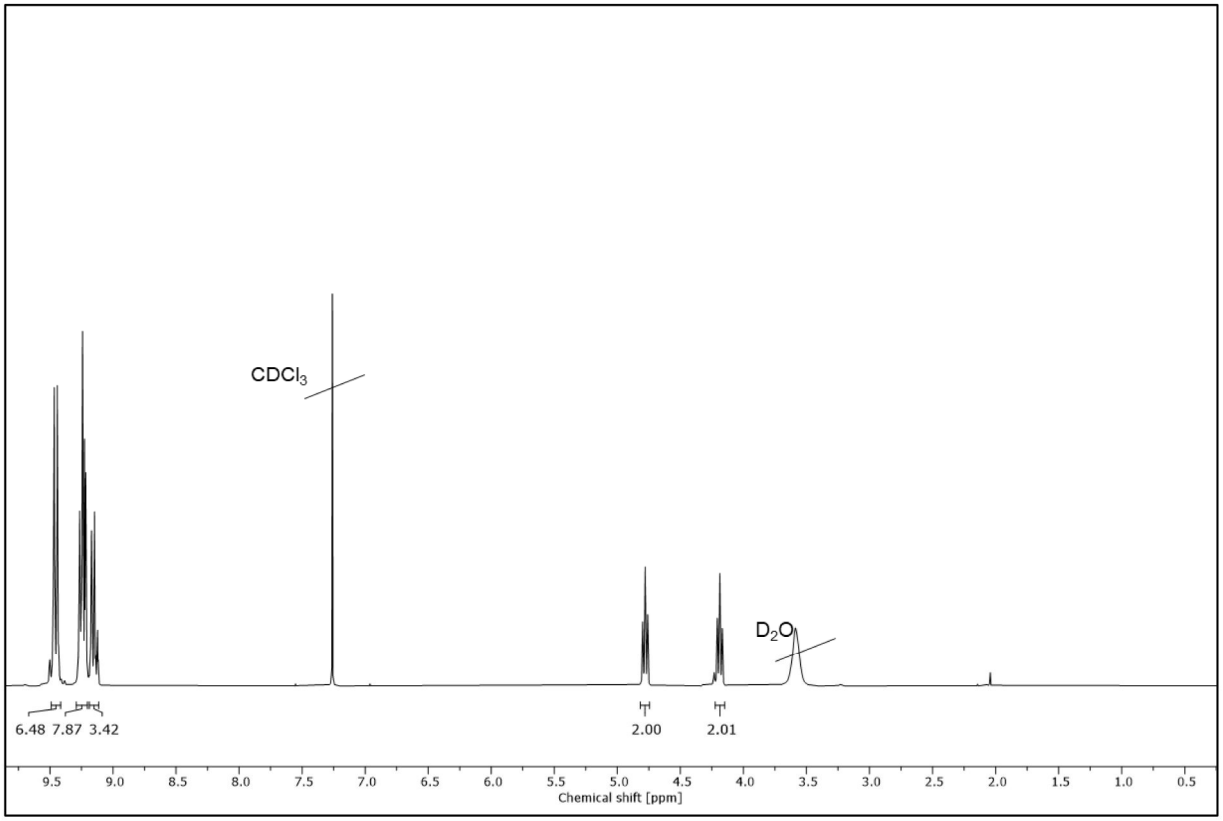


*Figure E12: $^{1}$H-NMR spectrum of single Trt-protected ethylene diamine linker (600 MHz, $CDCl_3$)*

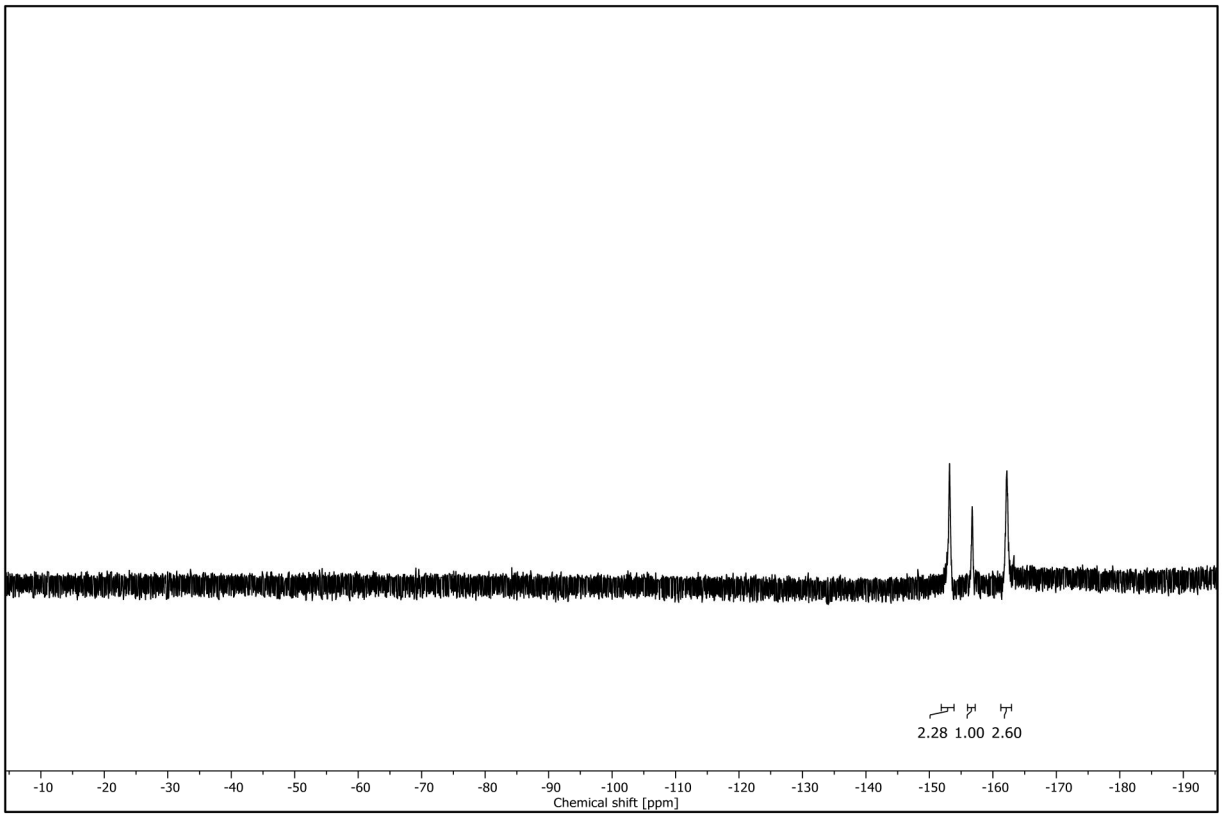


*Figure E13: $^{19}$F-NMR spectrum of $P_{100}$(EDA-Trt) (600 MHz, $CDCl_3$)*

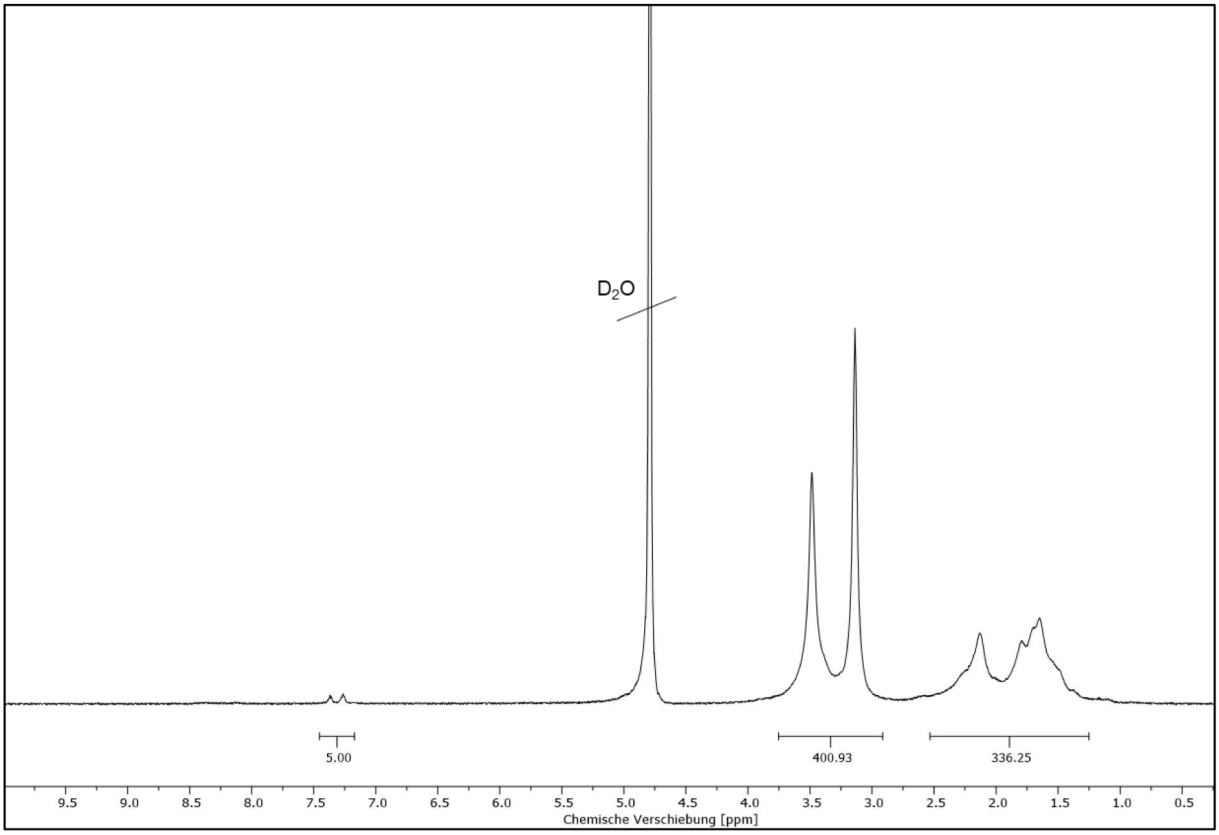


*Figure E14: $^{1}$H-NMR spectrum of $P_{100}$(+) (600 MHz, $D_2O$)*

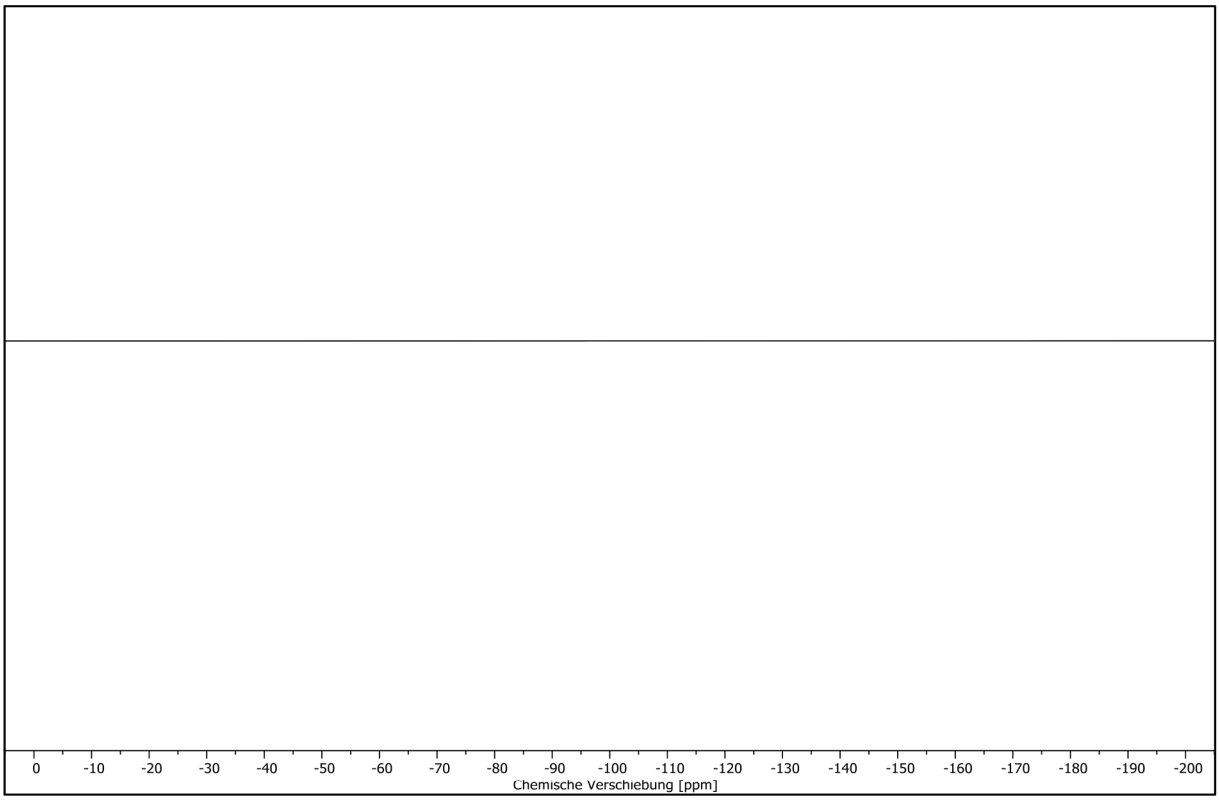


*Figure E15: $^{19}$F-NMR spectrum of $P_{100}$(+) (600 MHz, $D_2O$)*

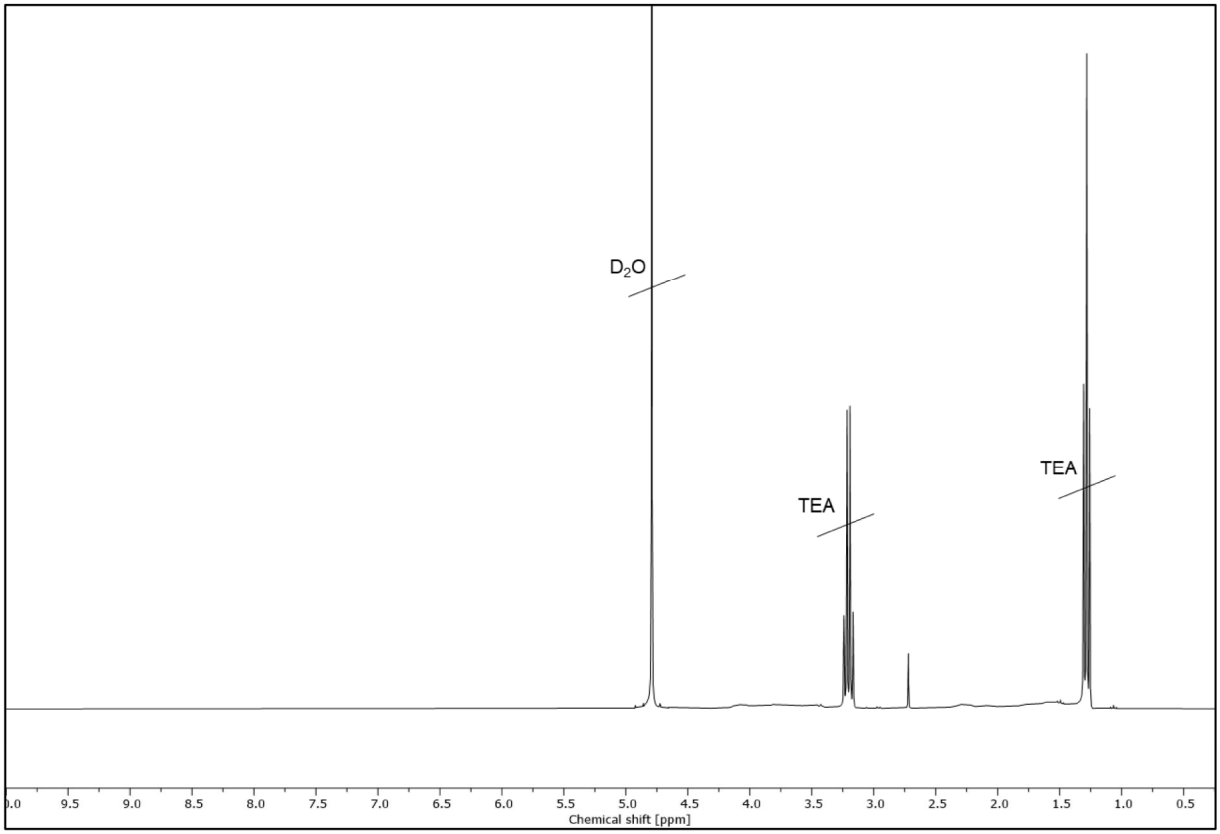


*Figure E16: $^1$H-NMR spectrum of $P_{100}$(-) with triethyl amine (TEA) impurities (600 MHz, $D_2O$)*

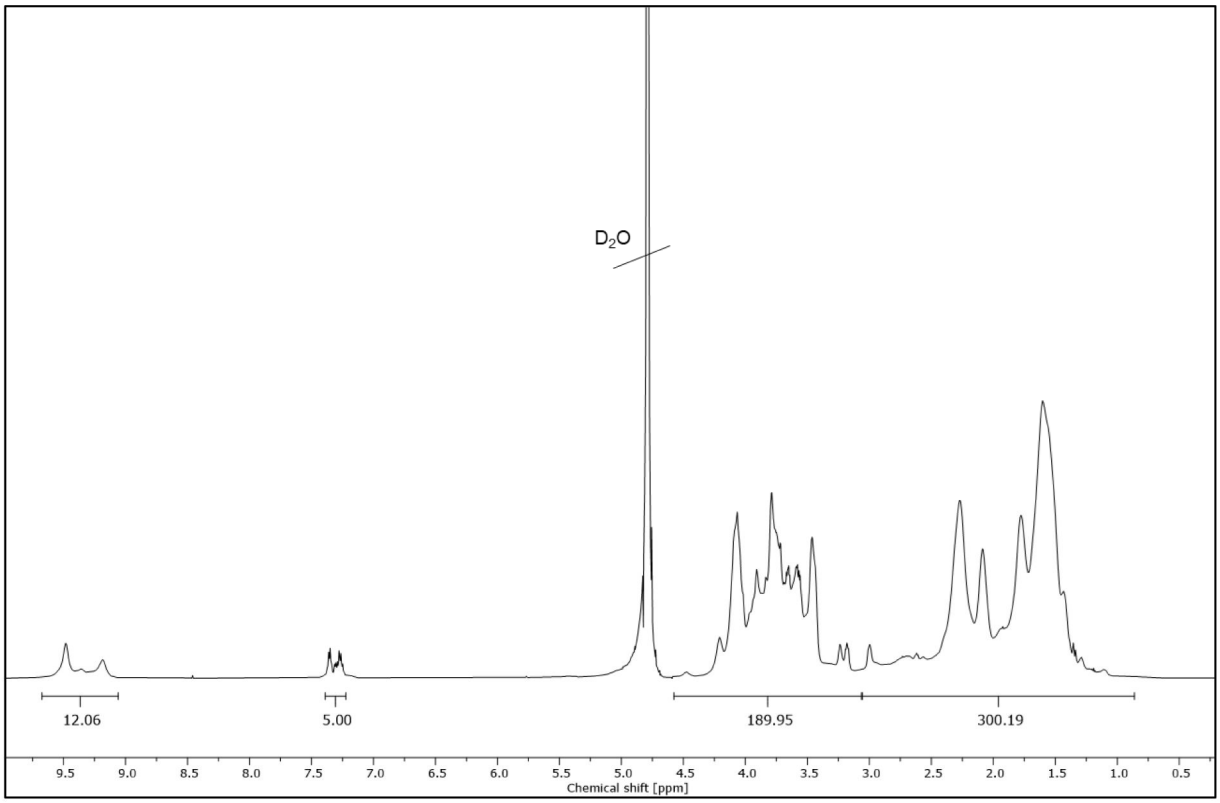


*Figure E17: $^1$H-NMR spectrum of $P_{100}$(-) (600 MHz, $D_2O$)*

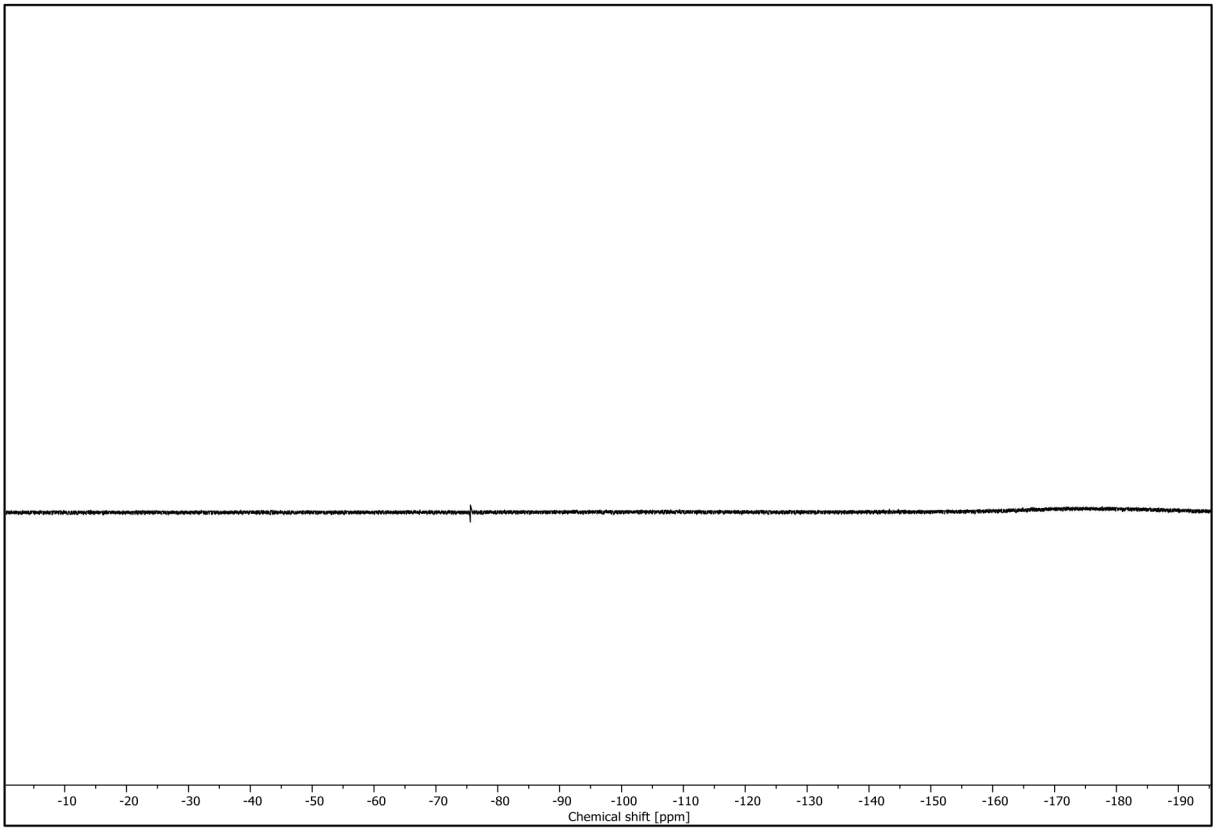


*Figure E18: $^{19}$F-NMR spectrum of $P_{100}$(-) (600 MHz, $D_2O$)*

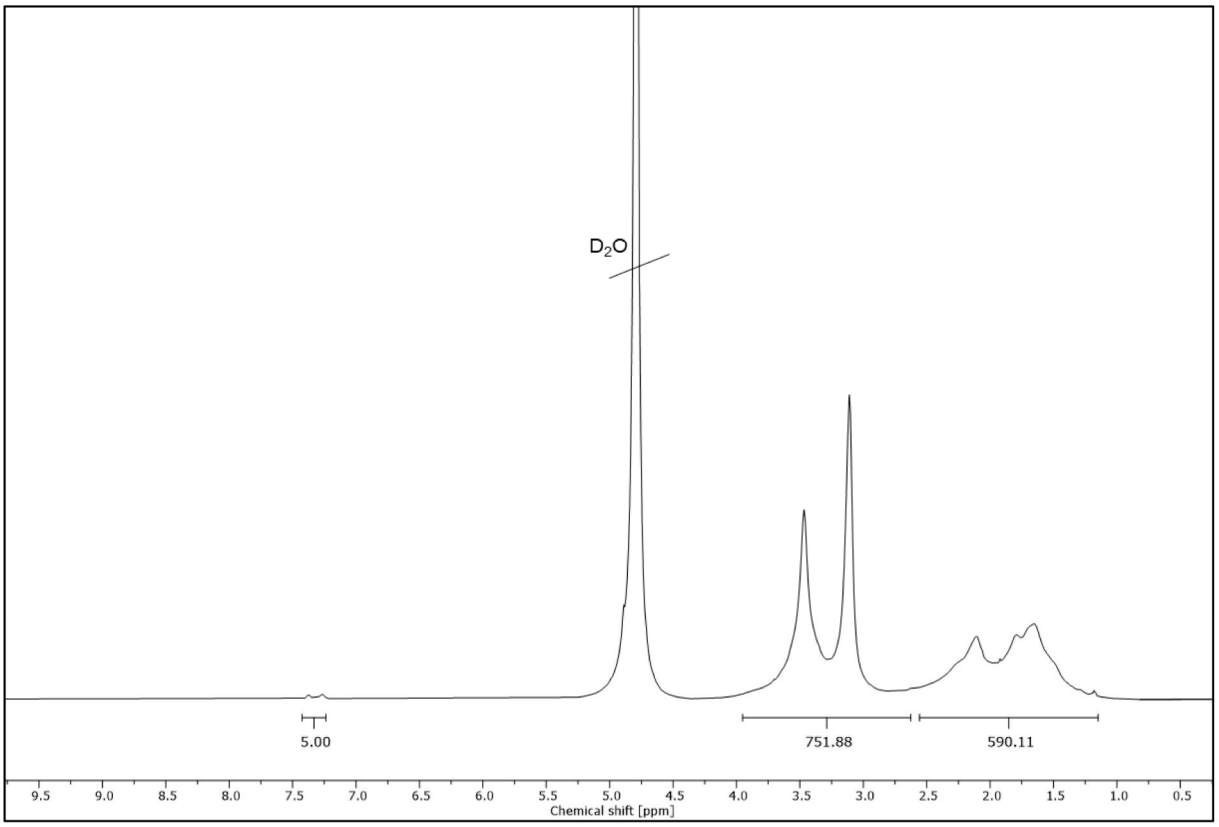


*Figure E19: $^{1}$H-NMR spectrum of $P_{200}$(+) (600 MHz, $D_2O$)*

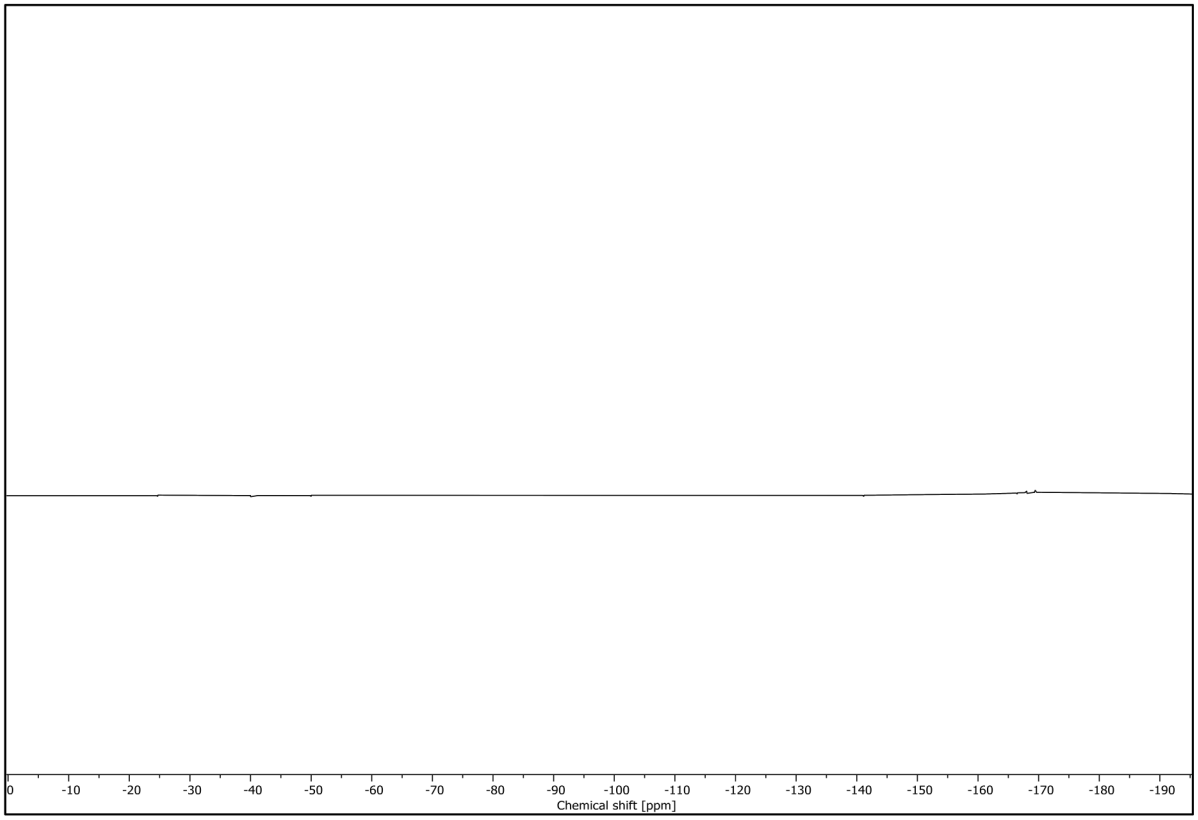


*Figure E20: $^{19}$F-NMR spectrum of $P_{200}$(+) (600 MHz, $D_2O$)*

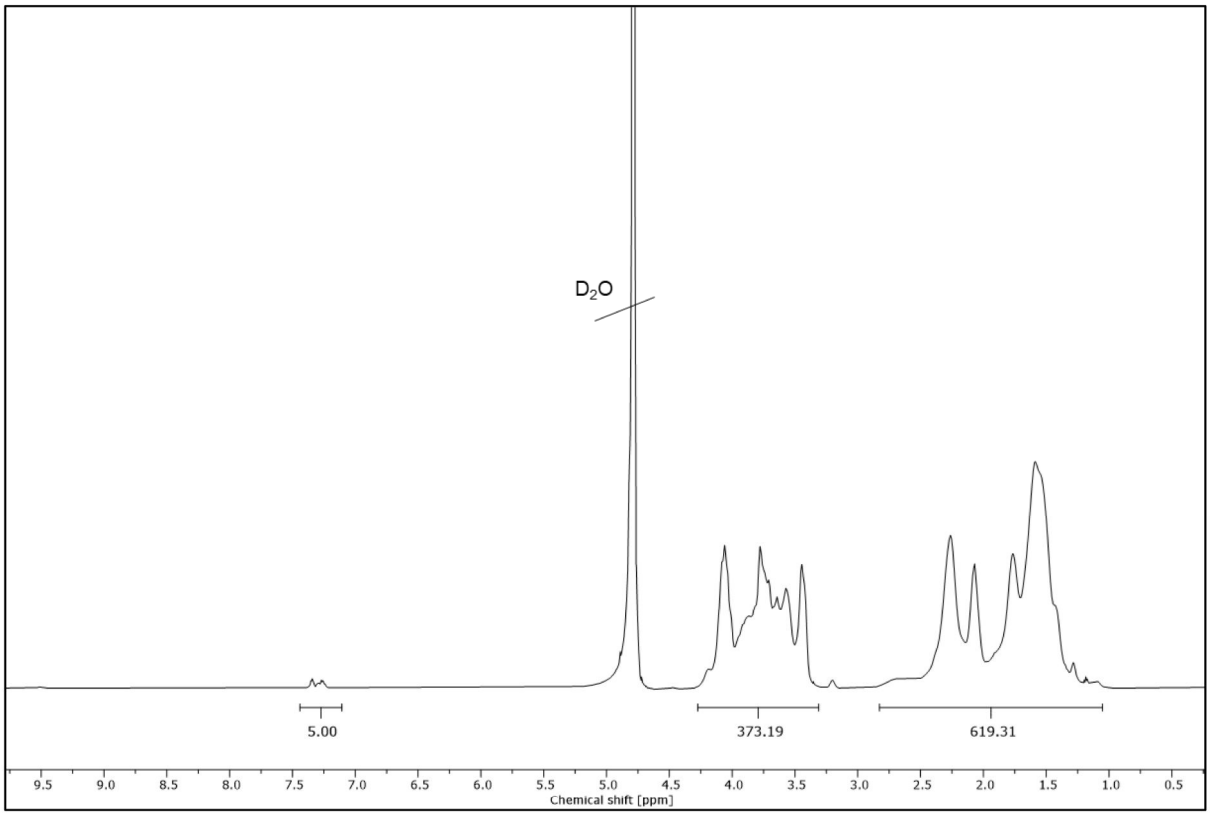


*Figure E21: $^{1}$H-NMR spectrum of $P_{200}$(-) (600 MHz, $D_2O$)*

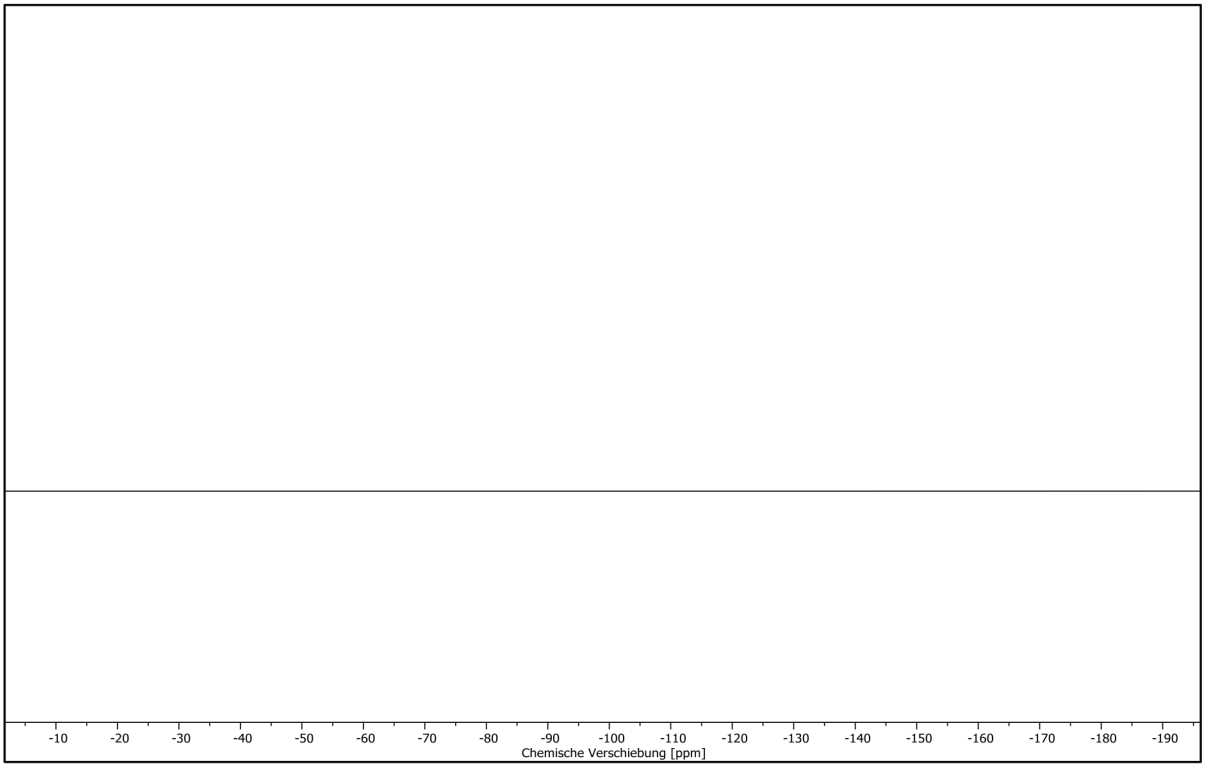


*Figure E22: $^{19}$F-NMR spectrum of $P_{200}$(-) (600 MHz, $D_2O$)*

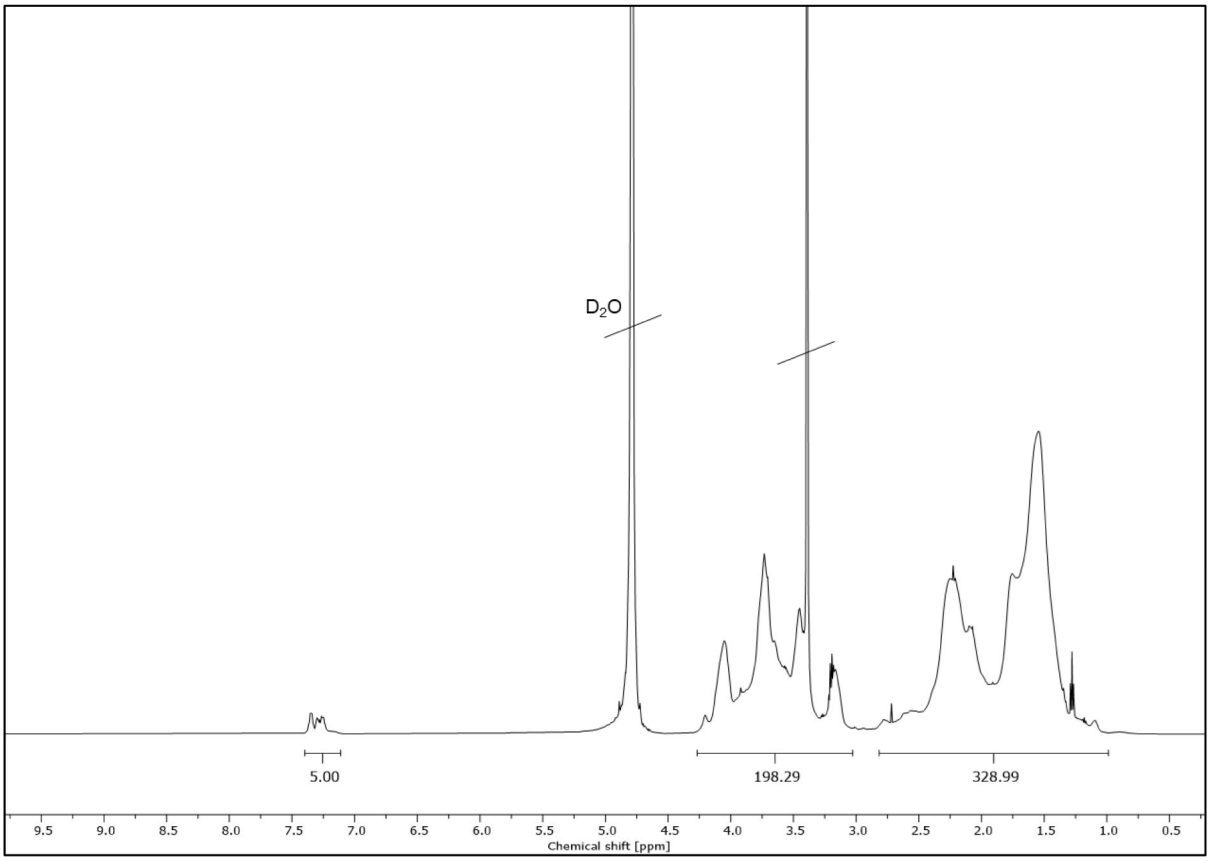


*Figure E23: $^{1}$H-NMR spectrum of $P_{100}$(+/-) (600 MHz, $D_2O$)*

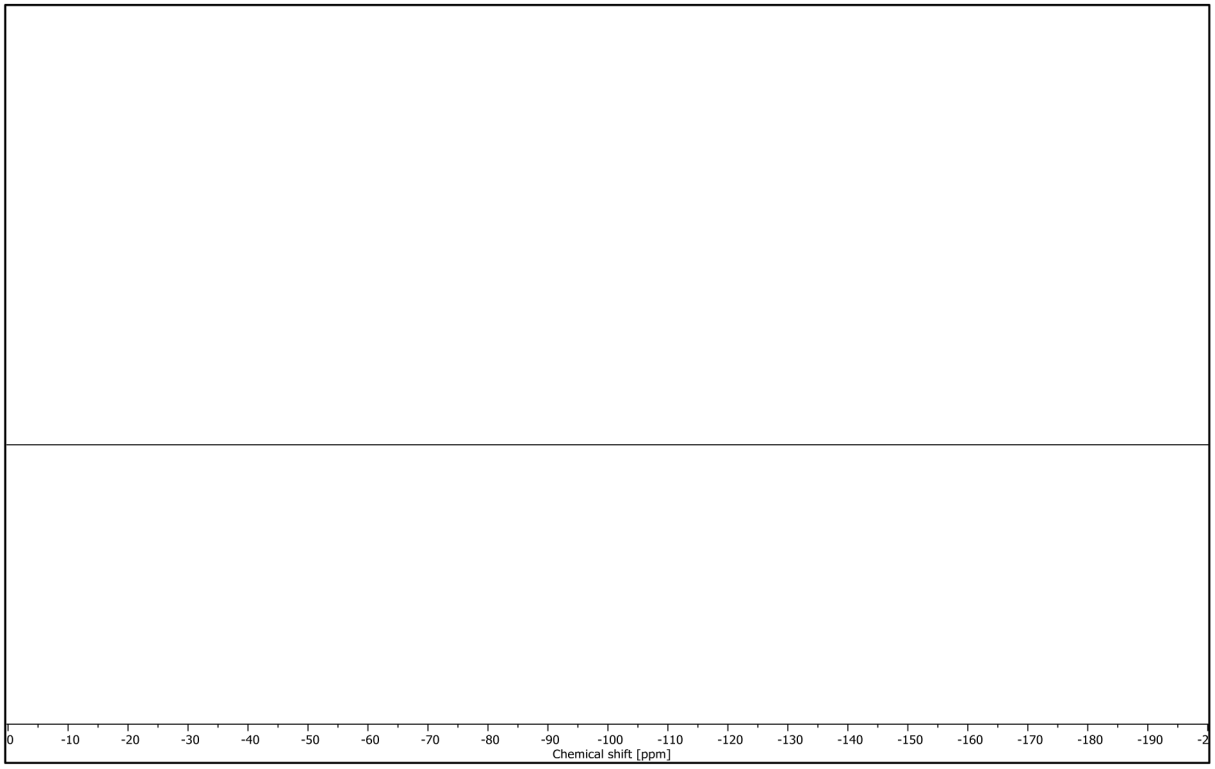


*Figure E24: $^{19}$F-NMR spectrum of $P_{100}$(+/-) (600 MHz, $D_2O$)*

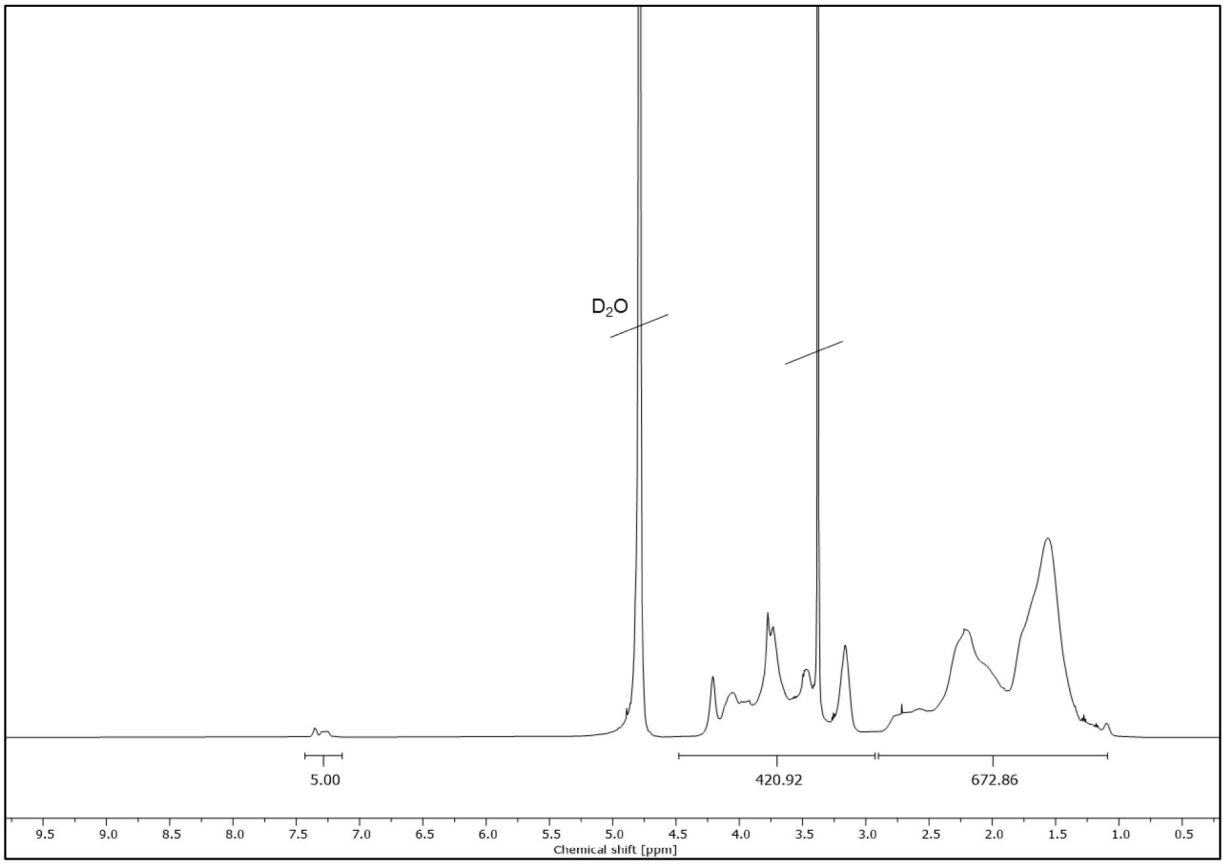


*Figure E25: $^{1}$H-NMR spectrum of $P_{200}$(+/-) (600 MHz, $D_2O$)*

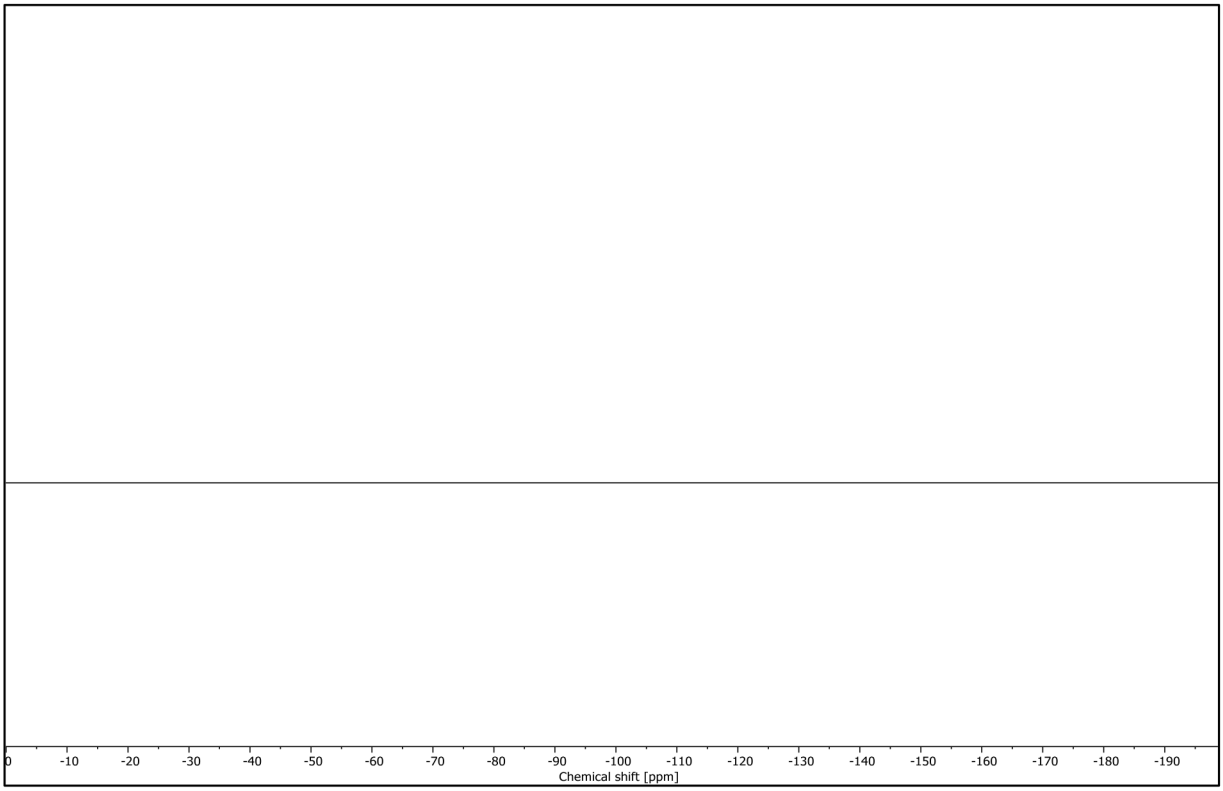


*Figure E26: $^{19}$F-NMR spectrum of $P_{200}$(+/-) (600 MHz, $D_2O$)*

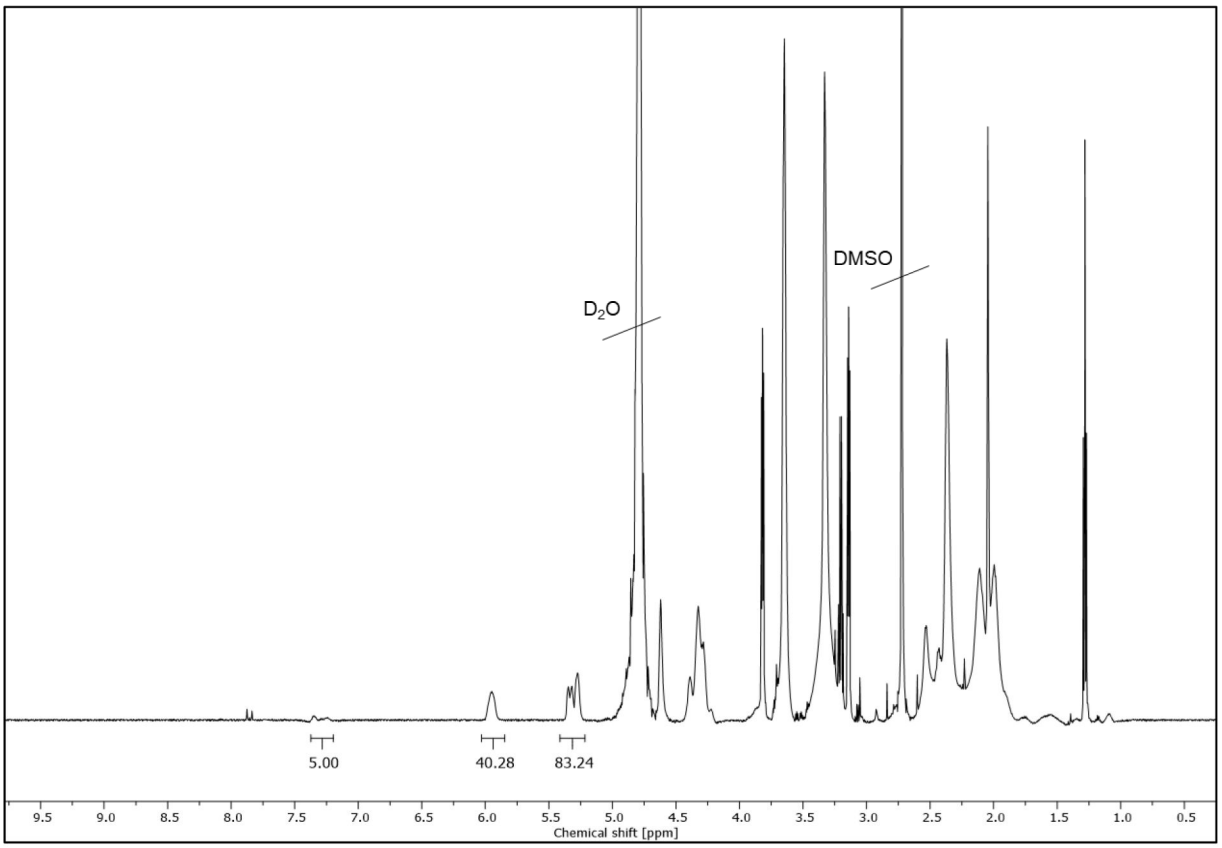


*Figure E27: $^{1}$H-NMR spectrum of $P_{100}$(EEEE) (600 MHz, $D_2O$)*

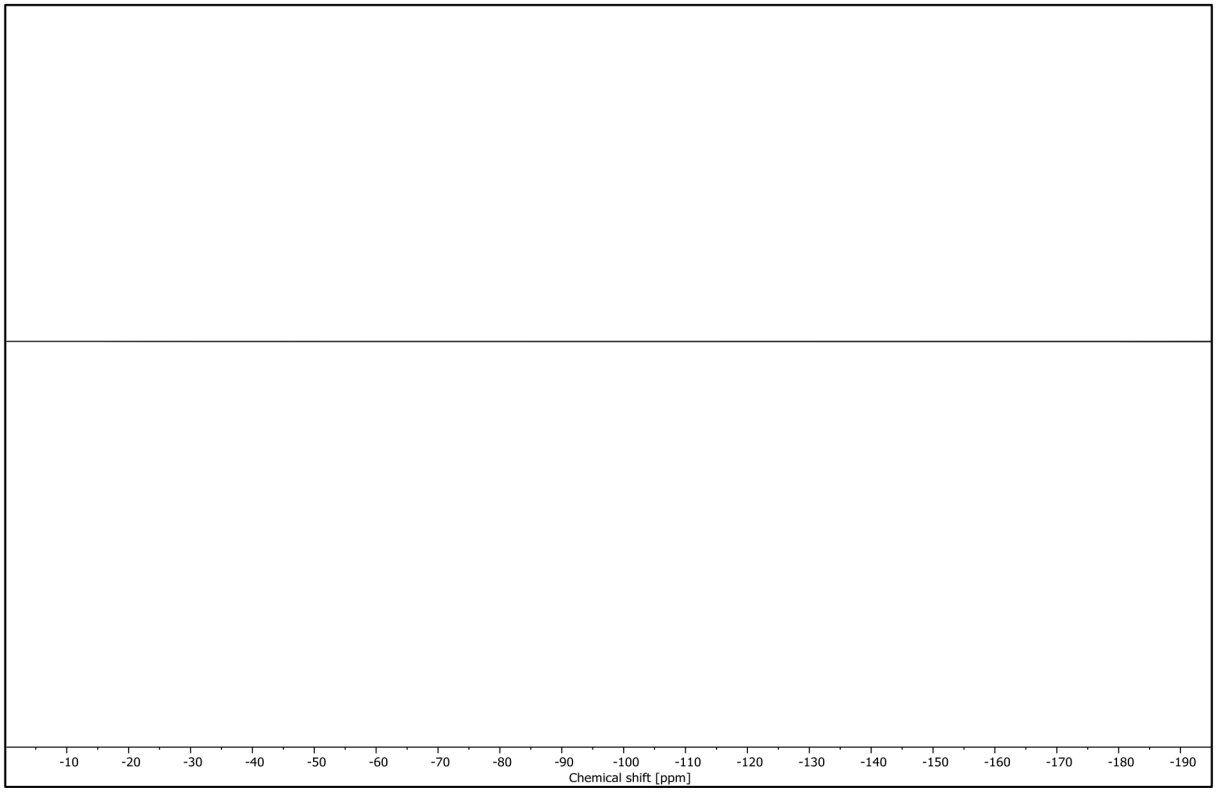


*Figure E28: $^{19}$F-NMR spectrum of $P_{100}$(EEEE) (600 MHz, $D_2O$)*

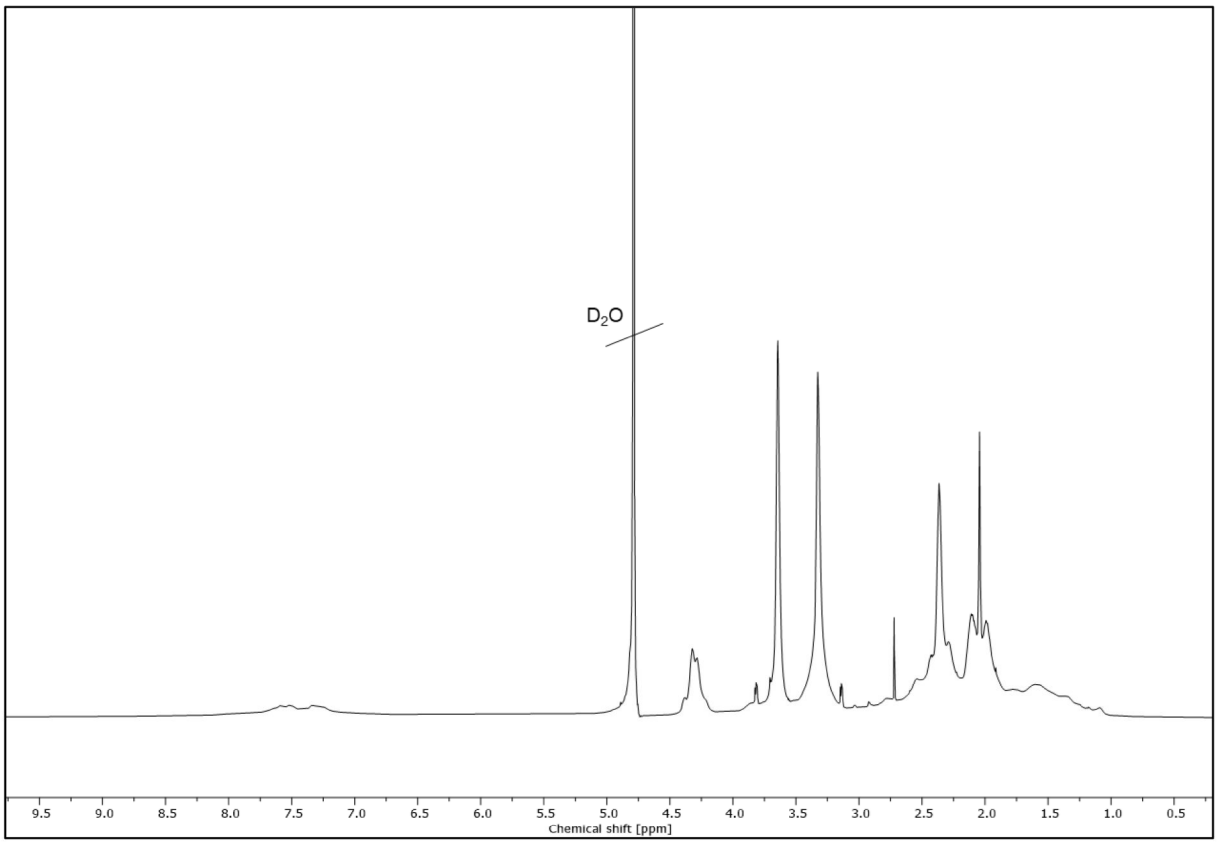


*Figure E29: $^{1}$H-NMR spectrum of $P_{100}$(- - - -) (600 MHz, $D_2O$)*

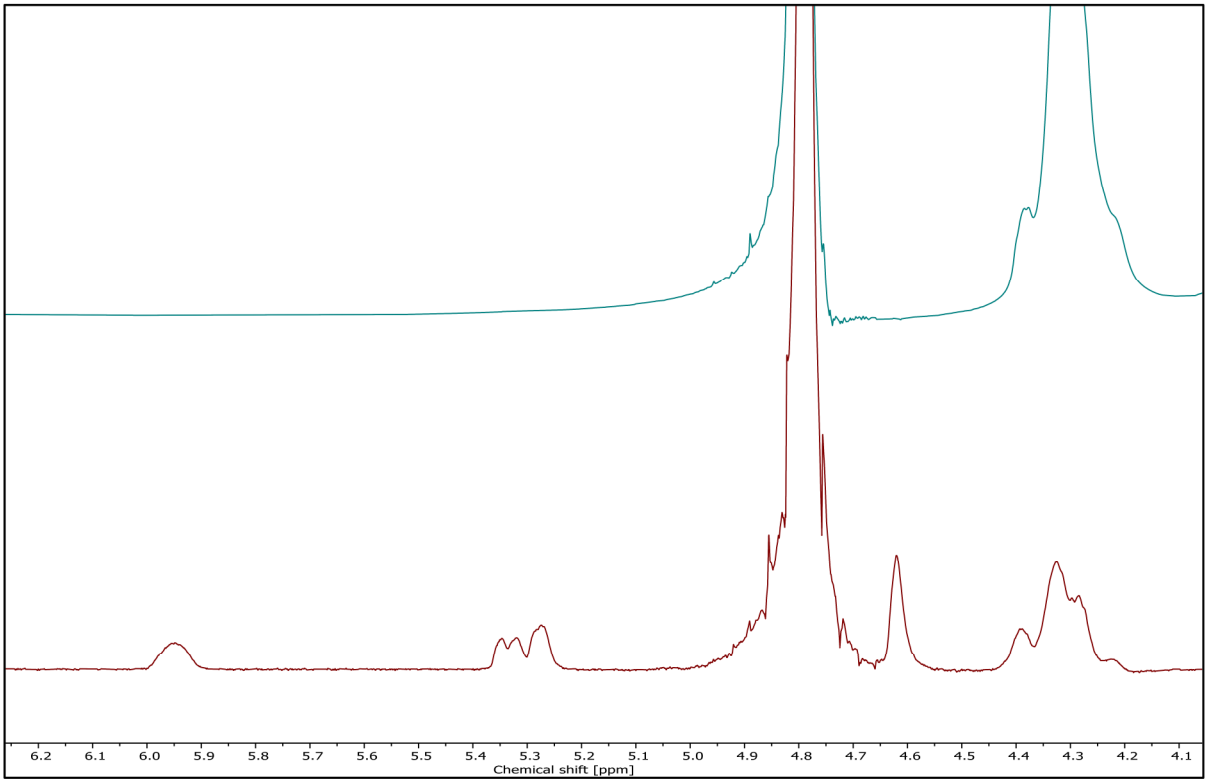


*Figure E30: Comparison of $^{1}$H-NMR of $P_{100}$(EEEE) (bottom) and $P_{100}$(- - - -) (top)*

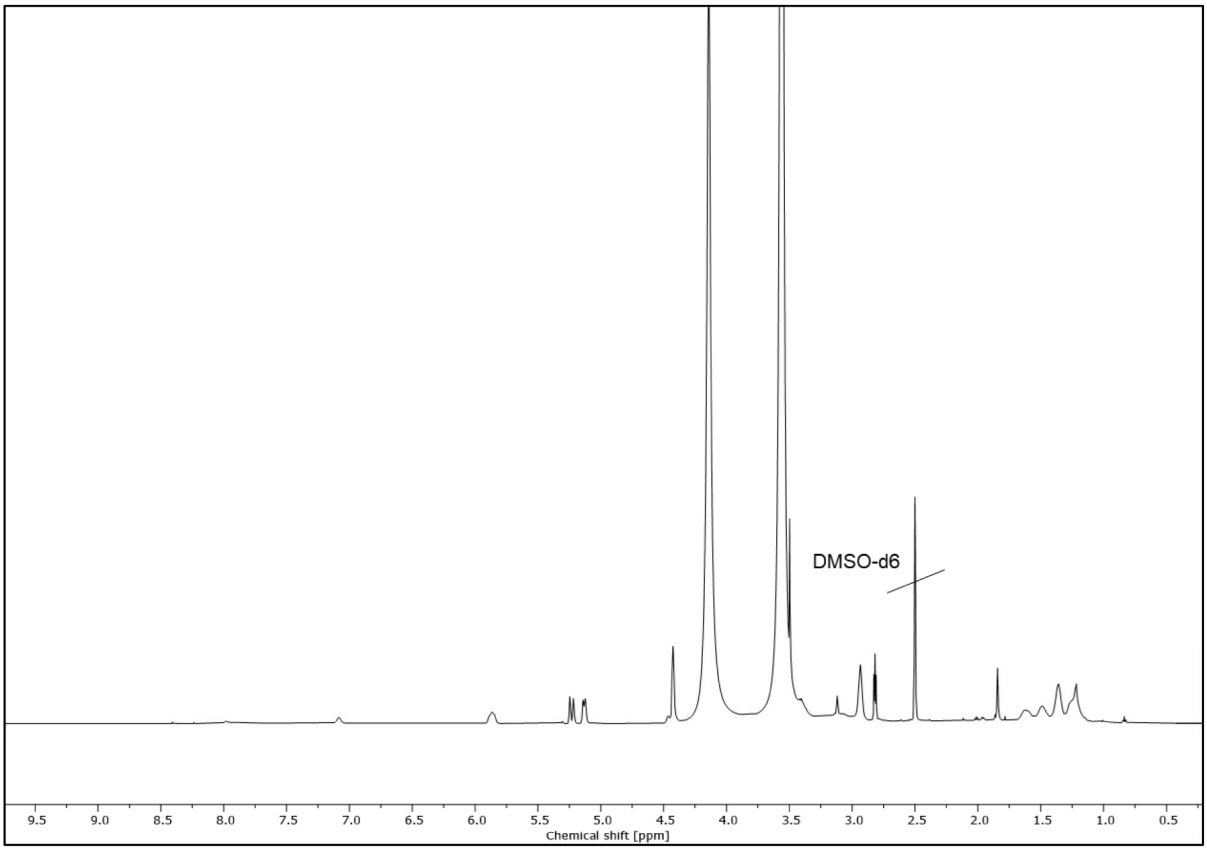


*Figure E31: $^{1}$H-NMR spectrum of $P_{100}$(KKKK) (600 MHz, DMSO-d6)*

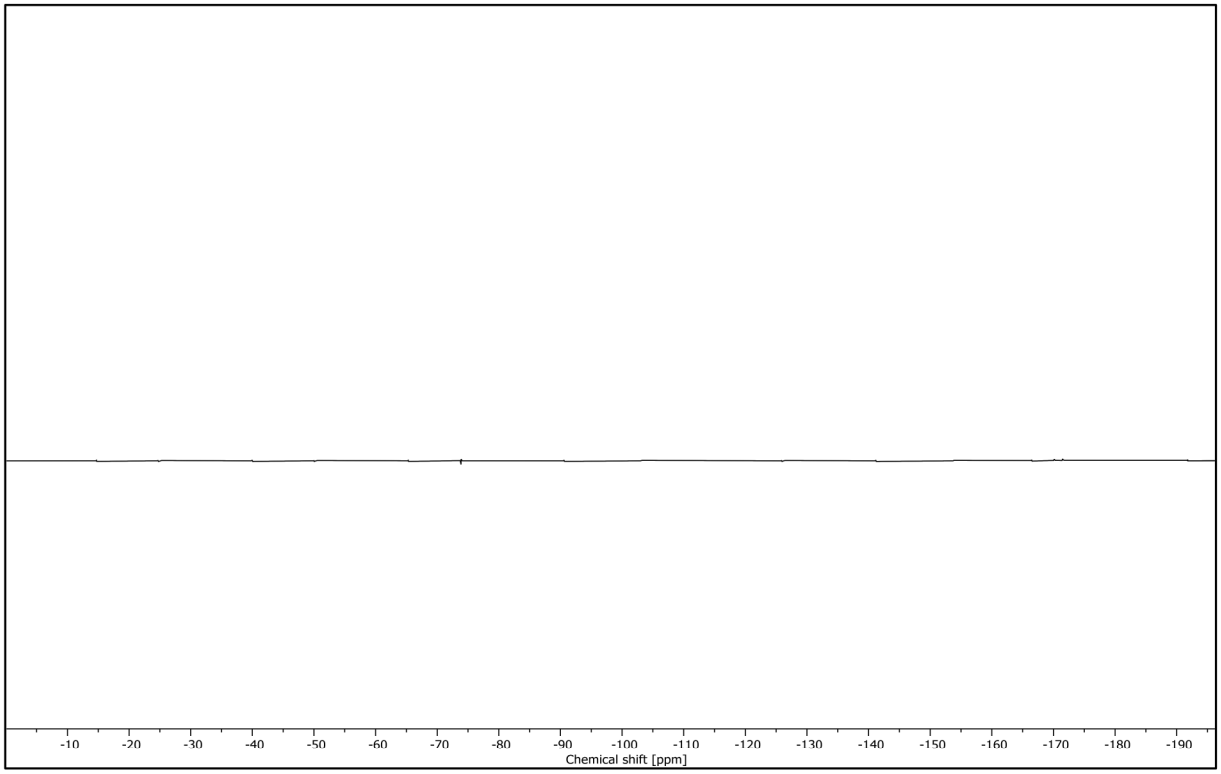


*Figure E32: $^{19}$F-NMR spectrum of $P_{100}$(KKKK) (600 MHz, DMSO-d6)*

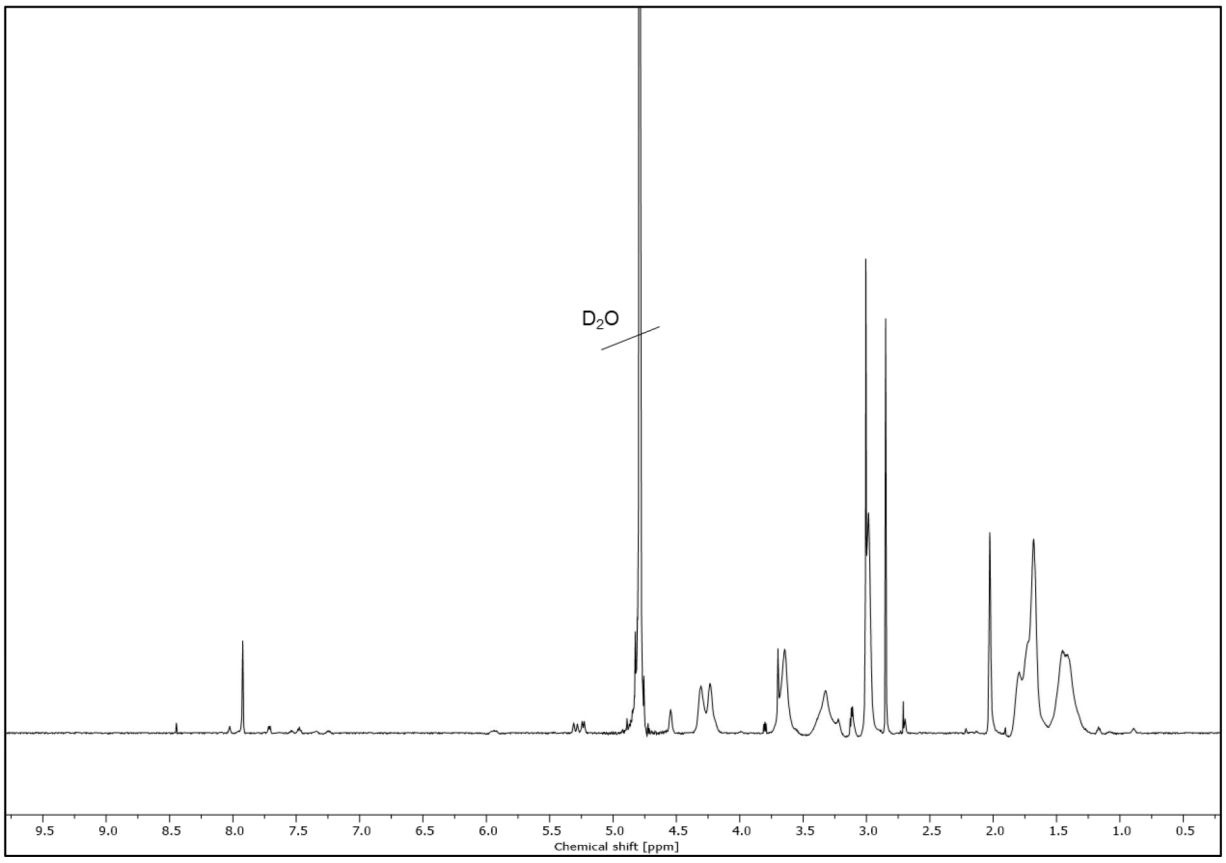


*Figure E33: $^{1}$H-NMR spectrum of $P_{100}$(++++) after first deprotection (600 MHz, $D_2O$)*

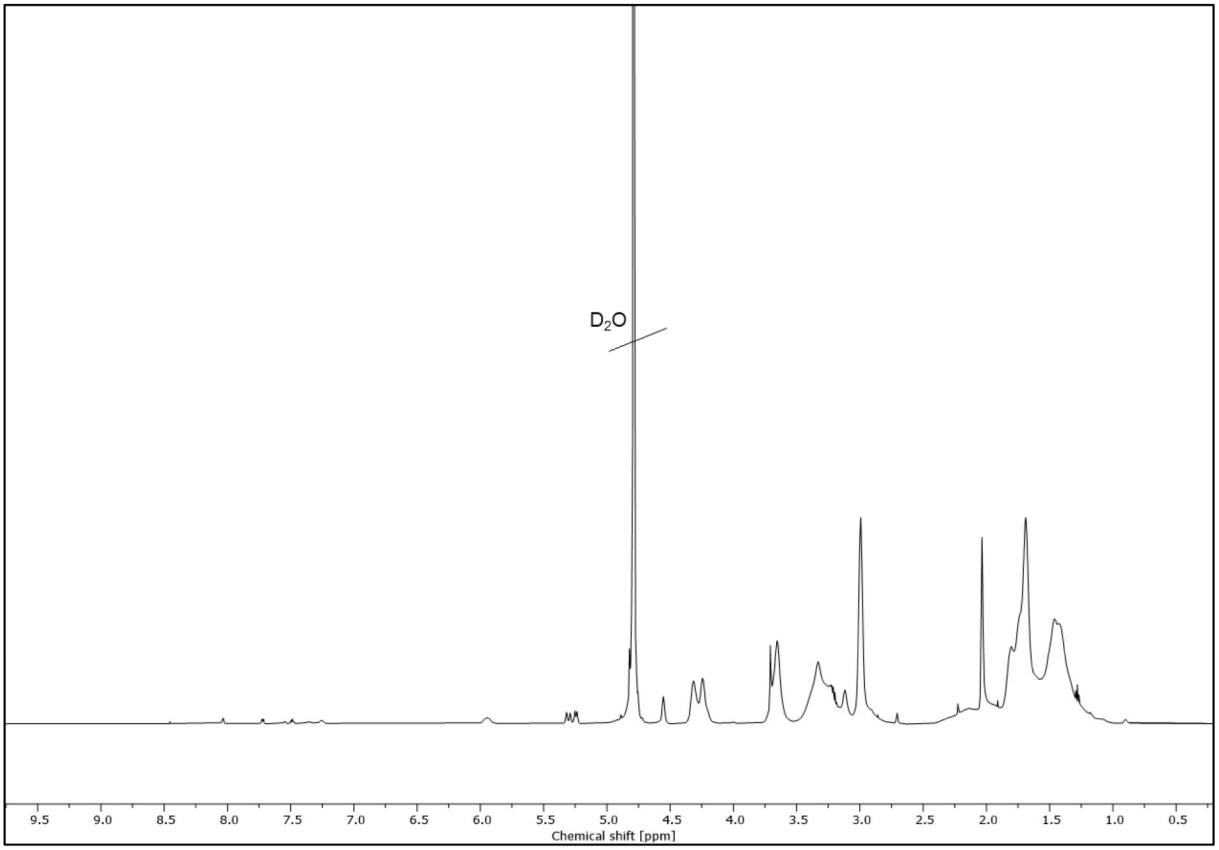


*Figure E34: $^{1}$H-NMR spectrum of $P_{100}$(++++) after second deprotection (600 MHz, $D_2O$)*

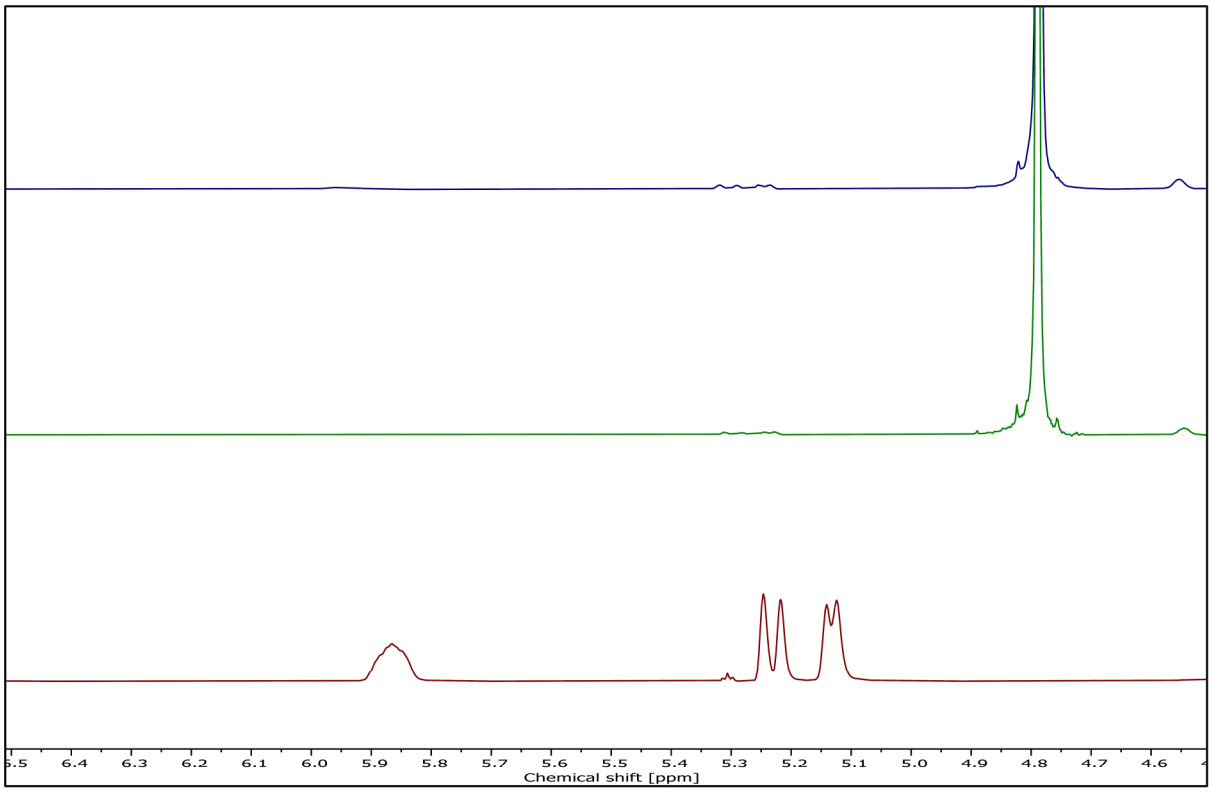


*Figure E35: Comparsion of $P_{100}$(KKKK) (bottom), $P_{100}$(++++) after first deprotection (middle) and $P_{100}$(++++) after second deprotection (top)*

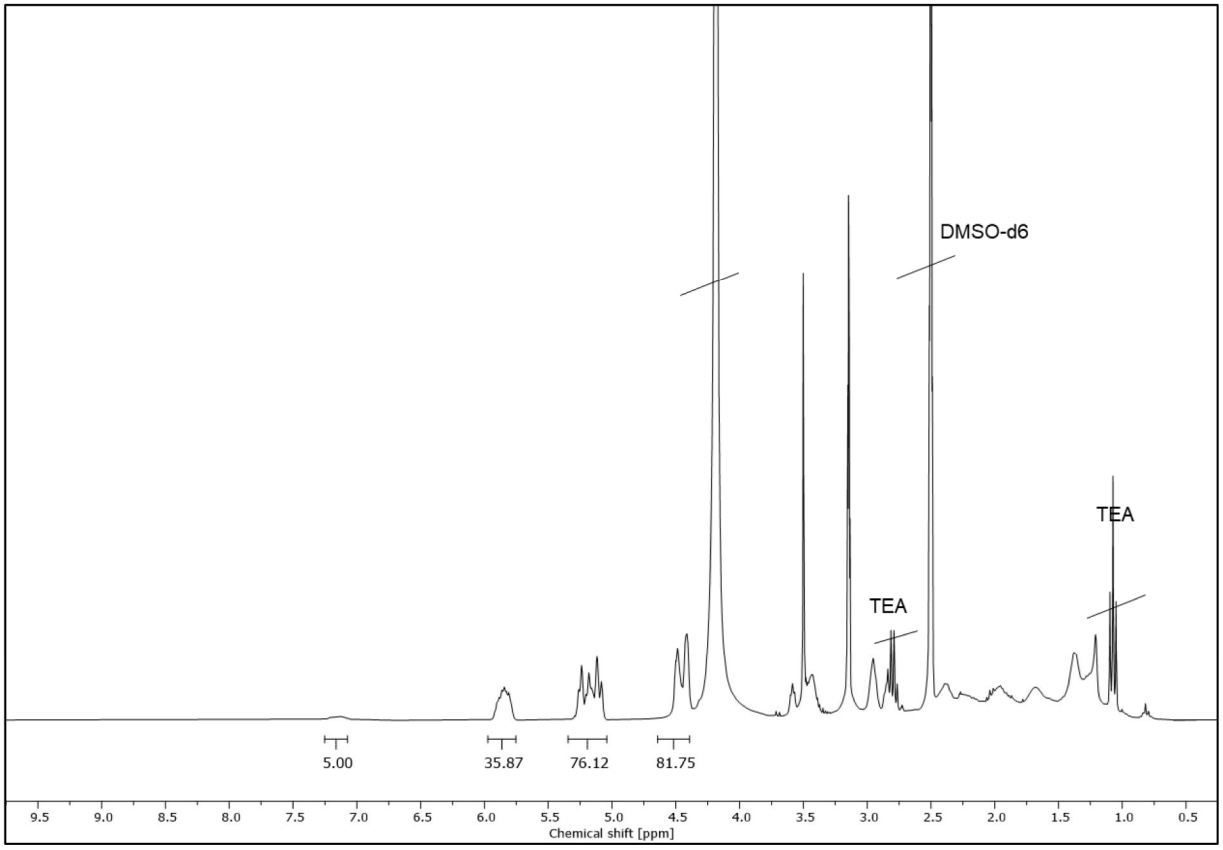


*Figure E36: $^{1}$H-NMR spectrum of $P_{100}$(KEKEKEKE) (600 MHz, DMSO-d6)*

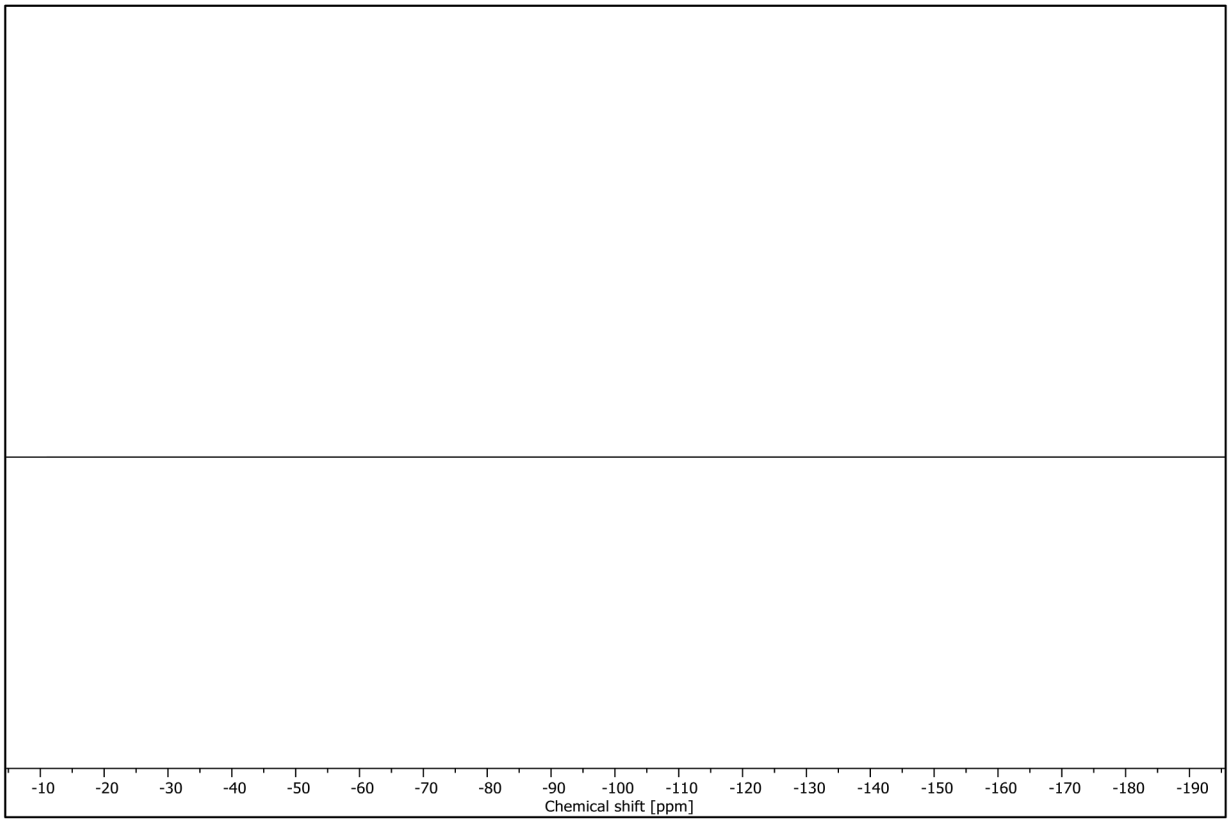


*Figure E37: $^{19}$F-NMR spectrum of $P_{100}$(KEKEKEKE) (600 MHz, DMSO-d6)*

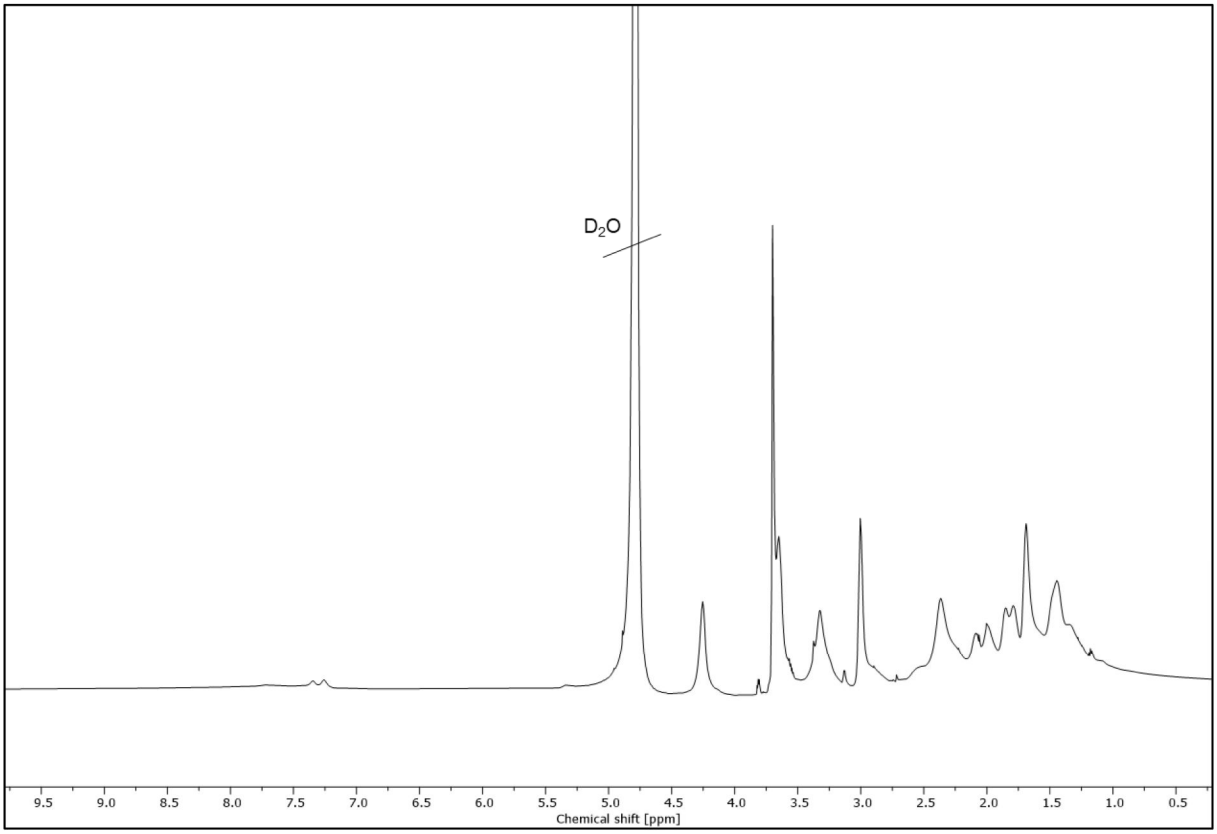


*Figure E38: $^{1}$H-NMR spectrum of $P_{100}$(+-+-+-+-) (600 MHz, $D_2O$)*

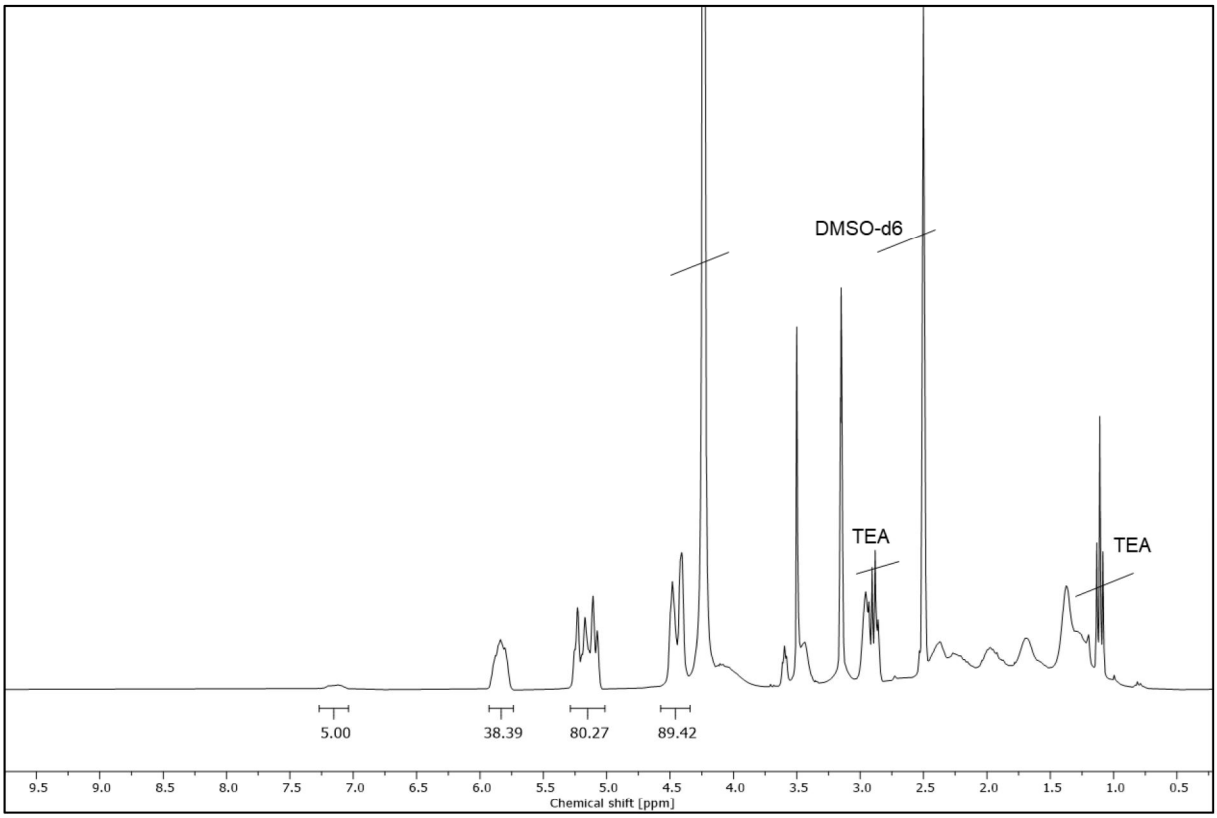


*Figure E39: $^{1}$H-NMR spectrum of $P_{100}$(KKEEKKEE) (600 MHz, DMSO-d6)*

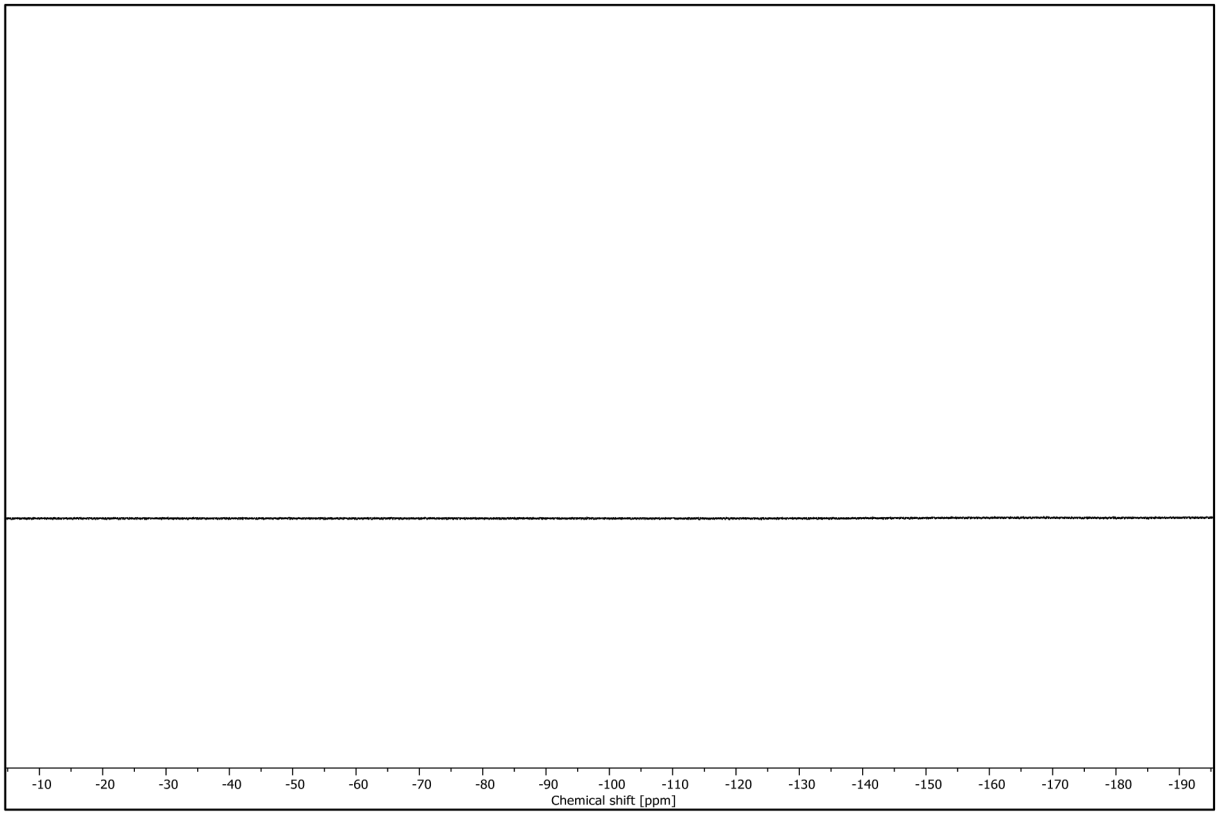


*Figure E40: $^{19}$F-NMR spectrum of $P_{100}$(KKEEKKEE) (600 MHz, DMSO-d6)*

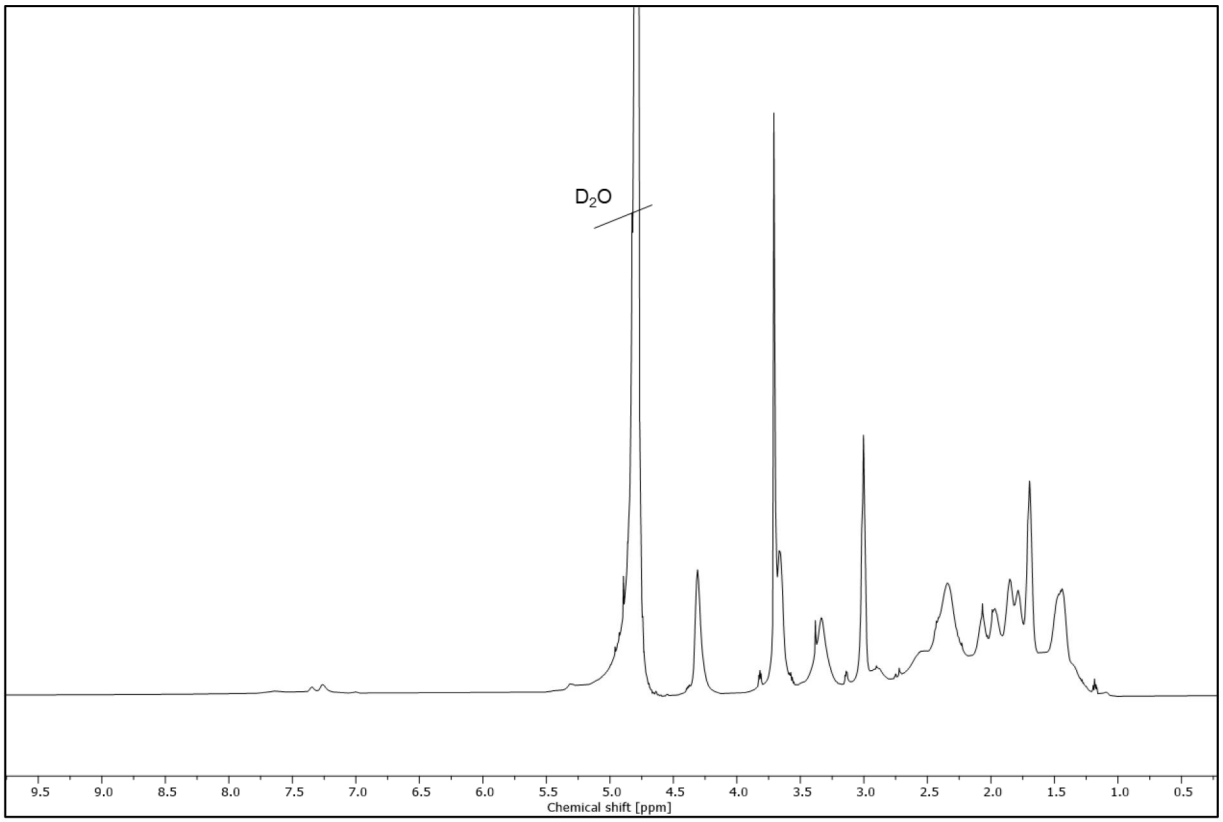


*Figure E41: $^{1}$H-NMR spectrum of $P_{100}$(++- -++- -) (600 MHz, $D_2O$)*

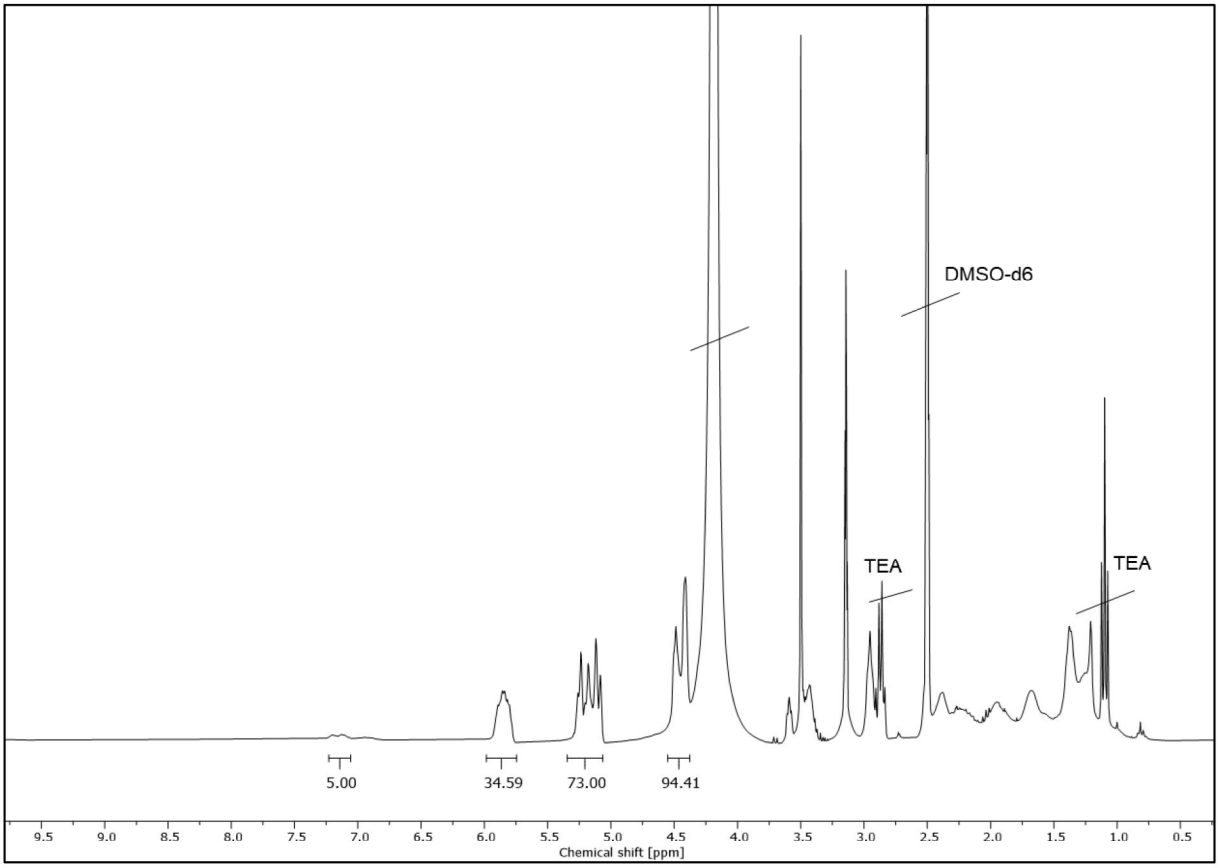


*Figure E42: $^{1}$H-NMR spectrum of $P_{100}$(KKKKEEEE) (600 MHz, DMSO-d6)*

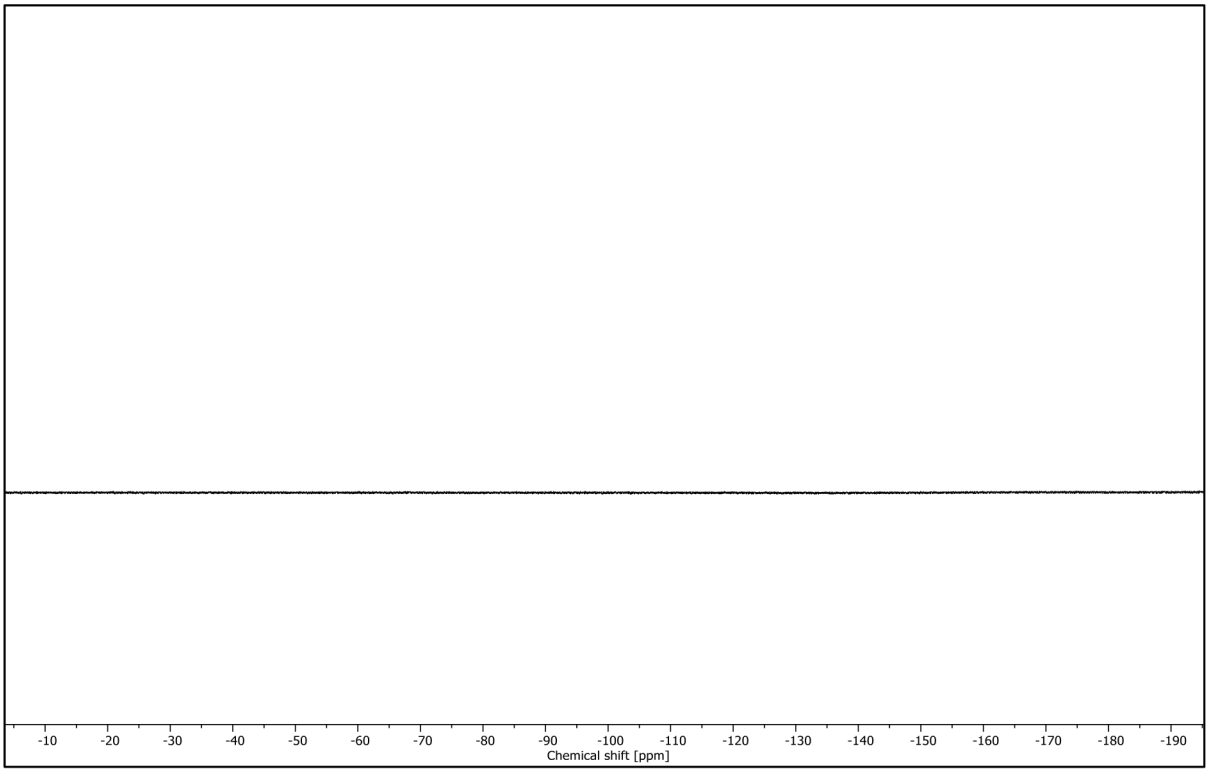


*Figure E43: $^{19}$F-NMR spectrum of $P_{100}$(KKKKEEEE) (600 MHz, DMSO-d6)*

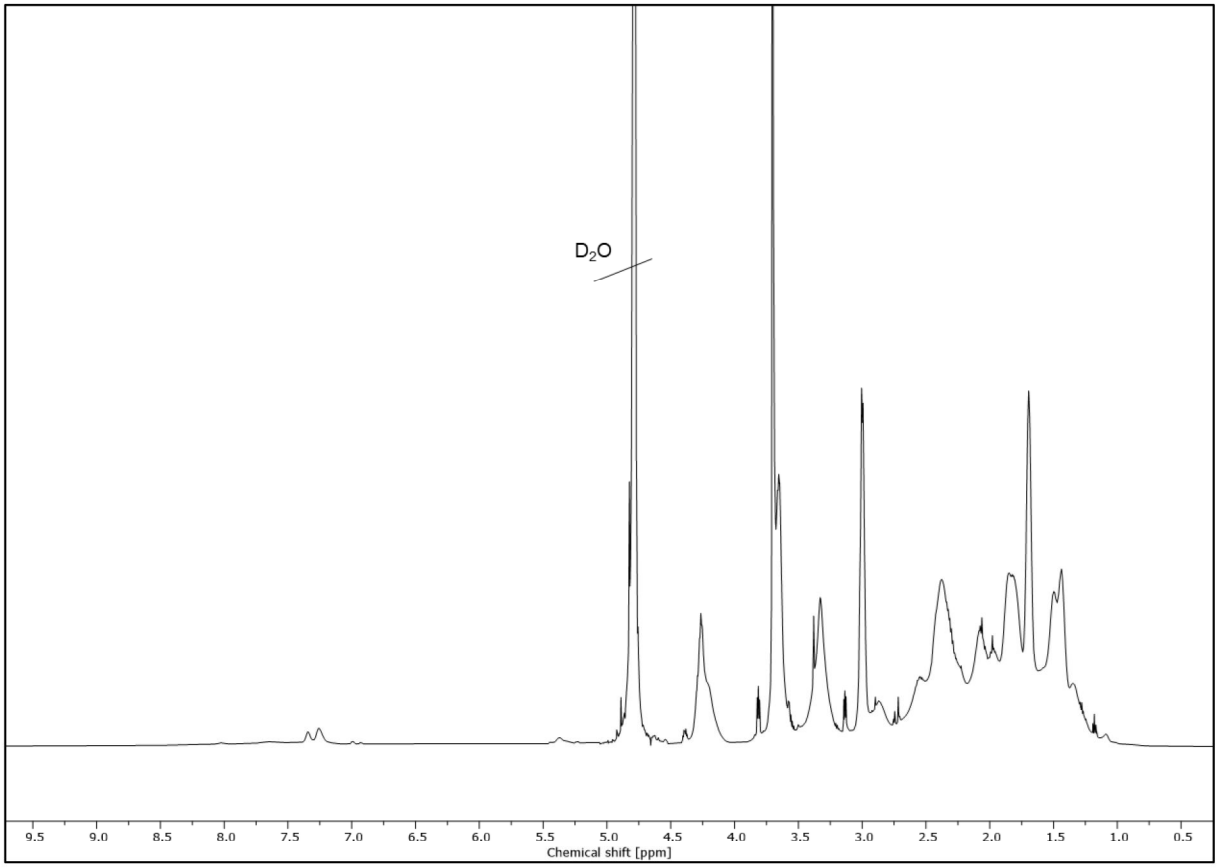


*Figure E44: $^{1}$H-NMR spectrum of $P_{100}$(++++- - - -) (600 MHz, $D_2O$)*

## 6.2. RP-HPLC

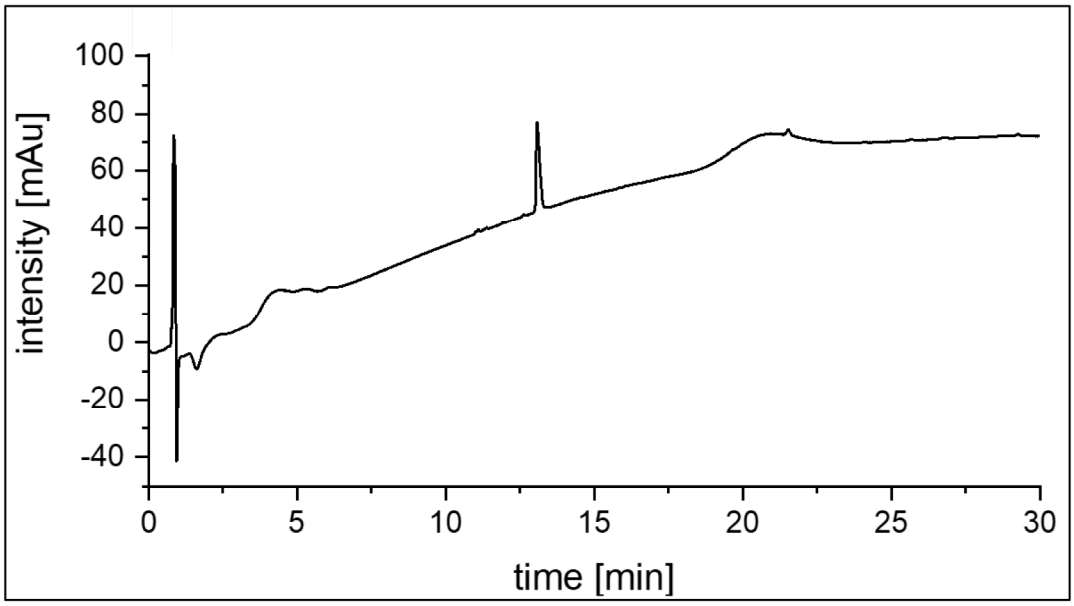


*Figure E45: RP-HPLC Run of EEEE*

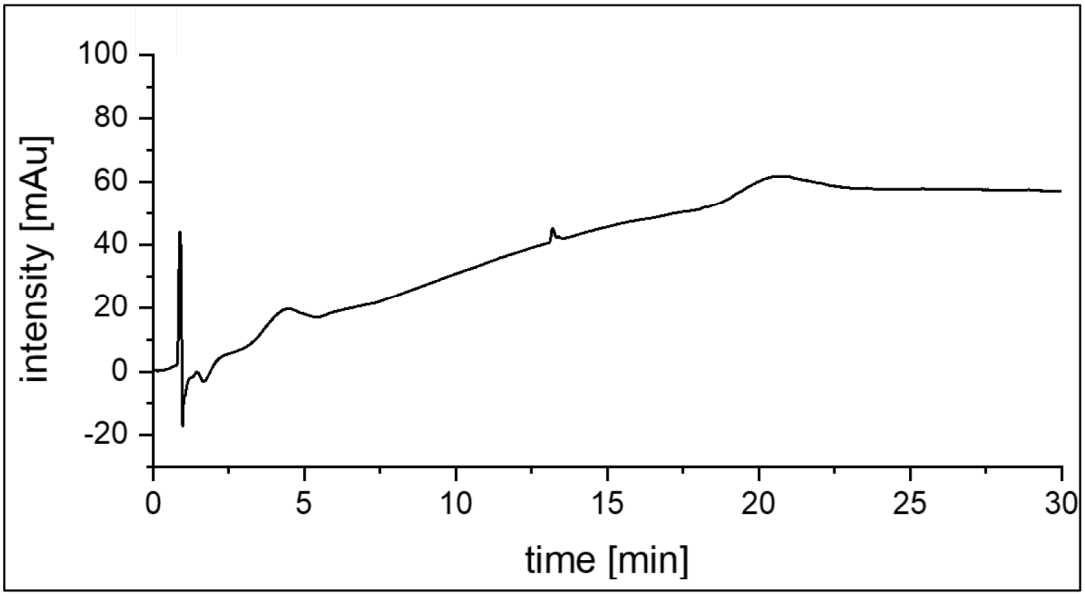


*Figure E46: RP-HPLC Run of KKKK*

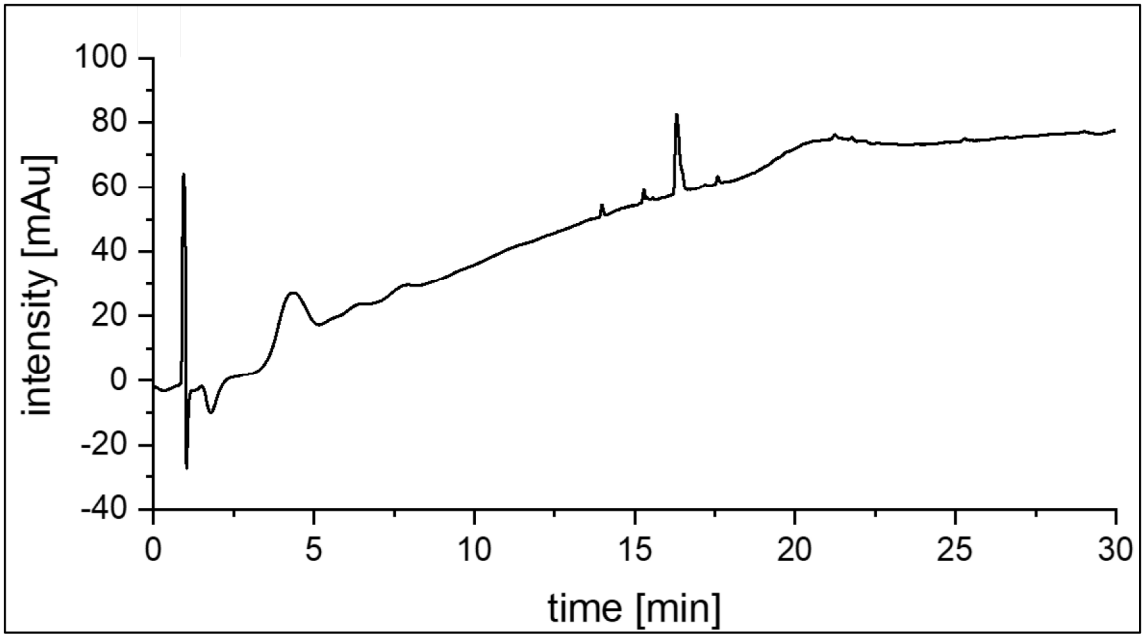


*Figure E47: RP-HPLC of KEKEKEKE.*

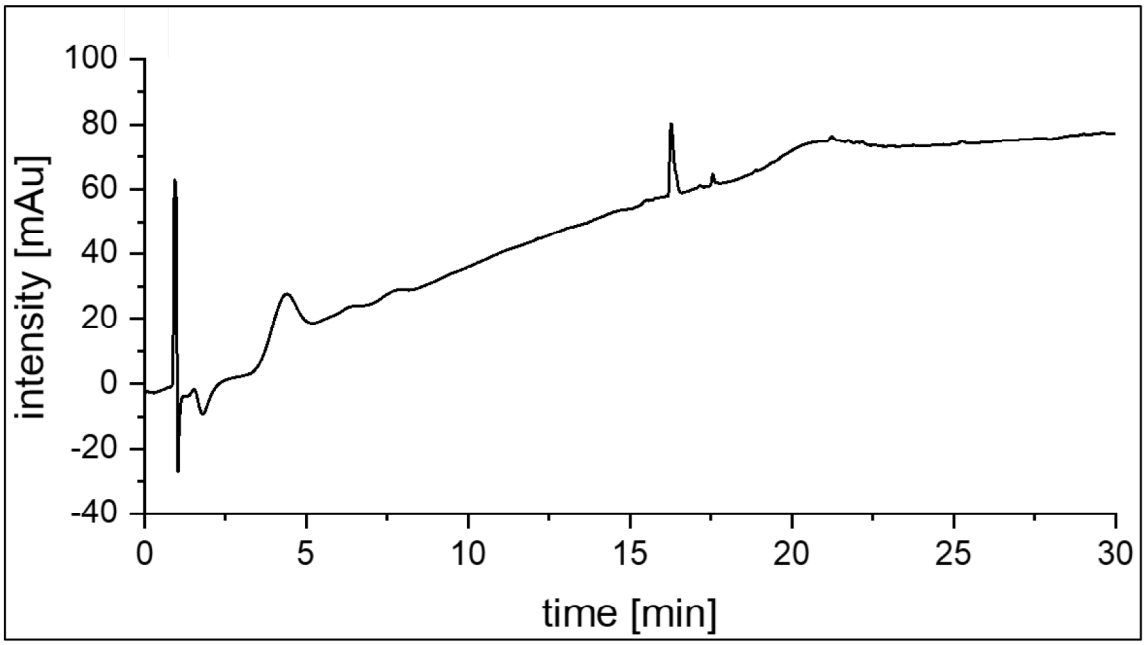


*Figure E48: RP-HPLC of KKEEKKEE.*

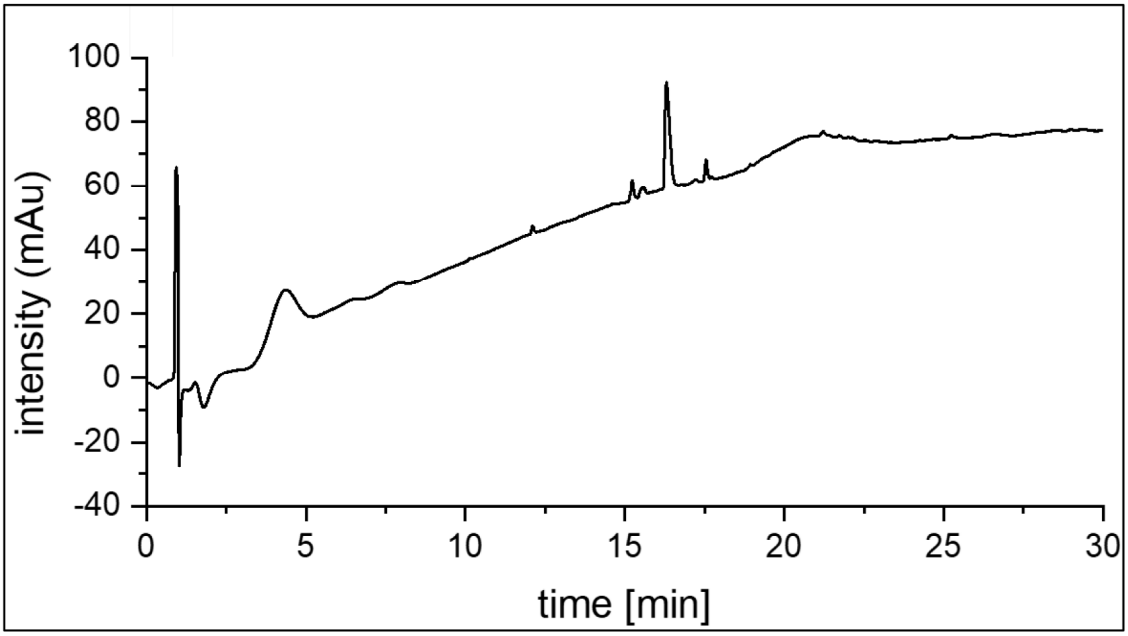


*Figure E49: RP-HPLC of KKKKEEEE.*

## 6.3. ESI-MS

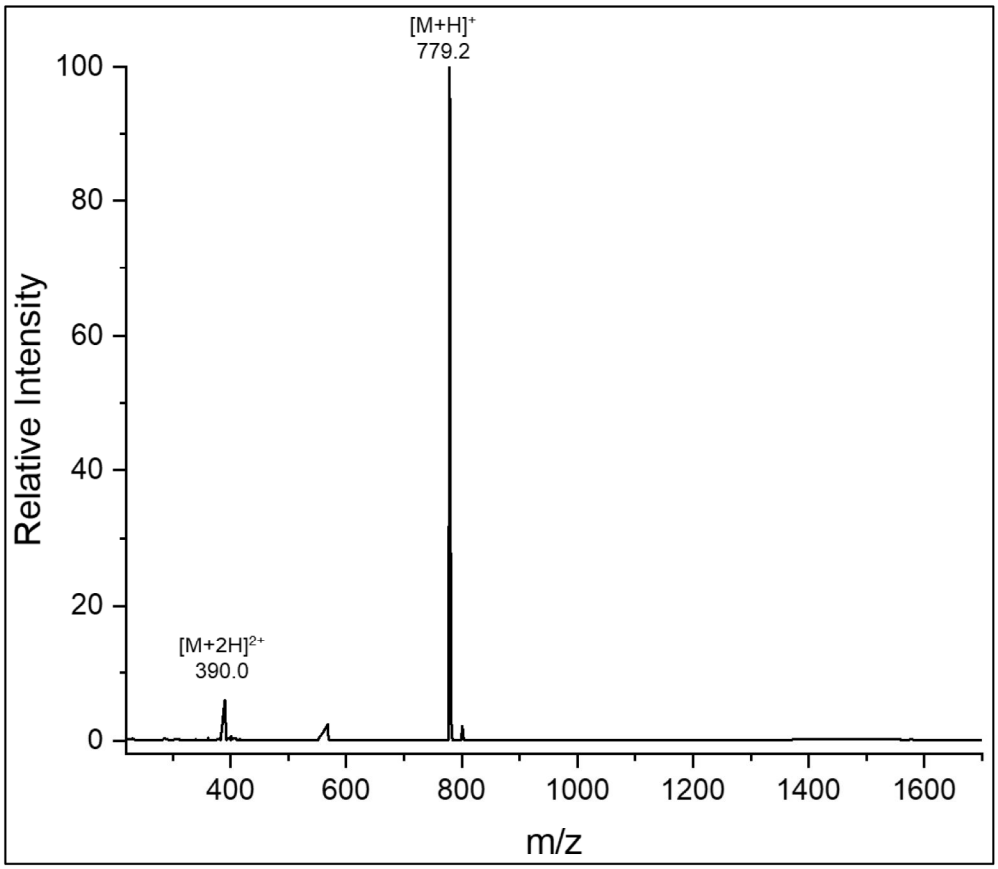


*Figure E50: ESI-MS spectrum of oligomer EEEE (positive mode).*

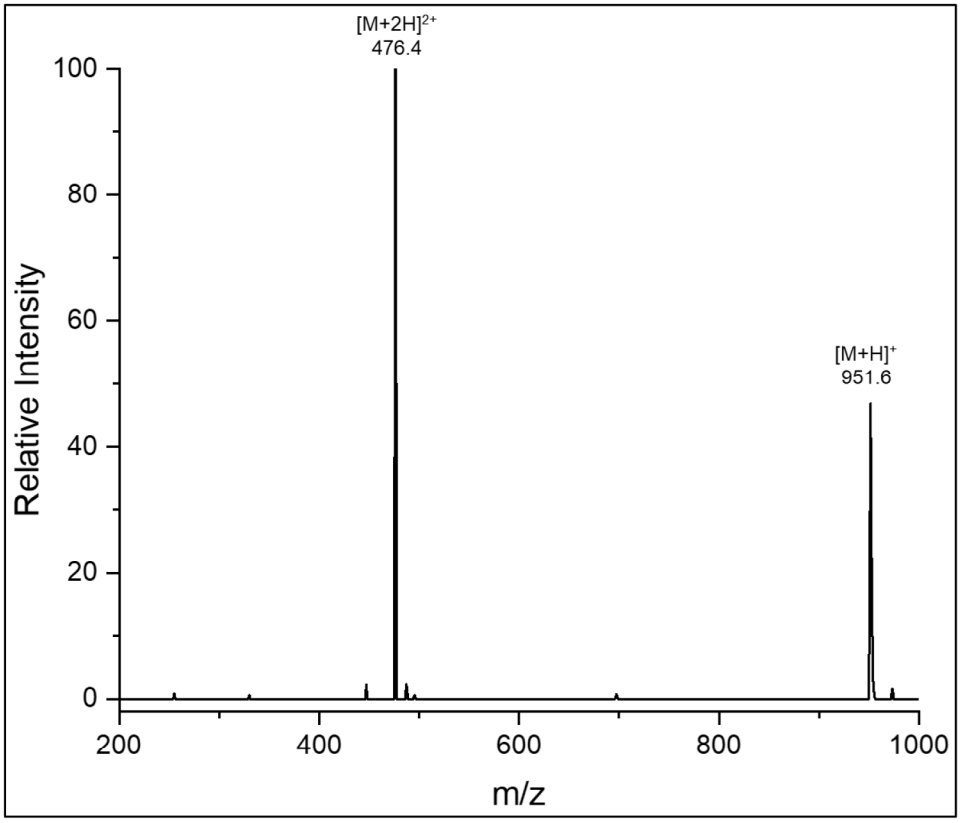


*Figure E51: ESI-MS spectrum of oligomer KKKK (positive mode)*

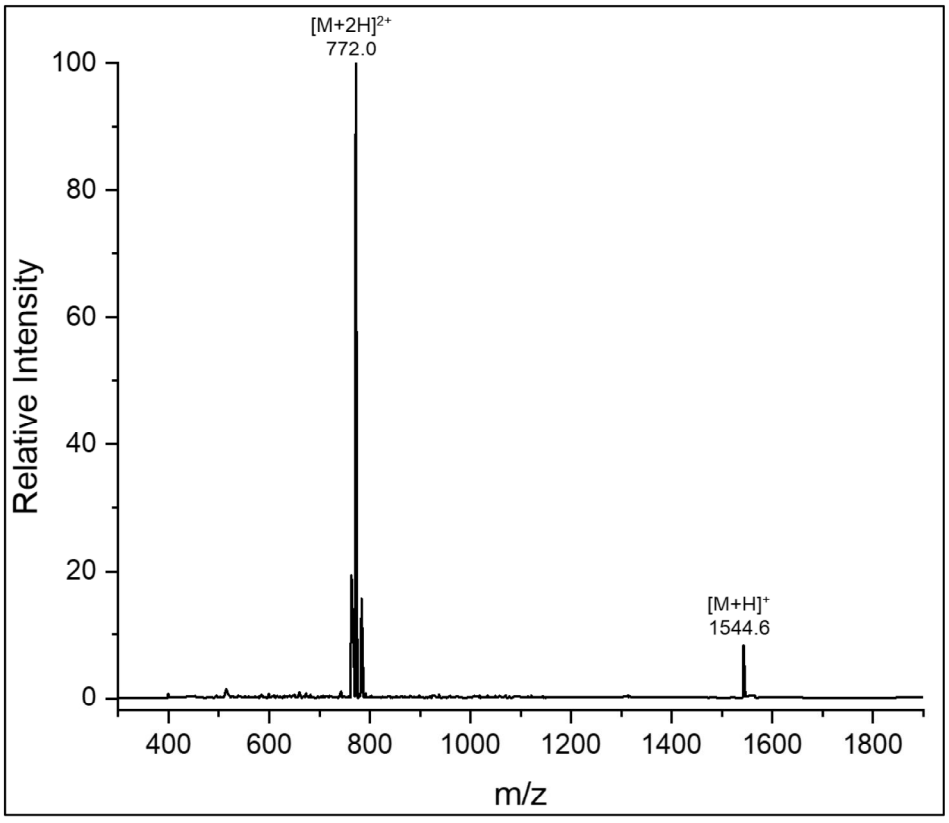


*Figure E52: ESI-MS spectrum of oligomer KEKEKEKE (positive mode)*

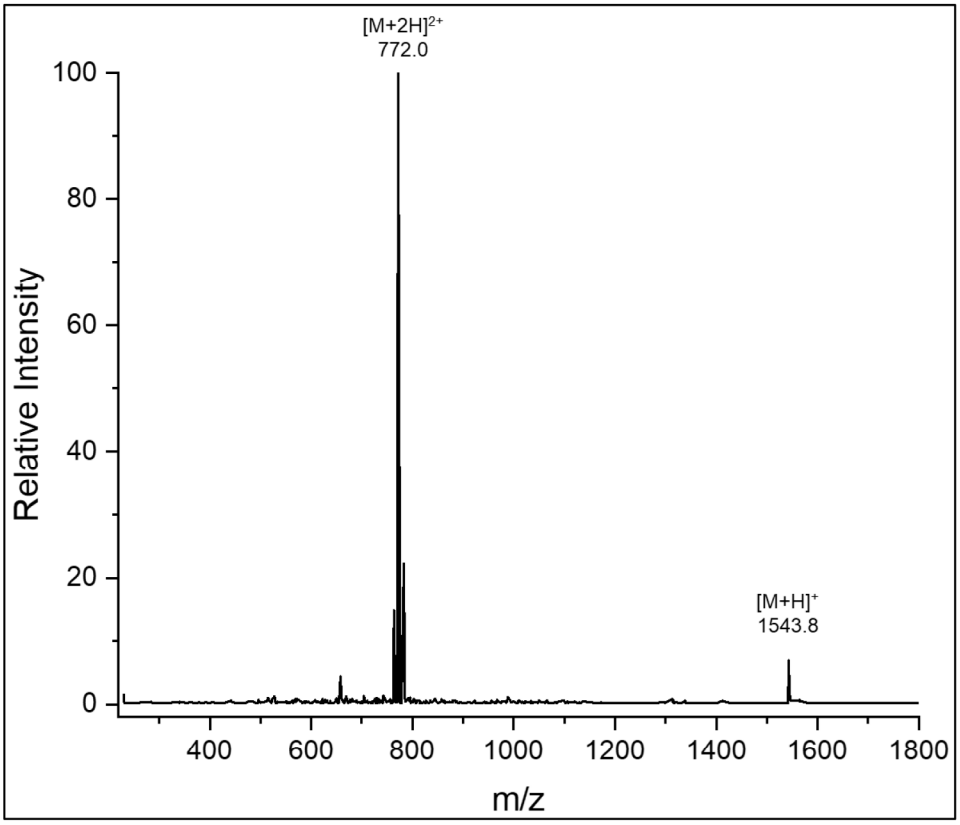


*Figure E53: ESI-MS spectrum of oligomer KKEEKKEE (positive mode)*

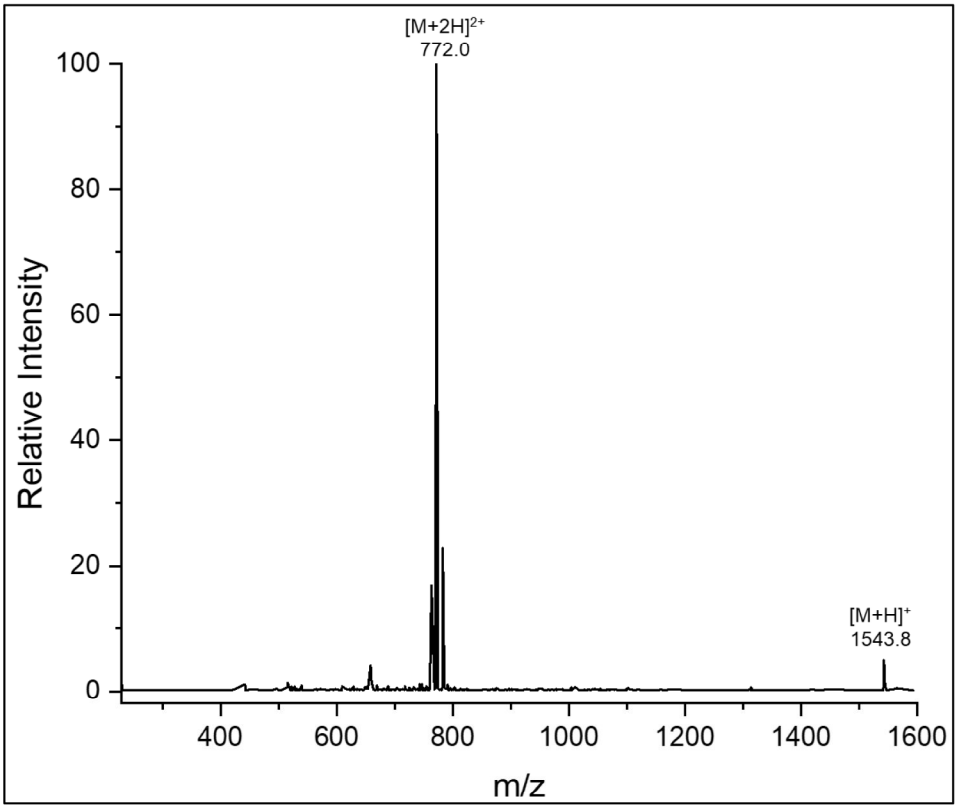


*Figure E54: ESI-MS spectrum of oligomer KKKKEEEE (positive mode).*

## 6.4. GPC

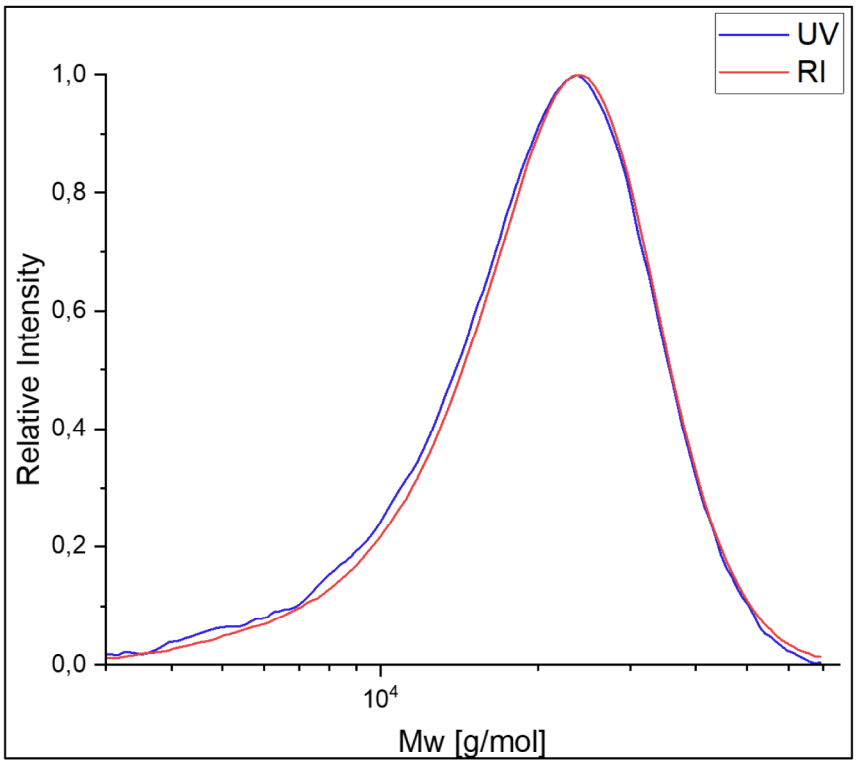


*Figure E55: GPC measurement (Eluent:THF) of Poly(Pentafluoro phenyl acrylate) 100 ($PPFP_{100}$)*

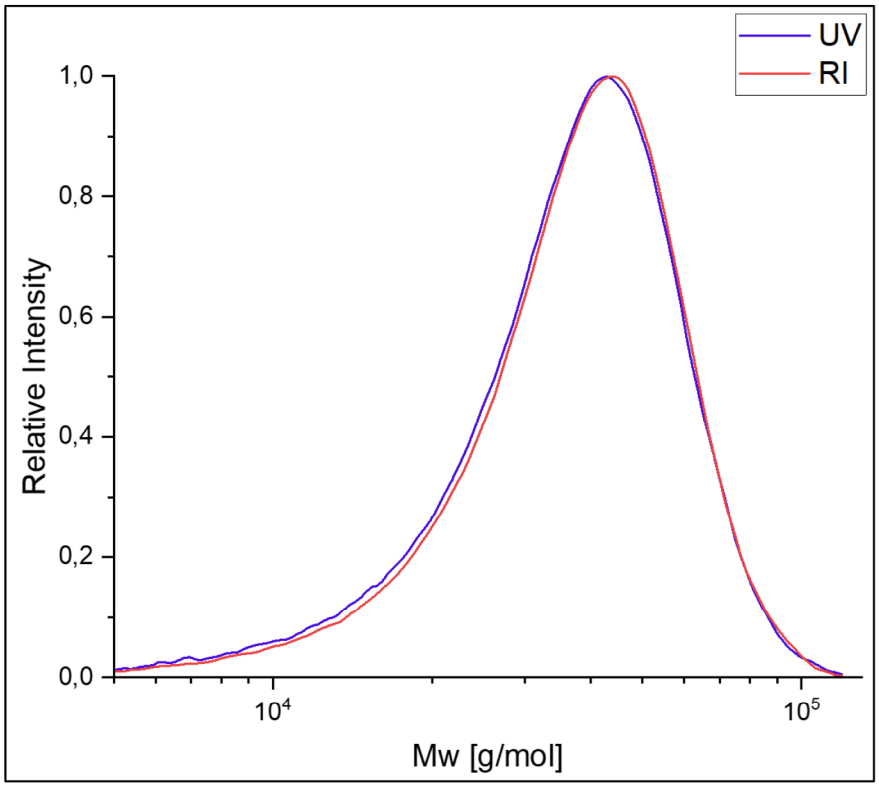


*Figure E56: GPC measurement (Eluent:THF) of Poly(Pentafluoro phenyl acrylate) 200 ($PPFP_{200}$)*

## 6.5. List of Abbreviations

| | |
|---|---|
| °C | Degree Celsius |
| µM | mikromolar |
| AA | Amino acid |
| AIBN | Azobisisobutyronitrile |
| Alloc | Allyloxy-carbonyl |
| Allyl | Allylether |
| BB | Building block |
| BSPA | Benzylsulfanylthiocarbonylsufanylpropionic acid |
| ConA | Concanavalin A |
| CRD | Carbohydrate recognition domain |
| CSC | Critical salt concentration |
| Đ | Dispersity |
| DCM | Dichloromethane |
| DIPEA | Diisopropylethylamine |
| DMF | Dimethylformamide |
| E. coli | Escherichia coli |
| EDA | Ethylene diamine |
| EDA-Trt | Trityl-protected ethylene diamine |
| EDS | Ethylene glycol diamine succinic acid |
| ESI-MS | Electrospray Ionization mass spectroscopy |
| eq. | equivalent |
| Fmoc | Fluorenylmethoxycarbonyl |
| Glc | α-D-glucopyranoside |
| GPC | Gel permeation chromatography |
| Hz | Hertz |

| | |
|---|---|
| IDP | Intrinsically disordered proteins |
| Man | α-D-mannopyranoside |
| $MgSO_4$ | Magnesium sulfate |
| MHz | Megahertz |
| min | Minute |
| mL | Millilitre |
| mM | Millimolar |
| MS | Mass spectrometry |
| MWCO | Molecular weight cut-off |
| $NaHCO_3$ | Sodium bicarbonate |
| nm | Nanometer |
| nM | Nanomolar |
| NMR | Nuclear magnetic resonance spectroscopy |
| PE | Polyelectrolyte |
| PEC | Polyelectrolyte complex |
| PEG | Polyethylene glycol |
| PFP | Pentafluoro phenyl |
| PFPA | Pentafluoro phenyl acrylate |
| PPFP | Poly(pentafluoro phenyl) |
| ppm | parts per million |
| PPV | Porcine parvovirus |
| PyBOP | Benzotriazol-1-yloxytripyrrolidinophosphonium hexafluorophosphate |
| RAFT | reversible-addition-fragmentation chain-transfer polymerization |
| RP-HPLC | Reversed-phase high pressure liquid chromatography |
| SPS | Solid-phase synthesis |
| S-RAM | Tentagel S-Ram resin |

| | |
|---|---|
| TEA | Triethylamine |
| TFA | Trifluoroacetic acid |
| TIPS | Triisopropylsilane |
| tBu | *tert*-Butyl |
| TDS | Triple bond diethylenetriamine succinic acid |

## 6.6. List of Figures

## 6.7. List of Tables

# 7. Acknowledgements

First of all, I would like to thank Prof. Dr. Laura Hartmann for the opportunity to complete my dissertation in her research group. Thank you for the great support and encouragement during my studies. Your passion and dedication to research have always been a great motivation for me and enabled me to pursue creative solutions.

An equally big thanks goes to Jun. Prof. Dr. Stephan Schmidt for his valuable guidance in this project. The inspiring conversations and discussions on the topic of coacervates helped me to better understand this project and provided further inspiration.

Furthermore, I would like to thank my mentor PD Dr. Klaus Schaper for taking the time to evaluate my dissertation.

I would also like to thank Dr. Monir "Mina" Tabatabai for reviewing my analytical data, especially the NMR spectra. Many thanks also to Michaela Kitzia, who always took the time to help with organizational problems. Special thanks to Stefanie Scheelen, Sonja Coors, Birgit Ohler, and Narges Irani, who have always taken care of the general tasks in the lab.

For recording mass spectra and nuclear magnetic resonance spectra I further want to thank CeMSA@HHU (Center for Molecular and Structural Analysis @ Heinrich Heine University), namely, Mohanad Aian, Ralf Bürgel, Dr. Klaus Schaper and Dr. Peter Tommes.

Ich danke dem gesamten AK Hartmann und AK Schmidt für die wunderbare Zeit während meiner Promotion. Trotz einer Pandemie hatte ich nie das Gefühl, allein zu sein. Ich danke euch für die schönen Momente während der „Klassenfahrten“, die unterhaltsamen Mittagessen und die geselligen Abende im Sozialraum.

Ein großer Dank geht an meine Bachelor- und Masterstudenten Joschua Pruisken, André Wassenberg, Jonathan Köpp, Basti Theisen, Peter Busch und Lea Schäfl. Danke für die gemeinsame und lustige Zeit im und außerhalb des Labors.

Besonders möchte ich mich bei Theresa Seiler und Tanja Paul bedanken. Ihr beide habt die Zeit für mich unvergesslich gemacht. Wir haben gemeinsam so viele Höhen und Tiefen durchgemacht, dass ich mir nicht vorstellen kann, wie ich das ohne euch beide geschafft hätte. Danke, dass ihr immer für mich da seid!

Ich danke meinen Kollegen aus dem „Makro-Praktikum“ – Melina Feldhof, Luca-Cesare Blawitzki und Patrick Konietzny – für den ganzen Spaß während der Praktikumszeit. In diesem Ausnahmezustand von zwei Monaten, der einmal im Jahr stattfand, habt ihr es mit eurer humorvollen Art geschafft, dass ich mich freute auf das Labor von morgens bis abends,

Kolloquien zu halten und Protokolle zu kontrollieren. Ich hoffe unser Stempel wurde noch zahlreich genutzt!

Auch meinen Freunden Victoria Ernst, Bianca Merz und Jasmin Konietzny, die immer an meiner Seite waren und mir auch in den stressigen Momenten ein Lächeln aufs Gesicht zaubern konnten, gilt mein Dank. Ein besonderer Dank geht auch an Laura Mayer für die zahlreichen „Dach“-Momente, Feierabend-Biere und Kneipenbingo-Abende. Danke, dass du immer ein offenes Ohr für mich hast.

Der größte Dank gilt meiner Familie! Danke an meinen Bruder Justin „Helga“ Illmann und meine Eltern Melanie und Uwe Illmann. Ihr habt mich wie kein anderer unterstützt. Dank euch gab es für mich keine Grenzen, und ich konnte herausfinden, wohin mich die Reise des Chemiestudiums führt. Heute kann ich gar nicht beschreiben, wie unendlich dankbar ich für eure bedingungslose Unterstützung bin!

Abschließend möchte ich mich bei Marco Lehmann bedanken. Danke, dass du mir während der gesamten Zeit beigestanden hast. Ich wüsste nicht, wie ich das ohne dich geschafft hätte. Danke, dass du mir auch in den schwierigen Momenten Sicherheit gegeben hast, wenn ich vor lauter Stress nicht wusste, wohin. Du bist der Grund, wieso ich nicht (ganz) durchgedreht bin.

# 8. References

**[1]** Meka, V. S.; Sing, M. K. G.; Pichika, M. R.; Nali, S. R.; Kolapalli, V. R. M.; Kesharwani, P. A comprehensive review on polyelectrolyte complexes. *Drug Discov Today* **2017**, *22* (11), 1697-1706.

**[2]** Lankalapalli, S. K., V.R.M. Polyelectrolyte Complexes: A Review of their Applicability in Drug Delivery Technology. *Indian Journal of Pharmaceutical Sciences* **2009**, *71* (5), 481-487.

**[3]** Solis, F. J.; de la Cruz, M. O. Collapse of flexible polyelectrolytes in multivalent salt solutions. *The Journal of Chemical Physics* **2000**, *112* (4), 2030-2035.

**[4]** De Robertis, S.; Bonferoni, M. C.; Elviri, L.; Sandri, G.; Caramella, C.; Bettini, R. Advances in oral controlled drug delivery: the role of drug-polymer and interpolymer non-covalent interactions. *Expert Opin Drug Deliv* **2015**, *12* (3), 441-453.

**[5]** Kwon, H. J.; Osada, Y.; Gong, J. P. Polyelectrolyte Gels-Fundamentals and Applications. *Polymer Journal* **2006**, *38* (12), 1211-1219.

**[6]** De Geest, B. G.; De Koker, S.; Sukhorukov, G. B.; Kreft, O.; Parak, W. J.; Skirtach, A. G.; Demeester, J.; De Smedt, S. C.; Hennink, W. E. Polyelectrolyte microcapsules for biomedical applications. *Soft Matter* **2009**, *5* (2), 282-291.

**[7]** Rabiee, A.; Ershad-Langroudi, A.; Zeynali, M. E. A survey on cationic polyelectrolytes and their applications: acrylamide derivatives. *Reviews in Chemical Engineering* **2015**, *31* (3).

**[8]** Alvarado, N.; Abarca, R. L.; Linares-Flores, C. Use of Chitosan-Based Polyelectrolyte Complexes for Its Potential Application in Active Food Packaging: A Review of Recent Literature. *Int J Mol Sci* **2023**, *24* (14).

**[9]** Vandenberg, E. J.; Diveley, W. R.; Filar, L. J.; Patel, S. R.; Barth, H. G. The synthesis and solution properties of some rigid-chain, water-soluble polymers: Poly[N,N'-(sulfo-phenylene)phthalamide]s and poly[N,N'-(sulfo-p-phenylene)pyromellitimide]. *Journal of Polymer Science Part A: Polymer Chemistry* **2003**, *27* (11), 3745-3757.

**[10]** Perry, S. L.; Leon, L.; Hoffmann, K. Q.; Kade, M. J.; Priftis, D.; Black, K. A.; Wong, D.; Klein, R. A.; Pierce, C. F., 3rd; Margossian, K. O.; et al. Chirality-selected phase behaviour in ionic polypeptide complexes. *Nat Commun* **2015**, *6*, 6052.

**[11]** Kossel, A. Über die basischen Stoffe des Zellkerns. *Hoppe-Seyler´s Zeitschrift für physiologische Chemie* **1897**, *22* (2), 176-187.

**[12]** Tiebackx, F. W. Gleichzeitige Ausflockung zweier Kolloide. *Zeitschrift für Chemie und Industrie der Kolloide* **1911**, *8*, 198-201.

**[13]** Michaels, A. S. M., R.G. Polycation-Polyanion Complexes: Preparation and Properties of Poly(Vinylbenzyltrimethylammonium) Poly-(styrenesulfonate). *Journal of physical Chemistry* **1961**, *65*, 1765-1773.

**[14]** Tsuchida, E. Formation of Polyelectrolyte Complexes and Their Structures. *Journal of Macromolecular Science, Part A* **1994**, *31* (1), 1-15.

**[15]** Kulkarni, A. D. V., Y.H.; Sancheti, K.H.; Patel, H.M.; Belgamwar, V.S; Surana, S.J.; Pardeshi, C.V. . Polyelectrolyte complexes: mechanisms, critical experimental aspects, and applications. *Artifical Cells, Nanomedicine and Biotechnology* **2016**, *44* (7), 1615-1625.

**[16]** A. Tripathi, J. S. M. *Advances in Biomaterials for Biomedical Applications*; Springer, 2017.

**[17]** E. Spruijt, M. A. S., J. van der Gucht. Linear Viscoelasticity of Polyelectrolyte Complex Coacervates. *Macromolecules* **2013**, *46* (4), 1633-1641.

**[18]** H.G. Bungenberg de Jong, H. R. K. Coacervation. *Proc. Koninkl. Med. Akad. Wetershap* **1929**, *32*, 849-856.

**[19]** J. van der Gucht, E. S., M. Lemmers, M.A.C. Stuart. Polyelectrolyte complexes: Bulk phases and colloidal systems. *Journal of Colloid and Interface Science* **2011**, *361* (2), 407-422.

**[20]** Dobrynin, A. V.; Colby, R. H.; Rubinstein, M. Polyampholytes. *Journal of Polymer Science Part B: Polymer Physics* **2004**, *42* (19), 3513-3538.

**[21]** Danielsen, S. P. O.; McCarty, J.; Shea, J. E.; Delaney, K. T.; Fredrickson, G. H. Molecular design of self-coacervation phenomena in block polyampholytes. *Proc Natl Acad Sci U S A* **2019**, *116* (17), 8224-8232.

**[22]** Blocher, W. C.; Perry, S. L. Complex coacervate-based materials for biomedicine. *Wires Nanomed Nanobi* **2017**, *9* (4).

**[23]** Perry, S.; Li, Y.; Priftis, D.; Leon, L.; Tirrell, M. The Effect of Salt on the Complex Coacervation of Vinyl Polyelectrolytes. *Polymers* **2014**, *6* (6), 1756-1772.

**[24]** Priftis, D.; Tirrell, M. Phase behaviour and complex coacervation of aqueous polypeptide solutions. *Soft Matter* **2012**, *8* (36), 9396-9405.

**[25]** McClements, D. J. Encapsulation, protection, and delivery of bioactive proteins and peptides using nanoparticle and microparticle systems: A review. *Adv Colloid Interface Sci* **2018**, *253*, 1-22.

**[26]** Blocher McTigue, W. C.; Perry, S. L. Protein Encapsulation Using Complex Coacervates: What Nature Has to Teach Us. *Small* **2020**, *16* (27).

**[27]** Schroder, H. C.; Neufurth, M.; Zhou, H.; Wang, S.; Wang, X.; Muller, W. E. G. Inorganic Polyphosphate: Coacervate Formation and Functional Significance in Nanomedical Applications. *Int J Nanomedicine* **2022**, *17*, 5825-5850.

**[28]** Liang, H.; de Pablo, J. J. A Coarse-Grained Molecular Dynamics Study of Strongly Charged Polyelectrolyte Coacervates: Interfacial, Structural, and Dynamical Properties. *Macromolecules* **2022**, *55* (10), 4146-4158.

**[29]** Wang, Q.; Schlenoff, J. B. The Polyelectrolyte Complex/Coacervate Continuum. *Macromolecules* **2014**, *47* (9), 3108-3116.

**[30]** Lytle, T. K.; Sing, C. E. Tuning chain interaction entropy in complex coacervation using polymer stiffness, architecture, and salt valency. *Molecular Systems Design & Engineering* **2018**, *3* (1), 183-196.

**[31]** Lytle, T. K.; Chang, L. W.; Markiewicz, N.; Perry, S. L.; Sing, C. E. Designing Electrostatic Interactions via Polyelectrolyte Monomer Sequence. *ACS Cent Sci* **2019**, *5* (4), 709-718.

**[32]** Madinya, J. J.; Chang, L.-W.; Perry, S. L.; Sing, C. E. Sequence-dependent self-coacervation in high charge-density polyampholytes. *Molecular Systems Design & Engineering* **2020**, *5* (3), 632-644.

**[33]** Perry, S. L. Phase separation: Bridging polymer physics and biology. *Current Opinion in Colloid & Interface Science* **2019**, *39*, 86-97.

**[34]** van Stevendaal, M.; Vasiukas, L.; Yewdall, N. A.; Mason, A. F.; van Hest, J. C. M. Engineering of Biocompatible Coacervate-Based Synthetic Cells. *ACS Appl Mater Interfaces* **2021**, *13* (7), 7879-7889.

**[35]** Cook, A. B.; Novosedlik, S.; van Hest, J. C. M. Complex Coacervate Materials as Artificial Cells. *Acc Mater Res* **2023**, *4* (3), 287-298.

**[36]** Mi, X.; Blocher McTigue, W. C.; Joshi, P. U.; Bunker, M. K.; Heldt, C. L.; Perry, S. L. Thermostabilization of viruses via complex coacervation. *Biomater Sci* **2020**, *8* (24), 7082-7092.

**[37]** Dong, D.; Cui, B. Comparison of rheological properties of different protein/gum arabic complex coacervates. *Journal of Food Process Engineering* **2019**, *42* (6).

**[38]** Forenzo, C.; Larsen, J. Complex Coacervates as a Promising Vehicle for mRNA Delivery: A Comprehensive Review of Recent Advances and Challenges. *Mol Pharm* **2023**, *20* (9), 4387-4403.

**[39]** Lim, S.; Moon, D.; Kim, H. J.; Seo, J. H.; Kang, I. S.; Cha, H. J. Interfacial tension of complex coacervated mussel adhesive protein according to the Hofmeister series. *Langmuir* **2014**, *30* (4), 1108-1115.

**[40]** Riggleman, R. A.; Kumar, R.; Fredrickson, G. H. Investigation of the interfacial tension of complex coacervates using field-theoretic simulations. *J Chem Phys* **2012**, *136* (2), 024903.

**[41]** Uversky, V. N. Protein intrinsic disorder-based liquid-liquid phase transitions in biological systems: Complex coacervates and membrane-less organelles. *Adv Colloid Interface Sci* **2017**, *239*, 97-114.

**[42]** Yewdall, N. A.; André, A. A. M.; Lu, T.; Spruijt, E. Coacervates as models of membraneless organelles. *Current Opinion in Colloid & Interface Science* **2021**, *52*.

**[43]** A.A. Hyman, K. S. Beyond Oil and Water - Phase Transition in Cells. *American Association for the Advancement of Science* **2012**, *337* (6098), 1047-1049.

**[44]** Hyman, A. A.; Weber, C. A.; Julicher, F. Liquid-liquid phase separation in biology. *Annu Rev Cell Dev Biol* **2014**, *30*, 39-58.

**[45]** Brangwynne, Clifford P.; Tompa, P.; Pappu, Rohit V. Polymer physics of intracellular phase transitions. *Nature Physics* **2015**, *11* (11), 899-904.

**[46]** Baer, A.; Hansch, S.; Mayer, G.; Harrington, M. J.; Schmidt, S. Reversible Supramolecular Assembly of Velvet Worm Adhesive Fibers via Electrostatic Interactions of Charged Phosphoproteins. *Biomacromolecules* **2018**, *19* (10), 4034-4043.

**[47]** Baer, A. O., I.; Schmidt, S.; Harrington, M.; Mayer, G. Strategien der Natur als Vorbild für nachhaltige Biomaterialien - Der "Sekundenkleber" der Stummelfüßer. *Biologie Unserer Zeit* **2019**, *49*, 418-425.

**[48]** Baer, A.; Horbelt, N.; Nijemeisland, M.; Garcia, S. J.; Fratzl, P.; Schmidt, S.; Mayer, G.; Harrington, M. J. Shear-Induced beta-Crystallite Unfolding in Condensed Phase Nanodroplets Promotes Fiber Formation in a Biological Adhesive. *ACS Nano* **2019**, *13* (5), 4992-5001.

**[49]** Baer, A.; Schmidt, S.; Haensch, S.; Eder, M.; Mayer, G.; Harrington, M. J. Mechanoresponsive lipid-protein nanoglobules facilitate reversible fibre formation in velvet worm slime. *Nat Commun* **2017**, *8* (1), 974.

**[50]** Yang, B.; Jin, S.; Park, Y.; Jung, Y. M.; Cha, H. J. Coacervation of Interfacial Adhesive Proteins for Initial Mussel Adhesion to a Wet Surface. *Small* **2018**, *14* (52), e1803377.

**[51]** Lemetti, L.; Scacchi, A.; Yin, Y.; Shen, M.; Linder, M. B.; Sammalkorpi, M.; Aranko, A. S. Liquid-Liquid Phase Separation and Assembly of Silk-like Proteins is Dependent on the Polymer Length. *Biomacromolecules* **2022**, *23* (8), 3142-3153.

**[52]** Black, K. A.; Priftis, D.; Perry, S. L.; Yip, J.; Byun, W. Y.; Tirrell, M. Protein Encapsulation via Polypeptide Complex Coacervation. *Acs Macro Lett* **2014**, *3* (10), 1088-1091.

**[53]** Kim, S.; Huang, J.; Lee, Y.; Dutta, S.; Yoo, H. Y.; Jung, Y. M.; Jho, Y.; Zeng, H.; Hwang, D. S. Complexation and coacervation of like-charged polyelectrolytes inspired by mussels. *Proc Natl Acad Sci U S A* **2016**, *113* (7), E847-853.

**[54]** Wang, F.; Xu, X.; Zhao, S. Complex Coacervation in Asymmetric Solutions of Polycation and Polyanion. *Langmuir* **2019**, *35* (47), 15267-15274.

**[55]** Werz, D. B.; Seeberger, P. H. Carbohydrates as the next frontier in pharmaceutical research. *Chemistry* **2005**, *11* (11), 3194-3206.

**[56]** Cecioni, S.; Imberty, A.; Vidal, S. Glycomimetics versus multivalent glycoconjugates for the design of high affinity lectin ligands. *Chem Rev* **2015**, *115* (1), 525-561.

**[57]** Kato, K.; Ishiwa, A. The role of carbohydrates in infection strategies of enteric pathogens. *Trop Med Health* **2015**, *43* (1), 41-52.

**[58]** Üclü, S.; Marschelke, C.; Drees, F.; Giesler, M.; Wilms, D.; Kohler, T.; Schmidt, S.; Synytska, A.; Hartmann, L. Sweet Janus Particles: Multifunctional Inhibitors of Carbohydrate-Based Bacterial Adhesion. *Biomacromolecules* **2024**, *25* (4), 2399-2407.

**[59]** Alberts, B. J., A. D.; Lewis, J.; ;organ, D.; Raff, M.; Roberts, K.; Wlater, P. *Molekularbiologie der Zelle*; John Wiley & Sons, 2017.

**[60]** Voets, D. V., J. G.; Pratt, C. W. *Fundamentals of biochemistry: life at the molecular level*; John Wiley & Sons, 2016.

**[61]** Varki, A. *Essentials of Glycobiology* Cold Spring Harbor Laboratory Press,U.S., 2017.

**[62]** Rini, J. M. Lectin Structure. *Annu. Rev. Biophys. Biomol. Struct.* **1995**, *24*, 551-577.

**[63]** Boyd, W. C.; Snavely, P. D., Jr.; Brown, R. D., Jr.; Roberts, A. E.; Rau, W. W.; Hoover, L.; Pease, M. H., Jr. Specific Precipitating Activity of Plant Agglutinins (Lectins). *Science* **1954**, *119* (3091), 419-420.

**[64]** Nitta. Molecular and sugar bining heterogenity of C-type lectins. **2005**.

**[65]** Mahajan, S.; Ramya, T. N. C. Nature-inspired engineering of an F-type lectin for increased binding strength. *Glycobiology* **2018**, *28* (12), 933-948.

**[66]** Kumamoto, Y.; Higashi, N.; Denda-Nagai, K.; Tsuiji, M.; Sato, K.; Crocker, P. R.; Irimura, T. Identification of sialoadhesin as a dominant lymph node counter-receptor for mouse macrophage galactose-type C-type lectin 1. *J Biol Chem* **2004**, *279* (47), 49274-49280.

**[67]** Tasumi, S.; Ohira, T.; Kawazoe, I.; Suetake, H.; Suzuki, Y.; Aida, K. Primary structure and characteristics of a lectin from skin mucus of the Japanese eel Anguilla japonica. *J Biol Chem* **2002**, *277* (30), 27305-27311.

**[68]** Edelman, G. M. C., B.A.; Reeke, G.N. Jr.; Becker, J.W.; Waxdal, M.J.; Wang, J.L. The covalent and three dimensional structure of Concanavlin A. *Proc Natl Acad Sci USA* **1972**, *69*, 2580-2584.

**[69]** Sumner, J. B. The Globulins of the Jack Bean, Canavalia Ensiformis. *Journal of Biological Chemistry* **1919**, *37* (1), 137-142.

**[70]** Brewer, C. F. Thermodynamic studies of lectin carbohydrate interactions by isothermal titration calorimetry. **2002**.

**[71]** Cavada, B. S.; Pinto-Junior, V. R.; Osterne, V. J. S.; Nascimento, K. S. ConA-Like Lectins: High Similarity Proteins as Models to Study Structure/Biological Activities Relationships. *Int J Mol Sci* **2018**, *20* (1).

**[72]** Hernando, P. J.; Dedola, S.; Marin, M. J.; Field, R. A. Recent Developments in the Use of Glyconanoparticles and Related Quantum Dots for the Detection of Lectins, Viruses, Bacteria and Cancer Cells. *Front Chem* **2021**, *9*, 668509.

**[73]** Heymann, F.; Hamesch, K.; Weiskirchen, R.; Tacke, F. The concanavalin A model of acute hepatitis in mice. *Lab Anim* **2015**, *49* (1 Suppl), 12-20.

**[74]** Ballerstadt, R.; Evans, C.; McNichols, R.; Gowda, A. Concanavalin A for in vivo glucose sensing: a biotoxicity review. *Biosens Bioelectron* **2006**, *22* (2), 275-284.

**[75]** Chung, N. J.; Park, Y. R.; Lee, D. H.; Oh, S. Y.; Park, J. H.; Lee, S. J. Heterometal-Coordinated Monomeric Concanavalin A at pH 7.5 from Canavalia ensiformis. *J Microbiol Biotechnol* **2017**, *27* (12), 2241-2244.

**[76]** Di Iorio, D.; Huskens, J. Surface Modification with Control over Ligand Density for the Study of Multivalent Biological Systems. *ChemistryOpen* **2020**, *9* (1), 53-66.

**[77]** Kaushik, S.; Mohanty, D.; Surolia, A. The role of metal ions in substrate recognition and stability of concanavalin A: a molecular dynamics study. *Biophys J* **2009**, *96* (1), 21-34.

**[78]** Alvarez Dorta, D.; Sivignon, A.; Chalopin, T.; Dumych, T. I.; Roos, G.; Bilyy, R. O.; Deniaud, D.; Krammer, E. M.; de Ruyck, J.; Lensink, M. F.; et al. The Antiadhesive Strategy in Crohn's Disease: Orally Active Mannosides to Decolonize Pathogenic Escherichia coli from the Gut. *Chembiochem* **2016**, *17* (10), 936-952.

**[79]** Bouckaert, J.; Mackenzie, J.; de Paz, J. L.; Chipwaza, B.; Choudhury, D.; Zavialov, A.; Mannerstedt, K.; Anderson, J.; Pierard, D.; Wyns, L.; et al. The affinity of the FimH fimbrial adhesin is receptor-driven and quasi-independent of Escherichia coli pathotypes. *Mol Microbiol* **2006**, *61* (6), 1556-1568.

**[80]** Martinez, J. J.; Hultgren, S. J. Requirement of Rho-family GTPases in the invasion of Type 1-piliated uropathogenic Escherichia coli. *Cell Microbiol* **2002**, *4* (1), 19-28.

**[81]** Han, Z.; Pinkner, J. S.; Ford, B.; Obermann, R.; Nolan, W.; Wildman, S. A.; Hobbs, D.; Ellenberger, T.; Cusumano, C. K.; Hultgren, S. J.; et al. Structure-based drug design and optimization of mannoside bacterial FimH antagonists. *J Med Chem* **2010**, *53* (12), 4779-4792.

**[82]** Mayer, K.; Eris, D.; Schwardt, O.; Sager, C. P.; Rabbani, S.; Kleeb, S.; Ernst, B. Urinary Tract Infection: Which Conformation of the Bacterial Lectin FimH Is Therapeutically Relevant? *J Med Chem* **2017**, *60* (13), 5646-5662.

**[83]** Mydock-McGrane, L. K.; Hannan, T. J.; Janetka, J. W. Rational design strategies for FimH antagonists: new drugs on the horizon for urinary tract infection and Crohn's disease. *Expert Opin Drug Discov* **2017**, *12* (7), 711-731.

**[84]** Sauer, M. M.; Jakob, R. P.; Eras, J.; Baday, S.; Eris, D.; Navarra, G.; Berneche, S.; Ernst, B.; Maier, T.; Glockshuber, R. Catch-bond mechanism of the bacterial adhesin FimH. *Nat Commun* **2016**, *7*, 10738.

**[85]** Sauer, M. M.; Jakob, R. P.; Luber, T.; Canonica, F.; Navarra, G.; Ernst, B.; Unverzagt, C.; Maier, T.; Glockshuber, R. Binding of the Bacterial Adhesin FimH to Its Natural, Multivalent High-Mannose Type Glycan Targets. *J Am Chem Soc* **2019**, *141* (2), 936-944.

**[86]** Albertazzi, L.; Martinez-Veracoechea, F. J.; Leenders, C. M.; Voets, I. K.; Frenkel, D.; Meijer, E. W. Spatiotemporal control and superselectivity in supramolecular polymers using multivalency. *Proc Natl Acad Sci U S A* **2013**, *110* (30), 12203-12208.

**[87]** Liese, S.; Netz, R. R. Quantitative Prediction of Multivalent Ligand-Receptor Binding Affinities for Influenza, Cholera, and Anthrax Inhibition. *ACS Nano* **2018**, *12* (5), 4140-4147.

**[88]** Martinez-Veracoechea, F. J.; Frenkel, D. Designing super selectivity in multivalent nano-particle binding. *Proc Natl Acad Sci U S A* **2011**, *108* (27), 10963-10968.

**[89]** Meyer, T.; Knapp, E. W. Database of protein complexes with multivalent binding ability: Bival-Bind. *Proteins* **2014**, *82* (5), 744-751.

**[90]** Wittmann, V.; Pieters, R. J. Bridging lectin binding sites by multivalent carbohydrates. *Chem Soc Rev* **2013**, *42* (10), 4492-4503.

**[91]** Müller, C.; Despras, G.; Lindhorst, T. K. Organizing multivalency in carbohydrate recognition. *Chem Soc Rev* **2016**, *45* (11), 3275-3302.

**[92]** Chipowsky, S. L., Y. C.; Roseman, S. Adehsion of cultured fibrolbasts to insoluble analog of cell surface carbohydrates. *Proc. Nat. Acad. Sci. USA* **1973**, *70* (8), 2309-2312.

**[93]** Dam, T. K.; Roy, R.; Das, S. K.; Oscarson, S.; Brewer, C. F. Binding of multivalent carbohydrates to concanavalin A and Dioclea grandiflora lectin. Thermodynamic analysis of the "multivalency effect". *J Biol Chem* **2000**, *275* (19), 14223-14230.

**[94]** Pieters, R. J. Maximising multivalency effects in protein-carbohydrate interactions. *Org Biomol Chem* **2009**, *7* (10), 2013-2025.

**[95]** Gestwicki, J. E. C., C.W.; Strong,L.E.; Oetjen,K.A.; Kiessling,L.L. Influencing Receptor-Ligand Binding Mechanisms withMultivalent Ligand Architecture. *J Am Chem Soc* **2002**, *124*, 14922-14933.

**[96]** Nallan Chakravarthula, T.; Zeng, Z.; Alves, N. J. Multivalent Benzamidine Molecules for Plasmin Inhibition: Effect of Valency and Linker Length. *ChemMedChem* **2022**, *17* (22), e202200364.

**[97]** Manabe, Y.; Tsutsui, M.; Hirao, K.; Kobayashi, R.; Inaba, H.; Matsuura, K.; Yoshidome, D.; Kabayama, K.; Fukase, K. Mechanistic Studies for the Rational Design of Multivalent Glycodendrimers. *Chemistry* **2022**, *28* (61), e202201848.

**[98]** Schwarzenbach, G. Der Chelateffekt. *Helvetica Chimica Acta* **1952**, *35*, 2344-2359.

**[99]** Sun, M.; Liu, S.; Song, T.; Chen, F.; Zhang, J.; Huang, J. A.; Wan, S.; Lu, Y.; Chen, H.; Tan, W.; et al. Spherical Neutralizing Aptamer Inhibits SARS-CoV-2 Infection and Suppresses Mutational Escape. *J Am Chem Soc* **2021**, *143* (51), 21541-21548.

**[100]** Smith, D. K. From fundamental supramolecular chemistry to self-assembled nanomaterials and medicines and back again - how Sam inspired SAMul. *Chem Commun (Camb)* **2018**, *54* (38), 4743-4760. DOI: 10.1039/c8cc01753k From NLM Medline.

**[101]** Jacobi, F.; Wilms, D.; Seiler, T.; Queckborner, T.; Tabatabai, M.; Hartmann, L.; Schmidt, S. Effect of PEGylation on Receptor Anchoring and Steric Shielding at Interfaces: An Adhesion and Surface Plasmon Resonance Study with Precision Polymers. *Biomacromolecules* **2020**, *21* (12), 4850-4856.

**[102]** Garcia-Moreno, M. I.; Ortega-Caballero, F.; Risquez-Cuadro, R.; Ortiz Mellet, C.; Garcia Fernandez, J. M. The Impact of Heteromultivalency in Lectin Recognition and Glycosidase Inhibition: An Integrated Mechanistic Study. *Chemistry* **2017**, *23* (26), 6295-6304.

**[103]** Leino, R.; Ekholm, F.; Poláková, M.; Pawłowicz, A. Synthesis of Divalent 2,2′-Linked Mannose Derivatives by Homodimerization. *Synthesis* **2009**, *2009* (04), 567-576.

**[104]** Bücher, K. S.; Konietzny, P. B.; Snyder, N. L.; Hartmann, L. Heteromultivalent Glycooligomers as Mimetics of Blood Group Antigens. *Chemistry* **2019**, *25* (13), 3301-3309.

**[105]** Boden, S.; Reise, F.; Kania, J.; Lindhorst, T. K.; Hartmann, L. Sequence-Defined Introduction of Hydrophobic Motifs and Effects in Lectin Binding of Precision Glycomacromolecules. *Macromol Biosci* **2019**, *19* (4), e1800425.

**[106]** Fischer, L.; Steffens, R. C.; Paul, T. J.; Hartmann, L. Catechol-functionalized sequence-defined glycomacromolecules as covalent inhibitors of bacterial adhesion. *Polymer Chemistry* **2020**, *11* (37), 6091-6096.

**[107]** Freichel, T.; Heine, V.; Laaf, D.; Mackintosh, E. E.; Sarafova, S.; Elling, L.; Snyder, N. L.; Hartmann, L. Sequence-Defined Heteromultivalent Precision Glycomacromolecules Bearing Sulfonated/Sulfated Nonglycosidic Moieties Preferentially Bind Galectin-3 and Delay Wound Healing of a Galectin-3 Positive Tumor Cell Line in an In Vitro Wound Scratch Assay. *Macromol Biosci* **2020**, *20* (9), e2000163.

**[108]** Neuhaus, K.; Wamhoff, E. C.; Freichel, T.; Grafmuller, A.; Rademacher, C.; Hartmann, L. Asymmetrically Branched Precision Glycooligomers Targeting Langerin. *Biomacromolecules* **2019**, *20* (11), 4088-4095.

**[109]** Shamout, F.; Monaco, A.; Yilmaz, G.; Becer, C. R.; Hartmann, L. Synthesis of Brush-Like Glycopolymers with Monodisperse, Sequence-Defined Side Chains and Their Interactions with Plant and Animal Lectins. *Macromol Rapid Commun* **2020**, *41* (1), e1900459.

**[110]** Alfen, F.; Putscher, E.; Hecker, M.; Zettl, U. K.; Hermann, A.; Lukas, J. Abnormal Pre-mRNA Splicing in Exonic Fabry Disease-Causing GLA Mutations. *Int J Mol Sci* **2022**, *23* (23).

**[111]** Ponader, D.; Wojcik, F.; Beceren-Braun, F.; Dernedde, J.; Hartmann, L. Sequence-Defined Glycopolymer Segments Presenting Mannose: Synthesis and Lectin Binding Affinity. *Biomacromolecules* **2012**, *13* (6), 1845-1852.

**[112]** Wojcik, F.; O'Brien, A. G.; Gotze, S.; Seeberger, P. H.; Hartmann, L. Synthesis of carbohydrate-functionalised sequence-defined oligo(amidoamine)s by photochemical thiol-ene coupling in a continuous flow reactor. *Chemistry* **2013**, *19* (9), 3090-3098.

**[113]** Merrifield, R. B. Solid phase peptide syntehsis of tetrapeptide. **1963**, *85*, 2149-2154.

**[114]** Hill, S. A.; Gerke, C.; Hartmann, L. Recent Developments in Solid-Phase Strategies towards Synthetic, Sequence-Defined Macromolecules. *Chem Asian J* **2018**, *13* (23), 3611-3622.

**[115]** Chan, W. C. W., P.D. *Fmoc Solid Phase Peptide Synthesis: A Practical Approach*; OUP Oxford, 1999.

**[116]** Orain, D. E., J.; Bradley, M. Protecting Groups in Solid-Phase Organic Synthesis. *Journal of combinatorial chemistry* **2001**, *4*, 1-16.

**[117]** Baier, M.; Giesler, M.; Hartmann, L. Split-and-Combine Approach Towards Branched Precision Glycomacromolecules and Their Lectin Binding Behavior. *Chemistry* **2018**, *24* (7), 1619-1630. DOI: 10.1002/chem.201704179 From NLM Medline.

**[118]** Freichel, T.; Eierhoff, S.; Snyder, N. L.; Hartmann, L. Toward Orthogonal Preparation of Sequence-Defined Monodisperse Heteromultivalent Glycomacromolecules on Solid Support Using Staudinger Ligation and Copper-Catalyzed Click Reactions. *J Org Chem* **2017**, *82* (18), 9400-9409. DOI: 10.1021/acs.joc.7b01398 From NLM PubMed-not-MEDLINE.

**[119]** Shamout, F.; Fischer, L.; Snyder, N. L.; Hartmann, L. Recovery, Purification, and Reusability of Building Blocks for Solid Phase Synthesis. *Macromol Rapid Commun* **2020**, *41* (2), e1900473.

**[120]** Ebbesen, M. F.; Itskalov, D.; Baier, M.; Hartmann, L. Cu Elimination from Cu-Coordinating Macromolecules. *Acs Macro Lett* **2017**, *6* (4), 399-403.

**[121]** Ebbesen, M. F.; Gerke, C.; Hartwig, P.; Hartmann, L. Biodegradable poly(amidoamine)s with uniform degradation fragments via sequence-controlled macromonomers. *Polymer Chemistry* **2016**, *7* (46), 7086-7093. DOI: 10.1039/c6py01700b.

**[122]** Blumler, A.; Schwalbe, H.; Heckel, A. Solid-Phase-Supported Chemoenzymatic Synthesis of a Light-Activatable tRNA Derivative. *Angew Chem Int Ed Engl* **2022**, *61* (1), e202111613.

**[123]** He, M.; Wu, X.; Mao, S.; Haruehanroengra, P.; Khan, I.; Sheng, J.; Royzen, M. Non-Chromatographic Purification of Synthetic RNA Using Bio-Orthogonal Chemistry. *Curr Protoc* **2021**, *1* (9), e247.

**[124]** Naoum, J. N.; Alshanski, I.; Mayer, G.; Strauss, P.; Hurevich, M. Stirring Peptide Synthesis to a New Level of Efficiency. *Organic Process Research & Development* **2022**, *26* (1), 129-136.

**[125]** Tieke, B. *Makromolekulare Chemie*; Wiley-VCH, 2014.

**[126]** Sarsabili, M.; Parvini, M.; Salami-Kalajahi, M.; Ganjeh-Anzabi, P. In Situ Reversible Addition–Fragmentation Chain Transfer Polymerization of Styrene in the Presence of MCM-41 Nanoparticles: Comparing “Grafting from” and “Grafting through” Approaches. *Advances in Polymer Technology* **2013**, *32* (4).

**[127]** Zdyrko, B.; Luzinov, I. Polymer brushes by the "grafting to" method. *Macromol Rapid Commun* **2011**, *32* (12), 859-869.

**[128]** Obhi, N. K.; Peda, D. M.; Kynaston, E. L.; Seferos, D. S. Exploring the Graft-To Synthesis of All-Conjugated Comb Copolymers Using Azide–Alkyne Click Chemistry. *Macromolecules* **2018**, *51* (8), 2969-2978.

**[129]** Wang, Z.; Yoon, S.; Wang, J. Breaking the Paradox between Grafting-Through and Depolymerization to Access Recyclable Graft Polymers. *Macromolecules* **2022**, *55* (20), 9249-9256.

**[130]** Li, L.; Huang, J.; Zhang, Y. Synthesis of Comb-Like Macromolecules via Semi-Batch Miniemulsion RAFT Polymerizations. *Macromolecular Chemistry and Physics* **2018**, *219* (18).

**[131]** Luo, X.; Li, Z.; Zhang, L.; Chen, Y.; Tan, J. Mechanistic Investigation of the Position of Reversible Addition–Fragmentation Chain Transfer (RAFT) Groups in Heterogeneous RAFT Polymerization. *Macromolecules* **2022**, *55* (12), 4916-4928.

**[132]** Zhang, B.; Wang, X.; Zhu, A.; Ma, K.; Lv, Y.; Wang, X.; An, Z. Enzyme-Initiated Reversible Addition–Fragmentation Chain Transfer Polymerization. *Macromolecules* **2015**, *48* (21), 7792-7802.

**[133]** Aponte-Rivera, C.; Rubinstein, M. Dynamic Coupling in Unentangled Liquid Coacervates Formed by Oppositely Charged Polyelectrolytes. *Macromolecules* **2021**, *54* (4), 1783-1800.

**[134]** Chen, X.; Chen, E.-Q.; Yang, S. Multiphase Coacervation of Polyelectrolytes Driven by Asymmetry of Charged Sequence. *Macromolecules* **2022**, *56* (1), 3-14.

**[135]** Es Sayed, J.; Caito, C.; Arunachalam, A.; Amirsadeghi, A.; van Westerveld, L.; Maret, D.; Mohamed Yunus, R. A.; Calicchia, E.; Dittberner, O.; Portale, G.; et al. Effect of Dynamically Arrested Domains on the Phase Behavior, Linear Viscoelasticity and Microstructure of Hyaluronic Acid - Chitosan Complex Coacervates. *Macromolecules* **2023**, *56* (15), 5891-5904.

**[136]** Knoerdel, A. R.; Blocher McTigue, W. C.; Sing, C. E. Transfer Matrix Model of pH Effects in Polymeric Complex Coacervation. *J Phys Chem B* **2021**, *125* (31), 8965-8980.

**[137]** Liu, Y. L.; Santa Chalarca, C. F.; Carmean, R. N.; Olson, R. A.; Madinya, J.; Sumerlin, B. S.; Sing, C. E.; Emrick, T.; Perry, S. L. Effect of Polymer Chemistry on the Linear Viscoelasticity of Complex Coacervates. *Macromolecules* **2020**, *53* (18), 7851-7864.

**[138]** Priftis, D.; Farina, R.; Tirrell, M. Interfacial energy of polypeptide complex coacervates measured via capillary adhesion. *Langmuir* **2012**, *28* (23), 8721-8729.

**[139]** Rubinstein, M.; Liao, Q.; Panyukov, S. Structure of Liquid Coacervates formed by Oppositely Charged Polyelectrolytes. *Macromolecules* **2018**, *51* (23), 9572-9588.

**[140]** Chang, L. W.; Lytle, T. K.; Radhakrishna, M.; Madinya, J. J.; Velez, J.; Sing, C. E.; Perry, S. L. Sequence and entropy-based control of complex coacervates. *Nat Commun* **2017**, *8* (1), 1273.

**[141]** Eberhardt, M.; Théato, P. RAFT Polymerization of Pentafluorophenyl Methacrylate: Preparation of Reactive Linear Diblock Copolymers. *Macromolecular Rapid Communications* **2005**, *26* (18), 1488-1493.

**[142]** Xu, Q. G., W. G. N-to_C Solid-Phase Peptide and Peptide Trifluoromethylketone Synthesis Using Amino Acis tert-Butyl Esters. *Chem. Pharm. Bull.* **2002**, *50* (5), 688-691.

**[143]** Hunter, L.; Butler, S.; Ludbrook, S. B. Solid phase synthesis of peptides containing backbone-fluorinated amino acids. *Org Biomol Chem* **2012**, *10* (44), 8911-8918.

**[144]** Carbolution. https://www.carbolution.de/product_info.php?products_id=460 (accessed 2024 16 July).

**[145]** Handa, B. K.; Keech, E. FMOC solid phase synthesis of an endothelin converting enzyme substrate. Use of allyl ester as the third orthogonal protecting group. *Int J Pept Protein Res* **1992**, *40* (1), 66-71.

**[146]** Hudecz, D.; Sigurdardottir, S. B.; Christensen, S. C.; Hempel, C.; Urquhart, A. J.; Andresen, T. L.; Nielsen, M. S. Two peptides targeting endothelial receptors are internalized into murine brain endothelial cells. *PLoS One* **2021**, *16* (4), e0249686.

**[147]** Gibson, M. I.; Fröhlich, E.; Klok, H. A. Postpolymerization modification of poly(pentafluorophenyl methacrylate): Synthesis of a diverse water-soluble polymer library. *Journal of Polymer Science Part A: Polymer Chemistry* **2009**, *47* (17), 4332-4345.

**[148]** Wei, T.; Furgal, J. C.; Scott, T. F. In situ deprotection and dynamic covalent assembly using a dual role catalyst. *Chem Commun (Camb)* **2017**, *53* (27), 3874-3877.

**[149]** Yasuhara, A. K., A.; Sakamoto, T. An efficient method for the deallylation of allyl aryl ethers using electrochemically generated. *J. Org. Chem.* **1999**, *64*, 4211-4213.

**[150]** Hubbard, P. B., W. J.; Simonsick, W. J. Jr.; Ross, C. W. III. Synthesis and Ring-Opening Polymerization of Poly(alkylene 2,6-naphthalenedicarboxylate) Cyclic Oligomers. *Macromolecules* **1996**, *29*, 8304-8307.

**[151]** Takizawa, K. T., C.; Hawker, C. J. Molecularly defined caprolactone oligomers and polymers synthesis and characterization. *J. AM. CHEM. SOC* **2008**, *130* (5), 1718-1726.

**[152]** Yamauchi, H.; Inayama, S.; Nakabayashi, M.; Hayashi, S. Systematic Order-Made Synthesis of Sequence-Defined Polyurethanes with Length, Types, and Topologies. *Acs Macro Lett* **2023**, *12* (9), 1264-1271.

**[153]** Hoyle, C. E.; Bowman, C. N. Thiol-ene click chemistry. *Angew Chem Int Ed Engl* **2010**, *49* (9), 1540-1573.

**[154]** Hartweg, M.; Jiang, Y.; Yilmaz, G.; Jarvis, C. M.; Nguyen, H. V.; Primo, G. A.; Monaco, A.; Beyer, V. P.; Chen, K. K.; Mohapatra, S.; et al. Synthetic Glycomacromolecules of Defined Valency, Absolute Configuration, and Topology Distinguish between Human Lectins. *JACS Au* **2021**, *1* (10), 1621-1630.

**[155]** Deng, Z.; Shi, Q.; Tan, J.; Hu, J.; Liu, S. Sequence-Defined Synthetic Polymers for New-Generation Functional Biomaterials. *ACS Materials Letters* **2021**, *3* (9), 1339-1356.

**[156]** Theato, P. Synthesis of well-defined polymeric activated esters. *Journal of Polymer Science Part A: Polymer Chemistry* **2008**, *46* (20), 6677-6687. DOI: 10.1002/pola.22994.

**[157]** Shamout, F. Synthese von Kammpolymeren mit sequenzkontrollierten Seitenketten zur multivalenten Präsentation von Zuckerliganden und deren Einsatz als Glykomimetika. Heinrich-Heine Universität, 2019.

**[158]** Bregant, S. T., A. B. Orthogonally protected lanthionines synthesis and use for the solid phase synthesis of an analogue. *J. Org. Chem.* **2005**, *70* (7), 2430-2438.

**[159]** Wu, H. A., M. N.; Niu, Y.; Qiao, Q.; Harfouch, N.; Nimer, A.; Cai, J. Solid phase synthesis of γ aapeptides using a submonomeric approach. *Org. Lett.* **2012**, *14* (13), 3446–3449.

**[160]** Grieco, P.; Gitu, P. M.; Hruby, V. J. Preparation of 'side-chain-to-side-chain' cyclic peptides by Allyl and Alloc strategy: potential for library synthesis. *J Pept Res* **2001**, *57* (3), 250-256.

**[161]** Tiwari, P.; Bharti, I.; Bohidar, H. B.; Quadir, S.; Joshi, M. C.; Arfin, N. Complex Coacervation and Overcharging during Interaction between Hydrophobic Zein and Hydrophilic Laponite in Aqueous Ethanol Solution. *ACS Omega* **2020**, *5* (51), 33064-33074.

**[162]** Yang, S.; Li, X.; Hua, Y.; Chen, Y.; Kong, X.; Zhang, C. Selective Complex Coacervation of Pea Whey Proteins with Chitosan To Purify Main 2S Albumins. *J Agric Food Chem* **2020**, *68* (6), 1698-1706.

**[163]** Li, L.; Srivastava, S.; Andreev, M.; Marciel, A. B.; de Pablo, J. J.; Tirrell, M. V. Phase Behavior and Salt Partitioning in Polyelectrolyte Complex Coacervates. *Macromolecules* **2018**, *51* (8), 2988-2995.

**[164]** Zhao, M.; Eghtesadi, S. A.; Dawadi, M. B.; Wang, C.; Huang, S.; Seymore, A. E.; Vogt, B. D.; Modarelli, D. A.; Liu, T.; Zacharia, N. S. Partitioning of Small Molecules in Hydrogen-Bonding Complex Coacervates of Poly(acrylic acid) and Poly(ethylene glycol) or Pluronic Block Copolymer. *Macromolecules* **2017**, *50* (10), 3818-3830.

**[165]** Hastings, D. E.; Bozelli, J. C.; Epand, R. M.; Stöver, H. D. H. Investigating the Effects of Charge Arrangement in Stimuli-Responsive Polyelectrolytes. *Macromolecules* **2021**, *54* (24), 11427-11438.

**[166]** Huang, J.; Morin, F. J.; Laaser, J. E. Charge-Density-Dominated Phase Behavior and Viscoelasticity of Polyelectrolyte Complex Coacervates. *Macromolecules* **2019**, *52* (13), 4957-4967.

**[167]** Illmann, M. D.; Schafl, L.; Drees, F.; Hartmann, L.; Schmidt, S. Glycan-Presenting Coacervates Derived from Charged Poly(active esters): Preparation, Phase Behavior, and Lectin Capture. *Biomacromolecules* **2023**.

'Cause I'm a real tough kid

I can handle my shit

They said, "Babe, you gotta fake it 'til you make it" and I did

…

I cry a lot, but I am so productive, it's an art

Taylor Swift, “I can do it with a broken heart”